A Study of the Effects of Friction and Mixing on the Exchange Flow through the Bosphorus (Strait of Istanbul)

by

Frank Gerdes
Diploma, Carl von Ossietzky Universität, 1996
Diploma, von Karman Institute for Fluid Dynamics, 1997

A Dissertation Submitted in Partial Fulfillment of the
Requirements for the Degree of

DOCTOR OF PHILOSOPHY

in the School of Earth and Ocean Sciences

We accept this dissertation as conforming
to the required standard

Dr. D.M. Farmer, Supervisor (Graduate School of Oceanography, University of Rhode Island)

Dr. R.G. Lueck, Departmental Member (School of Earth and Ocean Sciences)

Dr. K.L. Denman, Departmental Member (School of Earth and Ocean Sciences)

Dr. C.J.R. Garrett, Outside Member (Department of Physics and Astronomy)

Dr. R.A. Pawlowicz, Additional Member (Department of Earth and Ocean Sciences, University of British Columbia)

Dr. G.A. Lawrence, External Examiner (Department of Civil Engineering, University of British Columbia)

Supervisors: Dr. David M. Farmer and Dr. Chris J.R. Garrett

ABSTRACT

This thesis presents observations from the Bosphorus (Strait of Istanbul), Turkey, made to study the effects of mixing, entrainment and frictionally induced shear on the dynamics of an exchange flow.

The well known two-layer structure with an upper layer of brackish Black Sea water over an opposing undercurrent of salty Mediterranean water was observed. It is likely that the exchange was maximal as it seemed to be bounded by two hydraulic controls at the strait's ends; a sill control at the Black Sea was readily identifiable and the exchange also appeared to be controlled at the south exit toward the Sea of Marmara. The lower layer lost 15 to 20% of its volume to the upper layer because of upward mixing caused by interfacial shear and turbulence created at bends and lateral protuberances. The exchange was quasi-steady, except during a so-called Orkoz when strong winds caused a reversal of the upper layer flow. Between the controls the interface sloped steeply throughout the strait indicating that mass and momentum exchange between the layers and friction along the interface and sidewalls were important.

The hydraulics of a single layer flow with entrainment is examined with a reduced gravity model. Expressions are derived for the local change of layer thickness and Froude number as function of the entrainment velocity. It is shown that entrainment, like friction, acts to force the flow toward criticality, although the layer thickness can increase if the Froude number is smaller than $1/2$. For certain Froude numbers the effects of friction and entrainment on the layer thickness and the hydraulic state of the flow are found to be of comparable magnitude. A two-layer model with entrainment is developed. Predicted and observed interfacial slopes are found to be in reasonable agreement.

The classical definition of hydraulic control assumes layers with uniform velocity so that further consideration is required if there is frictionally induced shear as observed in the Bosphorus. If a shear flow preserves the shape of its velocity profile, a standard formula suggests that hydraulic control is achieved when the depth-averaged flow speed is less than $(gh)^{1/2}$. On the other hand, shallow water waves have a speed relative to the mean flow of more than $(gh)^{1/2}$, suggesting that information could propagate upstream. This

apparent paradox is solved by showing that the internal stress required to maintain a constant velocity profile depends on flow derivatives, thus altering the wave speed without introducing damping. By contrast, an inviscid shear flow does not maintain the same profile shape, but is shown to exhibit hydraulic control when the depth-averaged speed equals the inviscid long wave speed. In the Bosphorus the similarity assumption was found to approximately hold indicating that hydraulic control could not be defined using classical inviscid theory.

Examiners:

Dr. D.M. Farmer, Supervisor (Graduate School of Oceanography, University of Rhode Island)

Dr. R.G. Lueck, Departmental Member (School of Earth and Ocean Sciences)

Dr. K.L. Denman, Departmental Member (School of Earth and Ocean Sciences)

Dr. C.J.R. Garrett, Outside Member (Department of Physics and Astronomy)

Dr. R.A. Pawlowicz, Additional Member (Department of Earth and Ocean Sciences, University of British Columbia)

Dr. G.A. Lawrence, External Examiner (Department of Civil Engineering, University of British Columbia)

Table of Contents

List of Tables

List of Figures

Acknowledgements

I am grateful to Dr. David Farmer for inviting me to join the Acoustical Oceanography Research Group at the Institute of Ocean Sciences (IOS) and for giving me the opportunity to work on this challenging research project. I thank both Drs. Chris Garrett and David Farmer for their encouragement and enthusiasm, insight and guidance in teaching me how to approach physical oceanography problems. I can only hope to someday follow their example as scientists. I also thank my committee members Dr. Rolf Lueck, Dr. Ken Denman, and Dr. Rich Pawlowicz for their help and suggestions offered to improve this dissertation. Special thanks go to Dr. Rich Pawlowicz for enduring the frequent, early morning ferry trips made to join my committee meetings. I am grateful to Dr. Greg Lawrence for serving as external examiner.

The core of my work came out of ship time on the TCG Mesaha I and TCG Mesaha II provided by the Department of Navigation, Hydrography and Oceanography (DNHO) in Istanbul, Turkey. I would like to state my appreciation of the exceptional level of coorporation and skill of all the participants with whom I worked during all phases of the experiments. I am not able to list all the people involved in these experiments, but I want to especially thank Lt.Cdr Erhan Gezgin who put much effort in taking care of the logistics and Lt.JG Ahmet N. Unlu for his help during and after the survey. I will always remember Mr. Mustafa Erol.

I have enjoyed my time at IOS and this is due in large part to those I worked with. I thank my fellow students Mr. Burkard Baschek, Mrs. Roblyn Kendall and Mrs. Tetjana Ross for stimulating discussions on scientific and various other matters. Special thanks go to Mrs. Grace Kamitakahara-King and Mr. Ron Teichrob for outwitting stubborn hardware and software, to Mr. Alan Adrian and Mr. Ron Teichrob for their participation in the two Bosphorus experiments, to Mr. Nick Hall-Patch for knowing where to find

things that I always needed desperately and immediately, to Mr. Kevin Bartlett for help with data processing problems, and to Mrs. Pip Sumsion for ensuring that pay cheques kept arriving. Thanks to my other colleagues and friends at IOS and UVic; it has been a pleasure working with you.

Last but not least, I must thank all those outside the world of oceanography that made my stay in Canada such a wonderful experience; especially Mr. Koit Teng and Mrs. Uta Rach for sharing their home (and driveway) for many more months than they might have anticipated and for their friendship. Finally, I would not have achieved this thesis without the love of my wife Ulrike and the smile of my son Kilian. Both have shown truly remarkable patience during the trials of the last few months of completing this dissertation. Without them it would have been much less pleasant.

The author was funded partly by a fellowship from the German Academic Exchange Service (DAAD, HSP III).

"... I mentioned to your Majesty at the beginning of my discourse that my intention in embarking on these travels was not only to contemplate and observe these natural motions which are purely visual, but also to investigate those which are more concealed but just as marvelous to the human mind, and encourage one to discover, for the public good, the reasons. Emboldened by the observations of the surface motion of our channel, happily I was able to prepare myself as best I could, for greater and nobler research, more fruitful since it was more difficult and new, and consequently worthy of Your Majesty's spirited genius. ..."

Count Luigi Ferdinando Marsigli in his letter to ex-Queen Christina of Sweden. The letter entitled "Osservazioni intorno al Bosforo Tracio" was originally published in Rome in 1681 (English translation in Deacon, 1978).

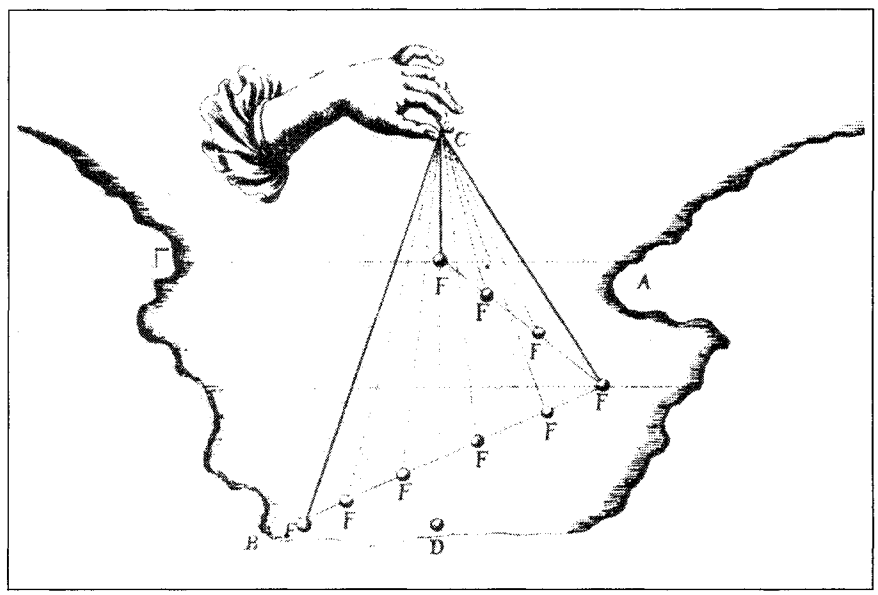

A figure from Marsigli (1681) illustrating how he measured the "Superior" (surface current) and the "Sottana" (under current) in the Bosphorus.

1. Introduction

1.1. Motivation

The major subject of this thesis is the circulation of water in a particular type of coastal feature called "sea strait", and my example of such a strait will be the Bosphorus, also known as Strait of Istanbul.

Geographically, the term sea strait is used to describe a narrow channel connecting two larger bodies of water, or more generally, any topographic relief obstructing the free flow of water between two water bodies. It may refer to narrow passages between an island and the mainland, such as the Strait of Messina, or to channels serving as the primary or sole connection between enclosed seas and the open ocean, such as the Bosphorus or the Strait of Gibraltar. Dynamically, a strait is any topographic constriction that imposes some type of control on the water flowing through it (Trowbridge *et al.*, 1998).

If one was given the task to study the circulation of the ocean with its basins and marginal seas interconnected by straits, one would do well by choosing the straits as observational starting points. First, mass, heat and chemical budgets for individual basins can be formulated in terms of the fluxes measured across the straits using a relatively small number of observations which can be done with relative ease. Second, it is reasonable to expect that straits impose some kind of constraint on the exchange between the basins. Third, strait-flow regularly exhibits fascinating physical processes like hydraulic control, hydraulic jumps, local instabilities, mixing, internal waves, and other hydraulic and fine scale phenomena which are well worth studying. It should also be noted that many straits are excellent natural laboratories for observing the above mentioned phenomena, because unlike the unpredictable open ocean, swift currents and topography reliably produce strong interactions at specific locations. Vessels can be scheduled with (some) confidence that

the targeted physical processes will occur, and the studies have a realism not available in artificial channels or numerical simulation. Finally, an understanding of exchange flows in straits may also be helpful in solving many environmental engineering problems.

Whenever a strait separates two basins containing waters of differing density, a baroclinic exchange may occur owing to the gravitational force that acts through internal horizontal pressure gradients to restore a stably stratified water column. The study of the baroclinic exchange in straits is an attempt to understand how a particular situation modifies the simplest possible flow configuration by including other effects, such as geometry, friction, rotation and mixing, and very often the main objective is to quantify the magnitude of the exchange.

Earlier studies invoked some type of friction as constraint mechanism on the flows (e.g. Defant, 1961*a*), but purely frictional constraint models require unrealistically large friction parameters (Trowbridge *et al.*, 1998). An important breakthrough occurred in the 1950s when Stommel & Farmer (1952, 1953) introduced the notion of hydraulic control and noted that internal hydraulic control at the mouth of an estuary could determine the exchange between an estuary and the open ocean. Their model was soon applied to strait flows. Coupled to mass and salt conservation statements, the hydraulic control condition provides an upper limit on the magnitude of the flows that are physically possible given the density difference between the two basins. This limit is set by a balance between the available potential energy, determined by the density difference, and the kinetic energy of the flow. Further improvements of the inviscid steady hydraulic theory came with the introduction of two topographic controls (Farmer & Armi, 1986) representing specific topographic features in the strait. An interesting consequence was the possibility of having a maximal exchange situation which requires the presence of two internal hydraulic controls separated by a region of subcritical flow. The exchange is maximal in the sense that for the given flow configuration the strait's subcritical region is effectively isolated from perturbations in the level of the interface in the adjoining water bodies that could possibly modify the exchange. Then the exchange is as large as the given flow configuration allows; the exchange is maximal (Armi & Farmer, 1987).

The inviscid Farmer & Armi (1986) model has been proven to be a powerful aid for the understanding and prediction of exchange in straits where friction and mixing effects

are relatively minor, such as the Strait of Gibraltar (Pratt, 1986; Farmer & Armi, 1988; Bryden & Kinder, 1991*a*). On the other hand, friction and entrainment can play an important role in longer, shallower, or narrower straits. The Bosphorus is a good example. There, substantial changes occur in the density structure of the water masses as they move through the strait. Moreover, the interface between the layers has an appreciable slope, even within the central portion which is well away from the controls points (Oğuz *et al.*, 1990). It seems likely under these circumstances that both mass and momentum flux between the layers, together with friction along the boundaries, contribute to the balance of forces within the strait. Frictional effects have been explored before by various authors - by Henderson (1966) for open channel flow, by Pratt (1986) for oceanic reduced gravity flows, and by Assaf & Hecht (1974) and Bormans & Garrett (1989*b*) for exchange flows in straits, just to name a few. On the other hand, until recently the effects of entrainment on the dynamics had not received much attention despite the fact that entrainment was found to be an important factor in numerical simulations of the exchange in the Bosphorus (Ünlüata *et al.*, 1990).

Most theoretical models make the assumption of homogeneous and uniform slab-like layers. However, not surprisingly observations and numerical simulations clearly show that the effects of friction and entrainment cause the transition from one layer to the other to be continuous rather than abrupt which means that vertical profiles of density and horizontal velocity show significant vertical gradients. In such circumstances it is often difficult to determine whether an exchange flow between two basins is hydraulically controlled. One reason is that hydraulic control is usually defined for layered flows. Unfortunately, using the results of layered hydraulic theory might depend sensitively on how one defines the layers (e.g. Pratt *et al.*, 1999). The problem is commonly resolved by extending the connection between long waves and hydraulic control, which is well established for layered flows, to continuously stratified and sheared exchange flows. However, this appears to be a bold step as there does not seem to be a well-founded model of hydraulic behaviour of such flows in hand (Pratt *et al.*, 2000). In fact, even for the simple case of a homogeneous but sheared fluid there is an apparent contradiction between control conditions based on an energy argument on one hand and on the speed of long waves on the other. These two arguments are commonly used in the engineering and oceanography literature,

respectively.

The study of the above mentioned theoretical topics was motivated by our observations at the Bosphorus which in turn were motivated not only by an interest in strait flows in general but also by a great necessity to gain a better understanding of the circulation in the Bosphorus. Worsening environmental problems associated with increasing international ship traffic and industrial pressures, in a region of rapidly developing hinterland and deteriorating marine environmental quality, have been a reason for great concern in recent years. They can be understood and solved only on the basis of a good knowledge of the physical processes at work (Ünlüata *et al.*, 1993; Özsoy *et al.*, 1996). Unfortunately, whereas much is known about the strait's hydrography, its currents are much less studied. For instance, both Oğuz *et al.* (1990) and Yüce (1996) point out that their interpretation of the Bosphorus internal hydraulics is only qualitative and solely based on hydrographic measurements. The reason is that current measurements, regardless of whether they are done from a vessel or from a mooring in the strait, are rather difficult under fast currents and heavy ship traffic. The first detailed observations of the flow had to wait until 1994 (Gregg *et al.*, 1999; Gregg & Özsoy, 2002). These observations, as well as the ones that will be shown in this thesis, reveal important discrepancies between reality and numerical simulations (Oğuz *et al.*, 1990). For example, hydraulic controls were not observed where hydrographic measurements and numerical simulations predicted them to be. Particularly challenging and rare are measurements at the southern end of the Bosphorus, because the surface layer becomes extremely shallow at this location and thus easily escapes detection (see Gregg *et al.*, 1999). We designed our measurements to avoid this problem enabling, us to investigate whether a hydraulic control might exist at the southern exit of the Bosphorus.

1.2. Thesis Layout

The overall objective of this project is to improve our understanding of the effects of mixing and entrainment on the dynamics of flows in straits, and in particular to gain a better understanding of the exchange flow in the Bosphorus. The emphasis will be on gaining physical insight through a combination of data analysis and simplified theoretical

description.

The thesis outline is as follows:

Chapter 2 summarises the relevant background; the Bosphorus and its adjoining seas are introduced and prior work pertinent to flow in straits in general and to the Bosphorus in particular is reviewed.

Chapter 3 is devoted to our observations and is split into 6 sections. The first describes the *Field Experiments.* I then describe and analyse the time-varying *Forcing and Flow* of the exchange, the *Evolution of the Flow along the Strait*, and *Friction at Bottom and Sidewalls.* The fifth section is the most important part of this chapter. It gives a qualitative and quantitative description of *Mixing and Entrainment* along the Bosphorus. Finally I discuss the key problems identified by our observations.

In chapter 4 I analyse the effects of entrainment and mixing on the dynamics of an exchange flow using a theoretical model. As this requires the use of the theory of hydraulics, I begin the chapter with a basic review of hydraulics of inviscid and frictional single-layer flows. I then analyse the effects of entrainment on the dynamics of a single-layer flow, and subsequently extend this model to two-layer hydraulics with entrainment. Finally I compare model predictions with our observations and discuss the findings.

In chapter 5 I will address the question of how hydraulic control can be defined and detected when the flow is not homogeneous and not uniform. I will describe a partial solution for the case of a homogeneous shear flow and discuss the implications for the determination of hydraulic controls and the exchange in the Bosphorus.

During one of our experiments we were fortunate to observe a highly unusual change of direction of the upper layer flow. Locally this phenomenon is called *Orkoz.* An Orkoz is very poorly documented in the literature so that our observations of it might actually be the first. I will introduce the Orkoz in chapter 3 but the main description will be done separately in chapter 6.

Finally, in chapter 7, I will summarise the findings of this thesis and review some of the outstanding difficulties in modelling the flow through the Bosphorus, in understanding the effects of entrainment on exchange in straits, and in resolving the question of maximal or submaximal exchange for stratified and sheared strait flows.

2. Background

In this chapter I will begin with an introduction to the Bosphorus and its adjoining seas. In the second section I will review the existing literature on exchange flows in straits thereby discussing some commonly used approximations and their applicability to the Bosphorus. The chapter ends with a summary.

2.1. The Bosphorus

The Bosphorus forms the northern part of the Turkish Straits which connect the Black Sea to the Sea of Marmara and the Aegean Sea (figures 2.1 & 2.2). Low salinity water from the Black Sea, formed as a result of excess precipitation and river discharge, flows through the straits to the Mediterranean as a surface flow. A flow of more saline, denser Mediterranean water returns to the Black Sea as an under-current (figure 2.3). The principal driving mechanism in the Bosphorus (as well as in the Sea of Marmara and Dardanelles) is simple: the upper southbound flow is caused by a hydraulic head due to excess fresh water in the Black Sea. It is underlaid by the north-flowing undercurrent which is driven by a longitudinal (along strait) pressure gradient as result of the marked density differences in the seas linked by the strait[1].

[1]This explanation was given as early as 1681 by the Italian military engineer, Count Luigi Ferdinando Marsigli (1658-1730). Marsigli went to Constantinople (today's Istanbul) in 1679. There he heard about the undercurrent in the Bosphorus from Turkish fishermen and from the British ambassador to the Sultan. He made a comprehensive survey of the Bosphorus, which was remarkable no less for its time than for the youth of the author. He observed the difference in density between the relatively fresh Black Sea and the more saline Sea of Marmara. He took samples of the surface current and the undercurrent and found that the bottom water was heavier than the surface water and must therefore have originated in the Sea of Marmara. He concluded that the heavier water flowed from the Sea of Marmara into the Bosphorus because of its greater density. In order to render his argument indisputable

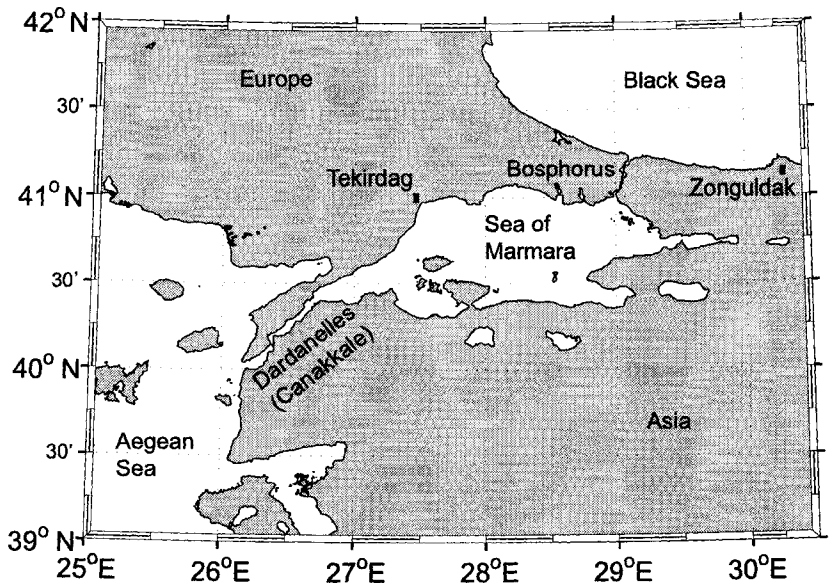

Figure 2.1.: *Map of the Turkish Straits system with Bosphorus (Strait of Istanbul), Sea of Marmara, and Dardanelles (Strait of Çanakkale).*

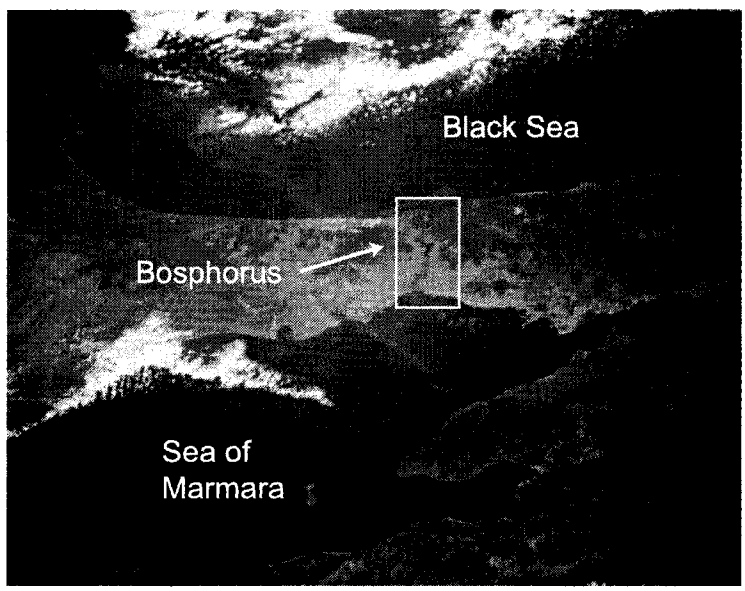

Figure 2.2.: *Photograph of the Bosphorus region taken from the Space Shuttle (NASA photo identification # STS066-0157-0192).*

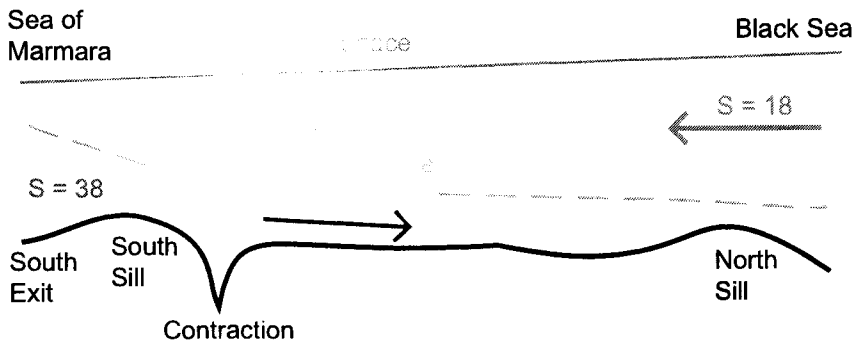

Figure 2.3.: *Sketch of the exchange flow in the Bosphorus with the upper brackish layer flowing southward and the lower salty layer flowing northward.*

Despite the relatively simple driving mechanism the exchange in the Bosphorus exhibits numerous subtleties which are due to the complicated strait geometry and the time varying forcing imposed by the adjoining basins. The following will serve as in introduction to these features.

2.1.1. Geometric Characteristics

The Bosphorus has a tortuous geometry (Figure 2.4). Over its length of about 32km the width varies between 0.7 and 3.5km with an average value of 1.6km at the surface and reduces toward the bottom to an average width of 500m at 50m depth. The depth varies between 30 and 110m (Yüce, 1990). The most prominent features affecting the flow are two sills and a contraction.

The South Sill is located 3km north of the South Exit at the Sea of Marmara (a map more detailed than in figure 2.4 is shown in figure 3.21, page 65). It is between 30m and

---

he designed a beautiful laboratory experiment which showed how the presence of adjacent bodies of water of differing density would set up and maintain a circulation as observed in the Bosphorus. Marsigli addressed his work to ex-Queen Christina of Sweden (Marsigli was employed by Queen Christina of Sweden in a diplomatic mission) in the form of a letter entitled *Osservazioni intorno al Bosforo Tracio.* An English translation including reproductions of Marsigli's drawings is given by Deacon (1978). A figure of Marsigli's experimental setup is also reproduced in (Gill, 1982, chapter 5). It is curious that Marsigli's study, although it came to the Royal Society in London, did not become generally known and had no influence over the controversy about a reported undercurrent in the Strait of Gibraltar. Hence, British scientists and engineers continued to puzzle fruitlessly over this problem for many more years until it was explained by von Waitz in 1755 (Deacon, 1971, 1985).

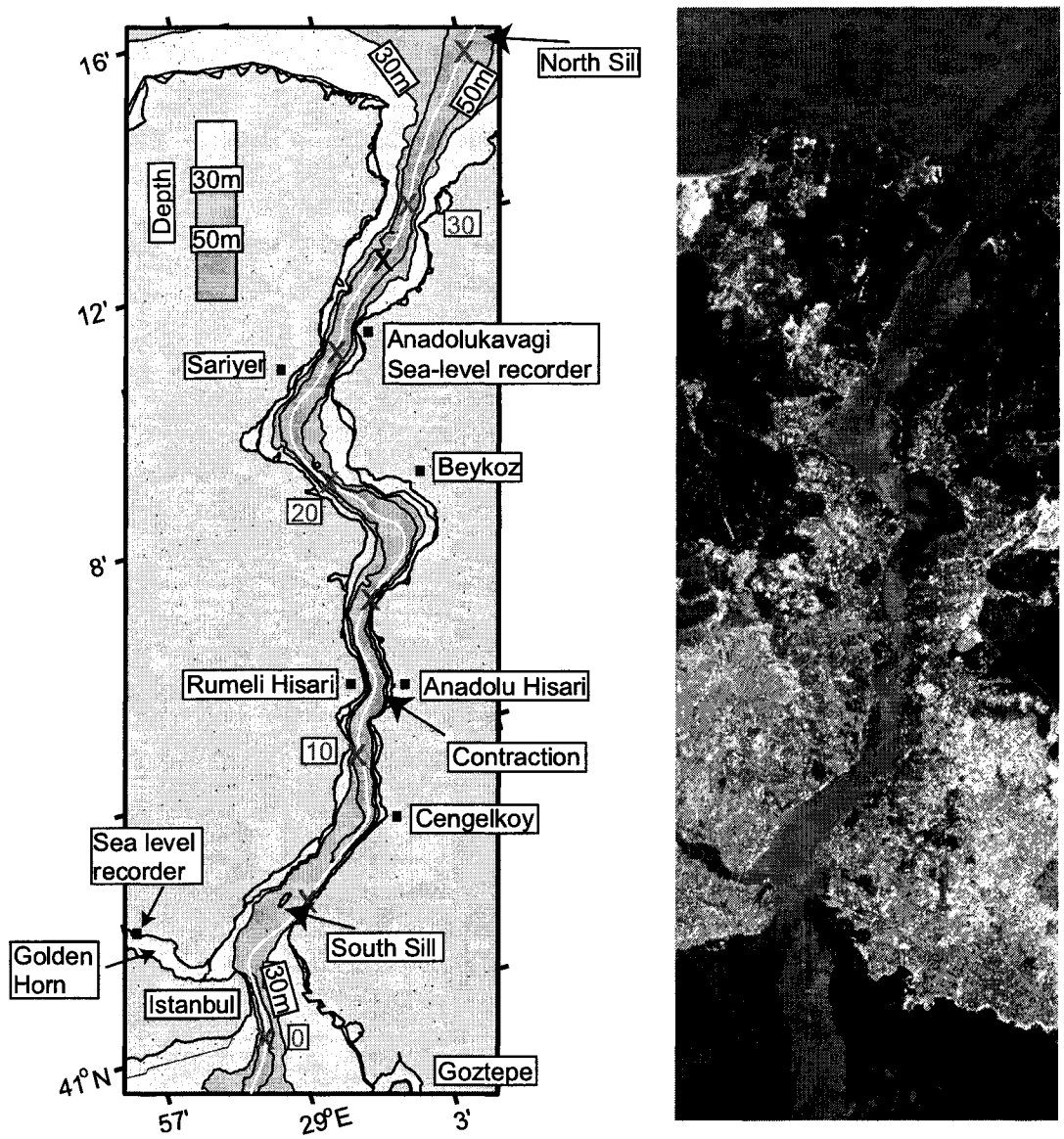

Figure 2.4.: ***Left:*** *Bathymetry of the Bosphorus. The thalweg or deepest path, shown by the white line, is marked in* 5km *increments by red crosses. The origin is at the Sea of Marmara entrance of the strait at* $41°00'01''N$ *and* $28°59'30''E$. ***Right:*** *ASTER satellite image from June 16, 2000 of the Bosphorus and its surroundings. The image is a gray-scale composite of visible and infrared spectral bands. It was provided by Dr. Michael Abrams from the ASTER Science Team at JPL.*

40m deep except for a central ridge that rises to about 28m. The ridge is flanked by two 40m deep channels that cut into the sill from the north whereby the one on the eastern side is the deeper one. From the south the sill is approached by the Marmara channel that runs along the western side of the strait. It does not connect to the northern channel on the eastern side. The second sill is the North Sill about 2km north of the Bosphorus - Black Sea junction, inside a narrow canyon, the so-called pre-Bosphorus channel, which extends in the northeast direction from the strait. The sill with a depth of 60m is found at the widest point of the canyon (Di Iorio & Yüce, 1999). The deepest part ($\approx$ 110m) of the strait roughly coincides with the narrowest section, called the Contraction (11 – 14km). It has a width of approximately 650m.

In addition to its irregular depth and width, the Bosphorus turns sharply about its average orientation of 23° from true north. Over the South Sill its orientation changes by 90°. Along the contraction the channel turns 60° and then bends back by nearly the same amount immediately to the north. Along the northern part it twists through 128° over a few kilometres, and then remains fairly straight north of position 22km. Some of these sharp bends lead to flow separation and eddy circulation in bays. These are sometimes visible in satellite images like the one shown in figure 2.4.

The present geometry of the Bosphorus appears to be the result of frequent tectonic activity (Gökaşan *et al.*, 1997). The Bosphorus' evolution began in the Early Pliocene ($\approx 4 \times 10^6$ years BP) with two streams separated from each other by the watershed of a plateau (near today's Anadolukavagi), one running to the Black Sea and the other to the Sea of Marmara (Gökaşan *et al.*, 1997, Figure 11). Block faulting formed a basin further south (near Beykoz). Over the next couple of years, or more precisely during the Pleistocene (1.6×10^6 to 11 000 years BP), the southern stream was transformed into a basin by means of intense faulting. On the other hand the watershed and northern stream were left mostly intact except for some deepening due to erosion. From 17 000 years BP onwards the global sea level began to rise and the Mediterranean waters passed the lowered barrier to reach the Black Sea (Gökaşan *et al.*, 1997)[2].

[2]The exact evolution of the Bosphorus is a matter of an ongoing heated debate which even caught the attention of the public and has been featured in several prominent publications including National Geographic and many scientific journals and magazines. The reason is that Ryan *et al.* (1997) released

2.1.2. The adjoining Basins: Black Sea and Sea of Marmara

The Black Sea is one of the largest land-locked basins in the world with a surface area of $4.2 \times 10^5 \text{km}^2$ and a volume of $5.3 \times 10^5 \text{km}^3$. Its only connection to other seas is the Bosphorus which controls the renewal of intermediate and deep waters of the basin. As a result of this limited exchange, Black Sea deep water has a very long mean residence time of about 2000 years. Below about 200m the water is rich in hydrogen sulfide, and except for bacteria, life is absent below 100 to 200m. The surface waters are strongly influenced by freshwater inflow from major European rivers such as Danube, Don, Dnieper, Dniester, and Southern Bug. Danube is the largest contributor, maintaining nearly half of the total inflow. The low salinity surface waters overlay the warmer and more saline Mediterranean influenced waters. In between them, there exists the so-called Cold Intermediate Layer (CIL) with temperatures typically less than 8°C. The CIL is easily detected during the summer but less so during the winter because of surface heating and cooling (Ünlüata *et al.*, 1993; Özsoy & Ünlüata, 1997). Tides are fairly small in the Black Sea because the natural period of oscillation of 5h differs considerably from that of the tide generating forces (Defant, 1961*b*, p. 404). At Anadolukavagi in the northern part of the Bosphorus the tide is mixed but mainly semi-diurnal as it is in the Black Sea itself, and the mean spring and mean neap tidal elevations are 3.6 and 1.5cm (Defant, 1961*b*; Alpar & Yüce, 1998).

The Sea of Marmara is a small inland sea with a surface area of 11500km^2 and a volume of 3380km^3. The maximum depth is 1400m. Being part of the Turkish strait system, it

an article in 1997 and a book in 1998 claiming to have found the location of the biblical flood. According to them, the passing of Mediterranean water into the Black Sea happened 7600 years BP as a sudden and catastrophic event. Their findings suggested that the terrifying and swift flood may have cast such a long shadow on succeeding cultures that it inspired the biblical story of Noah's ark. This is called the "Flood Hypothesis". However, other scientist dispute this theory. According to Aksu *et al.* (2002), the Marmara Sea was isolated from both the Black Sea and the Aegean Sea during glacial periods, when global sea-level lowering exposed the shallow sills at the Straits of Bosphorus and Dardanelles, and was reconnected through both straits during interglacial periods during the rise of the global sea level. Because it filled earlier, by about 10 000-12 000 years BP the Black Sea started spilling into the Marmara Sea (rather than the reverse), leading to the development of a brackish-water surface layer that has persisted to the modern day.

has a two-layer stratification. The low-salinity surface water (≈ 23 psu) is separated from the saltier (≈ 38 psu) Mediterranean water by a strong pycnocline located at a depth of about 25m. The Sea of Marmara receives an inflow from the Bosphorus which is about 50 times the cumulative annual discharge of the small rivers entering it. The residence times for the upper and lower layers are estimated to be 4 to 5 months and 6 to 7 years, respectively (Beşiktepe *et al.*, 1994). The Sea of Marmara is too small to generate its own tides, but a tidal signal reaches it through the Dardanelles and the Bosphorus. In the southern part of Bosphorus the mean spring tidal range is less than 4cm (Alpar & Yüce, 1998).

2.1.3. Forcing of the Flow

Barotropic Forcing

The flow of the surface water from the Black Sea to the Sea of Marmara is caused by the excess of riverine flow (350km^3 per year) and precipitation (300km^3 per year) over evaporation (350km^3 per year) in the Black Sea. The excess is balanced by an outflow of about 300km^3 per year through the Bosphorus (Ünlüata *et al.*, 1990). The mean sea-level difference along the strait is between 0.3 and 0.4m (e.g. Ünlüata *et al.*, 1990; Alpar & Yüce, 1998).

Instantaneous fluxes and sea-level differences can deviate significantly from these long term averages. The sea-level difference is generally greater between February and July (ranging from 28 to 56cm with an average of 40 ± 3cm), when the net freshwater influx to the Black Sea increases, and lower (between 19 and 35cm with an average of 23 ± 3cm) during autumn and winter (Alpar & Yüce, 1998).

I have already mentioned that tidal sea-level oscillations are small at the Bosphorus causing tidal currents with amplitudes of not more than $\pm 0.10\,\mathrm{m\,s^{-1}}$. (This was derived from our own current data shown in figure 3.7). They are never big enough to override the mean sea-level difference driving the exchange flow as, for instance, in the Strait of Gibraltar. In fact, meteorological effects dominate the time-dependent response of the flow. The region is affected by two distinct seasonal climatic regimes. During the summer, northerly winds from the Black Sea dominate. During the winter, the weather is

dominated by an almost continuous passage of cyclonic systems. These affect the region for periods between three to ten days, and often result in winds of $8\,\mathrm{m\,s^{-1}}$ to $10\,\mathrm{m\,s^{-1}}$ (hourly averages) sustained over one to two days. Maximum speeds of $30\,\mathrm{m\,s^{-1}}$ have been observed as gusts (Ünlüata *et al.*, 1990). On an annual basis, northerly winds are dominant with a frequency of 60%, with southerlies occurring 20% of the time. During the winter winds from either direction are equal both in strength and frequency. Changes in wind speed and direction occur on a variety of time scales ranging from a few hours (e.g. a daily land-sea breeze) to tens of days (passage of cyclonic systems) (Alpar & Yüce, 1998). The effect of the winds on the flow in the Bosphorus is through a change of sea-level in the exit regions of the Black Sea and Sea of Marmara. In general, onshore winds tend to raise and offshore winds tend to lower the sea-level. Because the orientation of the Bosphorus is approximately the same as the prevailing wind direction, Cetin (1999) speculates that wind stress along the surface of the Bosphorus itself might contribute to the forcing.

Another reason for sea-level changes is variations of barometric pressure. However, the barometric pressure difference between the western Black Sea and the Sea of Marmara is too small to influence the exchange in the strait. For instance, for the period from 1991 to 1994 the average pressure difference between Kumkoy (Black Sea side of the Bosphorus) and Tekirdag (north shore of Sea of Marmara) is 1 mbar (Cetin, 1999), and hourly averaged barometric pressure differences between the Sea of Marmara and the Black Sea during September 1994 show extrema of about ± 2 mbar (Özsoy *et al.*, 1998).

According to measurements by Arisoy & Akyarli (1990) exchange flow conditions prevail for about 95% of the time. Blocking of the flows in either layer occurs during extraordinary events. Lower layer blocking typically occurs during spring and summer months when the net freshwater influx to the Black Sea increases. It typically lasts for a few days. Upper layer blocking events, identified locally as *Orkoz*, are believed to occur in the autumn and winter months, when the surface flow reverses and the surface salinity increases in response to southwesterly winds. These events last for only a few days, too (Özsoy *et al.*, 1995).

In summary, barotropic forcing of the Bosphorus exchange ranges from weak to very strong and operates on a variety of time scales ranging from a few hours to seasons or even years (Peneva *et al.*, 2001). Despite a number of field observations in recent years,

the picture is still far from complete. Long term meteorological observations are easily available, and although there are no permanent tide gauges at the Bosphorus, several sea-level records, with durations of up to a few years, exist and have been studied (e.g Yüce & Alpar, 1997; Alpar & Yüce, 1998; Özsoy *et al.*, 1998; Cetin, 1999, and references therein). On the other hand, as pointed out by Özsoy *et al.* (1998), observations of currents are much sparser because measurements with current meters deployed in the Bosphorus are difficult under fast currents and heavy ship traffic. The long-term measurement strategy was therefore based on deploying instruments only into the lower layer. Deployments into the upper layer were carried out only during the duration of field experiments and are thus even rarer (Arisoy & Akyarli, 1990; Özsoy *et al.*, 1998; Gregg *et al.*, 1999; Gregg & Özsoy, 2002).

Baroclinic forcing

The waters below 40m depth in the Sea of Marmara exhibit very constant properties. Between 1987 and 1992 basin averaged potential temperature and salinity were 14.5°C and 38.5 psu (Beşiktepe *et al.*, 1994). These averages were obtained between March and September and show very little seasonal variation. These variations are essentially confined to the upper layer (< 25m). The upper layer salinity is in the range of 23 ± 2 psu, reaching a maximum in winter as a result of increased wind mixing and reduction of the influx from the Black Sea. Upper layer temperature varies between 7°C in the winter and 22°C in the summer and correspondingly density σ_θ varies between 14 and 19 kgm^{-3}.

A similar situation exists at the Black Sea side of the Bosphorus. Cetin (1999) shows 11 salinity and temperature profiles obtained at irregular intervals between 1992 and 1998. Upper layer temperatures vary between 4°C in the winter and 22°C in the summer. Upper layer salinity is 17.5 ± 1 psu, and density $\sigma_\theta = 13.5 \pm 1.5 \mathrm{kgm}^{-3}$. Relatively larger surface salinities in the winter period generally decrease somewhat late spring and summer as a result of increased fresh water inflow into the Black Sea. Lower layer temperature and salinity vary between 13°C and $15^{\circ}\mathrm{C}$ and 35 and 37 psu, respectively. The corresponding density range is 26 to 27.5 kgm^{-3}.

The above values are based on cruise data and, hence, have a sampling period of the order of months. However, significantly faster fluctuations are not likely as salinity changes

only seasonally. Surface temperatures are certainly influenced by changing solar radiation, but this has little effect on density.

It is worth noting that over the North Sill fluctuations of lower layer salinity of up to 3 psu over two days have been observed (e.g. Yüce, 1996) but this is not related to a change in stratification in the basins but rather to varying mixing rates within the Bosphorus in response to varying layer speeds.

In summary, one can expect that the baroclinic part of the exchange, which is driven by the large density contrast between the basins, is very steady on time scales of less than a month. On seasonal time scales the only significant variation seems to be that of salinity at the Black Sea side of the Bosphorus. It varies between 16.5 and 18.5 psu with lower values indicating summer conditions corresponding to the increased Black Sea river inflow.

2.1.4. Hydrographic Characteristics

The hydrographic characteristics of the water masses in the Bosphorus have been reported on by a number of authors (e.g. Möller, 1928; Oğuz *et al.*, 1990; Ünlüata *et al.*, 1990; Yüce, 1990, 1996). As an example, figure 2.5 shows salinity transects along the strait from (Yüce, 1996).

On the basis of the above studies a synopsis of what might be called an average situation in the strait might be as follows: The Bosphorus is stratified in two layers. In the absence of current measurements the interface may be identified by a transitional layer between the salinity limits of $18-23$ and $33-38$ psu (Oğuz *et al.*, 1990). It is relatively sharper at the northern part of the strait with an average thickness of about 5m located at the depth of 40 to 50m. It extends with a slope toward the southern part where significant changes take place with respect to its position and stratification characteristics. The widening of the interface south of the constricted region indicates vertical mixing. Mixing results in a total increase of about 3 psu in the upper layer between the two ends of the strait. Toward the southern end the interfacial layer becomes much thicker and attains a thickness of 10 to 15m above which the surface layer eventually joins the Marmara exit region in the form of a jet. It has a salinity of 21 to 22 psu at the southern exit region. The lower layer enters the strait below a depth of about 25m and proceeds northward by flowing over the South Sill. Most of the mixing takes place in the region to the south of the

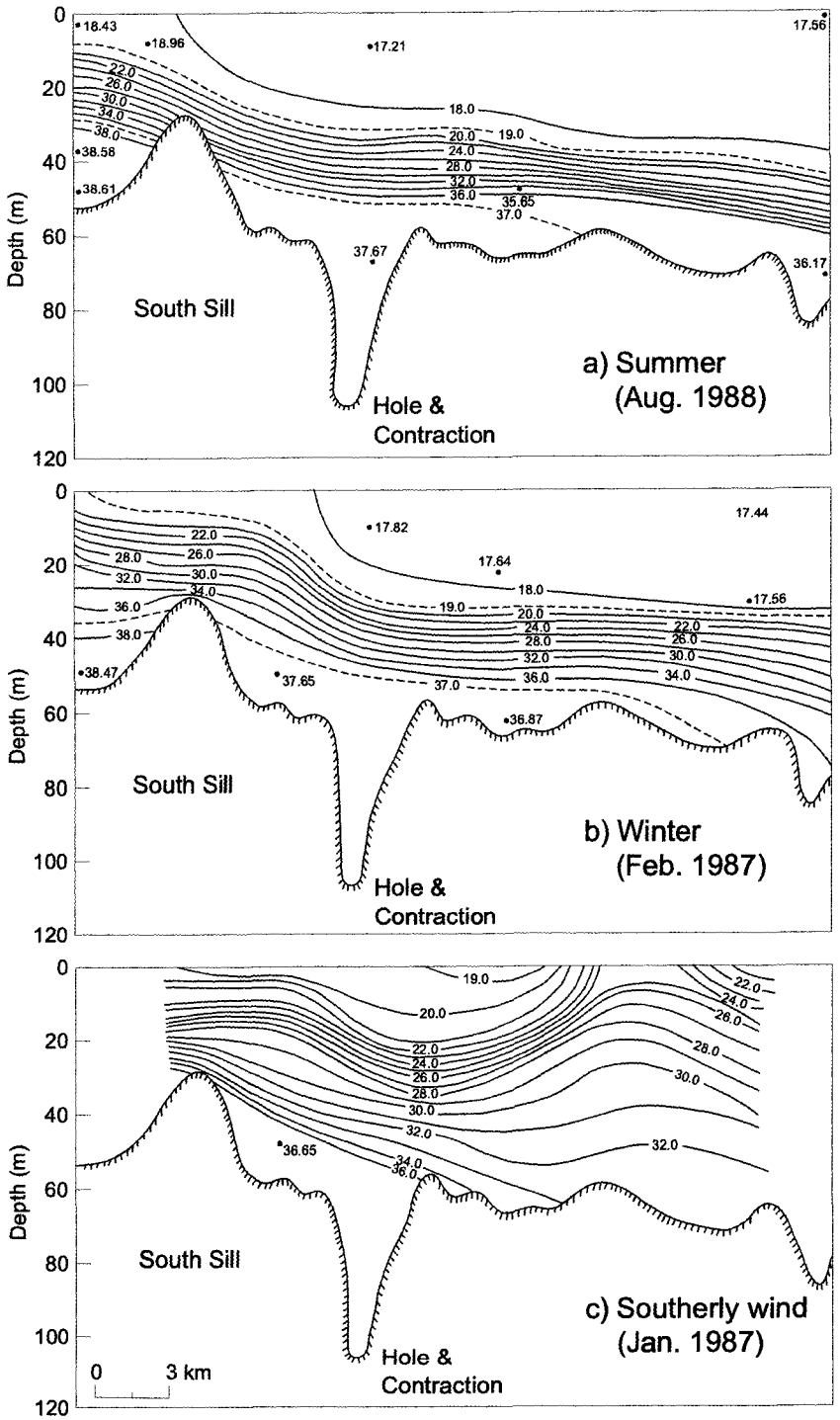

Figure 2.5.: *Salinity transects along the Bosphorus from a) August 1988 with moderate northerly winds b) February 1987 with moderate northerly winds, and c) January 1987 when strong south-westerly winds prevailed. Adapted from figure 2 in (Yüce, 1996).*

Contraction. Thereafter, the rate of vertical mixing is small and the Marmara water joins the pre-Bosphorus channel in the Black Sea with a maximum salinity of 36.5 psu below a depth of 50m.

Figure 2.5 indicates that the stratification is subject to temporal variations and might differ significantly from the average situation: A thick upper layer (Figure 2.5 a) results from a strong inflow from the Black Sea which may result from both increased riverine inflow into the Black Sea and/or strong northerly winds. In the winter the sea-level difference is typically reduced compared to the summer. Then the thickness of the upper layer is decreased whereas the thickness of the interface increases (Figure 2.5 b). During strong southwesterly winds the lower layer flow intensifies and the surface flow decreases significantly (Figure 2.5 c). Vertical mixing is increased and the interfacial layer becomes relatively thick throughout the strait as compared with the much stronger interfacial contrast in the case of intense upper layer flow conditions.

Oğuz *et al.* (1990) and Yüce (1996) emphasise that their hydrographic measurements are not supported by velocity measurements so that they are not able to establish a quantitative relation between the observed stratification and the strength of the exchange. They estimate the strength of the flow on the basis of visual observations and/or measurements of wind speed and direction.

2.1.5. Environmental Problems

I have mentioned before that the main motivation for several scientific studies in the Bosphorus in recent years was the increasing concern about the state of health of the Turkish Straits. Therefore I would like to give a few more details although this problem is not at the heart of my thesis. The two main areas of concern are sea-accidents due to an increasingly dense ship traffic in the Bosphorus and the worsening industrial and domestic pollution of the waters.

According to Öztürk & Öztürk (1996) and the Association of Turkish Maritime Pilots (see http://www.turkishpilots.org/) a total of 40000 to 48000 vessels passed the Bosphorus each year from 1996 to 2000. The total cargo transported is about 42 million tons, of which more than 16 million tons is crude oil. The number of oil tankers longer than 200m per

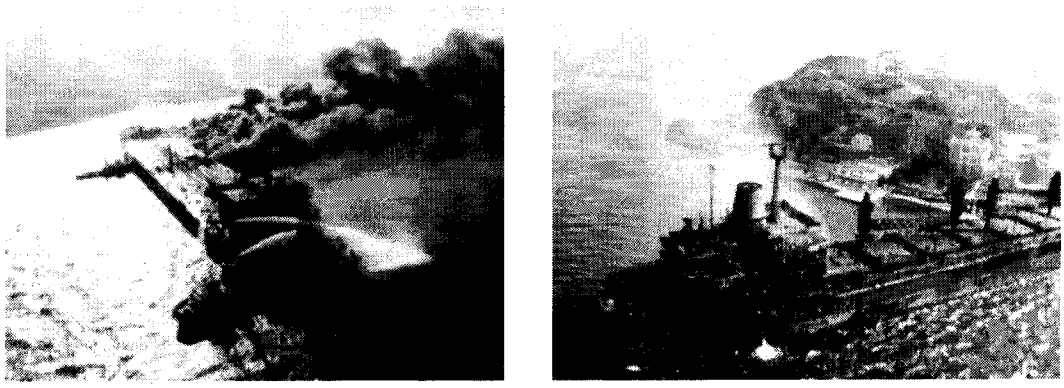

Figure 2.6.: *From 1982 to 1994 between 200 and 300 sea-accidents were registered in the Bosphorus. Most of them involved smaller to medium size vessels. One of the bigger accidents is shown in the above figures: M/T Nassia (left) collided with bulk carrier M/V Shipbroker (right) on 13 March 1994. 29 officers and crewmembers of both ships lost their lives. The fire on the tanker Nassia, fully loaded with crude oil, damaged the Strait and the environment. Approximately 20.000 tonnes of crude oil caused severe pollution, and a fire, which lasted almost 5 days. Istanbul was spared a disaster only because of a favourable wind (Öztürk & Öztürk, 1996).*

year is about 2200[3]. In the future nuclear waste might be added to the list of cargo if Russia goes ahead with its plans to import nuclear waste for disposal. In addition, 2000 trips/day across the Bosphorus are made by domestic small boats for commuting[4]. Considering the straits's complicated geometry, the strong currents with opposing surface and under currents, as well as quickly changing meteorological conditions, the probability for accidents with severe pollution and loss of human life on sea and land (the strait's shoreline is densely populated) is very high. However, under the Montreux Treaty from 1936, commercial vessels and tankers, whatever flag they carry, have freedom of passage and navigation day and night regardless of their cargo through the Turkish Straits and are under no obligation to take a pilot. Hence Turkey has very little power to reduce or even control the traffic, so that presently her only option is to reduce the likelihood of accidents by gaining a better understanding and forecasting of the complicated currents

[3]We saw tankers probably as long as 300m passing through the 650m wide Contraction. This is an impressive but also worrying sight.

[4]The reader is asked to pause for a moment to appreciate our effort in surveying the Bosphorus. The ship traffic was a major hindrance as it forced us to spend a considerable fraction of our survey time on "getting out of the way of ships" and "waiting for ships to pass".

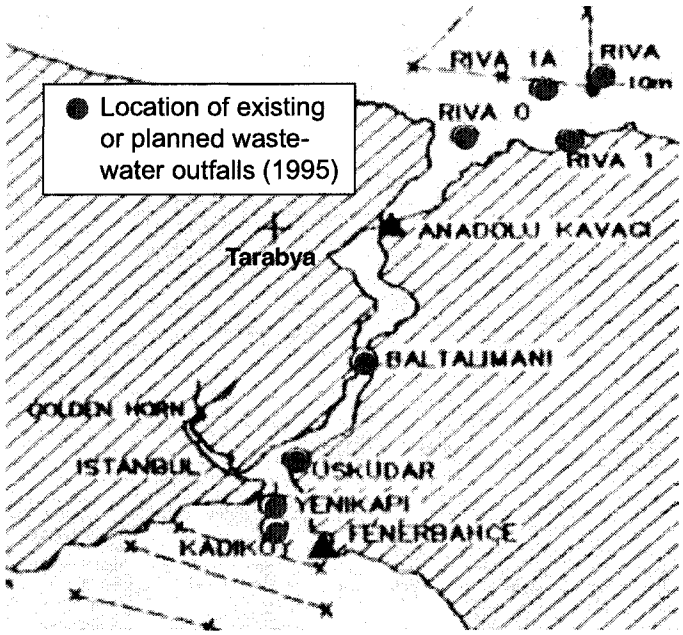

Figure 2.7.: *Location of existing or planned waste-water outfalls along the Bosphorus. Adapted from Hansen* et al. *(1995), figure 1.*

along the strait.

The second area of concern is the increasing pollution of the waters in the Sea of Marmara which has been declared a sensitive ecological area. The north-western Black Sea coastal waters are drastically polluted by large inputs of nutrients and organic matter via riverine and wastewater discharges. The polluted Black Sea surface flow, before spreading into the Sea of Marmara, is further contaminated by the waste discharged into the Bosphorus from the city of Istanbul by the numerous industries and the population of 10 million[5] (including suburbs) (e.g. Polat & Tügrul, 1996; Öztürk & Öztürk, 1996). In 1990 the wastewater flow for Istanbul was $15.5\mathrm{m}^3\,\mathrm{s}^{-1}$ (Orhon, 1995) compared to an average net transport of about $10\,000\mathrm{m}^3\,\mathrm{s}^{-1}$ through the Bosphorus. The pollution has reached levels such that many species ranging from zooplankton to dolphins that were resident in the Bosphorus in 1958 are now extinct or nearly extinct (Öztürk & Öztürk, 1996). A major effort seems to be necessary to avoid a similar situation in the Sea of Marmara. Unfortunately, reducing the levels of pollution resulting from Istanbul's wastewater is not an easy task. Problems related to a fast growing population and rapid urban development

[5]Estimates vary between 8 and 12 million.

as well as socio-economic and political issues have curtailed and restricted past investment in the sewerage system. The problem is probably best illustrated by an example: in implementation schemes defined by earlier studies, Istanbul's deep marine outfalls with no basic treatment were designed on the assumption that the major portion of the lower layer flow reaches the lower anoxic layer of the Black Sea, thus carrying all the pollutants away from the Marmara Sea and the coastal zone. This scheme is relatively inexpensive as the outfalls can be installed close to Istanbul (see figure 2.7) with mechanical or no treatment of the wastewater. However, findings of other oceanographic studies (e.g. Akyarli & Arisoy, 1995) indicate that the lower layer loses on average more than 40% of its flow to the upper layer before entering the Black Sea, the significant part of this mixing taking place in the transition zone between the Bosphorus and the Sea of Marmara (Akyarli & Arisoy, 1995). If this is indeed the case then it would be necessary to either build the outfalls at Riva at the coast of the Black Sea or to equip outfalls at Istanbul with mechanical, chemical and biological wastewater treatment facilities. Both options would be extremely expensive. The problem becomes even more convoluted if it is taken into account that much of the pollution originates in the Black Sea. Hence, it is being questioned if a reduction of pollution from within the Bosphorus area would even lead to a noticeable improvement for the Sea of Marmara (Akyarli & Arisoy, 1995; Gönenç *et al.*, 1995).

My understanding is that in 1995 the scientific database was still too sparse and controversial for a well-founded recommendation and the situation might have improved only little since then. In any event, it seems that the fate of pollutants, such as the waste-water from the city of Istanbul, is largely determined by the stability of the two-layer exchange in the Bosphorus, an understanding of which is hence highly desirable.

2.2. Flow in Straits: Theories and Approximations

In this section I will give an overview of prior studies of flow in straits. I will keep the discussion of the theory at a superficial level postponing an in-depth discussion of the physics and mathematics of hydraulics and hydraulic control until chapters 4 and 5.

The theory is perhaps best introduced by considering the along-strait momentum equation for two homogeneous layers, where the subscript $i(= 1, 2)$ indicates the (upper, lower)

layer:

$$\frac{\partial u_i}{\partial t} + u_i\frac{\partial u_i}{\partial x} + v_i\frac{\partial u_i}{\partial y} + w_i\frac{\partial u_i}{\partial z} - fv_i = -\frac{1}{\varrho_i}\frac{\partial P_i}{\partial x} + \text{friction} + \text{mixing} \tag{2.1}$$

where

$x,\ z$ = along channel and vertical coordinate,

t = time,

$u,\ v,\ w$ = along-strait, cross-strait, and vertical velocities,

f = Coriolis parameter,

ϱ = density,

P = pressure.

Typically, solutions are sought by assuming that some (or most) of the terms are negligible. As mentioned earlier the historical development of strait flow theories probably started with using friction as constraint mechanism on the flow (Defant, 1961*b*). However, that required unrealistically large friction coefficients. Later understanding supported by observations indicated a less central role for friction and the main balance was found to be between the nonlinear acceleration and the pressure gradient (Bryden & Kinder, 1991*a*).

In what follows I will depart from the historical development beginning with the inviscid theory which is the basis of most of the existing strait flow theory.

2.2.1. Inviscid Theory

The classical inviscid theory had its breakthrough when Stommel & Farmer (1953) introduced the concept of hydraulic control and applied it to the general case of calculating the flows through a constriction connecting two basins containing water of different densities. Their model assumes the flow to be steady, rotationless, and inviscid so that the nonlinear acceleration balances the pressure gradient:

$$u_i\frac{\partial u_i}{\partial x} = -\frac{1}{\varrho_i}\frac{\partial P_i}{\partial x}\,. \tag{2.2}$$

If the flow is hydrostatic then the pressure gradients can be written in terms of layer densities and layer thicknesses, and with the addition of mass continuity some manipulation

(e.g. Armi, 1986) yields ratios like:

$$F_i^2 = \frac{u_i^2}{g' h_i} , \tag{2.3}$$

called layer Froude numbers. Here, g denotes gravitational acceleration, h_i the layer thicknesses with the subscript i numbering the layers, and

$$g' = g\frac{\varrho_2 - \varrho_1}{\varrho_2}$$

is the reduced gravity. Hydraulic control occurs when the sum of the layer Froude numbers is unity:

$$G^2 = F_1^2 + F_2^2 = 1 . \tag{2.4}$$

At the control point the flow makes a transition from subcritical ($G^2 < 1$) to supercritical ($G^2 > 1$) conditions. Coupled to mass conservation statements, the control condition provides an upper limit on the magnitude of the flows. The limit is set by a balance between the available potential energy, determined by the density difference between the basins, and the kinetic energy of the flows. Another interpretation of hydraulic control involves the speed of long internal waves. At the control point where $G^2 = 1$ the speed is such that the wave cannot propagate upstream against the flow, and therefore information about the downstream conditions cannot pass the control. The Stommel & Farmer (1953) theory was extended by Assaf & Hecht (1974) who introduced the novel idea of having two controls at opposite ends of the strait instead of one.

A control typically occurs at a minimum in the cross-sectional area, which in the literature of open channel flows is often thought of as a sill (Henderson, 1966). However, a control can also occur at a minimum in channel width. A distinction has to be made between these two types because a sill primarily affects the lower layer, whereas a contraction affects both layers (Armi, 1986). Both sill and contraction control are called topographic control. Farmer & Armi (1986) introduced the concept of two topographic controls representing specific topographic features in the Strait of Gibraltar: one at the main sill (Camarinal Sill) and one at the narrowest section of the strait (Tarifa Narrows). An interesting result was the possibility of having a maximal exchange situation, which requires two controls separated by flow that is subcritical ($G^2 < 1$). The presence of

supercritical conditions on either side of a subcritical interior portion, ensures that adjustments in the level of the interface in the adjoining basins cannot propagate into the strait and thereby influence the exchange. The exchange within the strait is as large as the local geometry and the density of the exchanging water masses allow; thus the resulting exchange is maximal. If the maximal exchange requirements are not met, for example, if control occurs only on one end of the strait, the exchange can never be greater than the maximal rate and in general will be less (Armi & Farmer, 1987).

The inviscid theory considers the balance between the pressure and the non-linear term only. Clearly there are situations when the other terms are significant, too, that is when the effects of rotation, large vertical motion, unsteady forcing, friction, and mixing need to be taken into account. I will discuss these in the following section. Also, most of the hydraulic theories assume rectangular cross-sections for the straits. Applying these theories to real straits then entails the use of an equivalent rectangle whose area equals that of the actual cross-section. Assaf & Hecht (1974), Bormans & Garrett (1989*b*) and Dalziel (1992), however, have shown that more realistic cross-section shapes (triangles, trapezoids and parabolas) cause the solution for the interface to shoal and the net exchange to decrease by as much as 20%.

2.2.2. Unsteady forcing

Farmer & Armi (1986), Armi & Farmer (1987) and Bormans & Garrett (1989*b*) argued that as long as the time-varying barotropic forcing (changes in sea-level) did not violate the main assumptions required by the steady hydraulic theory, that is the existence of controls, its effects on the exchange could be investigated using the same formalism by considering a succession of steady states. This is called the quasi-steady approximation. However, Helfrich (1995) pointed out that if either the time for long internal waves to propagate through the strait is of the same order or longer than the time-scale of changes in the barotropic flow or if the temporal accelerations $\partial u/\partial t$ in (2.1) are not small compared to the nonlinear term $u\,\partial u/\partial x$, the quasi-steady approximation is suspect. He combined theoretical and laboratory models to determine the time-dependent exchange through a strait as a function of tidal forcing and of the length of the strait. He found the flow to be a function of two non-dimensional parameters: $\gamma \equiv (g'H_S)^{1/2}T/L$, which measures

the distance travelled by long internal waves in a forcing period T, relative to the strait's length L (H_S is the height of the sill), and $q_{b0} = u_{b0}/(g'H)^{1/2}$ which measures the strength of the barotropic forcing velocity u_{b0} compared to the buoyancy-driven exchange velocity $(g'H)^{1/2}$. Here, H and u_{b0} are the strait's depth and the barotropic velocity amplitude. The quasi-steady approximation assumes the first parameter to be infinite. An important conclusion was that, for the time dependent regime, complete information about the strait geometry, not just a finite number of control points, is required to determine the exchange.

Helfrich (1995) showed that the tidally forced exchange, for parameters applicable to the Strait of Gibraltar, is about 25% less than the quasi-steady exchange determined by Farmer & Armi (1986). For the Bosphorus it is not so easy to determine the value of the coefficients γ and q_{b0} because the exchange fluctuates in a much more irregular manner. I will analyse the role of unsteady forcing in the Bosphorus in section 3.2.

2.2.3. Rotation

The term $-fv_i$ in (2.1) corresponds to the alteration of momentum as fluid flows in a rotating system, i.e. the rotating earth. It is called the Coriolis force and acts at right angle to a fluid element that moves in a rotating frame. The first-order effect of rotation is the introduction of an across-strait tilt to the interface and the surface. In the northern hemisphere the Coriolis force causes the moving layers to bank up against the right of the strait when looking downstream with respect to the moving layer.

The internal radius of deformation (also called Rossby deformation radius) $R_c = (g'h_1)^{1/2}/f$ is used to classify straits into rotational and non-rotational flows (e.g. Whitehead *et al.*, 1974; Whitehead, 1998). When the strait is narrow compared to the deformation radius, then rotation can be ignored as it is in most hydraulic theory. Typical values for the Bosphorus are R_c = 15 to 30km greatly exceeding its 3km width. On the other hand, for Gibraltar the deformation radius is only slightly larger than the narrowest part of the strait and hence appears to be significant there (Bormans & Garrett, 1989*a*).

Because rotational effects are for the most part insignificant in the Bosphorus (a possible exception at the South Exit will be shown in section 3.4), I will here only mention the most relevant papers that deal with this topic: the benchmark models of steady rotating hydraulics are those of Whitehead *et al.* (1974) (zero absolute vorticity) and Gill (1977)

(non-zero but uniform potential vorticity). Reviews on these two papers and later developments are given by Borenas & Pratt (1990), Pratt & Lundberg (1991) and Whitehead (1998).

2.2.4. Vertical Motions

Hydraulic theory generally assumes a flow with negligibly small vertical velocities. Consequently, the pressure distribution can be considered hydrostatic with $\partial P/\partial z + \varrho g = 0$, and the hydraulic (or shallow water) equations can be applied to each layer as outlined above. The basic assumption is that the curvature of the streamlines is small. This is the case for flows over topography with much larger horizontal then vertical scales, that is for $\sigma \equiv (H/L)^2 \ll 1$.

Zhu & Lawrence (1998, 2000) incorporate non-hydrostatic effects as a correction into the classical hydraulic equations. While hydraulic theory gives the pressure and layer energy accurate to $O(\sigma)$, their extended theory gives pressure and layer energy accurate to $O(\sigma^2)$. They study the exchange flow through a channel with an underwater sill in a laboratory experiment, and compare predicted and measured flow rates and interface positions. They find the inclusion of non-hydrostatic effects to be necessary to accurately predict the flow rate and the interfacial position along the channel. For a relatively steep sill with a height to length ratio of $H/L_S = 0.29$ the inclusion of non-hydrostatic effects results in a 15% increase in the predicted flow rate compared to the hydrostatic prediction. The increase is caused by centrifugal forces as the flow passes over the sill effectively reducing g'.

Although $\sigma = (h_S/L_S)^2 \approx 0.08$ appears small, it is large compared to ratios found in sea straits. For example, in the Strait of Gibraltar Camarinal Sill is about 300m high and about 4km long (e.g. Farmer & Armi, 1988) giving $\sigma \approx 0.006$, and in the Bosphorus the South Sill has scales of $H_S = 40$m and $L_S = 1$km giving $\sigma \approx 0.001$, indicating that non-hydrostatic effects are negligibly small. On the other hand, they are likely to be significant in flows over sharp-crested weirs or spillways (Henderson, 1966), and possibly also in flows over relatively steep sills in fjords. The sill in Knight Inlet might be an example (e.g Farmer & Armi, 1999). They also need to be included for the study of so-called approach controlled flows, where hydraulic theory fails because of the neglect of streamline curvature (Zhu & Lawrence, 1998). Furthermore, non-hydrostatic effects need

to be taken into account if features such as internal solitary waves and wave generation by flow over topography are of interest (Helfrich, 1995).

For the purpose of the present work non-hydrostatic effects are very small so that I can safely ignore them.

2.2.5. Friction

The success of the inviscid hydraulic theory in describing the exchange in the Strait of Gibraltar indicates that there the main balance is between the pressure and non-linear terms. However, Gibraltar is a short, wide and deep strait, whereas other straits, like for instance the Bosphorus, are long, narrow and shallow. In the latter friction is more likely to be important.

As pointed out by Pratt (1986) it is difficult to treat friction in a purely deductive way in a non-linear flow. Therefore, friction is usually parameterised using a quadratic drag law and the flow is assumed to be slab-like. Then the relative importance of friction can by assessed by the dimensionless parameter $C_H L/H$, where C_H is the dimensionless drag coefficient. This parameter is the ratio between $C_H u^2/H$, which measures flow deceleration due to friction, and the non-linear term $u\,\partial u/\partial x \approx u^2/L$, which measures the acceleration of the flow. Pratt (1986) tabulates the parameter for a number of straits. Using $C_H = 10^{-3}$ he finds that the only strait listed in which friction is apparently weak is Gibraltar, with $C_H L/H = 0.1$. The other straits, including the Bosphorus, have $0.7 < C_H L/H < 2.0$. As a rule of thumb, a strait may be considered short enough to justify neglect of bottom friction, if its length is much less than a thousand times the sill depth (based on $C_H = O(10^{-3})$) (Anati *et al.*, 1977).

Friction was already used by Defant (1961*a*) to balance along-strait pressure gradients, but Assaf & Hecht (1974) were probably the first to include interfacial and sidewall/bottom friction in a hydraulic model for exchange in a strait. Their predictions for interface depths along the Strait of Gibraltar, the Bosphorus and the Bab-el-Mandab were in reasonable agreement with observations. Their model indicates correctly that the interface slopes throughout the strait. This success, in particular for the Strait of Gibraltar, is somewhat surprising considering that their friction coefficients were about 10 times larger than commonly accepted values (e.g. Bormans & Garrett, 1989*b*), and that their model

neglects width and depth variations along the strait. Subsequently, Bormans & Garrett (1989*b*) combined the Assaf & Hecht (1974) model with the Farmer & Armi (1986) model, and examined the effects of both interfacial and bottom-friction in the Strait of Gibraltar using realistic topography. They used $C_H = 3 \times 10^{-3}$ as bottom friction coefficient and $C_I \approx 10^{-4}$ as interfacial drag coefficient (in part based on direct dissipation measurements of Wesson & Gregg (1988)). They found that friction shifts the location of control sections and that it brings the maximal and submaximal solutions for the interface depth closer together than in the inviscid case. They concluded that for quantitatively accurate comparisons between theory and observations in a strait such as Gibraltar solutions for transport and interface depths require the inclusion of friction. However, friction is small enough that for a qualitative description the inviscid theory is sufficient.

On the basis of these findings and given that the Bosphorus has a much more rugged topography than Gibraltar it appears likely that friction is important in the former. This view is supported by the results of several numerical studies of the Bosphorus exchange (see Johns & Oğuz, 1990; Oğuz *et al.*, 1990; Stashchuk & Hutter, 2001).

I will estimate bottom and sidewall friction in the Bosphorus in section 3.5, and will review and discuss frictional effects in single and two-layer flows in chapter 4.

2.2.6. Mixing and Stratification

The theories reviewed so far ignore that there is always some mixing between two oppositely flowing layers in a strait. Associated with mixing is a vertical transfer of mass and momentum. In many cases, the mixing is confined to the vicinity of the interface and results in the formation of a well mixed intermediate layer whose thickness increases in the direction of its flow. An example is the thick interfacial region that develops at the eastern end of the Strait of Gibraltar; the inflowing water clearly entrains significant amounts of Mediterranean water that was otherwise heading toward the Atlantic (Farmer & Armi, 1988; Bray *et al.*, 1995). The situation in the Bosphorus is similar.

If mixing is not too strong - I will explain the meaning of this in a short while - it seems reasonable to formulate a model that incorporates mixing but retains the layer formalism. Then the effect of mixing is to entrain water from the lower into the upper and from the upper into the lower layer. This is represented by an entrainment velocity

w_e that carries fluid across the interface from one layer into the other. Second, it is assumed that entrained mass and momentum are instantly mixed across the section of the layers so that layer densities and velocities are constant over a cross-section. This concept of *entrainment mixing* at the interface with uniform conditions above and below might be as old as the Knudsen relations; at least I have not been able to track it down to a certain publication. For example, in chapter 5.3 of his monograph Officer (1976) applies this concept to determine the effect of entrainment on the various physically observable quantities (e.g. salinity) in an estuary in which water from the lower layer is entrained into the upper layer. The entrainment formulation is also used in numerical models of the dynamics of flows in estuaries and straits, see (Grubert & Abbott, 1972) and Oğuz & Sur (1989); Oğuz *et al.* (1990) for example. The latter authors add time dependence to the problem and apply their model to the exchange in the Dardanelles and the Bosphorus. However, the authors do not elaborate on the effects of entrainment on the dynamics of the flow. This will be the main purpose of the discussion in chapter 4.

If the exchange is dominated by turbulent mixing, it is possible to find a solution where velocity is limited by turbulent eddy viscosity. If it is assumed that the aspect ratio H/L is small and that the flow is weakly stratified in the vertical but still forced by a horizontal density contrast maintained at the ends of the strait, then the steady state force balance is between buoyancy and the vertical diffusive terms, and at leading order reduces to

$$\frac{1}{\varrho}\frac{\partial P}{\partial x} = A_v \frac{\partial^2 u}{\partial z^2}\,, \tag{2.5}$$

where A_v is the vertical eddy coefficient for momentum. Cormack *et al.* (1974) derived a formal asymptotic solution for this problem, and in the context of estuarine circulation it was also examined by Officer (1976). At leading order the density gradient is linear in the horizontal and the volume and mass fluxes can be given (Hogg *et al.*, 2001*a*). When non-dimensionalised by the fluxes obtained in the inviscid hydraulic limit they read

$$q_V = \frac{5(\mathrm{Gr_T}\sigma)^{1/2}}{96}\,, \tag{2.6}$$

$$q_M = \frac{4\,\sigma}{(\mathrm{Gr_T}\,\sigma)^{1/2}\,\mathrm{Pr_T}} + \frac{31\,(\mathrm{Gr_T}\sigma)^{3/2}\,\mathrm{Pr_T}}{90720}\,. \tag{2.7}$$

Here $\sigma = H^2/L^2$, the turbulent Grashof number is $\mathrm{Gr_T} = g'H^3/A_v^2$ with g' based on the density difference between the two reservoirs connected by the strait, and the turbulent

Prandtl number is $\mathrm{Pr_T} = A_v/K_v$, where K_v is the vertical eddy coefficient for mass. The fluxes due to advection are a function of the non-dimensional parameter $\mathrm{Gr_T}\sigma$, however the mass flux is also modulated by the effect of horizontal diffusion when $\mathrm{Gr_T}\sigma$ becomes small. The hydraulic limit occurs for large values of this parameter. Note that, taking $(g'H)^{1/2}$ as velocity scale, $(\mathrm{Gr_T}\sigma)^{-1/2}$ may be written as the ratio of viscous forces of order $K_v u/H^2$ to an inertial term of order u^2/L, in much the same way that this comparison is represented by $C_H L/H$ for a frictional flow.

Between the inviscid hydraulic and the viscous limit, the dynamics should be controlled by a three-way balance between inertia, buoyancy and viscous/diffusive effects. This regime was explored by Hogg *et al.* (2001*a*) in a numerical simulation. Assuming $\mathrm{Pr_T} = 1$ the non-dimensional mass flux was predicted over a range of $\mathrm{Gr_T}\sigma$ encompassing the viscous and hydraulic limits:

$$q_M = 0.052\,(\mathrm{Gr_T}\sigma)^{1/2} \qquad \text{for} \quad \mathrm{Gr_T}\sigma < 40 \quad \text{(viscous limit)}, \tag{2.8}$$

$$q_M = 1 - 1.7\,(\mathrm{Gr_T}\sigma)^{-1/4} \qquad \text{for} \quad 40 < \mathrm{Gr_T}\sigma < 10^6 \quad \text{(intermediate range)}, \tag{2.9}$$

$$q_M = 1 \qquad \text{for} \quad \mathrm{Gr_T}\sigma > 10^6 \quad \text{(hydraulic limit)}. \tag{2.10}$$

Hogg *et al.* (2001*a*) then determined in which of the three ranges typical field cases lie. They calculate $\mathrm{Gr_T}\sigma$ by two methods. The first uses field estimates of parameters to calculate it directly, and the second uses an estimate of the average interface thickness, and direct comparison with the numerical simulation. The latter is based on the relation

$$\frac{\delta}{H} = 3.4\ (\mathrm{Gr_T}\sigma)^{-1/4} \tag{2.11}$$

where δ is the thickness of the density interface. This is derived from a scaling argument which assumes that the value of the diffusivity determines the thickness of the density interface.

For Gibraltar the first method gives $\mathrm{Gr_T}\sigma \approx 10^6$, which is in the hydraulic limit, whereas the second gives $\mathrm{Gr_T}\sigma \approx 10^5$, which is somewhat into the intermediate range. For the Bosphorus A_v is not available. Using $\delta/H = 0.35$, the second method gives $\mathrm{Gr_T}\sigma = 9\times10^3$. Obviously the value could also be an order of magnitude higher. This puts the Bosphorus somewhere in or just above the middle of the intermediate range. For this range of $\mathrm{Gr_T}\sigma$ Hogg et.al.'s simulation of the exchange flow in a contraction does show an interface of finite thickness, however, the general layer structure of the velocity field remains intact.

I believe that the results by Hogg *et al.* (2001*a*) provide justification for analysing the effects of mixing in the Bosphorus in a framework that retains the layer formalism. Observations described in chapter 3 and the theoretical analysis in chapter 4 will support this view.

2.3. The Question of Submaximal or Maximal Exchange

Until about 1999 it was accepted knowledge in the literature that the Bosphorus represents a case of a "maximal exchange" strait (e.g. Yüce, 1996; Özsoy *et al.*, 1998). The presence of internal hydraulic controls was deduced from rapid changes in the depth of isohalines which coincided with the location of horizontal and vertical constrictions and abrupt expansions (section 2.1.4). This agreed with results from a two-layer numerical model (Oğuz *et al.*, 1990) which showed hydraulic controls at the North Sill, at the exit toward the Sea of Marmara and in the Contraction (figure 2.8). In the simulation the first two controls were found to be always present whereas the third depended on the magnitude of the net barotropic flow and was lost for sufficiently weak upper layer flow. However, until recently no velocity measurements existed to directly verify these conclusions. Whereas the first detailed current measurements from 1994 (Gregg *et al.*, 1999; Gregg & Özsoy, 2002) confirmed a control at the North Sill, the currents in the contraction were much too small for a hydraulic control in the two-layer sense. Detailed measurements from the South Exit have not yet been reported so that it is not yet clear whether a second control exists, i.e. whether the exchange in the Bosphorus is maximal.

In order to realise the relevance of this point, it is necessary to understand the implications of submaximal or maximal exchange flows for the Bosphorus. For the Strait of Gibraltar this question has been analysed in detail in a number of studies (e.g. Bryden & Stommel, 1984; Armi & Farmer, 1985, 1987; Farmer & Armi, 1988; Bormans & Garrett, 1989*b*; Garrett *et al.*, 1990; Bryden & Kinder, 1991*b*), whereas for the Bosphorus it appears to have received less attention.

Provided the exchange is maximal, it will have two controls at which, in the framework of classical inviscid two layer hydraulic theory, the conditions

$$G_S^2 \equiv \frac{u_{1S}^2}{g'h_{1S}} + \frac{u_{2S}^2}{g'h_{2S}} = 1 \qquad \text{and} \qquad G_C^2 \equiv \frac{u_{1C}^2}{g'h_{1C}} + \frac{u_{2C}^2}{g'h_{2C}} = 1 \tag{2.12}$$

are fulfilled. For the Bosphorus the subscripts S and C could indicate controls at the North Sill and the Contraction, respectively (see figure 2.3 or figure 2.8). With the conditions that the mass transport in each layer must be the same at the two controls and that the Bernoulli difference $u_1^2 - u_2^2 + 2g'h_1$ is constant between the controls, and with a prescribed net flow $Q = Q_1 + Q_2$ (where $Q_i = u_i h_i$, $i = 1, 2$), one obtains six equations which can be solved by numerical methods for the six unknowns u_{1S}, u_{2S}, h_{1S}, h_{1C}, u_{1C}, and u_{2C} (Bryden & Kinder, 1991*b*). The solution is unique and it is in this sense that the exchange is fully determined by the strait.

This maximal exchange solution is obtained for a given salinity difference between the basins, that is for given g' (assuming that the effect of temperature on density is negligibly small compared to the effect of salinity - as it is generally the case in sea straits). However, it can be combined with the overall mass and salt conservation statements for the Black Sea, as first attempted by Bryden & Stommel (1984) for the Mediterranean. This introduces a new equation and the salinity difference becomes one of the variables determined in the maximal exchange solution. Because density, and hence g', is primarily determined by salinity, the total maximal exchange solution for the flow through the strait can be shown to depend only on a single external parameter $P - E$ which is precipitation (and river discharge) minus evaporation. This is a powerful statement which implies that a well defined connection between the exchange in the strait and the basin exists.

To illustrate the relevance of maximal exchange for the Bosphorus consider two possible applications: If the exchange is maximal, that is bounded by two topographic controls, then changes of the strait's topography at these controls might significantly affect the salinity difference as well as the layer transports and hence the water renewal rates of the basins. This could be interesting for studies of the paleoceanography of the Black Sea and eastern Mediterranean as the strait's topography might have changed over time due to tectonic activity (Aksu *et al.*, 2002). A present-day application would be the assessment of the effects of a railway tube tunnel in the Bosphorus. Such a project has been under investigation for some time. The impact of a tube tunnel rising 10m above the sea-floor on the exchange could be significant if it was built at the location of an existing topographic control, thereby significantly changing the maximal exchange solution. On the other hand, it might have little effect if built elsewhere.

Note that the two controls of a maximal exchange flow isolate the strait from changes in, for instance, the interface depth in the basins. (In the Black Sea these could result from climate changes (Özsoy, 1999) or anthropogenic influences on river discharge (Tolmazin, 1984).) This means the strait would not be a good monitoring point to detect such changes. For the Strait of Gibraltar Garrett *et al.* (1990) have argued that a sub-maximal exchange, with only one topographic control, would allow a more rapid response of the strait to changing conditions in the Mediterranean (the flow was assumed to be sub-critical at the eastern exit), that is the strait would be a more suitable monitoring point. In the Bosphorus the exchange would be submaximal if, for instance, the control toward the Sea of Marmara did not exist. Then changes in interface depth in the Sea of Marmara could propagate upstream through the strait, that is they could be monitored in the Bosphorus. It is, however, beyond the scope of this thesis to analyse whether this is of any practical use as this would require a complete study of the circulation in the Sea of Marmara and an understanding of the exchange in the Dardanelles which might be regulated by its own hydraulic controls (Ünlüata *et al.*, 1990). Alternatively, the exchange would also be sub-maximal if the control at the North Sill was lost. This thesis will, however, indicate that this is less likely to occur.

Finally, it is worth pointing out that the maximal exchange concept also applies to flows subject to friction or mixing. These effects reduce the maximal exchange rate, but provided the fundamental requirement is met, the exchange is as great as it can be for the given density difference, friction, and mixing (Armi & Farmer, 1987). However, friction and mixing will make the exchange indeterminable, unless one knows how these effects change the control conditions as well as the frictional and entrainment rules to apply between the controls, i.e. along the subcritical section of the strait.

2.4. Summary

The flow through the Bosphorus is subject to a great degree of variability, depending on meteorological factors and the water budget of the Black Sea. Nevertheless a well defined two-layer structure prevails for most of the time. Upper or lower layer blockage are believed to be short-lived phenomena (Ünlüata *et al.*, 1990). However, the relation

between sea-level and layer transports is largely unknown.

The salinity sections indicate vertical mixing between the layers which appears to be particularly strong in the southern part of the strait. Ünlüata *et al.* (1990) estimate the total vertical mixing along the Bosphorus from long-term averaged layer fluxes using the steady state salt and mass conservation equations. They find downward and upward fluxes of $1200\text{m}^3\,\text{s}^{-1}$ and $2000\text{m}^3\,\text{s}^{-1}$, respectively, compared to upper and lower layer transports of $20\,000\text{m}^3\,\text{s}^{-1}$ and $10\,000\text{m}^3\,\text{s}^{-1}$, respectively (figure 2.8). Qualitatively it is clear that the vertical fluxes are larger in the southern part of the strait, but quantitative estimates are not known.

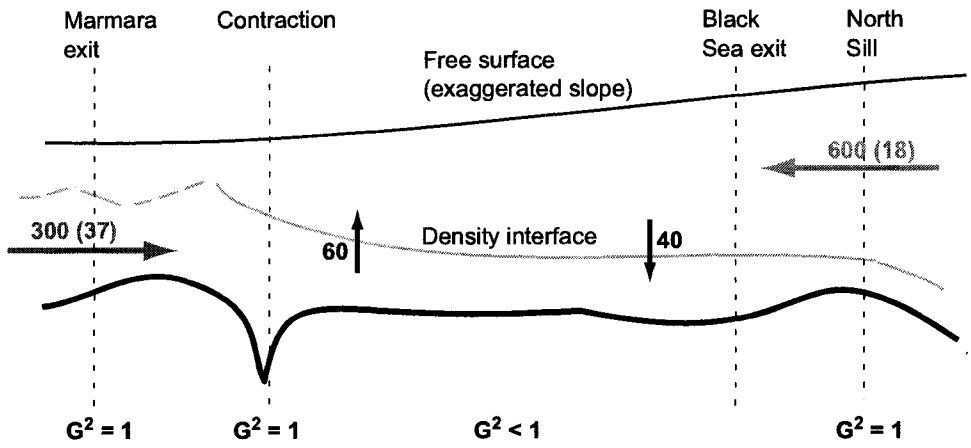

Figure 2.8.: *Summary sketch of the two-layer flow in the Bosphorus according to Özsoy* et al. *(1998). The layer transports are given in* km^3/yr. *The numbers in parentheses indicate layer salinities in psu.*

Whereas rotational and non-hydrostatic effects are likely to be negligible in the Bosphorus, time-dependence, friction and mixing appear to be important. The latter three have been included in numerical models of the Bosphorus flow but only time-dependence and friction have been studied in detail. Mixing and entrainment and as well as shear and stratification have been considered only very recently and it has yet to be explored how they affect the dynamics of exchange flows, including the issue of whether the exchange is submaximal or maximal.

I will address the above issues in the following chapters.

3. Observations

3.1. Field Experiments

The data used in this thesis were collected during four experiments in the Bosphorus. The two main data sets were obtained in August 1998 and March/April 2000. Two smaller data sets are from October 1997 and June 2000.

All experiments were a collaborative effort of the Institute of Ocean Sciences (IOS), British Columbia, Canada and the Department of Navigation, Hydrography and Oceanography (DNHO) of the Turkish Navy in Cubuklu, Istanbul.

In the following data description I will use a coordinate system that follows the thalweg, or deepest path, along the strait. Distances are positive northward from an origin close to Istanbul (figure 2.4). In along-strait (cross-strait) direction northward (eastward) and southward (westward) flow are positive and negative, respectively. Time is given as 'Coordinated Universal Time' (UTC) which was 3 hours behind local Istanbul daylight saving time during all our experiments[1].

3.1.1. October 1997

As part of the work on the installation of the Acoustic Scintillation Instrument SIREN in October 1997 (Di Iorio *et al.*, 1999) a one-day survey was carried out on October 9 which consisted of a run from the northern end to the southern end of the strait and two runs across the strait between Rumelihisari and Anadoluhisari. Nine casts with a Seabird 19 profiler were carried out and currents were measured with a 300kHz broadband ADCP (Acoustic Doppler Current Profiler) from R.D. Instruments (Model: Workhorse). The

[1]For the North American reader: Europe including Turkey changes to daylight saving time one week earlier than North America, for instance, on March 26, 2000 instead of April 2, 2000.

ADCP data suffered from problems with the heading data. Sounder images are available as print-outs from the vessel's onboard sonar.

3.1.2. August 1998

Observations took place on August 18, 19, 20, 21 and 24. They included an integrated survey of CTD (Conductivity, Temperature, Depth) profiles, ADCP measurements, and echo-sounder imaging together with GPS positioning. Shipboard measurements were carried out between 0900 and 1700 (local time) (0600 to 1400 UTC) from the Turkish Navy vessel TCG Mesaha II.

The Mesaha II carried an internally recording Seabird 19 profiling CTD for obtaining temperature and salinity versus depth profiles. Because of the strong currents it was necessary to attach a heavy weight to the bottom of the instrument as shown in figure 3.1.

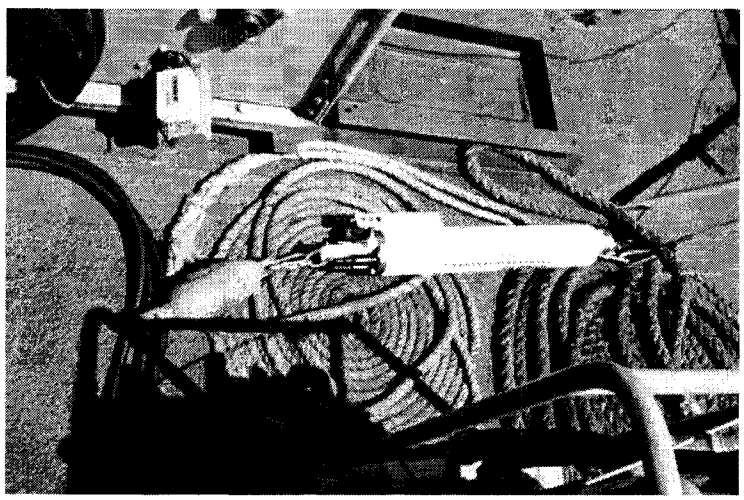

Figure 3.1.: *Seabird 19 Conductivity, Temperature, Depth profiler with weight attached to the bottom.*

For positioning a standard GPS system was used because differential GPS corrections were not available at the Bosphorus. We therefore recorded raw satellite range data and post-processed them following Héroux & Kouba (1995). This increased the horizontal position accuracy from ±40m to about ±2m. Details are given in appendix A.

For flow and transport measurements we again used a 300kHz broad-band ADCP. The unit kept excellent bottom tracking, which was checked against the post-processed GPS

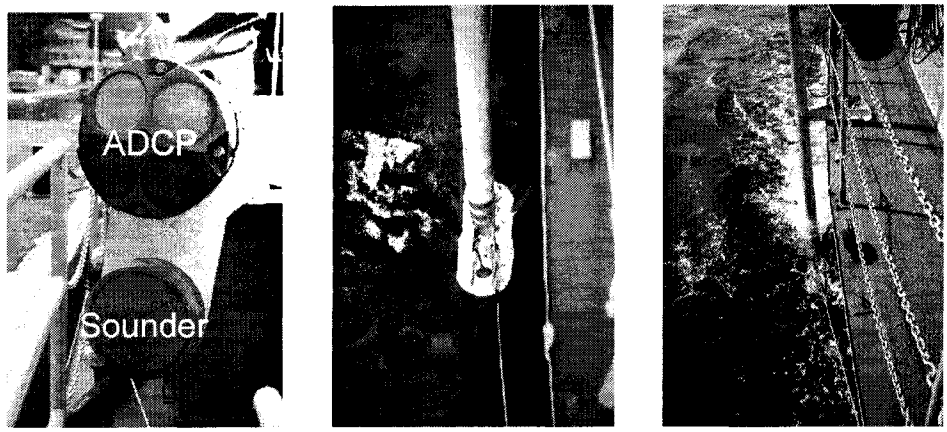

Figure 3.2.: *Left: ADCP unit and echo-sounder transducer. Middle: head of ADCP/echo-sounder mast in water. Right: same when moving. The figures are from March/April 2000 when the mast was mounted on the starboard side of the Mesaha I.*

data. The instrument, together with an echo-sounder transducer, was mounted at a depth of 0.5m on a mast deployed over the port side of the vessel (figure 3.2). The centre of the shallowest bin was at 3m. Velocity was usually recorded in 2m vertical bins (4m triangle filter) at 2s intervals.

A 120kHz BioSonics echo-sounder was used for two-dimensional flow imaging. The images were acquired with 45cm vertical resolution at uniform time intervals of 0.5s. In figures the data are horizontally stretched or compressed so as to compensate for changing ship speed consistent with the horizontally uniform GPS referenced distance scale. Note that features with horizontal scale L' in the images have a true length of $L = L'(1 - \frac{u_{water}}{u_{ship}})$ which means that upper and lower layer features scale differently. The scatter is due to both biota, which tends to concentrate at density interfaces, and also to sound speed gradients. The highly resolved images allow interpretation of distinctive signatures associated with distortion of the density field by the flow, such as turbulence (Farmer & Armi, 1999; Seim, 1999).

The survey data were supplemented by hourly averaged meteorological data (wind-speed, wind-direction, air temperature, and barometric pressure) from Sariyer (figure 2.4) and by daily averaged meteorological data from Tekirdag located on the northern coast of the Sea of Marmara (figure 2.1).

An ADCP/echo-sounder system which was deployed on the sea-floor in the middle of

the strait between Rumelihisari and Anadoluhisari failed shortly after deployment so that we did not obtain continuous current measurements in August 1998.

3.1.3. March/April 2000

Observations from the survey vessel TCG Mesaha I took place on March 31, from April 4 to 8 and on April 10. The philosophy of our experimental approach was, as in August 1998, to acquire an overview of the flow in the strait by surveying along the entire strait from the Black Sea to the Sea of Marmara and conducting detailed observations in the contraction and southern part of the strait in order to study mixing processes. However, based on our results from the previous experiment, we concentrated much of our effort on the contraction and southern part of the strait.

The ship-based instrumentation was essentially identical with the one described before except that the vertical resolution of the echo-sounder was increased to 0.15m. We also installed a weather station (from DAVIS instruments) on the vessel which recorded wind-speed, wind-direction, air temperature, barometric pressure, and humidity. The sensors were at a height of about 7.5m above water. Meaningful wind-speed and wind-direction data were obtained only during CTD stations when the vessel was stationary. These data supplemented the hourly meteorological data from Sariyer and Goztepe.

As improvement over the previous experiment, we were able to obtain continuous observations of sea-level and current in the strait. Float-type recorders operated by DNHO at Anadolikavagi and in the Golden Horn (Istanbul) (figure 2.4) provided hourly averaged sea-level data from both ends of the strait. The Golden Horn station was at a distance of about 3.9km to the centre line of the Bosphorus. The vertical datum planes were arbitrary at both recording sites.

Between March 31 and April 10, 2000 an upward looking 300kHz broad-band ADCP was deployed in the middle of the strait between Rumelihisari and Anadoluhisari at a depth of 60m (figure 3.3). It operated at a transmission rate of 2 pings per second, and used a vertical bin size of 1.2m. 24 pings were averaged into 12s ensembles, and stored internally.

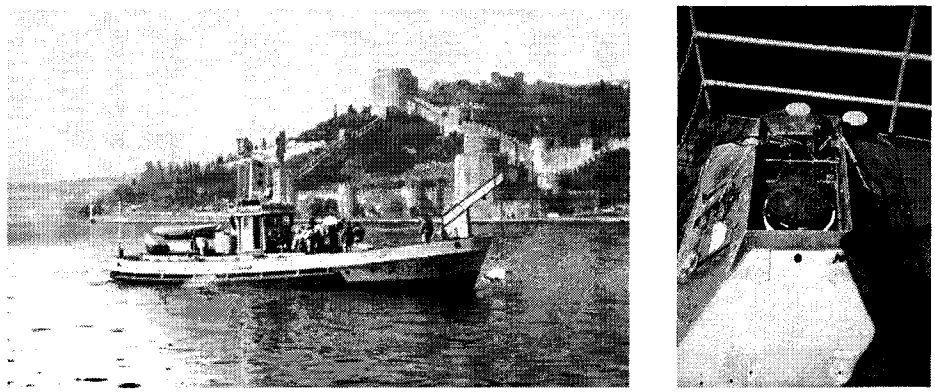

Figure 3.3.: *Left: Deployment of the ADCP with the Rumeli Hisari castle in the background. Right: The upward looking ADCP mounted in a gimbled bottom bracket. The second slot holds a battery pack.*

3.1.4. June 2000

Between June 19 and 23 Lt.JG Ahmet N. Unlu from DNHO carried out a survey from the TCG Mesaha II using our 300kHz ADCP and a Seabird 19 profiler. The main purpose was to familiarise the DNHO personnel with the operation of the ADCP. Because of various problems with the instrumentation and also because of some unexpected closures of the Bosphorus for all ship-traffic the survey time was much reduced so that useful data could only be obtained on June 22 and 23. Sea-level and meteorological data were not available.

3.2. Forcing and Flow

3.2.1. Baroclinic Forcing

I have already mentioned that the baroclinic part of the exchange, which is driven by the large density contrast between the basins, is believed to vary only on seasonal scales. Figure 3.4 shows that it was indeed quite steady for the duration of our experiments in August 1998 and March/April 2002. For the following recall that in the Bosphorus density is mainly determined by salinity with temperature playing only a secondary role.

The salinities of the upper layer entering the strait from the Black Sea and of the lower layer entering from the Sea of Marmara were a nearly constant 18 psu and 38 psu, respectively. Variations of temperature in the upper layer Black Sea water occurred in

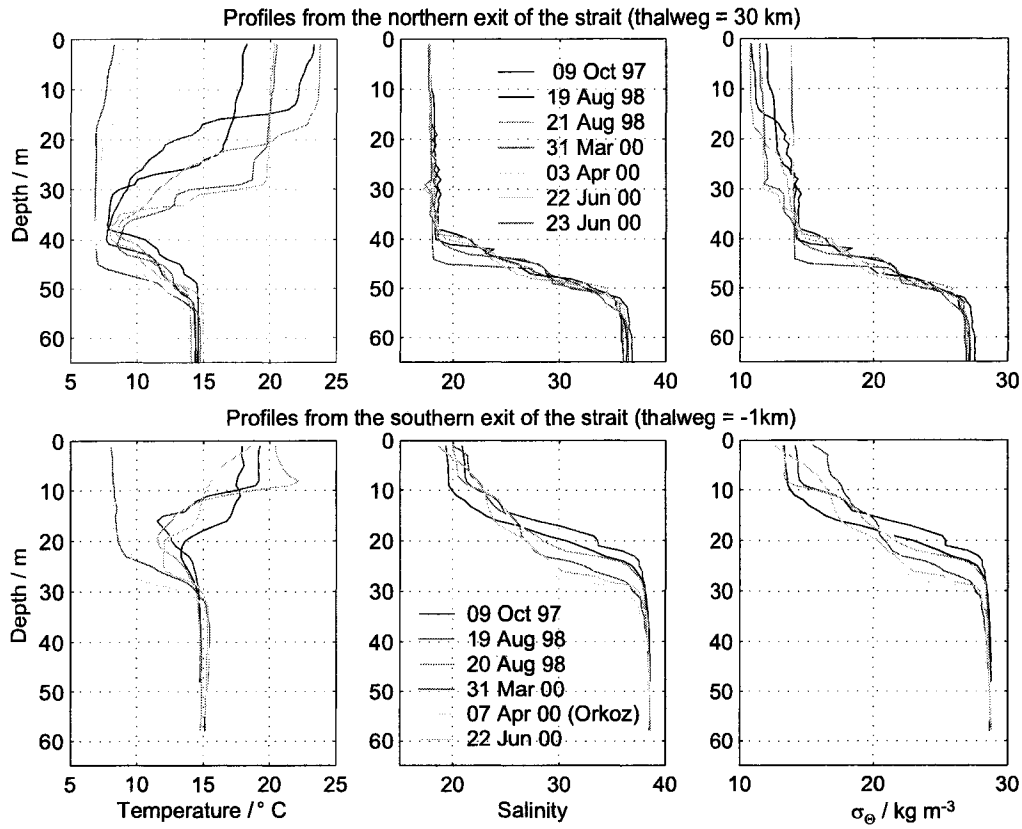

Figure 3.4.: *Vertical profiles of temperature (left), salinity (middle), and density (right) obtained during our 4 experiments which roughly correspond to three different seasons from spring to autumn. The upper row shows profiles from the northern Bosphorus (thalweg position = 30km, see figure 2.4) and the lower row shows profiles from the southern exit region (thalweg position = −1km).*

August 1998 and were due to variations in surface heating and cooling. In March/April and June 2000 upper layer temperature was practically constant.

The lower layer water entering from the Sea of Marmara is basically constant in salinity and exhibits only a small fluctuation in temperature of about 1°C.

3.2.2. Barotropic Forcing

In what follows I will concentrate on our observations from March/April 2000 as only during that experiment did we obtain a complete set of meteorological, sea-level and continuous current data.

Meteorological Conditions

Figure 3.5 shows meteorological data from two permanent stations for the period from March 27 to April 16, 2000. The northern station (Sariyer) is on the western side of the Bosphorus and the southern station (Goztepe) is on the Anatolian side, south of Kadidoy (see figure 2.4). The station air pressure was converted to sea-level pressure using the equation $p_{\text{sea-level}} = p_{\text{station}} \exp(z_{\text{station}}/H_s)$ with a scale height of $H_s = 8.4\text{km}$ (Gill, 1982).

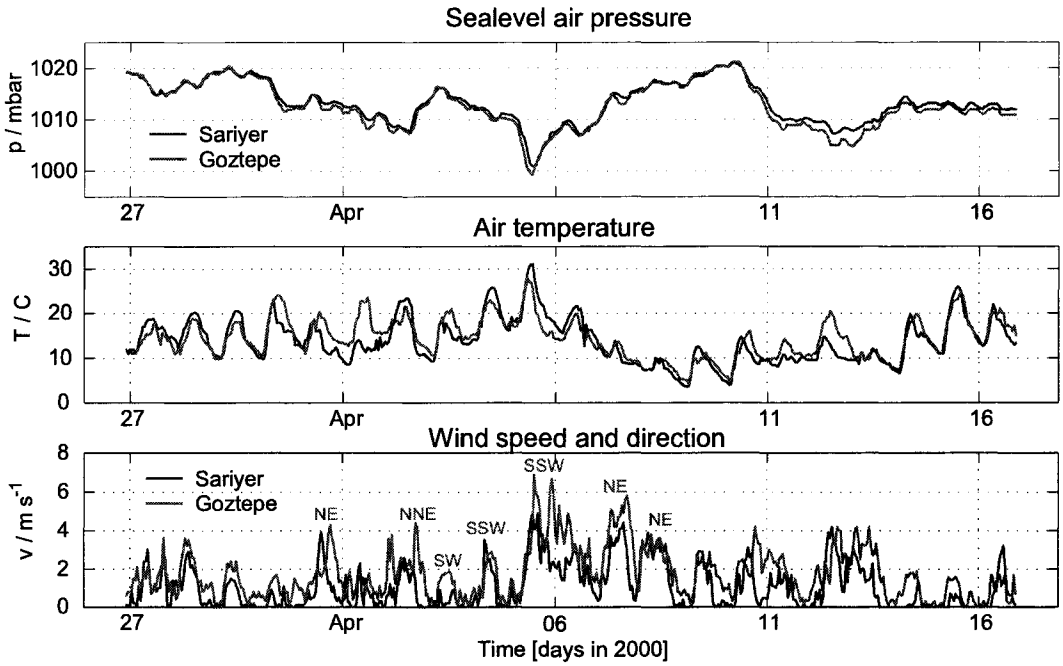

Figure 3.5.: *Local meteorological data from the March/April 2000 experiment. Data were obtained at* 1h *intervals (without averaging) at permanent meteorological stations at Goztepe (*$40^\circ 58'N$, $29^\circ 05'E$, *elevation* 33m*) and Sariyer (*$41^\circ 08'N$, $29^\circ 04'E$, *elevation* 58m*).*

The meteorological conditions at Goztepe and Sariyer were very similar. On average the magnitude of the barometric pressure difference was only $0.7 \pm 1\text{mbar}$. This is too small to significantly affect the sea-level difference which varies between 20 and 40cm. Furthermore, figure 3.6 shows that even between the Sea of Marmara and the Black Sea the sea-level difference was small so that we can rule out the possibility that larger scale air-pressure patterns affected the sea-level difference.

Wind speeds varied between 0 and $6\text{m}\,\text{s}^{-1}$ and shifted frequently between northerly and

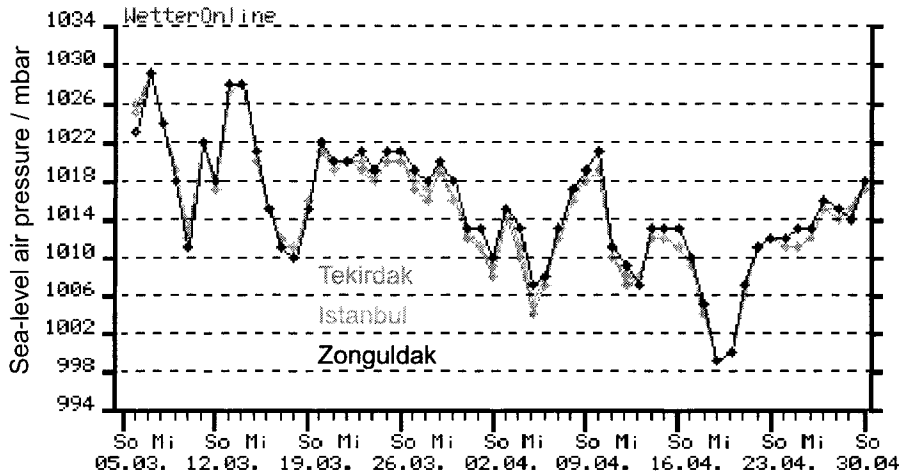

Figure 3.6.: *Sea-level air-pressure in March and April 2000 at Tekirdak (Sea of Marmara), Istanbul, and Zonguldak (Black Sea). The data were obtained from and are used with permission of Wetteronline Meteorologische Dienstleistungen GmbH, Bonn (www.wetteronline.de).*

southerly directions. For northerly winds Di Iorio & Yüce (1999) observed larger wind-speeds at the Black Sea exit region than at the sheltered Sariyer station. Our wind-speed data obtained on the vessel during 3 CTD casts in the Black Sea exit region indicate that this is also the case for southerly winds. The wind-speeds averaged over 5 to 10 minutes were between $2\,\mathrm{m\,s^{-1}}$ and $3.5\,\mathrm{m\,s^{-1}}$ larger than those measured at Sariyer.

Sea-level and Current

Figure 3.7 compares wind, sea-level and current data for the duration of the deployment of the bottom-mounted ADCP.

Let us first consider the periods from 30 March to 05 April and from 07 to 10 April. The upper layer moved southward from the Black Sea toward the Sea of Marmara with a speed varying between -0.75 and $-1\,\mathrm{m\,s^{-1}}$. The lower layer flowed northward with a somewhat smaller speed between 0.5 and $0.8\,\mathrm{m\,s^{-1}}$. Fluctuations occurred in response to sea-level changes: a sea-level increase at Anadolukavagi or a sea-level decrease at Istanbul, correlated with an increasing upper layer current and a decreasing lower layer current, as well with a thickening of the upper layer and thinning of the lower layer. On the other hand, we see little correlation between wind speed/direction (measured locally at the Bosphorus) and sea-level. This suggests that sea-level changes were caused by larger

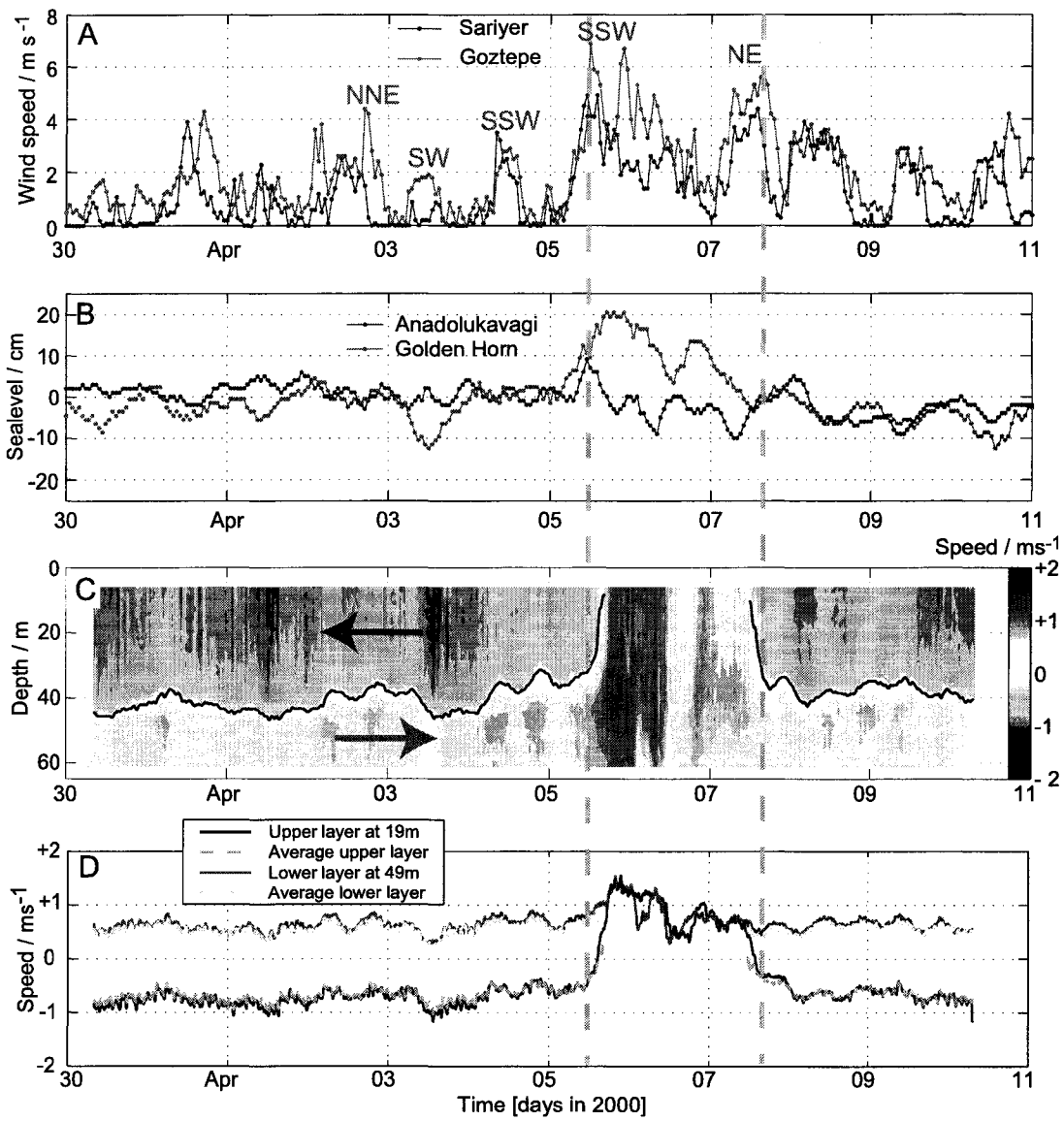

Figure 3.7.: *A: Wind speed at Sariyer and Goztepe meteorological stations. B: Sea-level variations at Anadolukavagi (north) and the Golden Horn (south). C: Horizontal along-channel component of the ADCP velocity vector. Blue indicates southward and red northward flow. C: Layer averaged currents, and currents obtained at depths of* 19m *and* 40m.

scale wind patterns over the Sea of Marmara and Black Sea rather than by wind-forcing along the strait.

The data from April 5, 3pm to April 7, 2pm show a reversal of the upper layer flow, locally called *Orkoz*. It was caused by a storm with strong southwesterly winds over the Aegean Sea and the Sea of Marmara. This raised the sea-level at the southern side above the level in the north, and subsequently reversed the upper layer flow.

The relation between the sea-level difference and upper and lower layer current is illustrated in figure 3.8. Note that the sea-level difference is not precisely known because the sea-level recorders were not geodetically levelled. After some investigations (see appendix C) I subtracted 28cm from the southern record. The Orkoz data are represented by the part of the curve with upper layer velocities above $-0.5\mathrm{m\,s^{-1}}$.

I have fitted regression lines through all data points (the line labelled *All data*) and through only those representing the exchange flow (the line labelled *Exchange only*). The first observation is that the relation between sea-level difference and upper layer current is indeed approximately linear. This is less so for the lower layer current. The second observation is that for the relation between upper layer current and sea-level difference the two regression lines have different slopes of about $-3\mathrm{s}^{-1}$ and $-8\mathrm{s}^{-1}$. This means that during the exchange flow situation a given sea-level change has a smaller effect on the upper layer current than during the Orkoz. Physically this means that the hydraulic head, which drives the upper layer, is balanced differently during the Orkoz than during the exchange: during the exchange the upper layer experiences both friction along side-walls and also along the interface whereas during the Orkoz only sidewall friction is important because interfacial shear should be minimal. For the lower layer current, which is driven by the density gradient between the basins, the slopes of both regression lines are about $2\mathrm{s}^{-1}$ with the slope of the *Exchange only* line being slightly smaller. We may use the same explanation as above. This explanation is also consistent with the fact that the presence or lack of interfacial friction has a large effect on the upper layer current but only a small effect on the lower layer current: the upper layer is only slightly influenced by sidewall friction making interfacial friction an important factor.

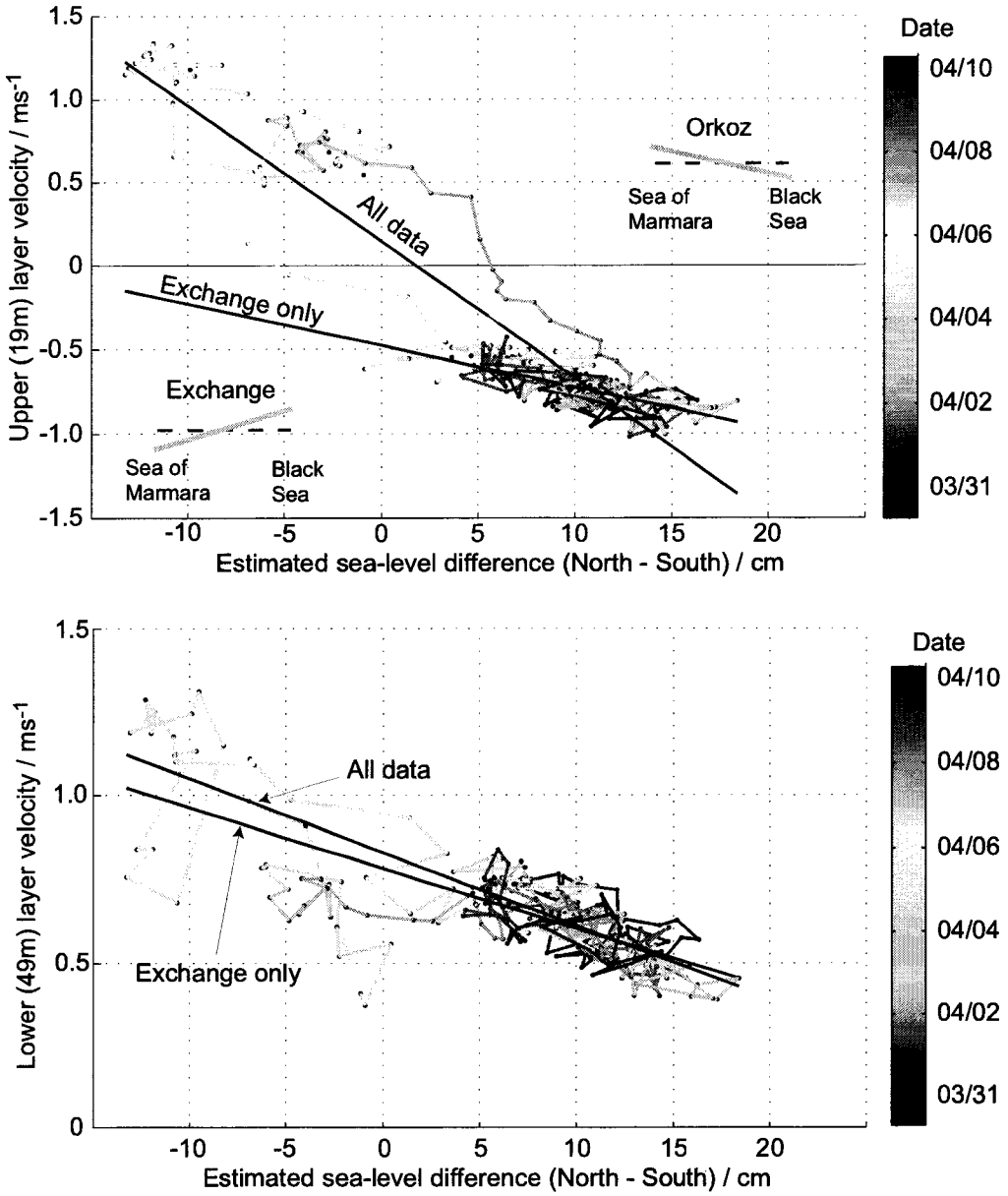

Figure 3.8.: *Upper and lower layer currents versus estimated sea-level difference. The tidal component was removed from sea-level and current (tidal amplitudes were about* 2.5cm *and* $0.1\,\mathrm{m\,s^{-1}}$*, respectively). The current data were* 1h *low-pass filtered and then re-sampled onto the hourly measured sea-level data. The original southern (Golden Horn) sea-level data were reduced by* 28cm*. The regression lines fit either all data points or only those obtained during exchange flow conditions (which excludes the Orkoz). Time is coded in colour.*

Layer Transports

It is well known (e.g. Özsoy *et al.*, 1998) and also clear from our observations that instantaneous fluxes can differ greatly from the long term mass balance estimates of Ünlüata *et al.* (1990) and Özsoy *et al.* (1998) (see section 2.1.3). This is illustrated by figure 3.9 which shows the transports in the upper and lower layer and the net transport during the duration of the deployment of the ADCP. The transports were derived by means of a regression analysis between the continuous current data from the ADCP and direct transport estimates from cross-channel transects. Details on the calculation are given in appendix D.2.2. Layer transports could not be determined during the Orkoz because the position of the interface was poorly defined.

Excluding the Orkoz, the average lower layer transport was $3800\text{m}^3\,\text{s}^{-1}$ with a standard deviation of $1300\text{m}^3\,\text{s}^{-1}$, and the average upper layer transport was $-16\,700\text{m}^3\,\text{s}^{-1}$ with a standard deviation of $3800\text{m}^3\,\text{s}^{-1}$. The net transport was $-12\,900\text{m}^3\,\text{s}^{-1}$ with a standard deviation of $5100\text{m}^3\,\text{s}^{-1}$. During the Orkoz the measured maximum net transport into the Black Sea was $26\,300\text{m}^3\,\text{s}^{-1}$. Note that the fluctuations of the layer transports (in percent of their mean value) are between 1.6 and 2 times larger than the fluctuations of the average layer velocities because the interface depth or, equivalently, the layer areas fluctuate as well.

The average upper layer transport is close to the long term average of $-600\text{km}^3\ \text{yr}^{-1}$ ($\approx -19\,000\text{m}^3\,\text{s}^{-1}$) given by Ünlüata *et al.* (1990) and Özsoy *et al.* (1998). On the other hand, the lower layer transport is significantly smaller than their estimate of $+300\text{km}^3\ \text{yr}^{-1}$. Interestingly, the same was noticed by Özsoy *et al.* (1998) and Cetin (1999) but the authors attribute the discrepancy to the poor quality of their transport estimates. A possible resolution of this discrepancy might be that the lower layer transport is larger in the second half of the year when the sea-level in the Black Sea is lower. This hypothesis is supported by our transport estimates of $+8500\text{m}^3\,\text{s}^{-1}$ from October 1997 (two transects at Rumelihisari), $7500\text{m}^3\,\text{s}^{-1}$ from August 1998 (20 transects along the strait), and an average value of $10\,700\text{m}^3\,\text{s}^{-1}$ reported by Gregg & Özsoy (2002) for September 1994.

It is clear that a long term record of the layer transports which captures seasonal fluctuations is very desirable. The results that I have presented here suggest that a

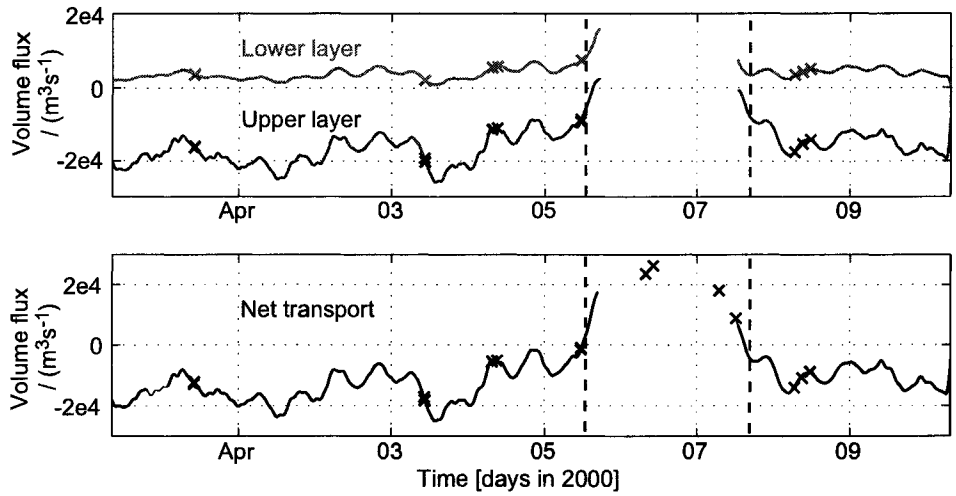

Figure 3.9.: *Upper and lower layer transports as well as net transport in the Bosphorus derived from direct transport estimates (indicated by 'X') and continuous current measurement with the bottom-mounted ADCP. The data outside the section enclosed by the dashed lines were used for the calculation of average transports given in the main text.*

relatively easy way for obtaining such a record is to use current measurements from a bottom mounted ADCP and calibrate those with precise layer transport measurements from a number of cross-channel transects. Note that our experiment produced transport estimates with a much better accuracy and resolution in time than previously reported. Even better results could have been obtained if additional and more precise cross-channel transects had been acquired.

Quasi-steady or not?

It is an interesting and for modelling purposes important question whether the exchange in the Bosphorus can be considered quasi-steady.

To answer this question, at least for our experiment, I will make use of Helfrich's (1995) analysis which I introduced in section 2.2.2. To this end we need to know both the strength and the time scales of the time-dependent barotropic forcing. A tidal and spectral analysis of the exchange **excluding the Orkoz** (appendix B) shows that between 25 and 50% of the fluctuations of southern and northern sea-level and of upper and lower layer currents were due to diurnal and semi-diurnal tidal forcing. The major part of the remaining variance was due to meteorological forcing with time-scales longer than tidal. This agrees

with findings by Alpar & Yüce (1998).

Using $g' = 0.13$, $L = 30$km and $H = 35$m for the minimum channel depth gives $\gamma \approx 34$, 6, and 3 for $T = 5$ days, 24 hours, and 12 hours, respectively (see section 2.2.2, p. 23 for definitions of γ and q_{b0}). I found the forcing strength q_{b0} associated with long term meteorological forcing to be about 0.25 in agreement with Helfrich (1995, Table 1), but the strength of the tidal forcing to be weaker so that $q_{b0} = 0.15$ should be used together with $\gamma = 3$ and 6. With these values Helfrich's figure 9 shows that the average transport in the time-dependent case is at most 5% smaller than the quasi-steady result. This difference is small enough to conclude that during our observations the exchange flow was quasi-steady, whereby the Orkoz is excluded.

My conclusion differs from that of Özsoy *et al.* (1998). They also find that $\gamma = O(1)$ for tidal forcing but argue that according to Helfrich (1995) $\gamma \gtrsim 30$ is required for the quasi-steady approximation to be valid. This is not correct because for $\gamma \gtrsim 30$ the flow would be quasi-steady for any, including a very large, forcing strength. In the Bosphorus, however, barotropic forcing appears to be usually weak.

Sea-level fluctuations at Anadolukavagi and lower layer currents at Anadoluhisari observed by Gregg *et al.* (1999) in September 1994 have about the same magnitude but with 3 to 5 days a larger time-scale than those reported here. Current observations are too sparse to decide whether the variability observed during our experiments and those of Gregg *et al.* (1999) is typical for the Bosphorus.

3.3. Evolution Along the Strait

I will give an overview of the flow along the entire length of the Bosphorus using data from two surveys from the Black Sea toward the Sea of Marmara. Our observations from March/April 2000 and August 1998 represent spring and summer conditions, respectively.

An Orkoz appears to be a very rare event (Arisoy & Akyarli, 1990) which stands out from the usual exchange flow situation. In what follows I will hence focus on the usual exchange flow situation. The Orkoz will be described at the end of this thesis in chapter 6.

March/April 2000

On March 31 our survey began just south of the North Sill and ended about 3km south of Istanbul. On April 5 we began about 3km north of the North Sill, but were cut short at position 10km by an oncoming storm. The data from these two days were merged at 30km (figure 3.10). Frequently heavy ship traffic forced us to deviate from the thalweg. This is obvious at 0km, 17km and 31km where the ADCP measurement were shallower than the thalweg depth. Furthermore, when reading the plots of temperature, salinity and density it should be kept in mind that the spatial resolution of our CTD data is rather coarse which creates some obvious artificial features in the contours.

The upper layer moved slowly at the broad northern entrance, accelerating as it entered the strait. At the North Sill it was homogeneous in density. From the surface down to a depth of 47m density was practically constant with $\sigma_\theta = 14\text{kgm}^{-3}$ ($S = 18\,\text{psu}$). The temperature of the Black Sea surface water was slightly higher on April 5 than on March 31 which explains the patch of warmer surface water from the northern exit toward 30km where the two data-sets were merged. Between the Black Sea and position 12km salinity increased by not more than 0.5 psu. The layer thickness, which I define using the depth of the zero-velocity isotach, decreased by about 10m, and the current speed increased to about $-0.7\text{m}\,\text{s}^{-1}$. Fluctuations of along-channel speed are for the main part due to variations in channel width. Between 9.5km and 11km and between 11km and 14km the strait has its deepest and narrowest section, respectively. Current speeds reached -1.8m/s at the surface and -1.5ms^{-1} within the layer. The density interface widened due to mixing, as will be explained later. The upper layer thickness continued to decrease and measured only about 18m at the Sea of Marmara which it entered with a average speed of -1ms^{-1}. Both velocity and salinity/density showed large vertical gradients south of the contraction. Salinity decreased from 20 psu at the surface to 26 psu at the interface at 18m depth giving an average salinity of about 23 psu.

The Mediterranean water entering the strait at the Sea of Marmara side had a salinity of $S = 38\,\text{psu}$ and a temperature of 15°C. During its transit toward the Black Sea salinity decreased by about 2.5 psu and temperature by about 1°C with most of the change occurring at the South and North Sills. Average current speeds were 0.5 to $1\text{m}\,\text{s}^{-1}$ and

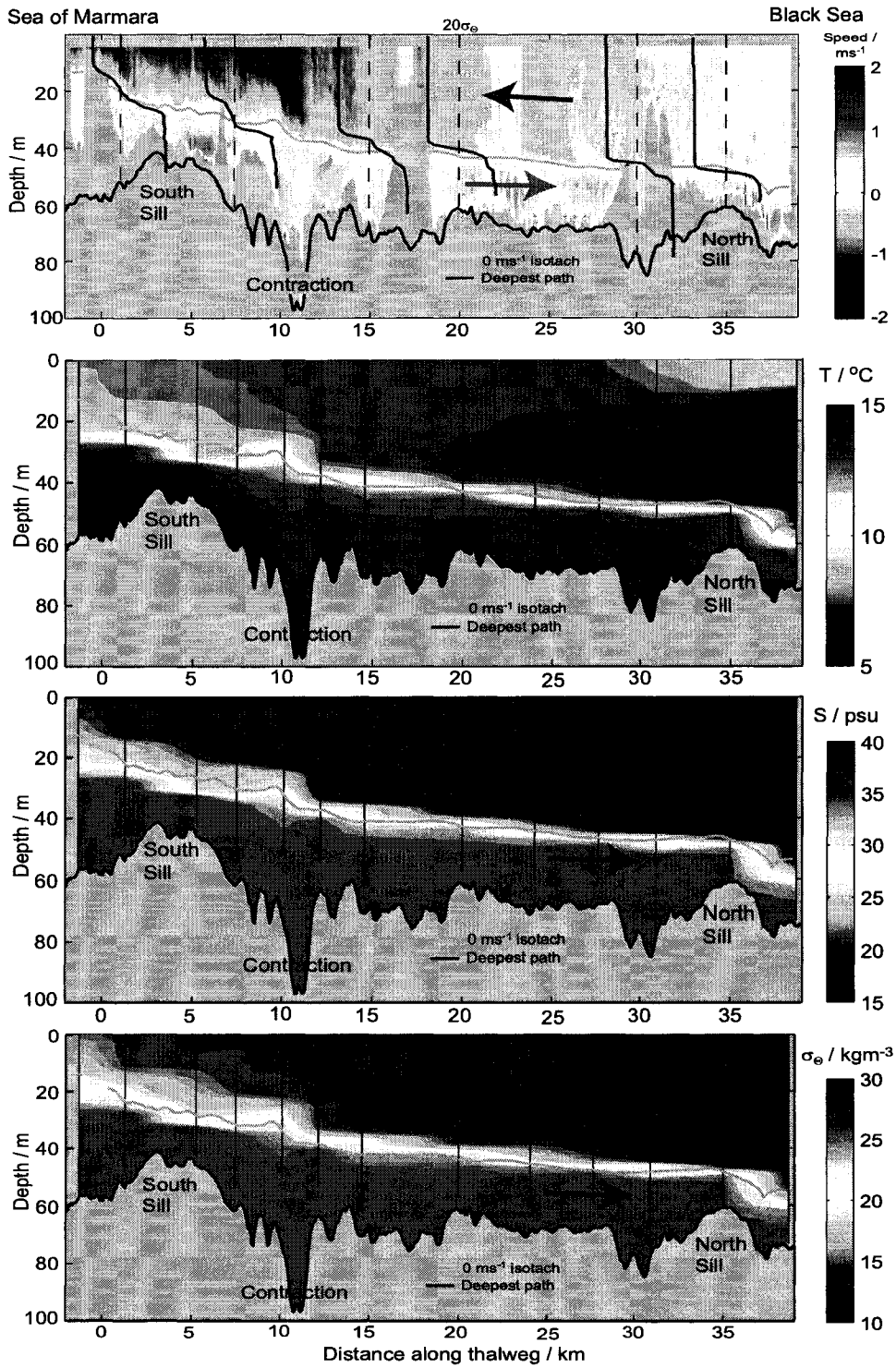

Figure 3.10.: *Composite of survey data obtained on March 31 and April 5, 2000.* ***1st panel:*** *Contours of along-channel current versus position along the thalweg. Northward flow is positive (red) and southward flow is negative (blue). The green solid line indicates the zero-velocity isotach. Density profiles are centred around* $\sigma_\theta = 20\mathrm{kgm}^{-3}$ *indicated by the dashed lines.* ***2nd panel:*** *Contours of temperature.* ***3rd panel:*** *Salinity.* ***4th panel:*** *Density in units of* σ_θ.

were fastest on the downstream slope of South and North Sill.

August 1998

The data from position 25.5km at Anadolukavagi to position −2.5km at the Sea of Marmara are from August 18, and those from position 35.4km at the Black Sea to position 25.5km were obtained one day later on August 19 (figure 3.11).

The general two-layer structure is similar to that of the flow in March/April 2000. However, there are some differences caused by seasonal changes of the conditions in the adjacent basins. Most obvious is the increase of the upper layer temperature. At the surface the temperature reached 24°C warmed by daytime air-temperatures of up to 28°C and nighttime temperatures falling to no less than 21°C. At the Black Sea side the water temperature dropped significantly at a depth of about 20m. This signifies the 8°C Cold Intermediate Layer (CIL) of the Black Sea which entered the Bosphorus at about 30m depth. Its signature was lost after 10km. On the other hand, the subdivision of the upper layer into a warm and a cold half was maintained almost throughout the entire strait because the temperature difference was large enough to have a noticeable effect on density (figure 3.4) and thereby stabilised itself against mixing. The lower layer had a temperature of about 14°C which is basically identical to the spring 2000 conditions.

The salinities of the upper layer water entering from the Black Sea and of the lower layer water entering from the Sea of Marmara were 17.5 psu and 38 psu, respectively, and were hence almost identical to those in spring 2000.

Along the northern part of the strait the depth of the interface (zero-velocity isotach, not shown here) was about 5m shallower than in March/April 2000. This correlates with a decreased upper layer transport and increased lower layer transport as consequence of a decreased freshwater influx into the Black Sea during autumn. Although meteorological conditions could also play a role, they do not explain the difference in this case; a steady northerly wind was present on August 18 and 19 which would increase the upper layer flow rather than weaken it.

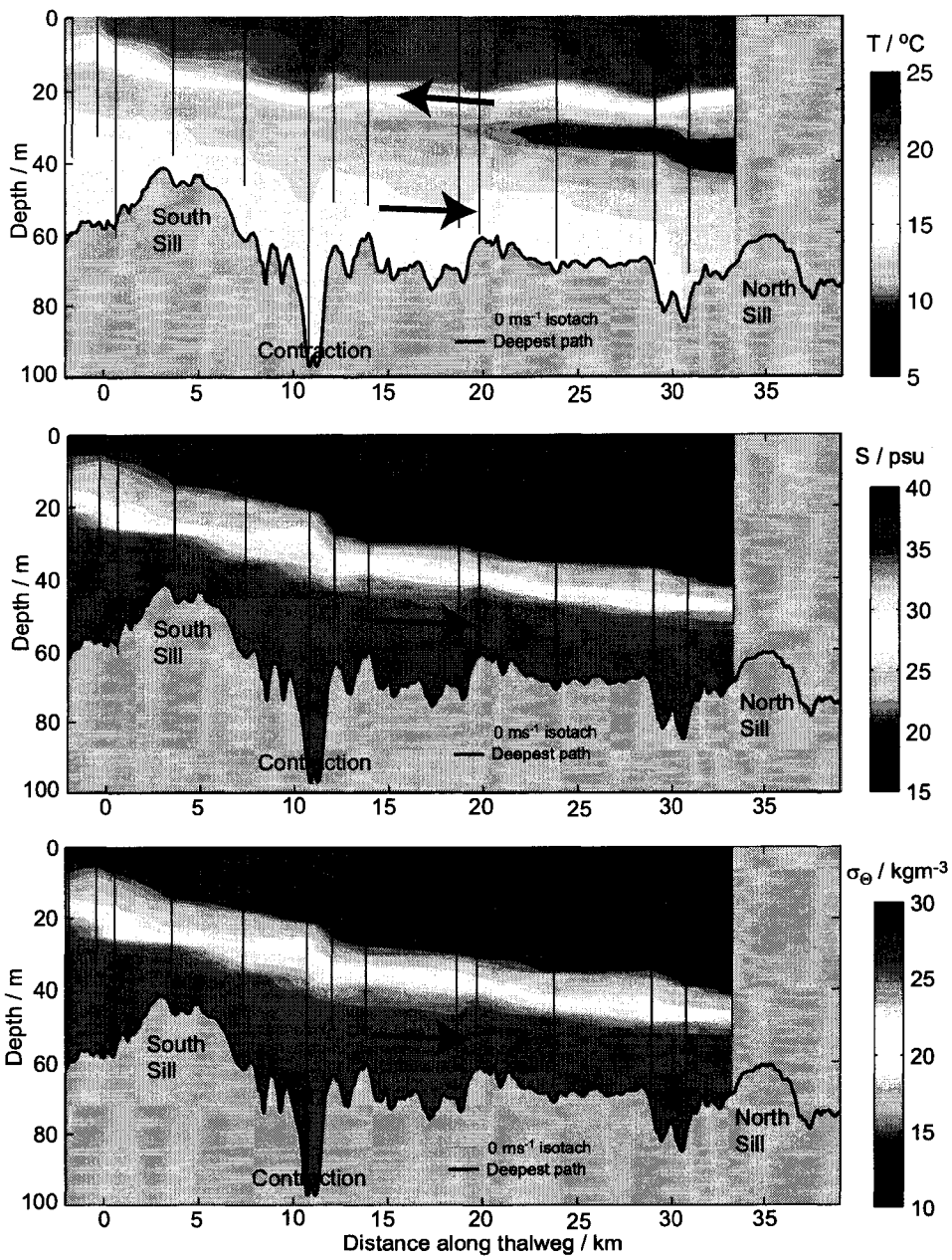

Figure 3.11.: *Composite of survey data obtained on August 18 and 19, 1998.* ***1st panel:*** *Contours of temperature. The location and depth of the CTD casts is shown by the black vertical lines. Constant temperature and salinity were assumed between the deepest CTD bin and the seafloor.* ***2nd panel:*** *Salinity.* ***3rd panel:*** *Density in units of* σ_θ.

June 2000: ASTER Surface Temperature Satellite Image

Figure 3.12 displays a satellite image which shows the surface water temperature along the Bosphorus from the Black Sea to the Sea of Marmara. The exact temperature scale is not known, but if we assume that conditions on June 16 were similar to those on June 22 and 23[2], then we can see from figure 3.4 that the light blue in the Black Sea indicates a surface temperature of 20.5°C, and the dark blue at the South Exit a surface temperature of 18.5°C. As the upper layer moved southward the surface temperature decreased because it entrained colder water (with $T = 15$°C, see figure 3.4) from the lower layer. Most of the entrainment occurred between the Contraction and the South Exit, and especially at the South Sill.

The surface flow entered the Sea of Marmara as a jet thereby spreading sideways, presumably because of its buoyancy or lateral mixing. The narrowing of the jet further south might not be real because clouds might have influenced the satellite data. We do not have any observations of the sub-surface waters in the Sea of Marmara because our surveys ended at the South Exit.

Change of Hydrographic Characteristics

A convenient way to visualise the change of the hydrographic characteristics of the water masses as they move through the strait is to show the spatial evolution of the TS-diagrams as done in figure 3.13 using data from August 1998.

Let us begin at the Black Sea side. The dark red curve shows the properties of the upper layer with a salinity of $S \approx 18$ psu and temperatures ranging from 7 to 23°C. As the upper layer progressed northward through the strait, its properties experienced little change until it reached the contraction. There salinity began to increase - first close to the interface and then throughout the entire upper layer. On the other hand, the properties of the lower layer changed relatively little as it moved from the Sea of Marmara to the Black Sea.

[2]It was checked that at least the meteorological conditions were indeed similar at these times.

Figure 3.12.: *ASTER satellite image from June 16, 2000 of the Bosphorus and its Black Sea and Sea of Marmara junction regions. Land area is shown as false colour composite of visible spectral bands with 15m spatial resolution. The water area image is derived from infrared bands with 90m resolution. Colour represents surface temperature with darker colours indicating colder waters. The scene is an extended version of that shown in figure 2.4.*

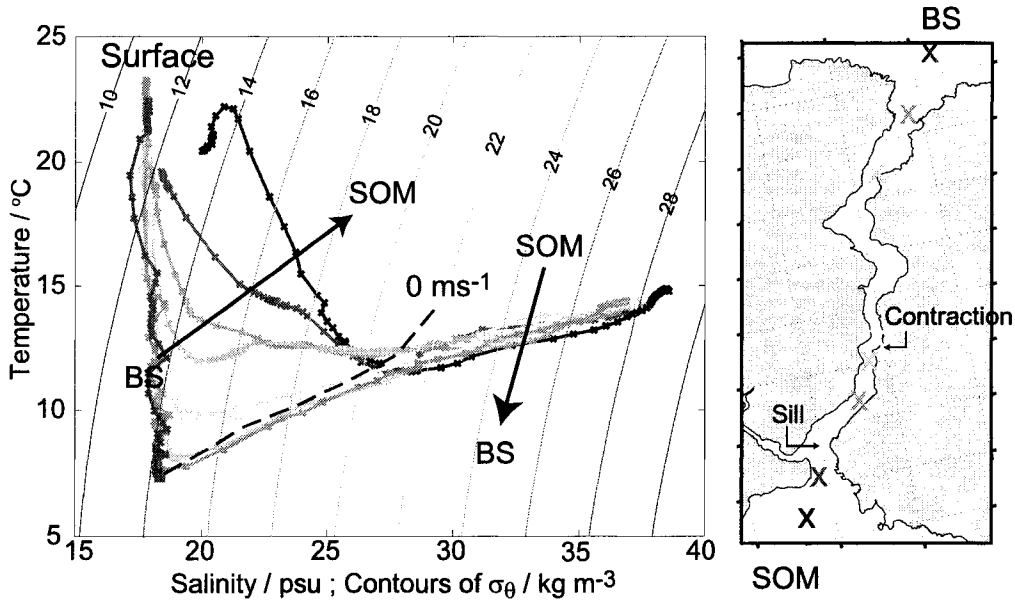

Figure 3.13.: *TS-diagrams from several locations along the Bosphorus in August 1998. The location of the CTD casts is shown in the right figure. The northernmost data are shown in red and the southernmost in blue. The dashed black line in the left figure indicates the position of the 0-velocity iso-tach. 'BS' and 'SOM' are abbreviations for 'Black Sea' and 'Sea of Marmara', respectively.*

Cross-channel Transect Along the Strait

Figure 3.14 shows velocity, salinity, and temperature data from 6 transects across the channel distributed along the strait from north to south. CTD casts were carried out approximately in the middle of the strait. The data are from April 3, 2000 whereby transect 1b was carried out at 07:50 UTC and transect 8 at 12:25 UTC. The upper layer flow was rather strong that day (see figure 3.7) so that the zero-velocity isotach was a little deeper than on other days.

We see that in the northern part of the strait (transects 1b, 2, and 5b) the flow is very uniform across the channel which has a simple cross-sectional shape between triangular and parabolic. I will show later (section 3.4) that significant cross-channel gradients occur in the upper layer at Beykoz. Those, however, did not have a lasting effect on the flow so that the upper layer was still very uniform in the Contraction.

On the other hand, the southern section shows a more complicated bathymetry which caused topographic steering of the flow and consequently horizontal gradients.

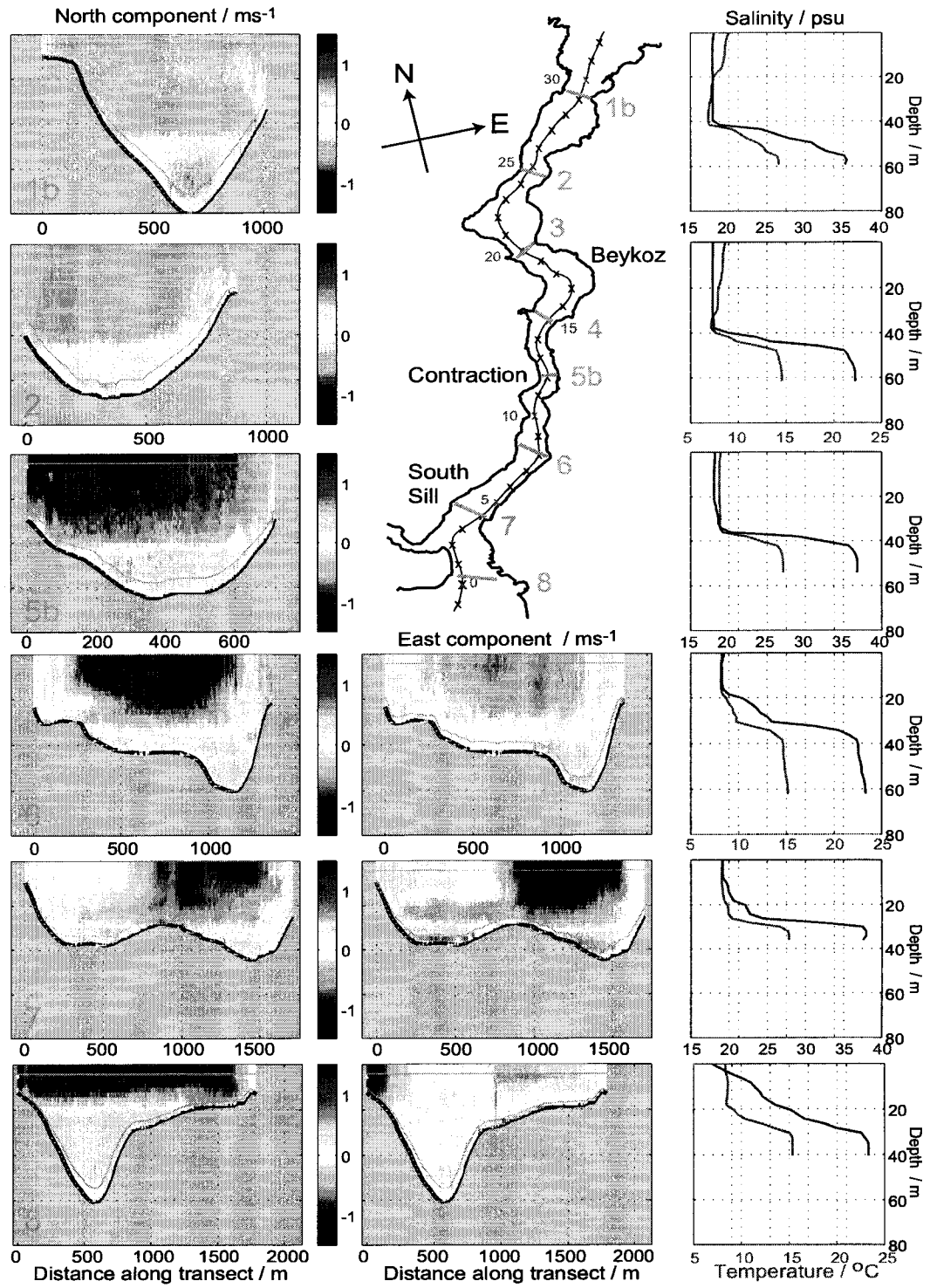

Figure 3.14.: *Velocity, temperature and salinity data from 6 cross-channel transects from April 3, 2000. The left and middle column show the north and east component of the horizontal velocity, respectively. For transects 1b and 2 the east component (not shown) is almost identical to the north component and for transect 5b the east component (not shown) is practically zero. Vertical scales are identical on all plots but horizontal scales vary. The map shows the location of the transects.*

Finally, note the very obvious difference in the depth of the zero-velocity iso-tach between the northernmost and southernmost transect.

Summary

Figures 3.10, 3.11 and 3.13 show that vertical mixing was small along the northern part of the strait. On the other hand, mixing appeared to be strong south of the Contraction and was directed mainly upwards. Hereinafter, I will call this process "upward entrainment" of water from the lower layer into the southward moving upper layer, and will reserve the word "mixing" for the simultaneous upward and downward entrainment between two layers. The observations suggest that the entrainment south of the contraction was related to the tortuous geometry in combination with the large currents which might have caused turbulence. In the next section I will discuss this in more detail and will also quantify the amount of mixing and/or entrainment along the Bosphorus.

3.4. Mixing and Entrainment

Long term mass and salt budgets provide estimates for the total average amount of mixing between the layers along the entire Bosphorus. Ünlüata *et al.* (1990) report downward and upward fluxes of $1200\mathrm{m}^3\,\mathrm{s}^{-1}$ and $2000\mathrm{m}^3\,\mathrm{s}^{-1}$, compared to upper and lower layer transports of $20\,000\mathrm{m}^3\,\mathrm{s}^{-1}$ and $10\,000\mathrm{m}^3\,\mathrm{s}^{-1}$. Qualitatively it is clear that the vertical fluxes are larger in the southern part of the strait, but quantitative estimates are not known.

Applying the principles of conservation of volume and salt I inferred the vertical fluxes from measurements of horizontal layer transports of salt and volume which were determined from salinity and current measurements along transects across the channel (figure 3.15). The transects were done at various locations along the strait with a spacing of 2km to 4km. Although this method is very simple in principle and is easily applied to, for instance, data from numerical simulations (e.g. Stashchuk & Hutter, 2001). Using it with our field data, however, proved more difficult. The main difficulties were measurement uncertainties and the temporal variability of the flow. See appendix D for details.

Determination of the vertical fluxes in itself does not reveal the physical reasons for

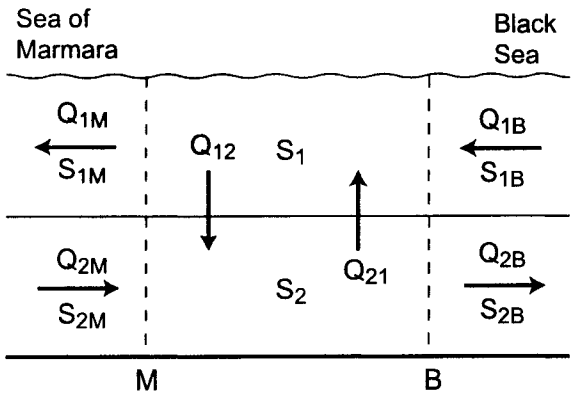

Figure 3.15.: *Compartment flows in the Bosphorus two-layer system.* $Q_{(1,2)(M,B)}$ *denote the layer transports in upper (1) and lower (2) layer whereby the subscripts M and B indicate the flows through boundaries toward the Sea of Marmara and Black Sea, respectively. Similarly,* $S_{(1,2)(M,B)}$ *denotes the layer salinities.* Q_{12} *and* Q_{21} *are the downward and upward entrainment fluxes and* S_1 *and* S_2 *the average salinities of the entrained waters. All quantities are positive.*

mixing. Therefore, I will compare the mixing rates with our other observations that provide information about the mixing processes. Echo-sounder imaging data will be the primary tool.

Figure 3.16 shows ADCP back-scatter intensity (average of all 4 beams) obtained during the run along the channel on March 31/April 5, 2000. High intensity signals correlate well with areas where we expect shear and turbulence, for instance, along the interface or in the southern part of the strait where currents are strong. Although, in principle, the backscatter could also be caused by biota, I will assume that here the acoustic backscatter is generated from turbulent refractive index fluctuations. This view is supported by Seim (1999) who used microstructure data from the Bosphorus obtained by Gregg *et al.* (1999) to demonstrate that salinity microstructure can dominate over temperature and/or biota by a factor of 10 when salinity controls the stratification - as it is certainly the case in the Bosphorus. Further evidence will be discussed in connection with the Orkoz in section 6.1. It is worthwhile noting that acoustic backscatter might also be caused by bubbles (entrained into the water by ship's propellers) and by other organic material (from sewage outfalls, for example).

In the lower panel figure 3.16 depicts average entrainment rates along the Bosphorus which I have divided into 4 sections: the North Sill, the Northern Section between North

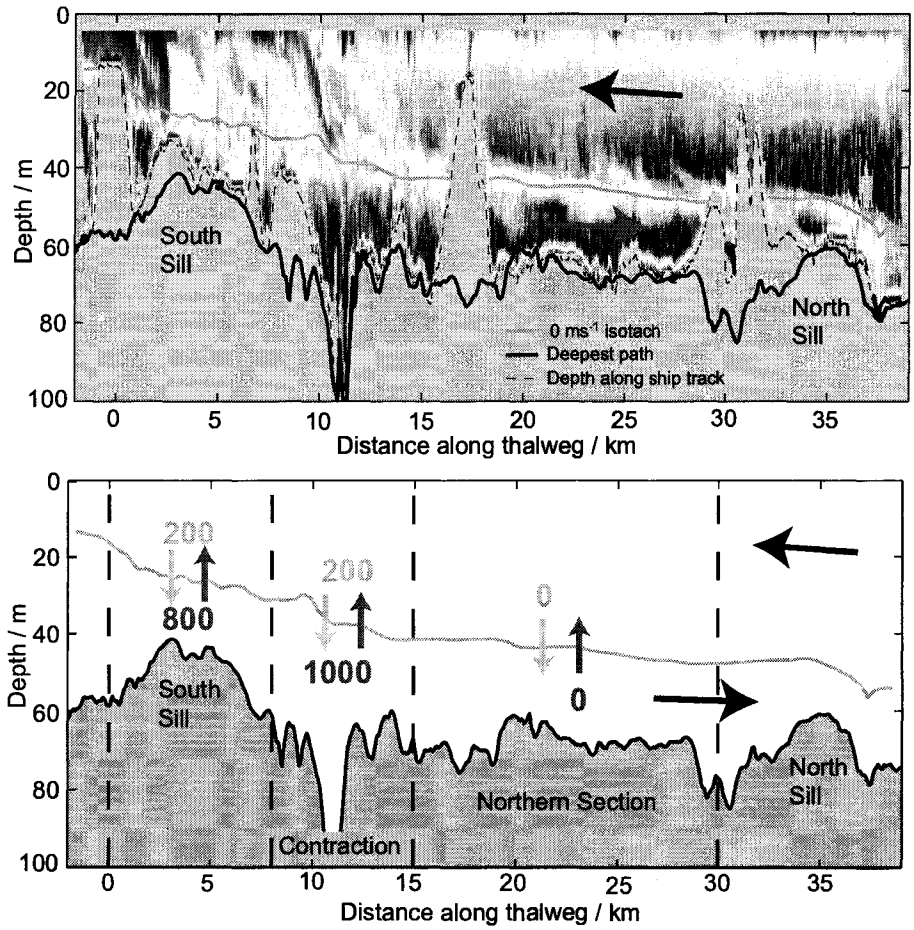

Figure 3.16.: ***Upper panel:*** *4-beam average of ADCP back-scatter intensity. Colour indicates the intensity of the back-scatter, red for intense and dark blue for weak or no return. The observations correspond to those shown in figure 3.10.* ***Lower panel:*** *Average entrainment rates in* $m^3 s^{-1}$ *along the strait with an uncertainty of about* $200 m^3 s^{-1}$.

Sill and Contraction, the Contraction itself, and the South Sill and South Exit. The averages are based on all entrainment rates from the 1998 and 2000 experiment. The numbers confirm the previous qualitative statements of little vertical mixing in the north and strong upward entrainment in the south. In what follows I will discuss flow and mixing in the 4 sections in detail.

3.4.1. North Sill

Figure 3.17 shows data from a 3.5km long transect along the thalweg at the North Sill. At the top of the sill the upper layer was about 47m thick. The density interface was very

sharp measuring only 4 to 5m. The lower layer was only 8 to 10m thick and its average speed about 0.6ms^{-1}. Reduced gravity was $g' = 0.13\text{ms}^{-2}$.

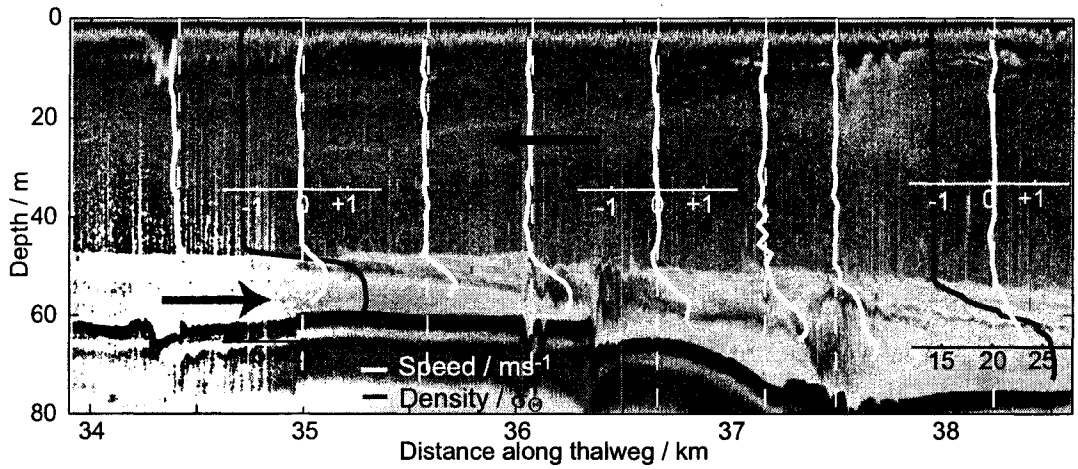

Figure 3.17.: *Acoustic back-scatter image taken on 05 April at the North Sill along the thalweg. Density profiles (black lines) and velocity profiles (white lines) are centred around* $\sigma_\theta = 20\text{kgm}^{-3}$ *and* 0m s^{-1}*, respectively.*

Di Iorio & Yüce (1999) show acoustic images of flow and channel bathymetry along and across the sill. These show that the cross-sectional shape is not rectangular but rather triangular. Then the composite Froude number of a two-layer flow is given by (e.g. Henderson, 1966; Bormans & Garrett, 1989*b*)

$$G^2 = F_1^2 + F_2^2\,, \qquad F_i^2 = \frac{u_i^2 W_I}{g' A_i}\,, \tag{3.1}$$

where subscripts 1 and 2 refer to the upper and lower layer, respectively, u_i is the layer averaged velocity, A_i is the cross-sectional layer area, and W_I is the channel width at the interface between the two layers. Note that for non-rectangular cross-sections W_I/A_i is larger than the layer thickness h_i, and recall that the flow is critical when $G^2 = 1$.

I estimated that $W_I = 1.1$ to 1.2km and $A_2 \approx 6000\text{m}^2$ at the top of the sill. With that $F_2^2 = 0.8$ so that the flow is marginally subcritical. This explains why it responded quite violently to irregularities in the sea-floor. Further downstream the channel deepens and narrows (see figure 3.iii by Di Iorio & Yüce (1999)) forcing the flow to accelerate so that the average layer velocity reached 0.9m s^{-1}. With $W_I \approx 500\text{m}$ and $A_2 \approx 3000\text{m}^2$ we obtain $F_2^2 \gtrsim 1$, i.e., the flow was critical to supercritical. At 37.2km it seemed to undergo a hydraulic jump after which the layer thickness increased and velocity decreased. These

observations confirm a simple hydraulic control at the North Sill as also reported by Di Iorio & Yüce (1999) and Gregg & Özsoy (2002).

Associated with the hydraulic jump was mixing which decreased the lower layer density by about 1kgm^{-3}. It was not possible to estimate the magnitude of the downward entrainment because we did not carry out a transect across the canyon north of the sill.

3.4.2. Northern Section

Mixing between the layers along the Northern Section was generally small. In figure 3.16 I have assigned values of $0\text{m}^3\,\text{s}^{-1}$ to both upward and downward entrainment. Obviously this is not to say that there is no mixing at all, but that it is approximately zero with an uncertainty of about $200\text{m}^3\,\text{s}^{-1}$.

That mixing is so small despite relatively fast currents and two major bends in the channel is perhaps surprising. For instance, one might expect that mixing would take place in the 90 degree bend at Beykoz (see figure 2.4 for the location) of which observations are shown in figure 3.18. The upper layer was concentrated on the western side of the strait whereas currents were almost zero within the bay at Beykoz. On the other hand, the lower layer was concentrated on the eastern side, and on the western side currents were even slightly negative, that is southward. The sounder-image shows three main areas with instabilities. The ones at (a) were probably due to separation of the southward flow from the inside bend and created turbulence within the upper layer. The ones at (b) were presumably due to vertical and perhaps horizontal shear within the upper layer. They existed and were visible to the acoustics because of the thermocline at about 20m (Recall figure 3.11 which shows that during the summer months a 10°C temperature step occurs in the upper layer.). Finally, instabilities were found at (c) roughly 5m above the zero-velocity iso-tach where the vertical velocity shear reached a maximum of 0.12s^{-1}. The gradient Richardson number Ri_g, which describes the relation between the stabilising effect of buoyancy and the destabilising effect of velocity shear (e.g Turner, 1973), was 0.4. This means that in theory there should be no instabilities as they can occur only if $\text{Ri}_g \leq 1/4$. Perhaps horizontal shear supports the onset of the instabilities or the problem lies in the limited vertical resolution of the data which is limited by the 2m vertical bins of the ADCP. At the pycnocline $\text{Ri}_g \approx 0.8$, and consequently we did see fewer instabilities

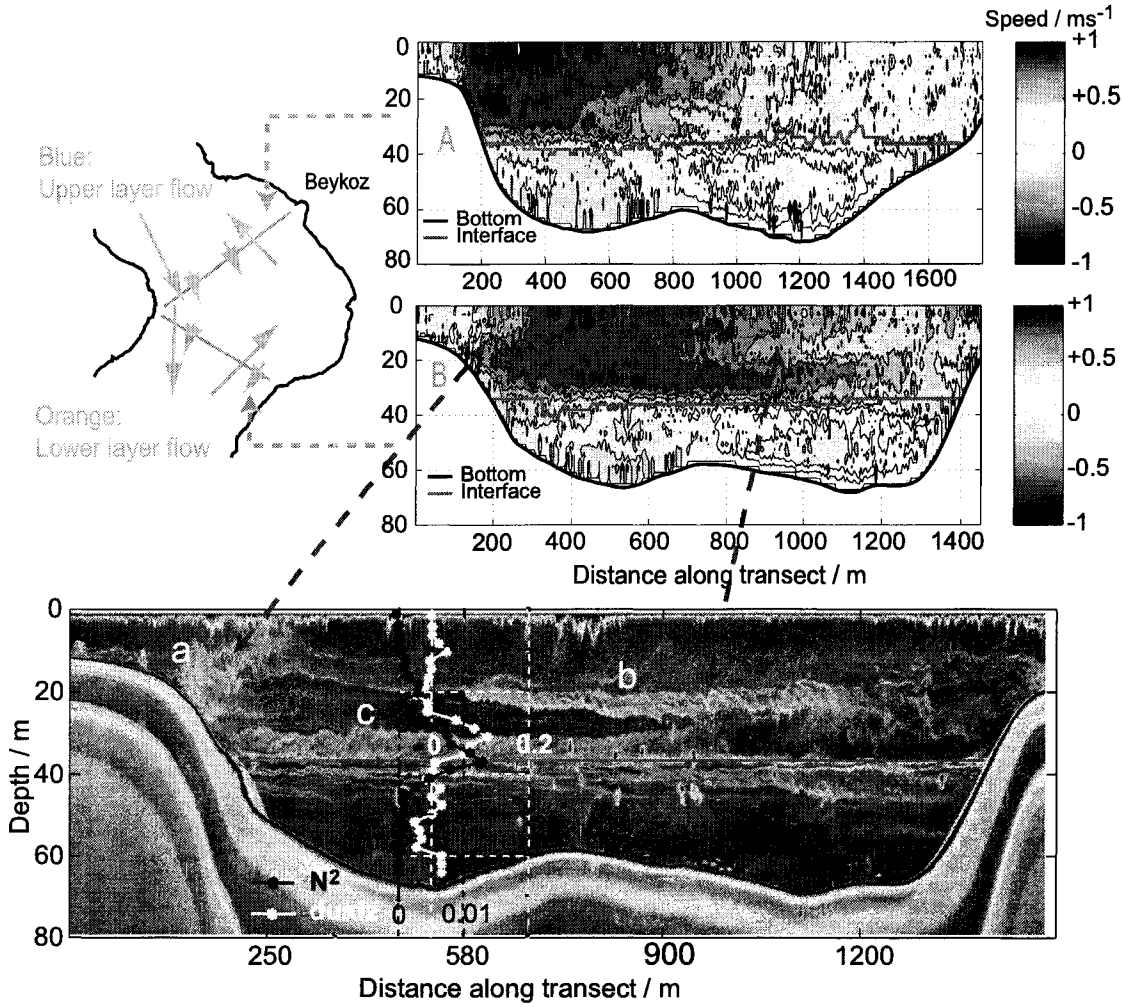

Figure 3.18.: *Observations of the flow in the curved section at Beykoz on 19 August 1998. The two panels in the upper right corner show contours of along channel velocity from the northern and southern transect. The lower panel shows the sounder image from the southern transect with the purple horizontal line indicating the position of the zero-velocity iso-tach. The vertical profiles in black and white show the vertical shear $du/dz/\mathrm{s}^{-1}$ and the buoyancy frequency N^2/s^{-2}, respectively, calculated from velocity and density with* 2m *vertical resolution.*

there.

In summary, along the Northern Section turbulence is created both by flow separation at bends and also by shear in the vicinity of the interface, but mixing between the layers is effectively limited by the strong stabilising effect of buoyancy at the pycnocline. This situation was observed not only at Beykoz but also at other locations which explains why the total vertical fluxes along the Northern Section were small.

3.4.3. Contraction

Strong upward entrainment of $1000\mathrm{m}^3\,\mathrm{s}^{-1}$ was observed in the section about the Contraction. This is a significant amount considering that the lower layer transport was only between 4000 and $9000\mathrm{m}^3\,\mathrm{s}^{-1}$. On the other hand, downward entrainment was only $200\mathrm{m}^3\,\mathrm{s}^{-1}$.

There is no doubt that the intense mixing is associated with the strong currents and the strait's tortuous geometry. Figure 3.19 shows acoustic back-scatter images and the along channel velocity from a run along the Contraction from 9km to 12km. During this

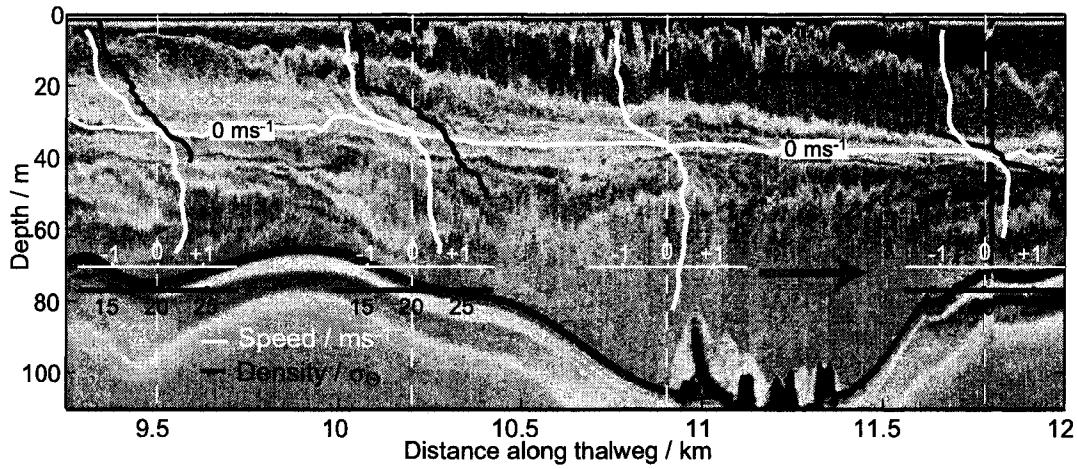

Figure 3.19.: *Acoustic back-scatter image taken on April 8, 2000 in the Contraction along the middle of the channel. Density profiles (black lines) and velocity profiles (white lines) are centred around* $\sigma_\theta = 20\mathrm{kgm}^{-3}$ *and* $0\mathrm{m}\,\mathrm{s}^{-1}$, *respectively.*

run we stayed in the middle of the channel thereby minimising the influence from the channel sides as much as possible. At 12km the zero isotach was at 40m and agreed well with the pycnocline and depth of intense back-scatter. The upper layer was about 750m wide. Note that we have to distinguish between the width of the channel and the width

of the active moving layer because at some bends flow separation occurred so that the effective layer width was smaller than the channel width. The layer widths were inferred from transects across the channel at 12km, 11km, 10km, 9.5km, and 8km. We obtain $G^2 \approx 0.12 + 0.08 = 0.20$. As the channel narrowed F_1^2 increased, but because it also deepened F_2^2 decreased so that at 10.5km we find $G^2 \approx 0.34 + 0.05 = 0.39$. At 10km the upper layer was only 600m wide. The flow was forced to accelerate and due to the Bernoulli effect the interface rose noticeably. The layer then widened again to about 750m at 9.5km and consequently the interface dipped down. At the southern end of the contraction at 9.5km we have $G^2 \approx 0.45 + 0.07 = 0.52$.

Associated with the strong currents in the contraction were strong shear and mixing. This can be inferred both from acoustic backscatter and from the change of velocity and density profiles. At the interface the vertical velocity shear du/dz reached values of 0.25s^{-1} (obviously with some temporal and spatial variability) and the gradient Richardson number was approximately 1/4 or less. Consequently Kelvin-Helmholtz like instabilities occur along the interface. However, turbulence originated not only at the interface, but also from the sharp bends where flow separation occurred. As one example, figure 3.20 shows sounder data from the vicinity of Akinti Burnu (Cape of the Current) which protrudes into the strait from the western shore. The fast upper layer impinges onto Akinti Burnu thereby creating turbulence. Unfortunately we do not have CTD profiles from this particular location to further support that the observed turbulence caused mixing.

3.4.4. South Sill and South Exit

The southern third of the Bosphorus is the most complicated section in terms of both bathymetry and flow. Figure 3.21 shows the coastline and bathymetry from 7km to the exit toward the Sea of Marmara. Most of the South Sill is between 30m to 40m deep except for a central ridge that rises to about 28m. The ridge is flanked by two 40m deep channels that cut into the sill from the north whereby the one on the eastern side is the deeper one. From the south the sill is approached by the Marmara channel that runs along the western side of the strait. It does not connect to the northern channel on the eastern side.

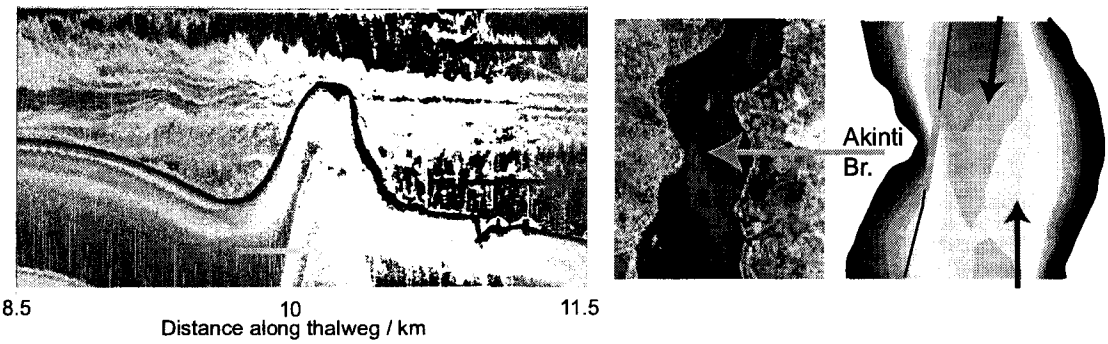

Figure 3.20.: *The left panel shows acoustic back-scatter image taken on 4 April 2000 in the vicinity of Akinti Burnu (at thalweg position* 10km*). The ship's path is shown as black line in the map in the right panel. The ASTER satellite image (from June 16, 2000) helps to visualise the strong currents (middle panel). The horizontal green line in the left panel indicates the section of the path along which the sounder data were taken which are marked by the green line in the left panel.*

Gregg & Özsoy (2002) gave the first detailed description of the flow around the South Sill. However, their shallowest ADCP bin was at 10m so that they missed much of the shallow southward flowing layer. Our data serve to complete the picture. I will present data from March 31 and April 3. On April 3 the upper layer current was about 20% stronger than on March 31.

Figure 3.22 shows data from track A which roughly follows the thalweg. The shallowest depth of 32m was encountered at 2.7km were we passed from the northern channel on the east side into the southern channel on the west side. The upper layer was strongly stratified and sheared except in a 10m thick surface layer. Sea of Marmara water was passing from the southern channel into the northern channel in a layer with thickness varying between 5m at 2.7km and 16m at 4km. Its upper boundary was clearly identified by a sharp density step and a thin layer of intense back-scatter intensity. The zero isotach was about 5m higher.

Figure 3.23 shows the data from three transects across the southern channel. Just south of the central ridge the southward flow was concentrated on the Asian side. At the surface the currents were stronger than $-1.5\mathrm{m\,s^{-1}}$ and decreased linearly to zero at a depth of 30m. West of the ridge the southward flow was practically zero. Similarly the northward current was stronger on the Asian side than on the European side so that at least 50% of

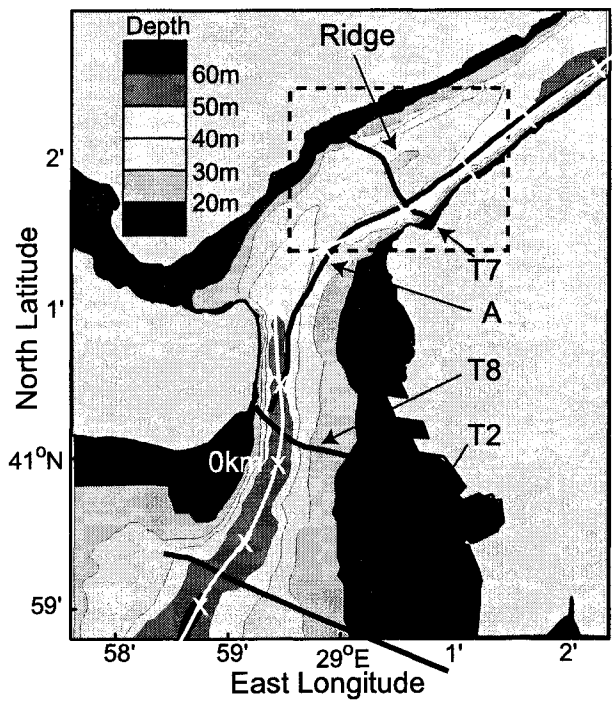

Figure 3.21.: *Bathymetry and ship tracks (black) in the southern part of the strait. The area of the South Sill is enclosed by the dashed line. The thalweg is shown as white line with* 1km *increments marked by crosses.*

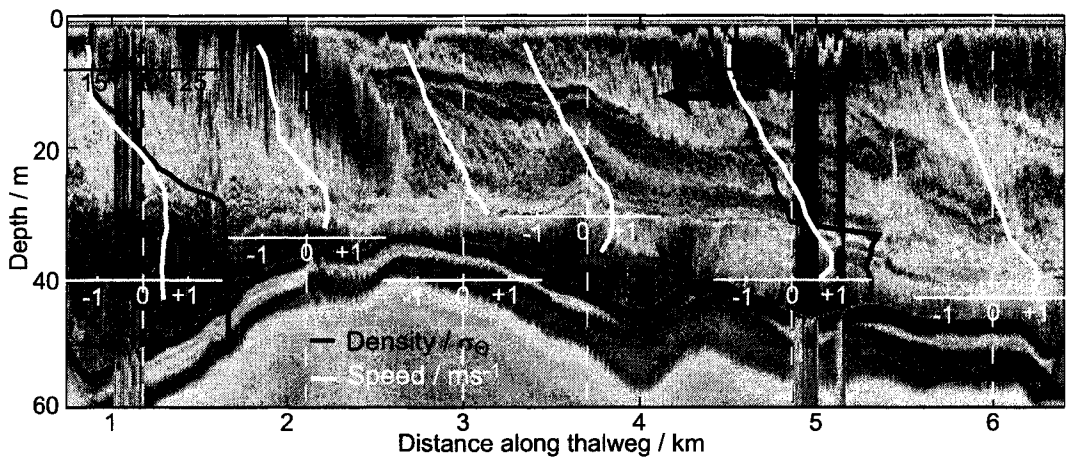

Figure 3.22.: *Acoustic back-scatter image taken on March 31, 2000 at the South Sill following track A in figure 3.21 from north to south. The patch of intense back-scatter at* 2km *was probably due to bubbles entrained by the propeller of a southbound oil-tanker that had passed us earlier.*

the Sea of Marmara water was directed over the eastern part of the sill. This differs from observations by Gregg & Özsoy (2002) who found that most of the deep flow was directed by the Marmara Channel over the western part of the sill. Presumably the flow path changes with the relative strength of upper and lower layer flow. During strong southward flow (our data) the lower layer appears to be weaker on the western than on the eastern side of the ridge.

About 3.5km further south on transect T8, at the exit toward the Sea of Marmara, the southward flow occupied almost the entire width of the channel. Surface currents were larger than $-1.5\mathrm{m\,s^{-1}}$ in the centre of the channel and larger than $-1.75\mathrm{m\,s^{-1}}$ along the European shore. The zero isotach was at 20m depth that is 10m higher than at transect T7. The gradient Richardson number $Ri_g = \frac{N^2}{(du/dz)^2}$ was less than 1/4 (often as small as 1/10) in the upper 15 to 20m. This supports the view that the high back-scatter intensities were due to turbulence. The lower layer was confined to the deep Marmara channel and moved northward with about $0.25\mathrm{m\,s^{-1}}$. The back-scatter in the lower western half of the channel was caused by outfall from Istanbul's main sewer which ends in the middle of the channel about 300m south of our transect (Beşiktepe *et al.*, 1995; Gregg & Özsoy, 2002). The presumably 'fresh' water appears to rise to the interface.

At the southern end of the strait the upper upper layer separated from the coast and shallows at Istanbul and entered the Sea of Marmara presumably like a jet (see transect T2 in figure 3.23 and also figure 2.4). Surface velocities were larger than $-1.5\mathrm{m\,s^{-1}}$ in the western half and larger than $-1\mathrm{m\,s^{-1}}$ in the eastern half. The gradient Richardson number was smaller than 1/4 in the upper 10m. The stratification in the upper layer supported internal waves, for instance at 2.2km, which can be seen both in the sounder image and also in the velocity contours (figure 3.23, lower panel). Wavelike signatures can also be seen along the pycnocline at 27m depth within the northward moving layer. Below the pycnocline the density was a constant $\sigma_\theta = 28.5\mathrm{kgm^{-3}}$ which is typical value for the lower Sea of Marmara waters (Beşiktepe *et al.*, 1994).

The zero isotach was noticeably tilted with a cross-channel slope of about -2.7×10^{-3}. Geostrophy gives

$$\frac{\Delta h}{W} = \frac{fU}{g'} \tag{3.2}$$

where $f = 10^{-4}$ is the Coriolis frequency, Δh is the change of the depth of the interface

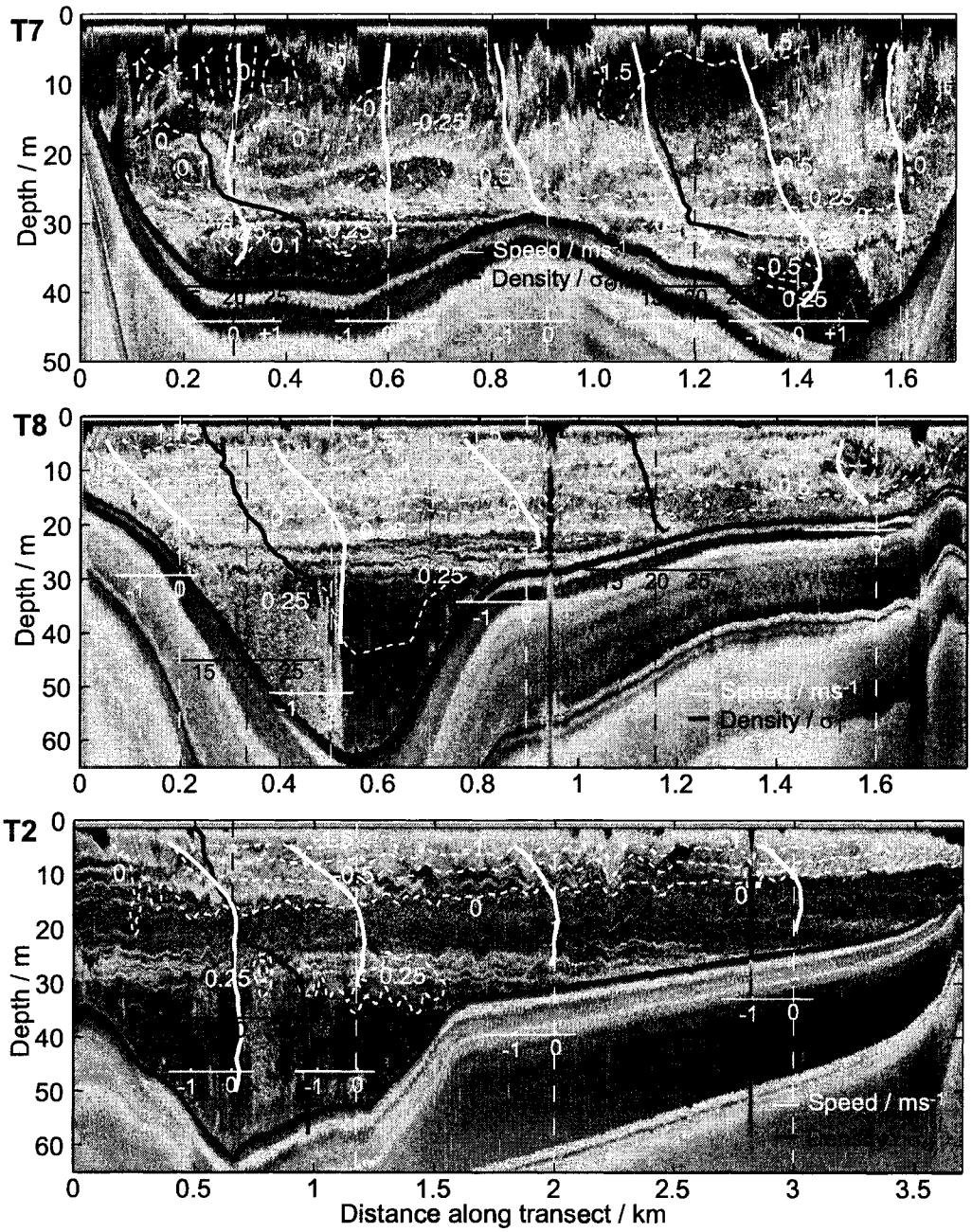

Figure 3.23.: ***Upper panel:*** *Acoustic back-scatter image taken on April 03, 2000 along track T7 across the strait from west to east. The white dashed lines are contours of along channel velocity. Density profiles (white lines) and velocity profiles (black lines) are centred around* $\sigma_\theta = 20\mathrm{kgm}^{-3}$ *and* $0\mathrm{m\,s}^{-1}$*, respectively.* ***Middle panel:*** *Acoustic back-scatter image taken on April 03, 2000 along track T8 across the strait from west to east.* ***Bottom panel:*** *Acoustic back-scatter image taken on March 31, 2000 along transect T2 in the Sea of Marmara exit region from west to east.*

over the width W, and U is the average layer velocity. Because the lower layer was approximately motionless only the stratification beneath the moving upper layer should affect the dynamics so that g' was as small as $0.07\mathrm{m\,s^{-2}}$. Using $U = -1\mathrm{m\,s^{-1}}$ we obtain a slope of -1.4×10^{-3}. This is only about half of what we observed. This might indicate that lateral and vertical friction and/or mixing may have contributed to the balance of forces (Defant, 1961*a*, chapter XVI).

On the basis of their data from September 1994 Gregg & Özsoy (2002) concluded that the exchange might have been controlled at the crest of the South Sill. Figure 3.23 shows that during our observations currents were too small for a two-layer control. In the east side $F_1^2 \approx 0.4$ and $F_2^2 < 0.1$. The flow from the southern channel into the northern channel in figure 3.22 shows some dips in the position of the interface which could indicate that the flow was close to control, but also here we did not find F_2^2 close to 1. It is feasible that during stronger southward flow $F_2^2 = 1$ at some locations across the South Sill but it appears unlikely that F_1^2 could reach a value of 1 at this location .

Between transect T7 and T8 the zero isotach rose by 10m so that the current and also the shear increased. Using $h_1 = 19\mathrm{m}$ (defined by the zero iso-tach), $g' = 0.07\mathrm{m\,s^{-2}}$ and an average layer velocity of $u_1 = 1.1\mathrm{m\,s^{-1}}$ we obtain $F_1^2 = 0.9$. We have to take into account that the uncertainty in F_1^2 is about 0.1. Hence, the flow could have been critical or marginally subcritical.

3.5. Bottom and Sidewall Friction

As I have mentioned in section 2.2.5 it is likely that friction contributes significantly to the balance of forces in the Bosphorus. Friction on solid walls is perhaps well established with the quadratic drag law $C_H u^2$ being generally accepted whereby the friction coefficient C_H is generally larger if u is the current speed above some bottom boundary layer, and smaller if u is the current speed averaged over the layer depth. Using the latter approach it is believed to be of the order of 10^{-3} (e.g Pratt, 1986). In their two-layer numerical simulation of the exchange through the Bosphorus Oğuz *et al.* (1990) used $C_H = 2.3 \times 10^{-3}$. This value was determined by tuning the friction parameters (for instance, C_H) until the model results agreed with available hydrographic data. To my knowledge direct estimates

of the friction coefficient in the Bosphorus have not yet been published.

One way to estimate the bottom stress τ, the drag exerted on the flow by the seabed, is to use the so-called profile method. On the basis of dimensional arguments (Tennekes & Lumley, 1972) the mean velocity above the seabed should exhibit a logarithmic profile in the inertial sublayer (or log-layer)

$$U(z) = \frac{u_\star}{\kappa} \ln\left(\frac{z}{z_0}\right) , \tag{3.3}$$

where U is the ensemble mean velocity (averaged sufficiently to eliminate turbulent fluctuations), z is the height above the seabed, $\kappa \approx 0.4$ is the von Kármán's constant, z_0 is the bottom roughness scale, and $u_\star$ is the friction velocity that scales the turbulent velocity fluctuations (e.g. Soulsby, 1983). The bottom stress is related to $u_\star$ by

$$\tau = \varrho u_\star^2 . \tag{3.4}$$

A linear fit to a plot of observed u versus $\ln z$ allows a determination of $u_\star$, and, hence, of the bottom shear stress. The friction coefficient can then be determined by least-squares fit to the equation

$$u_\star^2 = C_H \, U_{\text{ref}}^2 , \tag{3.5}$$

where the reference velocity U_{ref} is chosen to be either the depth-averaged or a near-bottom velocity.

Velocity profiles were derived from 120min data averages from the bottom-mounted ADCP. The centre of the first velocity bin was 3.7m above the bottom. For the fitting procedures criteria given by Lueck & Lu (1997) were applied: the fitting starts with trying the lowest three velocity bins. If the error of the three-bin fit is less than 1% of the maximum streamwise speed, then the fourth bin is tried, and so on. Fits obtained with z_0 values larger than 0.02m are rejected. (This value was derived from a histogram of values of z_0 as shown by Lueck & Lu (1997).) The height of the log-layer, h_L is defined as the maximum height to which acceptable fits can be obtained. Hence the minimum value of h_L, if found, is 6.1m (the height of the third bin) above the bottom.

We obtained 130 averaged velocity profiles from the 10.5 days of velocity data. As examples, 5 of these profiles are shown in figure 3.24 whereby, for the sake of convenience, I have chosen to display the magnitude of the streamwise component of horizontal velocity.

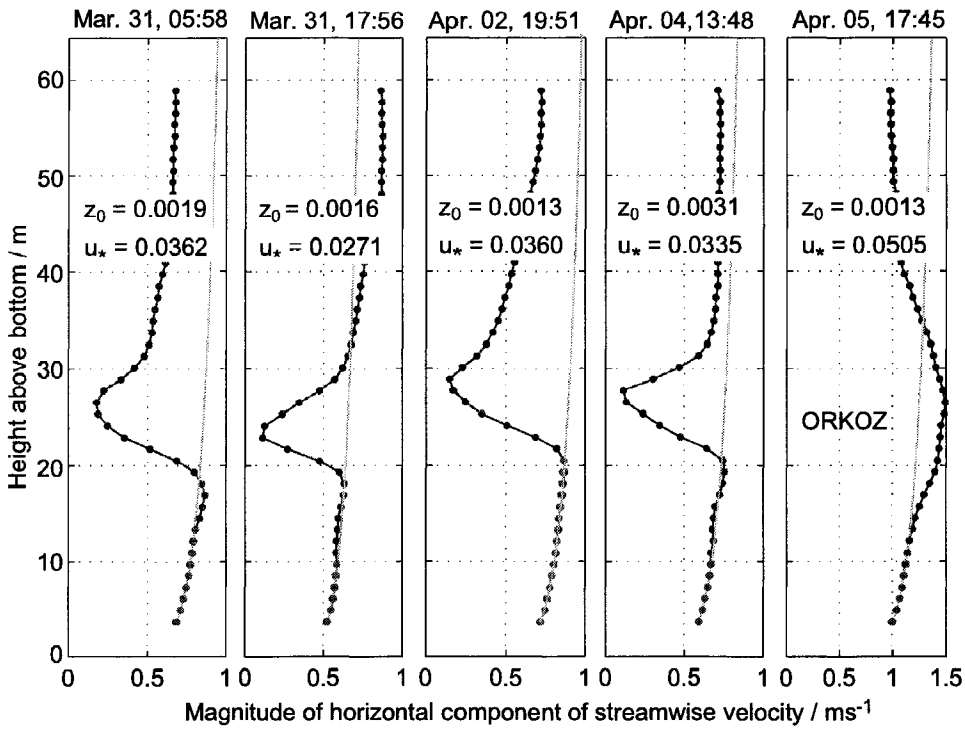

Figure 3.24.: *Sample profiles (in blue) of* 2h *averages of the* ***magnitude*** *of the streamwise component of horizontal velocity. The green lines are the fitted logarithmic velocity profiles. The red data points are those used for determining the fit, hence the topmost red point indicates the height of the log-layer. The roughness length* z_0 *and the friction velocity* u_* *are given in units of* m *and* $\mathrm{m\,s^{-1}}$*, respectively.*

For this figure, the streamwise direction was defined to be aligned with the mean flow of the lowest 8 velocity bins (the lowest 12m). The direction of the flow at the interface is slightly different and therefore the velocity does not reach zero. With these settings 123 of the 130 profiles fulfilled the fitting criteria and were used to obtain $C_H = 0.0022$ (or $C_H = 0.0027$ if the fit is forced through the origin) as shown in figure 3.25.

The values obtained during the Orkoz, readily identified by their larger velocity values, showed larger deviations from the fitting line than the other values. If we exclude these data from the fit, we obtain $C_H = 0.0020$ or $C_H = 0.0025$ for the unforced and forced fit, respectively. Just for the duration of the Orkoz 21 profiles fulfilled the criteria and with that the forced fit gives $C_H = 0.0030$. This value is, however, subject to great uncertainty because of large data scatter.

Reducing the averaging length from 120min to 60 or 20min had no influence on C_H

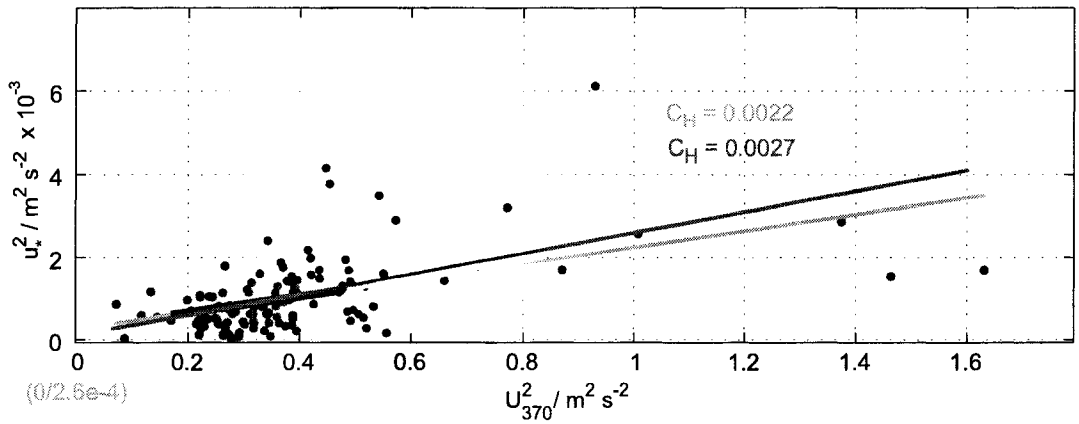

Figure 3.25.: *Friction velocity squared u_*^2 (proportional to bottom-stress) against U_{370}^2. U_{370} is the* 2h *mean velocity in the first velocity bin at* 3.7m *above the sea-floor. The solid lines have slopes equal to the drag coefficient C_H obtained from least-squares fits. Streamwise velocity was aligned with the direction of the mean velocity of the lower* 12.1m. *The green fit line crossed the ordinate at* 0.00026 *whereas the red fit line was forced to go through* $(0, 0)$.

and neither had a reduction of the maximum acceptable roughness length from 0.02m to 0.01m. Requiring the log-layer fit to use at least 4 instead of 3 data points reduced the scatter so that $C_H = 0.0024$ and 0.0026 for the unforced and forced fit, respectively, when all data were used. Without the Orkoz data the corresponding values are $C_H = 0.0020$ and 0.0023.

According to Ergin *et al.* (1991) the sea-floor along the Bosphorus consists mainly of sand and gravel with significant amounts of shell fragments because finer material is eroded and removed by the strong currents. For such a sand/gravel sea-floor Soulsby (1983) gives a roughness length of $z_0 = 0.0003$m (with a standard deviation for $\ln z_0$ of about 2). Curiously, the values I find are about 0.005m which is about an order of magnitude larger. The reason for this discrepancy is that Soulsby's values assume skin-friction which extends only about 1m above the sea-floor. The log-layer observed here, which was up to 20m thick, is not consistent with skin-friction and is more likely to be caused by form drag due to an irregular bed form as pointed out by Lueck & Lu (1997) and Sanford & Lien (1999). Indeed, at the South Exit side-scan sonar surveys revealed the presence of asymmetrical current ripples of sand ranging in lengths from 2 to 25m (Ergin *et al.*, 1991) and it would seem likely that ripples exist in the middle of the strait, too, indicating that it was indeed form drag, rather than skin-friction, that caused the log-layers we observed (figure 3.24).

The friction coefficients I have given are based on a reference velocity from the first velocity bin at 3.7m above the seafloor. For the flow in a tidal channel Lueck & Lu (1997) find that their $C_{H,360}$ is about 25% larger than $C_{\mathrm{H,m}}$ where the latter uses the mean of all velocity bins (up to the sea-surface) as reference velocity. In the Bosphorus it is not so clear how to calculate $C_{\mathrm{H,m}}$ because of the two layer structure. If I calculate the average velocity using all lower layer velocity bins between sea-floor and interface (and again exclude the Orkoz data), I obtain $C_H = 0.0023$ (unforced and forced fit). If I use the bottom 21m which seem to be little influenced by the interfacial shear, I obtain $C_H = 0.0018$ and 0.0022 for the unforced and forced fit, respectively. The difference is small so that we do not need to be overly worried about the definition of the reference velocity.

Using a value of $C_H = 0.0023$ as done by Oğuz *et al.* (1990) is consistent with this investigation. Of course, one has to question whether one value can be correct for the entire Bosphorus. For instance, the form drag along the sea-floor may vary along and across the strait, because the size of the ripples depends on the strength of the current. Unfortunately the accuracy of the vessel-mounted ADCP data is not sufficient to repeat the analysis with data from other locations. Alternatively, friction could be estimated from measurements of the turbulent kinetic energy dissipation ε. The results of such measurements, carried out by Gregg *et al.* (1999), have not yet been reported.

A further unknown is the effect of lateral protuberances along the Bosphorus. Some have a noticeable effect on the flow as shown in figure 3.20. Flow separation and the generation of waves seem to occur. Both processes cause a drag on the mean current. In theory the resulting effect on the flow can be represented by some form drag which is associated with the pressure drop across the topographic feature in question. It is determined by integrating the horizontal component of pressure along the surface of the topographic feature. For a 2-dimensional feature the drag per unit width is given by (Baines, 1995)

$$F = \int dx\, p(H) \frac{\partial H}{\partial x} \tag{3.6}$$

where $p(H)$ is the pressure at the sea-floor. This integral also includes the pressure drop due to bottom stress. Unfortunately this definition of form drag turned out to be very difficult to use with our data as it requires the density field and the free surface pressure gradient around the 3-dimensional topographic feature which our data do not provide.

Theoretical and numerical studies on wave and separation drag have been reported by MacCready & Pawlak (2001) for the case of an isolated Gaussian ridge on a slope in a uniformly stratified flow. One of their conclusions is, that the wave drag decreases with increasing slope. For the steep lateral protuberances in the Bosphorus this suggests that wave drag might be less important than separation drag. But, as mentioned before, we do not have the data to test this.

In conclusion, it seems reasonable to assume that the average friction coefficient for bottom and side-wall friction is about $C_H = 0.0023$ keeping in mind that the value might be larger at some isolated lateral protuberances.

3.6. Two Key Problems

Our observations confirm the long-known two-layer structure of the exchange through the Bosphorus. On the other hand, they show details which have not been reported before. Some seem to be at odds with previously accepted wisdom which was mainly based on hydrographic measurements and simulations with two-layer numerical models. The key problems are:

- The interface along the Bosphorus is markedly sloped along the thalweg. This can be explained by the influence of bottom/sidewall and interfacial friction as shown, for instance, by Assaf & Hecht (1974) and Bormans & Garrett (1989*b*). This, however, ignores mixing. In the Bosphorus we observe a significant amount of upward entrainment (that is entrainment of water from the lower into the upper layer) in the southern half of the strait, and clearly we must wonder what the effect on the dynamics will be. Mixing/entrainment will exchange momentum between the layers and is in this sense akin to interfacial friction. If we furthermore combine our observations of an increased interfacial slope in the southern section of the strait with that of increased entrainment, we may wonder whether entrainment might have a similar effect as friction on the flow.

  Price & Baringer (1994), for instance, estimated the effective mean entrainment stress at the interface as $\tau_I = \varrho_0 V w_e$ where V is their streamtube velocity and w_e is the entrainment velocity. However, this equation ignores that mixing will also

exchange volume and mass, the latter causing a horizontal density gradient within the layers. It is not clear a priori how the simultaneous exchange of volume, mass and momentum affects the dynamics of the flow. This will be investigated in the next chapter.

- Classical two-layer hydraulics assumes homogeneous and uniform layers. Observations clearly show that the effects of mixing and friction lead to stratified and sheared layers. If the layers are nearly homogeneous and uniform it is accepted practice to use values that are representative for the layer. Most often layer averages of velocities and densities are used to calculate Froude numbers, etc. This is the approach used in the previous sections.

  Along the southern Bosphorus, however, the velocity in the upper layer is far from being uniform. Can we then be sure that Froude numbers based on average layer quantities correctly represent the hydraulic state of the flow? This is a critical question as the whole classification of an exchange as being controlled, submaximal, maximal, etc. depends on the correct determination of the hydraulic state of the flow. This issue will be pursued in chapter 5.

Both points may also help decide a question regarding the flow through the Bosphorus contraction. Knowing that exchange flows may be controlled at lateral constrictions and also knowing that the associated hydraulic jump (the meaning will be explained in section 4.1.1) causes mixing, hydrographic data from the contraction, which showed mixing and a fairly abrupt change of the depth of isohalines, were thought to indicate a hydraulic control (e.g. Yüce, 1996; Ünlüata *et al.*, 1990). However, current measurements by us and Gregg *et al.* (1999) reveal that the composite Froude number is less than 1, i.e. the classical condition for hydraulic control $G^2 = 1$ is not met. Furthermore, the acoustic images do not indicate a hydraulic jump which, in theory, should have shown as a fairly sudden increase in upper layer thickness at the southern end of the contraction.

Hence, one may wonder about the following 3 possibilities: a) the classical two-layer theory is applicable and the flow is indeed not controlled, b) the classical two-layer theory is not applicable and the flow is controlled, or c) the classical two-layer theory is not applicable and the flow is nevertheless not controlled.

4. Effects of Mixing and Entrainment on an Exchange Flow

4.1. Review of Single Layer Hydraulics

I will review the basics of hydraulics for a single homogeneous and uniform layer with a free surface. This is probably the most simple hydraulics type problem and has been treated in detail in many hydraulics texts (e.g. Chow, 1959; Henderson, 1966). I will summarise results first for inviscid flow and then for frictional flow. None of this is original material and its only purpose is to familiarise the reader with the concepts and notation so that the following section in which entrainment is added to the problem will be understood more easily.

4.1.1. Inviscid Flow

The problem to be considered is illustrated in figure 4.1. The basic equations of hydraulics for one layer are the inviscid, rotationless, steady state shallow water equations. If we consider a layer of fluid flowing steadily over an obstacle of slowly varying height $H(x)$ in

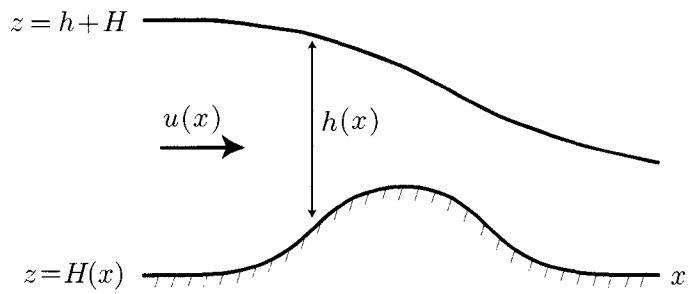

Figure 4.1.: *A single layer of fluid of depth $h(x)$ flows at speed $u(x)$ over a sill of height $H(x)$. The width of the rectangular channel is $W(x)$.*

a rectangular channel of slowly varying width $W(x)$, these equations are

$$u\frac{du}{dx} + g\frac{dh}{dx} = -g\frac{dH}{dx}\,, \tag{4.1a}$$

$$u\frac{dh}{dx} + h\frac{du}{dx} = -\frac{Q}{W^2}\frac{dW}{dx} \tag{4.1b}$$

where $Q = uhW$ is the layer transport and g is the gravitational acceleration. I will consider the problem further using two different approaches which I will refer to as Matrix Approach and Energy Approach. A third approach, which involves the speed of long waves, will be discussed in chapter 5.

Matrix Approach

The Matrix Approach examines the mathematical structure of equations (4.1) on the assumption that there is an asymmetry in the flow properties through a constriction. Following Benton (1954) and Armi (1986) the equations can be written in matrix form as

$$\mathbf{C}\mathbf{v}_\mathbf{x} = \mathbf{D}\mathbf{f}_\mathbf{x} \tag{4.2}$$

where $\mathbf{v}_\mathbf{x}$ are the derivatives of the dependent variables (u, h), $\mathbf{f}_\mathbf{x}$ are the derivatives of the independent topographic variables (H, W) and

$$\mathbf{C} = \begin{pmatrix} u & g \\ h & u \end{pmatrix}\,, \qquad \mathbf{D} = \begin{pmatrix} -g & 0 \\ 0 & -\frac{Q}{W^2} \end{pmatrix}\,. \tag{4.3}$$

We can try to solve (4.2) for the variables $\mathbf{v}_\mathbf{x}$ as functions of the variables $\mathbf{f}_\mathbf{x}$. However, solutions will exist only if $\det(\mathbf{C}) \neq 0$, or if in the neighbourhood of locations where $\det(\mathbf{C}) = 0$ certain regularity conditions are satisfied. In fact, these regularity conditions establish unique solutions; these solutions where $\det(\mathbf{C}) = 0$ are called controls since they establish these unique flows. Physically the regularity conditions are constraints on the flow which are required since the magnitude of the free-surface slope in the neighbourhood of a control is finite. The latter is an empirical fact (Armi, 1986)[1].

[1] In fact, drinking a pint of beer would be a much less enjoyable activity if the beer did not flow out of the glass with finite slope!

The last paragraph can be cast in equations as follows: after inverting the matrix $\mathbf{C}$, we find the following relations

$$\frac{1}{u}\frac{du}{dx} = \frac{\frac{hg}{W}\frac{dW}{dx} - g\frac{dH}{dx}}{u^2 - gh}\,, \tag{4.4a}$$

$$\frac{1}{h}\frac{dh}{dx} = \frac{\frac{u^2}{W}\frac{dW}{dx} - g\frac{dH}{dx}}{u^2 - gh}\,. \tag{4.4b}$$

At the controls the Froude number $F^2 = u^2/(gh) = 1$ (i.e. $\det(\mathbf{C}) = 0$) and the denominators vanish. The numerators also have to vanish (this is the regularity condition) so that velocity variation and surface slope remain finite. This gives the following conditions which determine the location of the control:

$$F^2 = \frac{u^2}{gh} = 1\,, \tag{4.5a}$$

$$\frac{dW}{dx} - \frac{g^{1/3}W^{5/3}}{Q^{2/3}}\frac{dH}{dx} = 0\,. \tag{4.5b}$$

The control fixes a relationship between layer thickness h and layer transport Q in its neighbourhood. Using $Q = uhW$ and (4.5a) we obtain

$$h = \left(\frac{Q^2}{gW^2}\right)^{1/3}\,. \tag{4.6}$$

This equation has great practical importance as it allows the determination of the layer transport Q from a measurement of layer thickness h and channel width W and vice versa.

From (4.5b) we see that for a sill alone (constant width), the flow is critical at the crest of the sill where $dH/dx = 0$. For a contraction alone (flat bottom) the flow is critical at the narrowest point where $dW/dx = 0$. For the case of both width and depth variations where sill crest and the narrowest section do not coincide, critical flow may occur at more than one point. In this case, the locations of the controls depend not only on the topography but also on the layer transport Q.

Energy Approach

Another approach to hydraulics is to classify the flow in terms of energy. This path is commonly taken in the literature on open channel hydraulics (e.g. Chow, 1959; Henderson, 1966) but is also used in many oceanography sources (e.g. Gill, 1977; Bormans, 1988; Pratt

& Lundberg, 1991). Equations (4.1) can be integrated with respect to x which leads to equations for the conservation of energy and volume flux

$$\frac{u^2}{2g} + h + H = E_R \,, \tag{4.7a}$$

$$Q = uhW = \text{const} \,. \tag{4.7b}$$

If it is assumed that the flow originates in a large reservoir, where hW tends to ∞ and the velocity u to 0 (such that Q stays finite), then E_R is the surface elevation of the reservoir. Eliminating u yields an equation for the layer thickness h,

$$\frac{1}{2}\left(\frac{Q^2}{gW^2}\right) h^{-2} + h = E_R - H \,. \tag{4.8}$$

The left hand-side has a minimum of $\frac{3}{2}\left(\frac{Q^2}{gW^2}\right)^{1/3}$ for $h = \left(\frac{Q^2}{gW^2}\right)^{1/3}$ so that, if $H_{\max}$ is the maximum height of a ridge over which the water flows, no solutions are possible if $E_R \leq H_{\max} + \frac{3}{2}\left(\frac{Q^2}{gW^2}\right)^{1/3}$. The level of the upstream reservoir is thus clearly 'controlled' at the level even if the level of a downstream basin is lowered further. It can be easily checked that for the calculated value of h the Froude number F^2 is equal to 1.

Using $F^2 = Q^2/(gW^2h^3)$ the energy equation (4.8) can be transformed into an equation for the Froude number (e.g. Benton, 1954)

$$\frac{1}{2}F^{4/3} + F^{-2/3} = (E_R - H)\left(\frac{gW^2}{Q^2}\right)^{1/3} \equiv \beta \,, \tag{4.9}$$

or into an equation for the non-dimensional layer thickness $h' = \left(\frac{W^2 g}{Q^2}\right)^{1/3} h$

$$\frac{1}{2}h'^{-1/2} + h' = (E_R - H)\left(\frac{gW^2}{Q^2}\right)^{1/3} \equiv \beta \,, \tag{4.10}$$

where $h' = F^{-2/3}$ was used by Gill (1977). β is shown as function of F^2 and h' in figure 4.2.

For a given volume flux Q and a given geometry ($W(x)$ and $H(x)$) the function β, as defined by (4.9), is only dependent on the value of E_R. As seen from figure 4.2 for a given E_R (and hence β), there are two values of F^2 and thus h' when $\beta > 3/2$, no possible values when $\beta < 3/2$, and a single value $F^2 = h' = 1$ when $\beta = 3/2$.

Both an increase of bottom height H and a decrease of the channel width W reduce the value of the right-hand side of (4.9) and force the flow towards criticality (into the

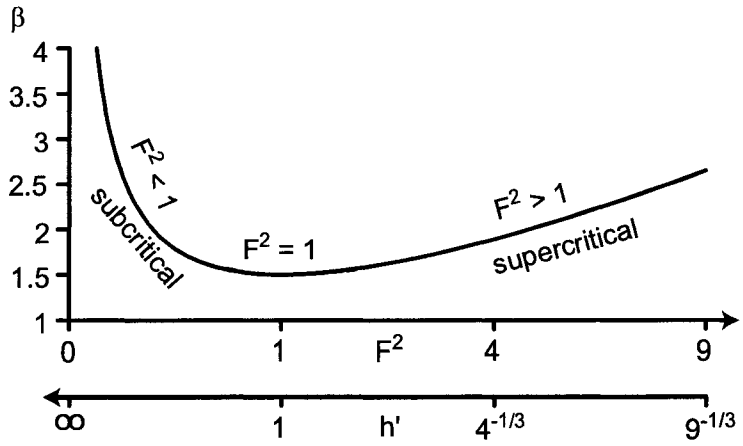

Figure 4.2.: *Relationship between* $\beta = \frac{1}{2}F^{4/3} + F^{-2/3}$ *and* F^2*, and between* β *and the non-dimensional layer thickness* h'*. The curve has two branches which meet at* $F^2 = h' = 1$ *and* $\beta = 3/2$*.*

minimum of β where $F^2 = 1$) . The flow is critical, with $F^2 = 1$, if the right-hand side equals 3/2. At that point, $d\beta/dx = 0$ and

$$W^{-1}\frac{dW}{dx} - \left(\frac{g'W^2}{Q^2}\right)^{1/3}\frac{dH}{dx} = 0\,, \tag{4.11}$$

which is identical to (4.5b) derived with the Matrix Approach.

Another useful set of equations which can be derived both from equations (4.4) and from (4.9) are the tendency equations for the layer thickness h and the Froude number F^2:

$$\frac{dh}{dx} = \frac{F^2}{1-F^2}\left(\frac{h}{W}\frac{dW}{dx} - F^{-2}\frac{dH}{dx}\right)\,, \tag{4.12a}$$

$$\frac{dF^2}{dx} = \frac{F^2}{1-F^2}\left(-(2+F^2)\frac{1}{W}\frac{dW}{dx} + \frac{3}{h}\frac{dH}{dx}\right)\,. \tag{4.12b}$$

The results show that for the present case of an inviscid single layer flow the Matrix Approach and the Energy Approach are equivalent and can be used to derive identical results.

Flow Configurations

The equations of motion (4.1) or the energy equation (4.8) are easily solved for the layer thickness along the channel. For simplicity we assume that the channel width is constant in the following discussion.

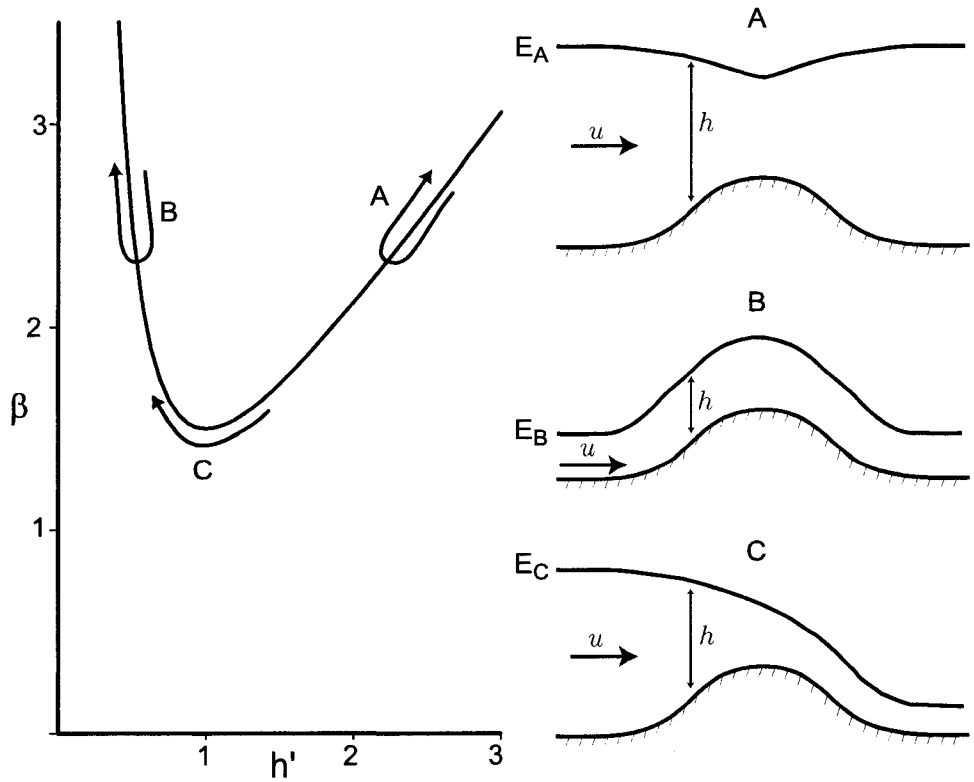

Figure 4.3.: *Sketch of function β versus non-dimensional layer thickness h' and three possible flow patterns for a single-layer flow over a sill. Arrows indicate change in β and non-dimensional layer depth in downstream direction. A: subcritical everywhere, B: supercritical everywhere, C: subcritical upstream of crest, critical at crest, and supercritical downstream of crest.*

Let us assume that far upstream E_R is large enough so that $\beta_{\min}$ is larger than 3/2, i.e. we assume that solutions exist (figure 4.3). As β varies along the channel, the nature of the flow will depend on the upstream value of h' and thus of F^2.

- **Subcritical Flow:** For $h'_{\text{ups}} > 1$, that is for $F^2_{\text{ups}} < 1$, the flow is subcritical upstream (figure 4.3 A). As it approaches the sill, the bottom height H increases and β decreases. h' decreases while F^2 increases. Note that this can also be seen from the tendency equations (4.12). At the sill crest where $H = H_{\max}$ the flow is still subcritical. Downstream of the sill, the function β will increase to its initial value, and h' and F^2 return to their upstream values. This means that the flow is subcritical everywhere and the layer depth h is large. It is symmetrical about the sill, with the surface slightly depressed over the sill (Bernoulli dimple!).

- **Supercritical Flow:** For $h'_{\text{ups}} < 1$, that is for $F^2_{\text{ups}} > 1$, the flow is supercritical upstream (figure 4.3 B). As β decreases to its minimum value, h' increases while F^2 decreases. The flow is supercritical at the sill crest. Downstream of the sill, the function β will increase to its initial value, and h' and F^2 return to their upstream values. This means that the flow is supercritical everywhere and the layer depth h is shallow compared to the layer depth for subcritical flow. The layer depth is symmetric about the sill and is maximal at the crest. Note that the supercritical solution B and the subcritical solution A may have the same value of the upstream energy E_R and therefore the same value of β_{min} ($E_A = E_B$ in the figure).

- **Critical Flow:** If we reduce the value of E_R upstream from the value E_A in figure 4.3 A, by decreasing either the depth or the current, such that $\beta_{\text{min}} = 3/2$, then $h' = F^2 = 1$ and the flow becomes critical at the sill crest (figure 4.3 C). Then the question arises as to how the flow will continue downstream of the sill. To see what happens we differentiate the tendency equation for h (4.12a) with respect to x and obtain

$$\frac{3F^2}{h}\left(\frac{dh}{dx}\right)^2 + \left(1 - F^2\right)\frac{d^2h}{dx^2} = -\frac{d^2H}{dx^2}\,. \tag{4.13}$$

At the crest $F^2 = 1$ so that the second term on the left vanishes. Because $-d^2H/dx^2 > 0$, dh/dx does not vanish at the crest. Hence, if the flow is subcritical upstream and critical at the crest, it will be supercritical just on the lee. The other mathematical possibility that the flow is supercritical upstream and subcritical downstream does not exist in reality because the flow is unstable (Long, 1954).

Note that it is not possible to further reduce the value of E_R so that $\beta_{\text{min}} < 3/2$ because then there is no solution. This means that the asymmetrical solution with subcritical flow upstream, critical flow at the crest, and supercritical flow downstream is the solution with the lowest possible energy $E = \frac{2}{3}\left(\frac{Q^2}{gW^2}\right)^{1/3} + H$.

Hydraulic Jump

Let us again consider the physical problem of flow from a larger reservoir to which fluid is supplied at a constant rate Q. Let us start with a flow that is subcritical everywhere ($F^2 < 1$, u slow and h large), see curve with energy level E_1 in figure 4.4. The surface level,

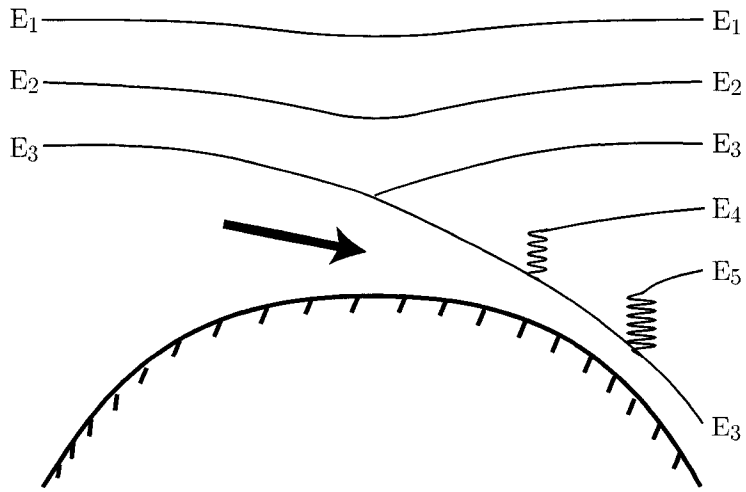

Figure 4.4.: *Examples of energy curves for different values of the downstream energy level E_R. The curve with $E_R = E_3$ is the one with the minimum upstream energy level necessary to go over the sill for given values of Q, W and H.*

and that includes the one upstream, depends on conditions applied at some downstream location, which effectively sets a surface level at some large value of x. If the downstream level is lowered (i.e. increase the drainage from the downstream reservoir), E decreases ($E_2 < E_1$), and the Bernoulli dimple deepens. Now we lower the downstream even more ($E = E_3$) such that the flow will have the minimum energy necessary to pass over the sill. The flow becomes critical at the crest. Any further decrease in E will be such that no solution exists.

Note that up to this point, the surface level in the upstream reservoir assumes the same level as is set downstream, i.e. the sill has no effect on the flow other than determining the local shape of the free surface. (I note in passing that the same applies to a flow that is supercritical everywhere. However, this is of no practical relevance here.)

If the downstream level is lowered to a very low level, e.g. on the lower downstream curve $E = E_3$, then the appropriate curve is the one with the high-level on the left ($F^2 < 1$), a smooth transition through $x = 0$ ($F^2 = 1$) and low levels on the right ($F^2 > 1$).

If the downstream level lies between the two solutions for $E = E_3$, that is for $E = E_4$ or E_5, the flow over the sill will be unaffected and will stay critical at the crest and the upstream level will still be given by E_3. However, downstream the solution has to be discontinuous. There will be a hydraulic jump connecting the solution in the downstream

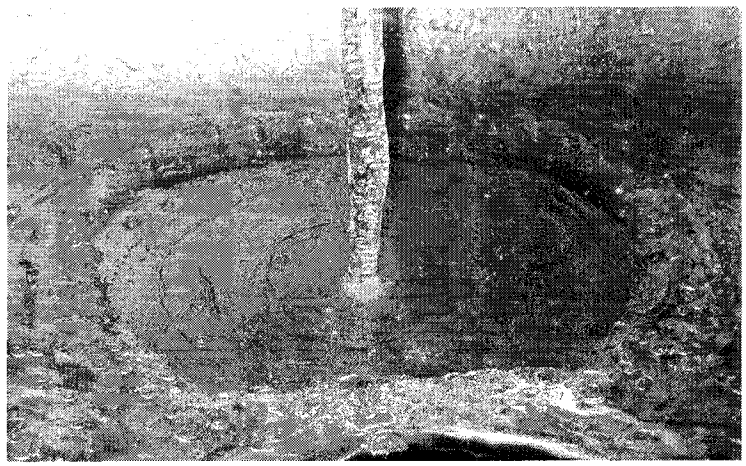

Figure 4.5.: *Rapid supercritical and tranquil subcritical radial flow produced by the impact of a jet of water on a horizontal surface. The hydraulic jump is the step in depth. Photograph by courtesy of Prof. M.S. Cramer, College of Engineering at Virginia Tech.*

to the solution immediately downstream of the crest. The hydraulic jump will dissipate energy and the loss will be proportional to the difference between E_3 and E_4. The position of the jump can be determined using the energy loss and the requirement of no change in momentum flux (Gill, 1977). The larger the energy difference between upstream and downstream reservoir, the larger the hydraulic jump and the further downstream it will be.

Note that whenever the downstream level is below the minimum value obtained for the minimum energy E_3 the upstream level is invariably given by that for $E = E_3$. Then the flow is said to be controlled by the sill at $x = 0$. The upstream level is independent of the downstream level, but is linked to the sill height. The link can be established by evaluating (4.8) at the control where (4.6) holds. The resulting relation

$$\frac{3}{2}\left(\frac{Q^2}{gW^2}\right)^{1/3} = E_R - H_C\,, \tag{4.14}$$

where H_C is the height of the sill at the crest, shows that Q and E_R cannot be varied independently of the sill height H_C.

To give the mathematics some physical reality I would like to point out that a hydraulic jump can be easily observed in the kitchen sink (figure 4.5). There the spreading of the water is equivalent to an increase in width of the flow.

Conclusion

- For an inviscid single layer flow through a constriction the Matrix Approach and the Energy Approach are equivalent.
- These approaches can be generalised to more complicated inviscid situations involving, for example, more than one layer or rotation. This was first recognised by Gill (1977). I will describe and use Gill's method in chapter 5.
- The fundamental difference between the controlled flow solution and the purely subcritical or supercritical solution lies in the role that the constriction plays in regulating the flow. In the latter case, the constriction has no influence on the flow other than modifying the shape of the surface. For the controlled flow, on the other hand, the upstream height is determined by the sill height.
- For an inviscid flow the controlled solution will be asymmetrical in some sense. This feature can be used to identify a control. The asymmetry is required since in inviscid flows the only mechanism that can dissipate energy and allow a flow to connect two different reservoir depths is the hydraulic jump. Hence, a hydraulic jump also indicates the existence of a control.

4.1.2. Frictional Single-Layer Flow

Frictional effects in open channel flow have been studied by Henderson (1966), and further explored by Pratt (1986), Bormans & Garrett (1989*b*), and Wajsowicz (1993) for the case of a single layer reduced gravity flow. In these studies the underlying assumption is that the flow can still be regarded as slab-like. Then the momentum equation is obtained by adding the term $-C_d u^2/h$ to the right-hand side of (4.1a), where friction is parameterised using a quadratic drag law in which C_d is the non-dimensional bottom drag coefficient (Pratt, 1986):

$$u\frac{du}{dx} + g\frac{dh}{dx} + g\frac{dH}{dx} = -\frac{C_d u^2}{h}\,. \tag{4.15}$$

This can be written as

$$\frac{d}{dx}\left(\frac{1}{2}\frac{u^2}{g} + h + H\right) = -C_d\frac{u^2}{gh}\,. \tag{4.16}$$

which shows that friction removes energy from the flow. There is no longer a simple functional expression connecting h to H as for the inviscid flow. However, using $Q = uhW$ and $F^2 = u^2/(gh)$ we obtain

$$\frac{d}{dx}\left\{\left(\frac{Q^2}{g'W^2}\right)^{1/3}\beta + H\right\} = -C_d F^2 \tag{4.17}$$

and hence

$$\frac{d\beta}{dx} = \frac{2}{3}\frac{3}{W}\frac{dW}{dx} - \left(\frac{g'W^2}{Q^2}\right)^{1/3}\left(\frac{dH}{dx} + C_d F^2\right), \tag{4.18}$$

where β is the hydraulic function $\frac{1}{2}F^{4/3} + F^{-2/3}$ as defined in the previous section.

The frictional term always reduces the hydraulic functional toward its minimum of 3/2 (remember figure 4.2) which means that friction acts to force the flow toward criticality, as one proceeds downstream, regardless of whether it is sub- or supercritical. At the control point $\beta = 3/2$, $d\beta/dx = 0$, and

$$W^{-1}\frac{dW}{dx} - \left(\frac{gW^2}{Q^2}\right)^{1/3}\frac{dH}{dx} = C_d\left(\frac{gW^2}{Q^2}\right)^{1/3}. \tag{4.19}$$

The control section is shifted downstream from its location in the inviscid case, as first pointed out by Henderson (1966).

The tendency of the Froude number is easily obtained from (4.18) using $\beta = \frac{1}{2}F^{4/3} + F^{-2/3}$

$$\frac{dF^2}{dx} = \frac{F^2}{1-F^2}\left\{-(2+F^2)\frac{1}{W}\frac{dW}{dx} + \frac{3}{h}\frac{dH}{dx} + \frac{3}{h}F^2 C_d\right\}, \tag{4.20}$$

confirming the conclusion from (4.18). The tendency of the layer thickness may be obtained, for instance, by writing the term in parentheses on the left-hand side of (4.16) as $(\frac{1}{2}F^2 h + h + H)$, whence

$$\frac{dh}{dx} = \frac{F^2}{1-F^2}\left(\frac{h}{W}\frac{dW}{dx} - F^{-2}\frac{dH}{dx} - C_d\right). \tag{4.21}$$

Friction causes the layer thickness h to increase in the direction of flow under supercritical conditions. When the flow is subcritical, however, the thickness decreases and, because Q = const, the velocity increases; that is friction causes the flow to accelerate! This is a curious result which seems to be at odds with intuition and the fact that friction removes energy from the flow. The physical meaning is that when the flow is subcritical, the energy is composed primarily of potential energy, the proportion of kinetic energy being small. Thus energy can effectively be removed only by removing potential energy, i.e. decreasing the layer thickness (Pratt, 1986).

Flow Configurations

I will now solve the equations of motion to obtain the layer thickness along the channel. For the sake of simplicity, I assume a channel with a constant width of $W = 1$. It is convenient to work with normalised variables of order one:

$$x^\star = x/L, \qquad h^\star = h/h_0, \qquad H^\star = H/h_0, \tag{4.22}$$
$$u^\star = u/\sqrt{gh_0}, \qquad C_d^\star = C_d \frac{L}{h_0}$$

Here, L and h_0 may be the length of the channel and the upstream layer thickness, respectively. Note that the Froude number is identical in both systems, that is $(F^\star)^2 = F^2$. Dropping the stars (*) the equations of motion are

$$u\frac{du}{dx} + \frac{dh}{dx} = -\frac{dH}{dx} - C_d\frac{u^2}{h} \tag{4.23a}$$
$$\frac{dQ}{dx} = \frac{d(uh)}{dx} = 0 \tag{4.23b}$$

Uniform Channel: The flow through a channel with a flat bottom and constant width is fully described by the equation for the surface slope

$$\frac{dh}{dx} = -C_d\left(\frac{h^3}{Q^2} - 1\right)^{-1} \tag{4.24}$$

where $Q = uh = \text{const}$. The control where $Q^2/h^3 = 1$ will be at the exit where the channel deepens or widens abruptly. Taking this to be at $x = 0$ and using $h_0 = Q^{2/3}$ the integral of (4.24) is

$$x = \frac{h}{C_d} - \frac{1}{4}\frac{h^4}{Q^2 C_d} - \frac{3}{4}\frac{Q^{2/3}}{C_d}\,. \tag{4.25}$$

Solutions for $Q = 1$ and $C_d = 0.3$ and 1.0 are shown in figure 4.6. Both frictional flows are controlled at $x = 0$ and are subcritical upstream. Friction clearly causes the surface to slope. At the control the slope becomes infinite thus violating the assumption of slowly varying flow, a problem that would disappear with realistic topography. If the flow was inviscid then the surface would be flat as indicated by the dashed lines in the figure. If we compare an inviscid solution and a frictional solution which have the same Q and the same layer thickness $h(x = -2)$, we see that, as predicted by (4.20), friction pushes the flow toward criticality whereas the inviscid flow remains subcritical.

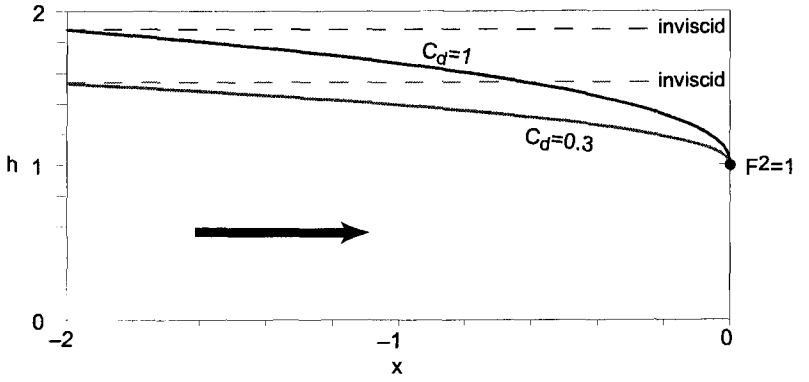

Figure 4.6.: *The scaled free surface for a single layer frictional flow through a uniform channel with exit control at $x = 0$. Red curve: $Q = 1$, $C_d = 0.3$. Blue curve: $Q = 1$, $C_d = 1$. The dashed lines show the flat surface for inviscid flows which have the same thickness as the frictional curves at $x = -2$.*

It is important to point out that the last statement applies only if we choose to prescribe Q as boundary condition. On the other hand, if upstream and downstream level are prescribed then friction will simply cause the flow to slow down and in this sense it is pushed away from criticality. This is the point of view taken by Winters & Seim (2000) as result of their numerical simulations of flow through a constriction subject to dissipation. Whether friction pushes a flow toward criticality or away from it is therefore a matter of choice of boundary conditions.

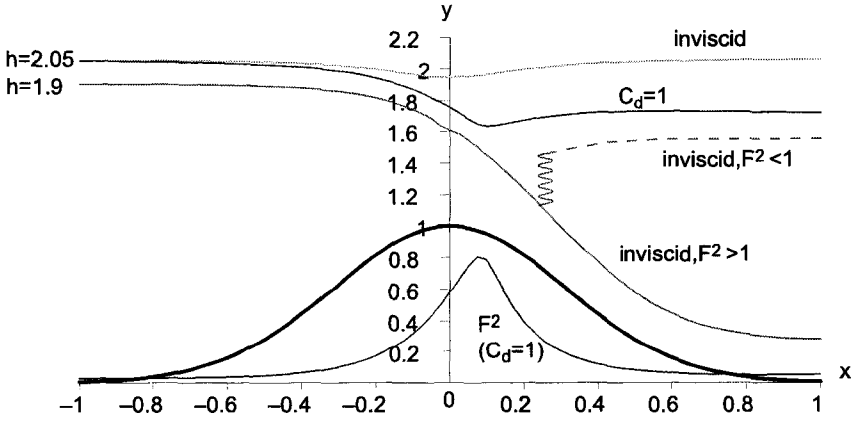

Figure 4.7.: *The scaled free surface for single layer frictional and inviscid flow over a sill. For all solutions $Q = 0.5$. Blue curves: $C_d = 0.3, h(-1) = 2.05$, the lower curve shows F^2. Green curve: $C_d = 0, h(-1) = 2.05$. Red curve: $C_d = 0, h(-1) = 1.9$.*

Flow over a Sill: For this configuration the solution was obtained numerically (Figure 4.7). The subcritical frictional solution ($C_d = 1, h(-1) = 2.05$) experiences a net decrease in elevation across the sill so that in contrast to the inviscid solution ($h(-1) = 2.05$) it is not symmetric about the sill crest. The Froude number reaches its maximum on the downstream side of the sill.

We now see that friction can cause purely subcritical flows to take on the 'overflow' character of inviscid controlled flows in which there is a net-decrease in elevation across the sill in the manner of a subcritical to supercritical transition (Pratt, 1986). In other words, whereas for inviscid flows asymmetry is a clear indicator for a control, this need not be true for frictional flow. However, asymmetry in combination with a hydraulic jump still indicates a control.

This is an issue in cases where the hydraulic state is deduced from the shape of the interface but where no flow measurements have been made to verify that the flow actually becomes critical. One example, which I mentioned already in section 2.4, is the interpretation of the change in depth of the pycnocline along the contraction in the Bosphorus as a hydraulic control (Ünlüata *et al.*, 1990; Yüce, 1996).

4.2. Single-Layer Flow with Entrainment

We are now in the position to tackle the problem of the effect of entrainment on a single layer flow. Some parts of the material in this section have been published by Gerdes, Garrett & Farmer (2002).

As before imagine a layer of fluid of density $\varrho(x)$ that flows steadily with a velocity $u(x)$ over a bottom profile of height $H(x)$ in a strait of rectangular cross-section with width $W(x)$. Above this lies a deep layer of density ϱ_0 moving with a constant velocity v (figure 4.8). Fluid from the passive upper layer is entrained into the active lower layer with an entrainment velocity u_e. Note that this situation is quite similar to that observed along the southern section of the Bosphorus if we change the active into the passive layer and vice versa.

As mentioned in section 2.2.6 the entrainment formalism assumes that the entrained water (mass and momentum) are instantly mixed across the section of the layer so that

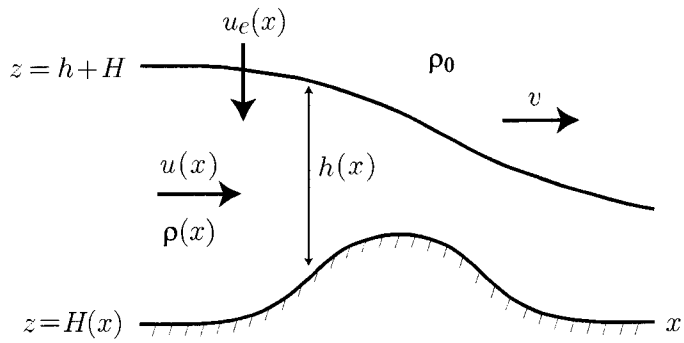

Figure 4.8.: *A single active layer of fluid of depth $h(x)$ and density $\varrho(x)$ flows at speed $u(x)$ over a sill of height $H(x)$. Fluid with density ϱ_0 is entrained with an entrainment velocity $u_e(x)$ from an overlying passive layer moving with a constant speed v.*

layer densities and velocities are constant over a layer cross-section. I will discuss this approximation at the end of this chapter.

Before delving into the mathematics I would like to point out that the problem we will consider is quite elementary: we want to know how the thickness and velocity of a single moving layer changes if it receives water of different density from somewhere. If the layer was motionless the added volume would clearly increase its thickness. It does not seem unreasonable that the same happens for a layer in motion. On the other hand, adding motionless water with zero momentum to a moving layer is very much akin to friction, and we know that the effect of that on a subcritical flow is to reduce the layer thickness. Third, if the added water has a different density, a density gradient develops which will accelerate the flow.

We will consider several increasingly complex situations. For the sake of simplicity we initially ignore friction and assume a constant channel cross section. More general results are presented subsequently.

4.2.1. Entrainment of water of the same density and zero horizontal momentum

The first problem is with no upper layer (so that $\varrho_0 = 0$) but with the entrained water having the same density as the lower layer. In this case ϱ remains constant. The problem is somewhat artificial, but describes a single layer receiving water from a sprinkler system.

The momentum equation is best derived by considering the momentum flux per unit width, given by

$$\int_0^h (\varrho u^2 + p)\, dz = \varrho \left(\frac{1}{2} g' h^2 + h u^2 \right) , \tag{4.26}$$

where $p = \varrho g'(h - z)$. (Really $g' = g$ for this problem, but let me write g' for easy comparison with other examples.) The added water has zero horizontal momentum and so the momentum flux remains constant, giving

$$\frac{1}{2} g' h^2 + h u^2 \ = \frac{1}{2} g' h_R^2 . \tag{4.27}$$

Here h_R is the layer thickness in an upstream reservoir where u approaches 0 (though this cannot actually happen with the present assumption, to be dropped later, of a constant channel width as well as flat bottom). Using $Q = uh$ and $F^2 = Q^2/(g'h^3)$ we obtain an algebraic expression relating F and Q:

$$\gamma \equiv F^{2/3} + \frac{1}{2} F^{-4/3} = \frac{1}{2} \left(\frac{g' h_R^3}{Q^2} \right)^{2/3} . \tag{4.28}$$

Although γ differs from β, which was derived for inviscid flow (figure 4.2), it also has a minimum of 2/3 at $F^2 = 1$. This means that the entrainment of fluid, which causes Q to increase, pushes the system towards criticality in a way that is similar to the effect of friction, as discussed in 4.1.2.

By differentiating (4.28) and (4.27) with respect to x we obtain expressions for the rate of change of the squared Froude number and layer thickness, respectively:

$$\frac{dF^2}{dx} = \frac{4}{Q} \frac{F^2(F^2 + 1/2)}{1 - F^2} \frac{dQ}{dx} , \tag{4.29}$$

$$\frac{dh}{dx} = -\frac{2h}{Q} \frac{F^2}{1 - F^2} \frac{dQ}{dx} . \tag{4.30}$$

Here dQ/dx is given by the entrainment velocity u_e. Note that the effect of entrainment is to decrease the layer thickness of a subcritical flow, notwithstanding the addition of entrained fluid.

4.2.2. Entrainment of lighter water with zero horizontal momentum

A more realistic situation occurs when the upper layer is less dense than the deeper, active layer. We expect that the entrained fluid of lower density will lead to a horizontal density gradient in the lower layer which will tend to accelerate the flow.

The conserved momentum flux is now

$$\int_0^{h_T} (\varrho u^2 + p)\, dz = \tag{4.31}$$

$$\varrho h u^2 + \frac{1}{2} g(\varrho - \varrho_0) h^2 + \frac{1}{2} g \varrho_0 h_T^2 \,, \tag{4.32}$$

where h_T is the height of a horizontal surface in the upper layer, with, consequently, no flux across it of horizontal momentum.

We combine $dQ/dx = u_e$ (conservation of volume) and $d(\varrho Q)/dx = \varrho_0 u_e$ (conservation of mass) to obtain $(\varrho - \varrho_0)Q = \text{const}$. It is now convenient to define $g' = g(\varrho - \varrho_0)/\varrho_0$, so that $g'Q = B^3 = \text{const}$, where B is the horizontal buoyancy flux per unit width (e.g. Turner, 1986), or

$$Q\frac{dg'}{dx} + g'\frac{dQ}{dx} = 0 \,. \tag{4.33}$$

Replacing ϱ by ϱ_0 in the first term of (4.32) (i.e. making the Boussinesq approximation) we now have

$$\frac{1}{2} g' h^2 + h u^2 = \frac{1}{2} g'_R h_R^2 \tag{4.34}$$

where g'_R , h_R are the reduced gravity and layer thickness in a fictitious reservoir. This may be rewritten as

$$F^{2/3} + \frac{1}{2} F^{-4/3} = \frac{1}{2} g'_R h_R^2 (QA)^{-1} \,, \tag{4.35}$$

whence

$$\frac{dF^2}{dx} = \frac{3}{Q} \frac{F^2(F^2 + 1/2)}{1 - F^2} \frac{dQ}{dx} \,. \tag{4.36}$$

As before entrainment acts to force the flow towards criticality, but at a slower rate than in (4.29), because of the presence of a density gradient.

The density gradient has a remarkable effect on the slope of the interface. In contrast to (4.30) we now obtain

$$\frac{dh}{dx} = -\frac{2h}{Q} \frac{F^2 - 1/4}{1 - F^2} \frac{dQ}{dx} \,. \tag{4.37}$$

For $F^2 < 1/4$ the layer thickness h increases instead of decreasing, even though the system is forced towards criticality, whereas for $F^2 > 1/4$ the layer thickness decreases. This may be clarified by considering the particular case of $F^2 = 1/4$. In this case the pressure gradient associated with the density gradient is just great enough to accelerate the flow and thus transport the entrained water downstream, such that the layer thickness remains constant.

4.2.3. Entrainment of lighter water with non-zero horizontal momentum

Finally, consider the case where the upper layer is moving with a constant velocity v. It can be shown that treating c as constant is a good approximation provided that the upper layer is much thicker than the lower layer. The fluid entrained into the lower layer has non-zero horizontal momentum and the lower layer momentum changes accordingly.

Starting with (4.31) as before and using conservation of volume, i.e. $hu + (h_T - H)v = \text{const} \Longrightarrow hv = hu + h_T v - \text{const}$, we obtain

$$\varrho h u^2 + \frac{1}{2} g(\varrho - \varrho_0) h^2 - \varrho_0 huv = \text{const}\,. \tag{4.38}$$

in place of (4.32), so that, with the Boussinesq approximation as before,

$$hu^2 + \frac{1}{2} g' h^2 = \frac{1}{2} g'_R h_R^2 + Qv \tag{4.39}$$

in place of (4.34). The derivative of this is

$$\frac{d}{dx}\left(hu^2 + \frac{1}{2} g' h^2\right) = v \frac{dQ}{dx}\,, \tag{4.40}$$

showing how the momentum flux of the active layer is changed by the entrainment of moving water. The extension of (4.35) is

$$F^{2/3} + \frac{1}{2} F^{-4/3} = \frac{1}{2} g'_R h_R^2 \,(QA)^{-1} + vA^{-1}\,, \tag{4.41}$$

where $g'Q = B^3$ is still constant.

The extensions of (4.36) and (4.37) are

$$\frac{dF^2}{dx} = \frac{3}{Q} \frac{F^2(F^2 + \frac{1}{2} - \frac{v}{u} F^2)}{1 - F^2} \frac{dQ}{dx}\,, \tag{4.42}$$

$$\frac{dh}{dx} = -\frac{2h}{Q} \frac{F^2 - \frac{1}{4} - \frac{1}{2}\frac{v}{u} F^2}{1 - F^2} \frac{dQ}{dx}\,. \tag{4.43}$$

It follows from (4.42) and (4.43) that the results for exchange flows ($v < 0$) are qualitatively similar to those obtained for $v = 0$. The magnitude of both dh/dx and dF^2/dx will be larger for $v < 0$ as the entrainment of negative momentum has an effect similar to that of additional friction.

For unidirectional flows v is positive. In principle dF^2/dx may change sign when v exceeds a certain value:

$$\frac{v}{u} = 1 + \frac{1}{2} F^{-2}\,. \tag{4.44}$$

The ratio v/u is $3/2$ when the flow is critical. As $F^2 > 1$ increases, v/u approaches unity, but rapidly increases for $F^2 < 1$ decreasing. In most examples of subcritical flow, one might expect the upper layer velocity to be not much larger than the lower layer velocity, so that dF^2/dx is unlikely to become negative. This means that for most unidirectional flows entrainment acts to force the flow towards criticality.

For entrainment of zero momentum fluid we found that the interface slopes upwards if $F^2 < 1/4$. For non-zero momentum of the upper layer the interface slopes upward if $F^2 < \frac{1}{4}\,(1 - \frac{1}{2}\,\frac{v}{u})^{-1}$ and is flat if

$$\frac{v}{u} = 2 - \frac{1}{2}F^{-2}\,. \tag{4.45}$$

Hence for $v > 0$ the slope dh/dx can be zero for Froude numbers larger than 0.5. The physical reason is that the entrained positive momentum supports the density gradient in accelerating the flow, so that the required density gradient can be smaller and correspondingly the Froude number can be larger for conditions of zero slope.

4.2.4. Flow Configuration

Evaluation of the layer properties as a function of the channel coordinate x, requires that (4.43) be evaluated simultaneously with $dQ/dx = u_e$ subject to given initial conditions in the upstream reservoir. The two equations are coupled and need to be solved iteratively because the entrainment velocity u_e is a function of some mean layer properties, usually involving the Froude number. For the sake of simplicity let us assume $v = 0$ in the following discussion.

We may relate u_e/u to the Froude number through an appropriate entrainment law. For example, Christodoulou (1986) proposes

$$\frac{u_e}{u} = C_E\,\mathrm{Ri}_b^{-1} = 0.002\,\mathrm{Ri}_b^{-1}\,, \quad \text{for} \quad 0.1 < \mathrm{Ri}_b < 10\,, \tag{4.46}$$

where C_E is the entrainment coefficient, and $\mathrm{Ri}_b = g'h/(\Delta u)^2$ is the bulk Richardson number with Δu the velocity difference between the layers. Then $\mathrm{Ri}_b = F^{-2}$ so that $u_e/u = 0.002\,F^2$. The factor $C_E = 0.002$ is empirically determined from water tunnel data and is subject to considerable uncertainty.

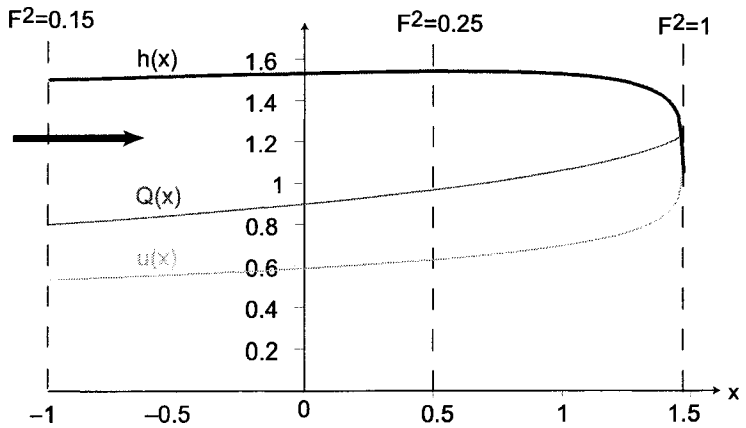

Figure 4.9.: *Solution of the non-dimensionalised equations of motion* (4.48) *for a uniform channel. The initial conditions at* $x = -1$ *are* $h = 1.5$ *and* $Q = 0.8$. *The entrainment coefficient is* $C_E = 1$. *The Froude number* F^2 *is equal to* u^3.

As for the case of the frictional flow, it is convenient to work with normalised variables:

$$x^\star = \frac{x}{L}, \qquad h^\star = \frac{h}{h_0}, \qquad H^\star = \frac{H}{h_0}, \tag{4.47}$$
$$u^\star = \frac{u}{B}, \qquad u_E^\star = \frac{u_E}{B}\frac{L}{h_0}, \qquad C_E^\star = C_E\frac{L}{h_0}.$$

Here, velocities are normalised using the third root of the buoyancy flux B^3. Note the following convenient relations: a) $(u^\star)^3 = (F^\star)^2 = F^2$, b) $g'^\star = 1/Q^\star$, and c) $B = \sqrt{g'_C h_C}$ where the subscript C indicates that the last relation is valid only at a control where $F^2 = 1$. Dropping the stars (*) a suitable set of equations of motion is

$$\frac{dQ}{dx} = C_e\frac{Q^4}{h^4}, \tag{4.48a}$$
$$\left(1 - \frac{Q^3}{h^3}\right)\frac{dh}{dx} = -\frac{dH}{dx} - 2\frac{dQ}{dx}\left(\frac{Q^2}{h^2} - \frac{1}{4}\frac{h}{Q}\right). \tag{4.48b}$$

The solution of (4.48) for a uniform channel is shown in figure 4.9. At $x = -1$ the flow is subcritical with $F^2 < 1/4$. Layer transport Q and velocity u (and hence F^2) increase steadily. The interface rise slowly until the point where $F^2 = 1/4$. Afterwards it decreases. At the control the interface slope becomes infinite which is an artefact of the unrealistic topography.

Note that a different relation between entrainment velocity and Froude number than (4.46) will give quantitatively different solutions, especially at locations where $F^2 \approx 1$.

4.2.5. Summary

- In all but one case it was found that entrainment acts to force the flow towards criticality in just the same way as friction. The exception is the unidirectional flow that occurs when the upper layer velocity is larger than the lower layer velocity by a certain, Froude number dependent, margin.

- For the artificial example in which the entrained fluid has the same density as the active layer, the layer thickness decreases for subcritical flow and increases for supercritical flow. If less dense fluid is entrained, the layer thickness increases for subcritical flow with $F^2 < 1/4$ (for $v = 0$).

- In (4.43) the entrainment term $-\frac{u_e}{u}(2 - \frac{v}{u} - \frac{1}{2}F_2^{-2})$ has a somewhat subtle interpretation. The combination of the first two terms represents the exchange of mass and momentum. For exchange flows with $v/u < 0$ it is always positive. The third term is always negative. It represents the contribution to the pressure gradient due to variations of the lower layer density. The entrainment of upper layer fluid causes the lower layer density to decrease in the direction of flow and hence to accelerate the flow. In terms of pressure, the effect is the same as if the interface elevation decreased in the direction of flow. However, only for very small Froude numbers does the third term dominate the first two. Hence, under most circumstances entrainment will cause a negative interface slope just like friction.

- Results with entrainment have been presented for zero friction and constant channel cross-section. However friction and variable cross-section can easily be included, thus combining the effects analysed separately here and in sections 4.1.1 and 4.1.2. The rate of change of the Froude number is given by

$$\frac{dF^2}{dx} = \frac{F^2}{1-F^2}\left\{\frac{3}{h}\frac{u_e}{u}\left(F^2 + \frac{1}{2} - \frac{v}{u}F^2\right)\right. \\ \left. -(2+F^2)\frac{1}{W}\frac{dW}{dx} + \frac{3}{h}\frac{dH}{dx} + \frac{3}{h}F^2 C_d\right\}, \tag{4.49}$$

where $Q = uhW$ and $dQ/dx = u_e W$ was used. This equation is equivalent to (4.18) if $u_e = 0$ and to (4.42) if W and H are constant and $C_d = 0$. The interface slope is

given by

$$\frac{dh}{dx} = \frac{F^2}{1-F^2}\left\{-2\frac{u_e}{u}\left(1-\frac{1}{4}F^{-2}-\frac{1}{2}\frac{v}{u}\right) + \frac{h}{W}\frac{dW}{dx} - F^{-2}\frac{dH}{dx} - C_d\right\}, \tag{4.50}$$

which reduces to (4.21) and (4.43) in the appropriate limits. In the derivation of these results it was assumed that the upper layer speed v is constant. This is really only possible if the channel width W is also constant. Consequently (4.49) and (4.50) with $dW/dx \neq 0$ seems to be valid only if $v = 0$.

- With $v = 0$ the ratio of the entrainment term and friction term is $\frac{0.002}{C_d}(F^2 + \frac{1}{2})$ and $\frac{0.004}{C_d}(F^2 - \frac{1}{4})$ in (4.49) and (4.50), respectively. For $C_d = 10^{-3}$ (Pratt, 1986) this suggests that the effects of entrainment and friction on the flow can be of roughly equal importance.

- I have shown in section 4.1.2 that bottom friction displaces the control downstream (e.g. Henderson, 1966; Pratt, 1986). The same is true for entrainment. Assuming constant width and a motionless upper layer, dh/dx remains bounded for $F^2 = 1$ only if

$$\frac{dH}{dx} = -C_d - \frac{3}{2}\frac{u_e}{u}. \tag{4.51}$$

  Using $C_d = 10^{-3}$ and (4.46) we find that the control location is displaced farther than in the case of friction alone. A sill must then be sufficiently steep on its lee side for control to be possible. Hence entrainment can totally inhibit control that would otherwise occur in an inviscid or purely frictional flow.

- Finally, we see that entrainment just as friction can cause purely subcritical flows to become asymmetric (see section 4.1.2), at least if $1/4 < F^2 < 1$ for $v = 0$. Since entrainment and friction are likely to occur together in real flows, this effect might be quite significant.

- I have arbitrarily assumed the upper and lower layer to be passive and active, respectively, but it is clear that the results are easily modified to apply to an active upper and passive lower layer with upward entrainment, recognising that the bottom

topography underlying the passive lower layer has no influence on the active layer. This would then be approximately the situation in the southern Bosphorus.

The theory does not apply, however, if entrainment is from an active into a passive layer, or if both layers are active with simultaneous upward and downward entrainment. These cases require a two-layer theory which is presented in the next section. The two-layer theory will also clarify the conditions under which a layer can assumed to be passive; in this section a layer was assumed passive provided it was deep and had a constant velocity. This seems intuitively plausible. On the other hand, with the theory of this section it is not possible to evaluate how deep the passive layer needs to be so that its velocity will remain sufficiently constant - despite the loss of fluid due to entrainment.

4.3. Two-Layer Flow with Entrainment

The main motivation for developing a two-layer theory was provided by the wish to understand the flow in the Contraction and at the South Sill in the Bosphorus. There upper and lower layers frequently have similar Froude numbers so that a clear distinction between active and passive is not given. Furthermore, although upward entrainment seems to dominate, some downward entrainment occurs and this might need to be taken into account.

4.3.1. Formulation of the Model

The two-layer formalism I am going to use is fairly standard. Starting equations, similar to those that I will be using, can be found in (Grubert & Abbott, 1972) or (Pedlosky, 1996, chapter 4). However, note that Grubert & Abbott (1972) and Pedlosky (1996) ignore interfacial friction and the density gradient, respectively. Because mixing has somewhat subtle effects particularly on the momentum balance it is worthwhile considering these carefully, and I will therefore present the derivations in some detail. The situation is sketched in figure 4.10.

The starting equations describing conservation of volume, mass and momentum are

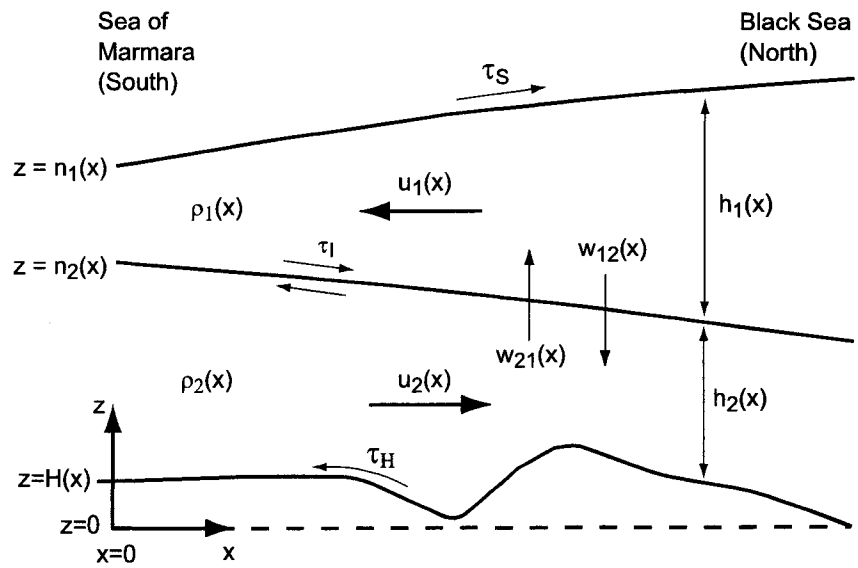

Figure 4.10.: *Basic flow configuration. The x-axis is positive toward the Black Sea, and the z-axis positive upwards. Layers of fluid of thickness $h_i(x)$, density $\varrho_i(x)$ flow at speed $u_i(x)$ over a bottom of height $H(x)$. The channel width is $W(x)$. Subscripts 1 and 2 indicate upper and lower layer, respectively. τ_S, τ_I, and τ_H represent surface, interface and bottom/side-wall friction, respectively. Mixing across the interface is represented by entrainment velocities w_{12} (downward) and w_{21} (upward), which are both understood to be positive. Note that layer velocities and volume fluxes are positive (negative) if their are towards the Black Sea (Sea of Marmara).*

most easily understood when written in flux form. For conservation of volume we have

$$\frac{d(u_1 A_1)}{dx} = W_I \left(w_{21} - w_{12}\right), \tag{4.52a}$$

$$\frac{d(u_2 A_2)}{dx} = W_I \left(w_{12} - w_{21}\right), \tag{4.52b}$$

where A_1 and A_2 are the cross-sectional areas of upper and lower layer, respectively, and W_I is the width of the channel at the interface. W_I may vary with interface depth if the channel has non-rectangular cross-section. Conservation of mass may be written as

$$\frac{d(\varrho_1 u_1 A_1)}{dx} = W_I \left(\varrho_2 w_{21} - \varrho_1 w_{12}\right) \tag{4.53a}$$

$$\frac{d(\varrho_2 u_2 A_2)}{dx} = W_I \left(\varrho_1 w_{12} - \varrho_2 w_{21}\right). \tag{4.53b}$$

Note that if upward and downward transport exactly cancel, there is no change of layer volume, but there may still be a change in density in both layers. Hence it does not suffice

to use only a net entrainment velocity $w \equiv (w_{12} - w_{21})$. We need to distinguish between upward and downward entrainment.

The mixing process not only exchanges mass but also momentum between the layers. The rate of change of momentum flux is given by

$$\frac{d(\varrho_1 u_1^2 A_1)}{dx} = W_I\,(\varrho_2 u_2 w_{21} - \varrho_1 u_1 w_{12}) - A_1 \frac{dP_1}{dx} - A_1 \varrho_1 (\tau_S + \tau_{I1} + \tau_{W1}) \tag{4.54a}$$

$$\frac{d(\varrho_2 u_2^2 A_2)}{dx} = W_I\,(\varrho_1 u_1 w_{12} - \varrho_2 u_2 w_{21}) - A_2 \frac{dP_2}{dx} - A_2 \varrho_2 (-\tau_{I2} + \tau_{W2} + \tau_{H2})\,. \tag{4.54b}$$

τ_S, τ_I, τ_W, and τ_H denote the friction terms at the surface, interface, side-walls, and bottom (Bormans & Garrett, 1989*b*), respectively, and $\frac{dP_k}{dx}, k = 1, 2$ the layer averaged horizontal pressure gradients. The left-hand sides of (4.54) represent the change of horizontal momentum flux over an infinitesimal distance δx. This change is caused by the flux of horizontal momentum across the interface (1st term on rhs), by horizontal pressure gradients (2nd term on rhs), and by frictional forces (3rd term on rhs).

Note that the set of equations (4.52), (4.53), and (4.54) can be solved numerically as soon as the friction terms and entrainment velocities have been parameterised and appropriate boundary conditions have been specified (e.g., Grubert & Abbott, 1972; Oğuz *et al.*, 1990). My approach is different as I will not integrate the equations but use them as diagnostic tools to predict the local rate of change of layer thickness and Froude number.

It is convenient to recast the equations in Eulerian form. Using (4.52) we obtain from (4.53)

$$u_1 \frac{d\varrho_1}{dx} = \frac{W_I}{A_1} w_{21} (\varrho_2 - \varrho_1)\,, \tag{4.55a}$$

$$u_2 \frac{d\varrho_2}{dx} = \frac{W_I}{A_2} w_{12} (\varrho_1 - \varrho_2)\,. \tag{4.55b}$$

and from (4.54)

$$u_1 \frac{du_1}{dx} = \frac{\varrho_2}{\varrho_1} \frac{W_I}{A_1} w_{21} (u_2 - u_1) - \frac{1}{\varrho_1} \frac{dP_1}{dx} - (\tau_S + \tau_{I1} + \tau_{W1})\,, \tag{4.56a}$$

$$u_2 \frac{du_2}{dx} = \frac{\varrho_1}{\varrho_2} \frac{W_I}{A_2} w_{12} (u_1 - u_2) - \frac{1}{\varrho_2} \frac{dP_2}{dx} - (-\tau_{I2} + \tau_{W2} + \tau_{H2})\,. \tag{4.56b}$$

Interestingly (4.53) and (4.54) contain both upward and downward transport terms, whereas (4.55) and (4.56) contain only either the upward or downward transport term. The explanation is as follows: we ignore friction and pressure gradients and assume we

have only downward entrainment ($w_{21} = 0$). Then (4.53a) and (4.54a) show that the upper layer loses mass and momentum, respectively. However, losing some of its fluid does not change the density of the upper layer as shown by (4.55a). And although the total momentum of the layer changes, (4.56a) shows that there is no change produced in the momentum density (momentum per unit mass) by motion out of the layer. Momentum leaves the layer, but as it leaves the density of the momentum remains unchanged[2].

The integrated horizontal pressure gradients per unit mass and unit area are given by

$$\frac{1}{\varrho_1}\frac{dP_1}{dx} = g\left(\frac{d\eta_1}{dx} + \frac{h_1}{2\varrho_1}\frac{d\varrho_1}{dx}\right), \tag{4.57a}$$

$$\frac{1}{\varrho_2}\frac{dP_2}{dx} = g\left(\frac{\varrho_1}{\varrho_2}\frac{d\eta_1}{dx} + \frac{\varrho_2-\varrho_1}{\varrho_2}\frac{d\eta_2}{dx} + h_1\frac{1}{\varrho_2}\frac{d\varrho_1}{dx} + \frac{h_2}{2\varrho_2}\frac{d\varrho_2}{dx}\right). \tag{4.57b}$$

where I have made the simplifying assumption that the channel has a rectangular cross-section and write W instead of W_I for the channel width. The pressure gradient in the upper layer is caused by the sea surface slope and by the density gradient in the upper layer. The pressure gradient in the lower layer additionally depends on the interface slope and on the lower layer density gradient.

Inserting (4.57) into (4.56) and then subtracting (4.56b) from (4.56a) yields an equation for the relative acceleration between the two layers

$$\begin{aligned} u_1\frac{du_1}{dx} - u_2\frac{du_2}{dx} = (u_2-u_1)\left(\frac{\varrho_2}{\varrho_1}\frac{w_{21}}{h_1} + \frac{\varrho_1}{\varrho_2}\frac{w_{12}}{h_2}\right) - g\frac{\varrho_2-\varrho_1}{\varrho_2}\left(\frac{d\eta_1}{dx} - \frac{d\eta_2}{dx}\right) \\ - g\left(h_1\left(\frac{1}{2\varrho_1} - \frac{1}{\varrho_2}\right)\frac{d\varrho_1}{dx} - h_2\frac{1}{2\varrho_2}\frac{d\varrho_2}{dx}\right) - \tau_0\,. \end{aligned} \tag{4.58}$$

Here all friction terms have been combined into $\tau_0 \equiv \tau_S + \tau_{I1} + \tau_{W1} + \tau_{I2} - \tau_{W2} - \tau_{H2}$. Since the horizontal density gradients are a consequence of mixing, it is possible to express them in terms of the entrainment velocities. Using (4.55) we obtain

$$\begin{aligned} u_1\frac{du_1}{dx} - u_2\frac{du_2}{dx} = (u_2-u_1)\left(\frac{\varrho_2}{\varrho_1}\frac{w_{21}}{h_1} + \frac{\varrho_1}{\varrho_2}\frac{w_{12}}{h_2}\right) - g\frac{\varrho_2-\varrho_1}{\varrho_2}\left(\frac{d\eta_1}{dx} - \frac{d\eta_2}{dx}\right) \\ - g\left(\frac{w_{21}}{u_1}\left(\frac{\varrho_2-\varrho_1}{2\varrho_1} - \frac{\varrho_2-\varrho_1}{\varrho_2}\right) + \frac{w_{12}}{u_2}\frac{\varrho_2-\varrho_1}{2\varrho_2}\right) - \tau_0\,. \end{aligned} \tag{4.59}$$

[2]The situation is similar to that of a train with passengers and baggage, all moving at speed u. If the passengers begin to throw baggage sideways out of the windows the total momentum of the train is decreased by the loss of mass but the train does not slow down. The loss of luggage has not altered the momentum per unit mass. Similarly, the loss of upper layer fluid does not alter the budget for momentum per unit mass (4.56a) but does alter the budget for total momentum (4.54a).

In the Bosphorus, as in most other straits, we are well justified in ignoring density variations of the order of $(\varrho_2 - \varrho_1)/\varrho_2$ and applying the rigid lid approximation. Then the equation for the relative acceleration between the two layers reads

$$u_1\frac{du_1}{dx} - u_2\frac{du_2}{dx} - g'\frac{d\eta_2}{dx} = (u_2 - u_1)(\frac{w_{21}}{h_1} + \frac{w_{12}}{h_2}) - \frac{g'}{2}\left(\frac{w_{12}}{u_2} - \frac{w_{21}}{u_1}\right) - \tau_0\,. \tag{4.60}$$

The first term on the right-hand side describes the effects of the exchange of momentum between the layers. The second term originates from the horizontal density gradients.

4.3.2. Local Change of Layer Thickness

Using (4.52) it is analytically straightforward, albeit tedious, to transform (4.60) into an equation for the local change of layer thickness. I write the expression in such a way that it is easily simplified for cases of small upper or lower layer Froude numbers:

$$\begin{aligned}\frac{dh_2}{dx} = &\frac{1}{1 - F_1^2 - F_2^2}\\ &\times\left\{(F_1^2 - 1)\frac{\partial H}{\partial x} - \frac{h_1F_1^2 - h_2F_2^2}{W}\frac{\partial W}{\partial x} + \frac{\tau_0}{g'}\right.\\ &+ w_{21}\frac{2F_1^2}{u_1}\left(1 - \frac{1}{2}\frac{u_2}{u_1} + \frac{1}{2}\frac{u_1}{u_2}\frac{F_2^2}{F_1^2} - \frac{1}{4}F_1^{-2}\right)\\ &\left. - w_{12}\frac{2F_2^2}{u_2}\left(1 - \frac{1}{2}\frac{u_1}{u_2} + \frac{1}{2}\frac{u_2}{u_1}\frac{F_1^2}{F_2^2} - \frac{1}{4}F_2^{-2}\right)\right\}\,.\end{aligned} \tag{4.61}$$

Here, I have arbitrarily chosen to present the change of the lower layer thickness, however, the change of the upper layer thickness is easily obtained using the rigid-lid approximation $d(H + h_2 + h_1)/dx = 0$.

dh_2/dx depends in a somewhat complicated way on changes in bottom elevation and channel width, on frictional effects, and on upward and downward entrainment. In what follows I will give physical meaning to (4.61) by discussing special cases.

Inviscid Flow

In the absence of friction ($\tau_0 = 0$) and entrainment ($w_{12} = w_{21} = 0$) we recover the steady differential solution for inviscid two-layer flows (See eqs. (A8) Armi, 1986). It can be integrated and possible flow solutions can be shown as curves in the Froude-number plane. Note that in a two-layer flow the composite Froude number $G^2 = F_1^2 + F_2^2$ in (4.61)

takes on the role of the single layer Froude number F^2 in (4.12a), that is critical conditions occur wherever $G^2 = 1$. A rigorous discussion is given, for instance, by Benton (1954), Armi (1986) and Lawrence (1990).

Frictional Flow

Results for the case where entrainment is absent but the flow is subject to interfacial and side-wall friction have been shown by Assaf & Hecht (1974) for a channel with constant trapezoidal cross-section (figure 4.11). The agreement between predicted and observed depths of the interface along the strait is, perhaps, surprisingly good considering that entrainment is not taken into account. The reason might be that Assaf & Hecht (1974) use rather large friction coefficients of $C_I = 1.2 \times 10^{-3}$ and $C_H = 15 \times 10^{-3}$ which are about an order of magnitude larger than commonly accepted values (Like those we will use later in section 4.4, p. 110). By doing so they partly account for the exchange of momentum due to mixing. Furthermore, their model is clearly limited in its neglect of width and depth variations; for instance, the interfacial slope becomes unrealistically steep at the controls because of the assumed abrupt deepening or widening of the channel. Also, numerical experimentation with Assaf & Hecht's constant topography model shows that the change in position of the interface, in response to reasonable variations of the net exchange or the friction coefficients, would hardly be observable, presumably because the control conditions very much define the interface depths at the strait's exits. Bormans & Garrett (1989*b*) avoided this problem in their study of the Strait of Gibraltar by using realistic topography. On the other hand, the salinity ratio S_1/S_2 appears to be a more sensitive and, hence, would be a more useful quantity for comparison, but can, in fact, not be used for comparison with the data from the Bosphorus because Assaf & Hecht's model ignores mixing.

The, nevertheless, important conclusion from Assaf & Hecht's study is that friction causes the interface to slope along the channel. Hence, there is a significant change in the thickness of each layer along the strait so that at each end one layer will be much thinner than the other. In the neighbourhood of the exit controls the flow will thus resemble that of a reduced gravity flow with one active and one passive layer.

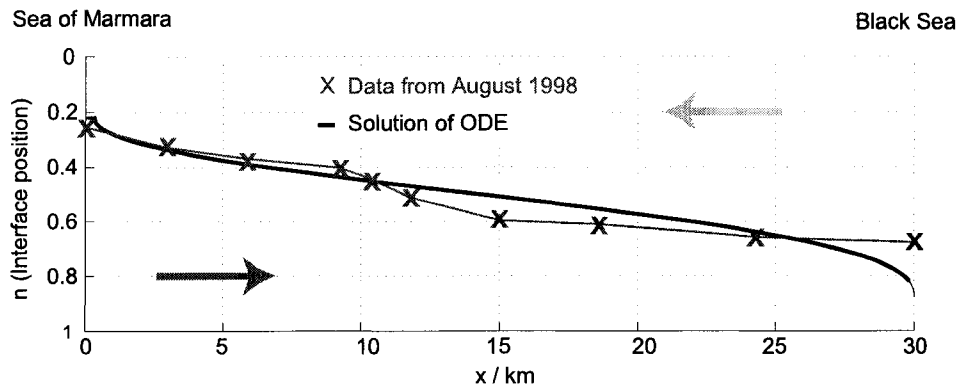

Figure 4.11.: *Black line: Assaf & Hecht (1974) solution for the depth of the interface ($n = A_1/(A_1 + A_2)$) along the Bosphorus. The trapezoidal cross-section was assumed to be constant. The net exchange and coefficients for interfacial and bottom friction were prescribed, and controls with $G^2 = 1$ were assumed at both channel exits. Line with crosses: Approximate depth of the interface based on our observations from August 1998.*

Entrainment From a Passive Upper Into an Active Lower Layer

This is the single-layer situation analysed in section 4.2. Assuming $F_1^2 \ll 1$ and $w_{21} = 0$, (4.61) immediately simplifies to (4.50). However, note that in order to derive (4.50) in the framework of the single-layer theory it was necessary to assume a motionless upper layer. We see now that this condition is unnecessarily strict and that $F_1^2 \ll 1$ is sufficient. Furthermore, (4.61) clarifies our assumption of a "passive" upper layer used in section 4.2: the upper layer can be considered passive if the layer velocities and layer thicknesses are such that (4.61) is well approximated by (4.50). For practical applications this statement is more useful than the requirement $F_1^2 \ll 1$.

Entrainment From a Passive Lower Into an Active Upper Layer

The equations for the case of upward entrainment from a passive lower layer ($F_2^2 \ll 1$) into an active upper layer are obtained from (4.61) for $F_2^2 \ll 1$

$$\frac{dh_1}{dx} = \frac{F_1^2}{1 - F_1^2}\left\{\frac{h_1}{W}\frac{dW}{dx} - \frac{\tau_0}{g'}F_1^{-2} - \frac{w_{21}}{u_1}\left(2 - \frac{u_2}{u_1} - \frac{1}{2}F_1^{-2}\right)\right\} \tag{4.62}$$

where $\frac{dh_1}{dx} = -\frac{\partial(H+h_2)}{\partial x}$ was used, and

$$\frac{dF_1^2}{dx} = \frac{F_1^2}{1-F_1^2}\left\{-(2+F_1^2)\frac{1}{W}\frac{dW}{dx} + \frac{3}{h_1}\frac{\tau_0}{g'} + \frac{3}{h_1}\frac{w_{21}}{u_1}\left(F_1^2 - \frac{u_2}{u_1}F_1^2 + \frac{1}{2}\right)\right\}, \tag{4.63}$$

where the total friction τ_0 is the sum of interfacial, side-wall and surface friction. As anticipated bottom topography lying within the passive layer has no influence on the active upper layer

Detrainment from an active lower into a passive upper layer

Recall that an important assumption in the two previous cases is that fluid is entrained from the passive layer into the active layer. According to standard entrainment laws this would appear to be the most usual case (Christodoulou, 1986). However, it has been shown that entrainment from the active to the passive layer can dominate in rapidly accelerating flows over sills (Farmer & Armi, 1999). Hence let us consider the case of an active lower layer that is ejecting fluid ($w_{12} = 0$ and $w_{21} > 0$) into an upper passive ($F_1^2 \ll 1$) layer that is thicker than the lower layer ($h_1 > h_2$). It might be more appropriate to call this process detrainment rather than entrainment.

The simplification of (4.61) is mathematically a bit more involved and is therefore presented in detail in appendix E. The result is

$$\frac{dh_2}{dx} = \frac{F_2^2}{1-F_2^2}\left\{-\frac{dH}{dx}F_2^{-2} + \frac{h_2}{W}\frac{dW}{dx} - C_H + \frac{w_{21}}{u_1}\left(\frac{u_1}{u_2} - \frac{1}{2}F_2^{-2}\right)\right\}. \tag{4.64}$$

The topographic and frictional influence on h_2 is the same as in (4.50). However, the detrainment term consists of only two components, because detrainment does not change the momentum density as pointed out earlier.

The term w_{21}/u_2 represents the loss of volume. For a subcritical flow this causes the layer thickness to increase notwithstanding the removal of fluid[3]. If the flow is supercritical the layer thickness decreases.

[3]Note that this term is also present if we consider the case of a single layer ejecting water into the air above. Then g' or rather g would be constant. From $d(uh)/dx = -w$, $u\,du/dx + g\,dh/dx = 0$ and $g = const$, we obtain $dh/dx = F^2/(1-F^2)\,w/u$.

The second term $(-\frac{1}{2}\frac{w_{21}}{u_1}F_2^{-2})$ represents the change of the density ratio between the two layers. In an exchange flow u_1 is negative. Then the upper layer density increases (approaching ϱ_2) and g' decreases with decreasing x. According to (4.64) this causes the layer thickness of a subcritical flow to increase in the direction of the lower layer flow. The magnitude of this effect is inversely proportional to the upper layer velocity for if it moves fast, detrainment causes only a small change of ϱ_1 over a given distance, but if it moves slowly the change in ϱ_1 will be large.

If u_1 is positive the two components of the detrainment term, which we can rewrite as

$$w_{21}\left(\frac{1}{u_2} - \frac{1}{2u_1}F_2^{-2}\right) ,$$

have opposite sign. The overall effect of detrainment depends on the magnitude of u_1 and F_2^2. We are assuming that $u_1 < u_2$. For example, for $u_1 = u_2/5$ the sum of the terms is negative unless $F_2^2 > 2.5$. This means that for subcritical to critical flows the effect of the loss of volume is small compared to that due to the decrease of g' and may be ignored[4]. On the other hand, for highly supercritical flow the loss of fluid must be taken into account.

It is interesting to compare these predictions with observations of the effects of detrainment on the flow over a sill in Knight Inlet (Farmer & Armi, 1999). There a relatively homogeneous active layer descends beneath a passive layer in which the density varies with position due to detrainment from the lower into the upper layer, as shown in their figures 7d and 13. Upper and lower layer velocity are both positive. Downstream of the sill crest, where $F_2^2 = 1$, the lower layer is supercritical and g' decreases. Following Farmer & Armi (1999) we ignore width variations and friction. Then (4.64) predicts that the decrease of bottom elevation H causes the layer thickness to decrease. This is counteracted by the effect of detrainment which causes the layer thickness to increase. This agrees with figure 13 in (Farmer & Armi, 1999) which shows that downstream of the control the observed interface location is indeed above the one predicted by inviscid theory.

[4]Equation (E.6) in appendix E shows that the volume loss term is even more negligible if $h_1 \gtrapprox h_2$ (with the upper layer still being passive) instead of $h_1 > h_2$.

Upward and downward entrainment in an exchange flow with $\mathbf{F_1^2 = F_2^2}$ and $\mathbf{h_1 = h_2}$

Let us consider another special case and evaluate the tendency equation (4.61) at a location where $h_1 = h_2$ and $-Q_1 = Q_2 > 0$. Also assume that the flow is subcritical ($G^2 = F_1^2 + F_2^2 < 1$). Surface and sidewall friction are ignored and interfacial and bottom friction are parameterised using quadratic drag laws (Bormans & Garrett, 1989*b*) so that total friction is given by

$$\frac{\tau_0}{g'} = C_I \frac{(u_1 - u_2)|u_1 - u_2|}{g'} \left(\frac{1}{h_1} + \frac{1}{h_2}\right) - C_H \frac{u_2|u_2|}{g' h_2} \tag{4.65}$$

where C_I and C_H are the interfacial and bottom friction coefficients. With these simplifications we obtain from (4.61) for the upper and lower layer

$$\frac{dh_1}{dx} = \frac{-1}{1-G^2} \left\{ -\frac{G^2}{2}\frac{dH}{dx} - \frac{G^2}{2}(8C_I + C_H) - \left(G^2 - \frac{1}{2}\right)\frac{w_{12} + w_{21}}{u_2} \right\}, \tag{4.66a}$$

$$\frac{dh_2}{dx} = \frac{1}{1-G^2} \left\{ -\left(1 - \frac{G^2}{2}\right)\frac{dH}{dx} - \frac{G^2}{2}(8C_I + C_H) - \left(G^2 - \frac{1}{2}\right)\frac{w_{12} + w_{21}}{u_2} \right\}. \tag{4.66b}$$

The first thing we note is that width variations have no effect on the layer thicknesses because we assume $\frac{dW_1}{dx} = \frac{dW_2}{dx}$. Interfacial and bottom friction cause the upper and lower layers to become thinner in their respective direction of movement (remember that $-u_1 = u_2 > 0$) and will have equal effect if $C_H = 8C_I$. Entrainment also thins the layers provided the composite Froude number G^2 is larger than 1/2, but it will have very little effect on the layer thicknesses if $G^2 \approx 1/2$ and will cause the opposite if $G^2 < 1/2$.

The purpose of the above paragraph is to point out that, in contrast to the case of single-layer reduced gravity flows, in a two-layer exchange entrainment does not necessarily have the same effect as friction. The physical reason seems to be that with two active layers, rather then one active and one passive, the effects of exchange of volume and momentum partly cancel whereas the effect of the density gradient does not. This means that depending on the hydraulic state of the flow, even a large amount of mixing may have little effect on the dynamics - provided the conditions $F_1^2 = F_2^2$ and $Q_1 + Q_2 = 0$ are met approximately. This might be a somewhat strict condition not often met in real strait flows.

4.4. Discussion and Comparison with Observations

The analysis in the two sections provided considerable insight into the effects of entrainment by relatively straightforward consideration of momentum conservation in control volumes and led to relationships for the evolution of flow properties, in particular, for the hydraulic state of the flow and the layer thicknesses. I will now discuss some of the assumptions made and will then attempt to test the theory by comparing the slope of the interface that we observed in the Contraction with the slope predicted by the theory.

Assumption of Slab-like Flow

The model assumes a slab-like flow homogeneous in density and uniform in velocity. Then the interface is well defined and, for instance, is completely independent of the value of the barotropic flow. In the Bosphorus this ideal was well approximated along the northern section of the strait up to the Contraction. For instance, velocity and density profiles at thalweg 11.7km at the northern end of the Contraction (figure 3.19) show a difference of only about 2.5m between the depth of the zero-velocity isotach and the depth of the $\sigma_\theta = 20\text{kgm}^{-3}$ isopycnal. Furthermore, the thickness of the interface, defined by the section with significant vertical gradients of velocity and density, was about 13m, i.e. only 20% of the total water depth. Hence, the assumption of slab-like flow seemed well justified. Further south the situation became more complicated as shear and stratification increased in the upper layer. In a sheared flow the position of the zero-velocity isotach relative to the depth of a given isohaline will vary with the barotropic flow and the effect will be the larger the stronger the shear. It might then be better to redefine the interface as the depths of maximal vertical shear or maximal vertical gradient of density. However, for our observations the depths of the zero-velocity isotach and of the $\sigma_\theta = 20\text{kgm}^{-3}$ isopycnal agreed quite well (see figures 3.19, 3.22, and 3.23), and were also at approximately the same depth as the surface of maximal vertical gradient of density.

The dynamics of the flow is not perfectly described when we approximate a stratified and sheared layer by a layer with constant velocity and density. Let us analyse this problem by example of the equation for the momentum flux per unit width (4.26) where the equal sign requires constant velocity and density. The typical approximation one would made

is to replace u by $\overline{u}$ and ϱ by $\overline{\varrho}$ where the averages are taken over the layer thickness h. Instead let us approximate the upper layer profiles at position 9.5km in the Contraction (figure 3.19) by linear velocity and density profiles with $u(z) = u_I + z\,(u_S - u_I)/h$ and $\varrho(z) = \varrho_I + z\,(\varrho_S - \varrho_I)/h$, where subscripts I and S denote interface and surface values, respectively, and $z_I = 0$ and $z_S = h$. Then we obtain instead of (4.26)

$$\int_0^h (\varrho u^2 + p)\,dz = \int_0^h \varrho(z')u^2(z')\,dz' + \int_0^h \left(\int_z^h \varrho(z')g\,dz'\right) dz' \qquad (4.67)$$

$$= \frac{1}{2}gh^2 \underbrace{\frac{2\varrho_S + \varrho_I}{3}}_{\lesssim(\varrho_S+\varrho_I)/2 \text{ Term 1}} + h \underbrace{\frac{u_S^2}{3}}_{>u_S^2/4 \text{ Term 2}} \underbrace{\frac{3\varrho_S + \varrho_I}{4}}_{\lesssim(\varrho_S+\varrho_I)/2 \text{ Term 3}},$$

where $u_I = 0$ was used. The expressions, set under the curly brackets, are obtained, if the velocity $u(z)$ and density $\varrho(z)$ are approximated by their vertical averages $\overline{u}$ and $\overline{\varrho}$, respectively. The differences between the exact and approximate density values in terms 1 and 3 are necessarily small since we have used the Boussinesq approximation in the theory. This indicates that it is a good approximation to ignore stratification and instead use layer averaged densities. On the other hand, we see from term 2 that the effect of shear should not be ignored as the exact value is about 30% larger than the approximate value.

The problem is that as a result of non-uniform distribution of velocity over a channel cross-section, the momentum of a homogeneous fluid passing through a channel cross-section with area A per unit time is generally greater than the value computed according to $wA\overline{u}^2/g$ where w is the unit weight of the fluid. The true value is given by $\beta wA\overline{u}^2/g$ where

$$\beta = \frac{\int u^2 dz}{\overline{u}^2 h}, \qquad (4.68)$$

is termed the "momentum coefficient" or "Boussinesq coefficient" (e.g. Chow, 1959, and also section 5.2 later in this thesis). This means that we have to replace $\overline{u}^2$ on the right-hand side of (4.26) by $\beta\overline{u}^2$. For a linear velocity profile $\beta = 4/3$ which is just the correction factor needed in term 2 in the example above. Similarly, in our expressions for the local rate of change of layer thickness or Froude number we have to replace F^2 by βF^2, where the Froude number is based on the depth averaged current, that is $F^2 = \overline{u}^2/(gh)$.

The third problem with the assumption of slab-like flow is a most difficult one. The

entrainment model makes the assumption that fluid with a well defined momentum, that is velocity and density, is entrained. However, if the fluid is entrained from a sheared and stratified layer, its momentum will depend on where, within the layer, it originates. This depends on the scale of the turbulence motions which in turn depends on the nature of the turbulence creating processes. In short, it is beyond the simple entrainment formulation which, although it considers the physical processes that cause entrainment (e.g. Turner, 1986; Christodoulou, 1986; Fernando, 1991; Sullivan & List, 1994), assumes uniform layers. Further details are hidden in the value of the entrainment coefficient which needs to be determined experimentally. Even if observations of turbulence are available, as in this thesis in form of acoustic images, it is difficult to devise something like a correction factor. A definitive solution is beyond the scope of this study.

Comparison with Observations

Along the contraction the interface rose from north to south by about 8m (figure 3.19). We describe the slope of the interface in terms of the local rate of change of the thickness of the upper layer which follows from (4.61):

$$\begin{aligned}\frac{dh_1}{dx} = & \frac{1}{1-F_1^2-F_2^2} \\ & \times \left\{ F_2^2 \frac{dH}{dx} + \frac{h_1 F_1^2 - h_2 F_2^2}{W} \frac{dW}{dx} - \frac{\tau_0}{g'} \right. \\ & - w_{21} \frac{2F_1^2}{u_1} \left(1 - \frac{1}{2}\frac{u_2}{u_1} + \frac{1}{2}\frac{u_1}{u_2}\frac{F_2^2}{F_1^2} - \frac{1}{4}F_1^{-2} \right) \\ & \left. + w_{12} \frac{2F_2^2}{u_2} \left(1 - \frac{1}{2}\frac{u_1}{u_2} + \frac{1}{2}\frac{u_2}{u_1}\frac{F_1^2}{F_2^2} - \frac{1}{4}F_2^{-2} \right) \right\} ,\end{aligned} \tag{4.69}$$

whereby we recall that the x-coordinate increases positive northward, that is opposite to the direction of flow of the upper layer.

Let us first assume that the flow was inviscid in order to investigate whether the interface rise can be explained by the Bernoulli effect, i.e., by a change in bottom height or channel width. To this end, we approximate (4.69) by

$$\frac{\Delta h_1}{L} = \frac{1}{1-\beta F_1^2 - F_2^2} \times \left\{ F_2^2 \frac{\Delta H}{L} + \frac{h_1 \beta F_1^2 - h_2 F_2^2}{W} \frac{\Delta W}{L} \right) \tag{4.70}$$

where the Boussinesq coefficient β is introduced to account for the shear in the upper layer. The Froude numbers and layer thicknesses vary along the Contraction, but let us

be conservative and use average values weighted somewhat towards their values at position 10.5km where the slope is maximal: $\beta = 1.2$, $F_1^2 = 0.35$, $F_2^2 = 0.08$, $h_1 = 35$m, $h_2 = 40$m, and $W = 750$m. With these values an 8m change in upper layer thickness would require $\Delta W = 260$m or $\Delta H = 60$m. Both values are much too large to be achieved, as in fact, both W and H are almost identical at the two ends of the Contraction. A 2m interface rise would require $\Delta W = 65$m which is 10m larger than the estimated error[5] in W of about 55m. On the other hand, the Bernoulli dimple of 4m at 10km requires $\Delta W = 130$m in good agreement with the actual reduction in layer width from 750m to 650m. This shows that (4.70) is applicable here. In summary, changes in bottom height H and W cannot explain the observed change in interface depth at the Contraction.

Let us next estimate the effect of friction. Total friction is the sum of surface friction, side-wall friction acting on the upper layer, interfacial friction acting on the upper and lower layer, and bottom friction acting on the lower layer. For a rectangular channel we obtain, using quadratic drag laws (Bormans & Garrett, 1989*b*; Oğuz *et al.*, 1990),

$$\begin{aligned} \tau_0 &= \tau_S + \tau_{H1} + \tau_{I1} + \tau_{I2} - \tau_{H2} \,, \\ &= \underbrace{C_S \frac{\varrho_{air}}{\varrho_1} \frac{|W|W}{h_1}}_{8\times10^{-7}} + \underbrace{\tau_{H1}}_{?} + \underbrace{C_I(u_1-u_2)|u_1-u_2|\left(\frac{1}{h_1}+\frac{1}{h_2}\right)}_{-1.2\times10^{-5}} - \underbrace{C_H \frac{u_2|u_2|}{h_2}}_{1.4\times10^{-5}} \,, \end{aligned} \tag{4.71}$$

where W is the mean wind-speed at 10m, $C_S = (1.3 \pm 0.3) \times 10^{-3}$ and ϱ_{air} is the density of air (Kraus, 1972, chapter 5). Using $C_H = 2.3 \times 10^{-3}$ (see section 3.5), $C_I = 1 \times 10^{-4}$ (see Oğuz *et al.* (1990); Bormans & Garrett (1989*b*), but to be discussed later), $h_1 = 35$m, $h_2 = 40$m, $u_1 = -1.1\,\mathrm{m\,s^{-1}}$, $u_2 = 0.5\,\mathrm{m\,s^{-1}}$, and a wind speed of $W = -4\,\mathrm{m\,s^{-1}}$, we obtain the values set under the curly brackets in (4.71). We see that surface friction is negligible and that bottom and interfacial friction have almost equal magnitude. Bottom-friction in the upper layer remains unspecified for now. Finally, using $L = 2700$m and the Froude

[5] I compared cross-channel transects taken along the Contraction. The width of the upper layer can be estimated easily and was found to be 750m ± 50m at both ends of the contraction. Although the wetted perimeter of the lower layer changes from triangular in the north to trapezoidal in the south, the cross-sections of the moving parts of the lower layer are similar. Furthermore the influence of the lower layer on the final result for dh_1/dx is relatively small because $F_2^2 < \beta F_1^2$. This hand-waving argument was confirmed by reformulating (4.70) using layer transports and layer areas as shown by Bormans & Garrett (1989*b*).

numbers and Boussinesq coefficient from above, we obtain $\Delta h_1 = 2.2\text{m}$ (with the correct sign!).

Finally let us estimate the effect of entrainment. On April 8, upward and downward entrainment were estimated to be $Q_{21} = (1300 \pm 200)\text{m}^3\,\text{s}^{-1}$ and $Q_{12} = (200 \pm 200)\text{m}^3\,\text{s}^{-1}$. Dividing by the interfacial area $A_I = L \times W \approx 2700\text{m} \times 750\text{m}$ gives entrainment velocities of $w_{21} = 6.5 \times 10^{-4}\text{m}\,\text{s}^{-1}$ and $w_{12} = 1 \times 10^{-4}$. Using the other values as given above and inserting them in (4.69) we find that upward entrainment raises the interface by 2.1m but downward entrainment lowers the interface by 0.4m.

In summary, it seems that we can predict only a little less than 50% of the observed change in depth of the interface. Considering the simplicity of the model in view of the complexity of the real flow, this is not a bad result. Furthermore, the reader might have noticed that my estimate is very conservative. For example, I have not taken into account that most of the entrainment takes place along the southern half of the Contraction where Froude numbers and velocities are larger (see acoustic image in figure 3.19). After taking this into account, the total effect of mixing is to raise the interface by 3.5m. As far as friction is concerned I have ignored a) that the effect of bottom-friction will be somewhat larger because the cross-sectional shape is not rectangular (see transect #5b in figure 3.14), b) that there is probably some form drag exerted on the upper layer which could not be quantified, and c) that the exact value of the interfacial friction coefficient is actually unknown, as will be discussed below. For instance, if we increased C_I from 1×10^{-4} to 4×10^{-4}, the layer thickness h_1 would increase by another 4m.

Interfacial Friction

The value of the coefficient C_I for interfacial friction was estimated from two publications: a) in their numerical simulation Oğuz *et al.* (1990) had to use $C_I = \text{O}(10^{-4})$ because the results depended sensitively on C_I, and b) Bormans & Garrett (1989*b*) used dissipation rates of $\varepsilon \approx 10^{-6}\text{Wkg}^{-1}$, measured in the eastern end of Gibraltar by Wesson & Gregg (1988), to infer an interfacial drag coefficient of $C_I \approx 10^{-4}$. Microstructure measurements have been carried out along the Bosphorus by Gregg *et al.* (1999) but the results have not yet been reported.

Aside from not knowing the exact value of C_I, a further problem is that we may have

over-represented the exchange of momentum in the calculation. The physical effect of interfacial friction is to exchange momentum between two moving layers without exchanging volume or mass. On the other hand, the effect of entrainment is to exchange momentum and mass. It seems necessary to retain both terms, because it is possible to exchange momentum without exchanging mass: a parcel of fluid may be injected from a lower layer into a upper layer, but having a higher density it might return to the lower layer without losing its integrity so that only momentum was exchanged but no mass. On the other hand, Pedersen (1972) argues that interfacial shear stresses are accounted for entirely by momentum fluxes between the layers due to entrainment. In addition Baringer & Price (1997) estimate the effective mean entrainment stress by $\tau_I = \varrho_0 V w_e$ where V is their streamtube velocity and w_e is the entrainment velocity. Based on the theory presented here these approaches appear to be incorrect. If values for C_I reported in the literature (e.g. Pedersen, 1986) are based on Pedersen's argument, we might be overestimating the momentum exchange when using these values with our theory which includes both interfacial friction and entrainment. But note that this has little practical implications as the uncertainty in any of these coefficients is probably more than just a factor of two.

The significant uncertainty in the coefficients is also one of the reasons why in this thesis no attempt has been made to numerically solve, for instance, equation (4.61) for the position of the interface, say, along the strait - as done by Assaf & Hecht (1974) and Bormans & Garrett (1989*b*) with models without mixing. In addition to finding values for the friction coefficients, we would have to find an appropriate entrainment law involving a so-called entrainment coefficient as additional unknown (e.g. Christodoulou, 1986). Furthermore, such a two-layer model (with added time-dependence) has already been solved for the position of the interfaces along the Dardanelles and the Bosphorus by Oğuz & Sur (1989) and Oğuz *et al.* (1990), respectively. The authors parameterise interfacial and bottom friction using quadratic drag-laws and entrainment using an entrainment concept proposed by Pedersen (1980). The Bosphorus model correctly captures the salient features of the exchange (slope of the interface, upward entrainment along the southern section), but incorrectly predicts a control with $G^2 \approx 1.7$ in the contraction and composite Froude numbers of $G^2 \approx 2$ at the North Sill and South Exit which are much larger than ob-

served. It seems likely that the discrepancies are due to the model's neglect of shear and stratification, and an over-simplification of the actual complicated topography. The first point was addressed by Johns & Oguz (1990) with a two-dimensional model using a turbulence parameterisation scheme instead of friction and entrainment laws, however, the agreement of the model results with observations was rather worse than better. It seems that ultimately three-dimensional models with accurate bathymetry and realistic parameterisations of friction and mixing will be required. Recent developments by Winters & Seim (2000), Hogg *et al.* (2001*b*), and Sözer & Özsoy (2002) are steps towards that goal but these models use much simplified geometries consisting of only a single constriction and are hence far from representing the topography along the Bosphorus.

Developing a numerical model to accurately predict the flow in the Bosphorus is not the purpose of this study. Instead we rely on simplified theoretical description to gain physical insight into the effects of entrainment on the dynamics of the flow. In this sense, our above comparison between theory and observations should be understood as qualitative rather than quantitative check of the equations.

5. Hydraulic Control in Non-Uniform Flows

One of the fundamental assumptions of the theory described in chapter 4 is that at any cross-section the layers are homogeneous in density and uniform in velocity. If the assumptions of uniformity and homogeneity are met, the Froude number, which describes the hydraulic state of the flow, is well defined.

As we have seen, any real flow will be bounded and along the boundaries friction will act on the flow creating shear. In case of two layers with different water masses mixing will cause continuous stratification to occur. If the gradients are not too large, common sense suggests that one may define the Froude number using average layer quantities, i.e., we use $F^2 = \overline{u}^2/(gh)$ where $\overline{u}$ is the average layer velocity. Alternatively we may use some other representative value for the layer velocity, for instance, the velocity from a portion of the profile that is uniform (e.g Farmer & Armi, 1988). Furthermore, at the end of the previous chapter I have shown that to a good approximation the density of a stratified flow can be represented by the average density and the effect of shear can be taken into account by introducing the Boussinesq coefficient β.

It remains, however, the question if and/or how shear and stratification affect the definition of hydraulic control. This problem is not new and 'solutions' are given in the literature. In physical oceanography it is accepted wisdom to exploit the connection between the propagation of long waves and hydraulic behaviour. This connection is well established for the case of layered models. The essence of it is that at a control an inviscid long wave is arrested, i.e. information cannot propagate through the control. (I will explain this point in detail in the next section). The solution to the problem then consists of defining a control as the location where an inviscid long wave is arrested because the inviscid wave speed is easily calculated also for stratified and sheared flows. This is a convenient but also a slightly worrying approach because, surprisingly enough, the con-

nection between long waves and hydraulic behaviour is not well established for sheared and stratified flows (Pratt *et al.*, 2000, page 2516).

This issue arose at the end of the work on this thesis and the reader should not expect completely satisfying answers. I would like to point out that, although I can perhaps claim to have raised this issue, Dr. Garrett developed the solutions presented in the sections entitled 'Resolving the Paradox' and 'Control Conditions for an Inviscid Shear Flow'. I have nevertheless included them in this thesis because they are important for an understanding of the question of hydraulic control at the Bosphorus. The material has been accepted for publication in the Journal of Fluid Mechanics (Garrett & Gerdes, 2002).

First, I will introduce the concept of information propagation in layered hydraulic flows as well as of Gill's (1977) functional formalism for hydraulic control situations. For the special case of a sheared homogeneous flow two different approaches for defining hydraulic control will be presented. Curiously they yield contrary results. This problem is then analysed and a partial resolution is presented. At the end, implications for the Bosphorus will be discussed.

5.1. The Connection Between Hydraulic Control and the Speed of Long Waves

Time-dependent Single Layer Flow

Let us re-consider the problem introduced in section 4.1.1. We want to determine the speed of propagation of inviscid waves in a single-layer flow of uniform density and velocity, and hence begin with the time-dependent momentum and continuity equations

$$\frac{\partial u}{\partial t} + u\frac{\partial u}{\partial x} + g\frac{\partial h}{\partial x} = -g\frac{\partial H}{\partial x}\,, \tag{5.1a}$$

$$\frac{\partial h}{\partial t} + \frac{\partial (uh)}{\partial x} = 0\,. \tag{5.1b}$$

We assume that H is zero, and that $h = h_0 + h'$ and $u = u_0 + u'$ where h' and u' are small quantities caused by a small disturbance and superimposed on the mean quantities h_0 and u_0 which are invariant with respect to x and t. Then the linearised governing equations

become (e.g. Gill, 1982)

$$\frac{\partial u'}{\partial t} + u_0 \frac{\partial u'}{\partial x} + g \frac{\partial h'}{\partial x} = 0 \,, \tag{5.2a}$$

$$\frac{\partial h'}{\partial t} + u_0 \frac{\partial h'}{\partial x} + h_0 \frac{\partial u'}{\partial x} = 0 \,. \tag{5.2b}$$

which after cross-differentiation turn into the wave equation

$$\left(\frac{\partial}{\partial t} + u_0 \frac{\partial}{\partial x} \right)^2 h' - c^2 \frac{\partial^2 h'}{\partial x^2} = 0 \,, \tag{5.3}$$

where $c = (g h_0)^{1/2}$ is the wave speed. The solution is

$$h'(x,t) = \mathcal{F}(x - (u_0 + c)t) + \mathcal{G}(x - (u_0 - c)t) \tag{5.4}$$

where $\mathcal{F}$ and $\mathcal{G}$ are arbitrary functions. The Froude number is defined as $F^2 = u_0^2/(g h_0) = h_0^2/c^2$. Hence, from (5.4) and assuming that $u_0 > 0$ we find that

- for subcritical flow with $F^2 < 1$ and $u_0 < c$ small disturbances can propagate upstream or downstream,
- for supercritical flow with $F^2 > 1$ and $u_0 > c$ small disturbances cannot propagate upstream (against the flow) but they can propagate downstream (with the flow),
- for critical flow with $F^2 = 1$ and $u_0 = c$ small disturbances are stationary or propagate downstream at speed $2u_0$ relative to a fixed coordinate system.

In a related approach we can make the a priori assumption that the small disturbances are wave-like, that is of the form

$$h' = h_A \exp(ik(x - \lambda t)) \qquad \text{and} \qquad u' = u_A \exp(ik(x - \lambda t)) \,, \tag{5.5}$$

where λ is the phase speed, k the wave number, and h_A and u_A the height and velocity amplitudes of the wave. This can directly be substituted into (5.2) and we obtain

$$\begin{pmatrix} u_0 - \lambda & g \\ h_0 & u_0 - \lambda \end{pmatrix} \begin{pmatrix} u_A \\ h_A \end{pmatrix} = 0 \tag{5.6}$$

which has a non-trivial solution only if

$$\det(\mathbf{C} - \lambda \mathbf{I}) = 0 \tag{5.7}$$

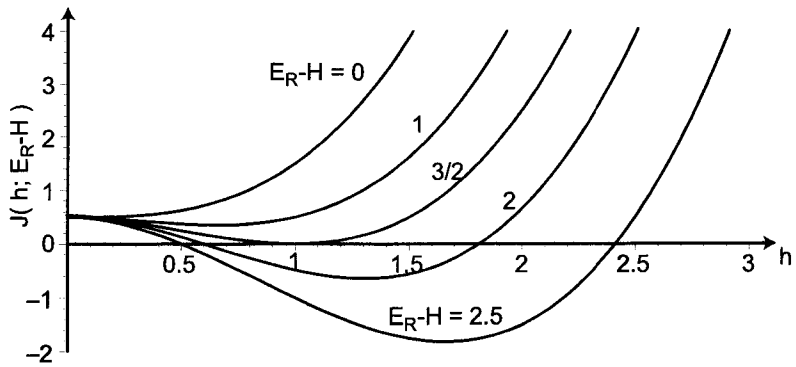

Figure 5.1.: *The functional $\mathcal{J}(h; E_R - H)$ defined in* (5.10) *plotted against h for various values of $E_R - H$. Q and g are assumed to be unity which is equivalent to using non-dimensionalised quantities in* (5.10).

where

$$\mathbf{C} = \begin{pmatrix} u_0 & g \\ h_0 & u_0 \end{pmatrix} \tag{5.8}$$

and $\mathbf{I}$ is the unity matrix. The eigenvalues λ are given by

$$\lambda = u_0 \pm c = u_0 \pm (gh_0)^{1/2} . \tag{5.9}$$

The wave is stationary when $\lambda = 0$ which leads to $u_0 = \pm(gh_0)^{1/2}$. Again the result is that the wave is arrested when $F^2 = 1$.

Gill's Functional Formalism for Hydraulic Flow

This formalism developed by Gill (1977) is closely related to what I called the 'Energy Approach' in section 4.1.1. For the sake of simplicity let us assume a channel of unit width. We rewrite (4.8) as

$$\mathcal{J}(h, E_R - H) \equiv h^3 + (H - E_R)h^2 + \frac{1}{2}\frac{Q^2}{g} = 0 \tag{5.10}$$

where the volume flux $Q = uh$ is constant. A physically acceptable solution with $h(x) > 0$ exists if and only if

$$E_R - H(x) \geq \frac{3}{2}\left(\frac{Q^2}{g}\right)^{1/3} \tag{5.11}$$

which is the result obtained earlier on page 78. A way of illustrating the solutions is a plot of $\mathcal{J}$ versus h for various values of $E_R - H$, as shown in figure 5.1. A solution, with

$E_R = E_1$ say, is obtained by tracing **along** the h-axis from the intersection of the axis with the curve $E_R - H = E_1$ in the direction of decreasing h, if $h(H = 0) > (Q^2/g)^{1/3}$ (supercritical flow), or in the direction of increasing h if $h(H = 0) < (Q^2/g)^{1/3}$ (subcritical flow). The curves $E_R - H = \text{const}$ do not intersect the h-axis if $E_R - H < 3/2(Q^2/g)^{1/3}$. Therefore solutions will not exist if either E_R or H is such that the sum $E_R - H$ is less than this value (or in the language of the 'Energy Approach' if the sill is too high or the upstream reservoir level too low). The solution with $E_R - H = 3/2(Q^2/g)^{1/3}$ has a minimum for $h = 2/3(E_R - H)$ and after inserting this in $\mathcal{J}(h, E_R - H)$ we readily obtain the control condition $F^2 = Q^2/(gh^3) = 1$. This approach is just another way of looking at the standard problem described in section 4.1.1.

It was Gill (1977) who first recognised that a common property of hydraulic control situations is that the flow can be described in terms of a functional expression connecting a *single* flow variable, which varies only with position along the channel, with geometric parameters $H(x)$, $W(x)$, etc. describing the cross-section of the channel. Gill stresses that the dependence of the flow variable on x is entirely implicit in terms of the geometric parameters. This functional expression, say $\mathcal{J}(h; H, W, etc.) = \text{const}$ must be multiple-valued in that h may take on several values for given geometric parameters. This requirement is a consequence of the non-linear term in the equation of motion. A merging of the different solution branches or roots occurs when

$$\frac{\partial \mathcal{J}}{\partial h} = 0\,, \tag{5.12}$$

which in combination with the other conditions defines the control section. We recognise in this our simple example from above where the single flow variable is the layer thickness h and the only geometric parameter is the bottom height H, and where solving $\partial \mathcal{J}/\partial h = 0$ for h yields $h = \frac{2}{3}(E_R - H)$ and $F^2 = 1$.

As argued by Gill (1977), at a control section not only $\mathcal{J}(h; H) = \text{const}$ is satisfied but because of $\partial \mathcal{J}/\partial h = 0$ the condition $\mathcal{J}(h + \delta h; H) = \text{const}$ is satisfied as well. This means that a slightly perturbed flow also satisfies the equations for steady flow, implying that waves are stationary there, i.e. stationary long-wave disturbances always exist at the control section. This general proof explains why the Froude number is unity at the control.

Summary

Recall the discussion of the hydraulic jump around figure 4.4 where we noted that any change in the downstream reservoir level cannot influence the upstream level provided the flow is critical in between. In the spirit of this section this means that waves cannot propagate from the downstream reservoir to the upstream reservoir, or in other words, any information on changes downstream cannot be communicated upstream.

The connection between hydraulics and inviscid long waves is not limited to single layer flows. For inviscid two and/or multi layer flows internal hydraulic control is related to the speed of inviscid long internal waves (e.g Armi, 1986; Lawrence, 1990). These situations can also be analysed by use of an extended version of Gill's formalism (Dalziel, 1991; Lane-Serff *et al.*, 2000).

5.2. Hydraulic Control of Open Channel Flow With Shear

The problem of hydraulic control becomes more subtle in a situation where friction leads to vertical shear as well as an overall retarding force. In this case pressure may still be hydrostatic if the horizontal scale is much greater than the water depth. We will also assume that the layer is homogeneous in density. It is not a priori clear how we should define hydraulic control for such a situation. There are two different approaches in the literature which curiously yield conflicting results.

The Engineering Approach

Because of the shear it is no longer appropriate to neglect the advective term involving the vertical shear. The momentum equation is then

$$u\frac{\partial u}{\partial x} + w\frac{\partial u}{\partial z} + g\frac{d}{dx}(h+H) = \frac{\partial \tau}{\partial z} \tag{5.13}$$

where τ represents internal frictional forces. The continuity equation is simply $\partial u/\partial x + \partial w/\partial z = 0$.

It is sometimes assumed that the horizontal velocity component u maintains a similar shape, with horizontal variations only of the depth-averaged speed $\overline{u}(x)$. Thus

$$u(x,z) = \overline{u}(x)P(\zeta) \quad \text{where} \quad \zeta = \frac{z-H}{h} \tag{5.14}$$

and $P(\zeta)$, with $\int_0^1 P d\zeta = 1$, is just a function describing the velocity profile. The continuity equation, along with its vertical integral $d(h\overline{u})/dx = 0$ and kinematic boundary conditions at $z = H$ and $z = H + h$, then gives

$$w = \overline{u}(x)P(\zeta)\left(\frac{dH}{dx} + \zeta\frac{dh}{dx}\right) \tag{5.15}$$

and the advective terms in (5.13) can be written as $P^2\,\overline{u}\,d\overline{u}/dx$. This will have implications for the form of the frictional term on the right hand side of (5.13), but for now we note that, if this term is ignored, the vertically integrated momentum and continuity equations become

$$M_2\overline{u}\frac{d\overline{u}}{dx} + g\frac{d}{dx}(h + H) = 0 \qquad \text{and} \qquad \frac{d}{dx}(h\overline{u}) = 0\,, \tag{5.16}$$

where $M_2 = \int_0^1 P^2 d\zeta$. The first equation here may be derived directly from consideration of the momentum budget for an element of the fluid between the bottom and the free surface and between x and $x + dx$.

The governing equations (5.16) are now similar in form to the governing equations for a flow with no shear (for instance, (4.1) with $W = \text{const}$). Following the procedure used to investigate these, we conclude that control occurs where the Froude number $\overline{u}/(gh)^{1/2}$ based on the depth-averaged current is $M_2^{-1/2}$. This is ≤ 1 as the Cauchy-Schwartz inequality $\int(P \cdot 1)d\zeta \leq \sqrt{\int P^2 d\zeta} \times \sqrt{\int 1^2 d\zeta}$ gives $M_2 \geq 1$.

An alternative way, implied by some texts, is to start from an assumption that the energy flux for the layer is conserved with x. This involves $M_3 = \int_0^1 P^3 d\zeta$ and leads to a critical Froude number, based on $\overline{u}$ as before, of $M_3^{-1/2}$, a different value from $M_2^{-1/2}$ but also ≤ 1. In the engineering literature (Chow, 1959; Henderson, 1966) the third moment, M_3 here, is denoted α and termed the energy coefficient or Coriolis coefficient. The second moment M_2 is denoted β and termed the momentum coefficient or Boussinesq coefficient. (We will comment on the use of α or β at the end of this chapter.)

The shortcoming of these arguments is, of course, the neglect of the frictional term on the right hand side of (5.13), even though such a term is required to maintain the profile in the presence of varying $\overline{u}(x)$. We return to this later, but first investigate whether long waves are arrested at the implied control section.

The Physical Oceanography Approach

We take $H = 0$ and a basic flow $u(z)$ in water of depth h. We consider infinitesimal perturbations u', w', h' of the horizontal and vertical velocity components and free surface elevation. The linearised momentum equation is

$$\frac{\partial u'}{\partial t} + u\frac{\partial u'}{\partial x} + w'\frac{du}{dz} + g\frac{\partial h'}{\partial x} = 0 \tag{5.17}$$

Seeking a wavelike solution with the perturbation variables proportional to $\exp[ik(x-ct)]$ and using the continuity equation $\partial u'/\partial x + \partial w'/\partial z = 0$ leads to

$$(c-u)\frac{\partial w'}{\partial z} + w'\frac{du}{dz} = -gikh'. \tag{5.18}$$

After dividing this by $(c-u)^2$, the left hand side may be written as a differential. Integrating the resulting equation vertically and using the linearised free surface kinematic boundary condition $w' = \partial h'/\partial t + u\partial h'/\partial x$ at $z = h$ we obtain

$$\int_0^h \frac{g dz}{(c-u)^2} = 1. \tag{5.19}$$

This result is well-established (Thompson, 1949; Burns, 1953)[1] but has been derived here to illustrate the simplicity of the derivation. It clearly gives the correct limits that $c^2 = gh$ if $u = 0$ and $(c-u)^2 = gh$ if u is independent of depth. Burns (1953) shows that, with the reasonable restrictions that $0 \leq u(0) < u(h), du/dz > 0$ and $d^2u/dz^2 \leq 0$, there are two solutions for c and these do not lie between $u(0)$ and $u(h)$. Moreover, the magnitude of c relative to $\overline{u}$ is greater than $(gh)^{1/2}$. For example, for a small departure from depth-uniform flow, and taking $\overline{u} = 0$ for convenience, we take $u = (gh)^{1/2}\epsilon(z)$ with $|\epsilon| \ll 1$ and $\int_0^h \epsilon\, dz = 0$. Expansion of the integrand in (5.19) then gives

$$c^2 = gh\left(1 + 3h^{-1}\int_0^h \epsilon^2 dz\right) \tag{5.20}$$

as effectively given on page 54 of (Baines, 1995) where it is derived from the Taylor-Goldstein equation assuming no stratification so that the buoyancy frequency $N = 0$. Thus the magnitude of the speed of long waves is greater than $(gh)^{1/2}$, in agreement with Burns' (1953) general result. The speed of these waves is apparently sufficient to carry information upstream through an alleged control point at which the mean flow is, as shown earlier, less than $(gh)^{1/2}$.

[1] More easily accessible might be the paper by Freeman & Johnson (1970) and the review by Peregrine (1976) which both reproduce Burn's result.

Resolving the Paradox

For a sheared flow of a homogeneous fluid in an open rectangular channel there is a disagreement between two accepted conditions for hydraulic control. One must be wrong.

One possibility for reconciliation might be that the speed of long waves is reduced by the friction that must accompany the maintenance of the shear. We recall, however, that for a slab-like flow the presence of bottom friction merely shifts the control section downstream of a ridge crest (Pratt, 1986); the *inviscid* waves are still arrested there as $u = (gh)^{1/2}$ there. Moreover, in that situation it is easy to show (e.g. Wajsowicz, 1993) that the damped waves have a *group* speed that is greater than $(gh)^{1/2}$. (If the bottom friction is represented by a linear term $-\lambda u$ instead of the quadratic term used in (4.15), the wave group speed is $(gh)^{1/2}[1-(4ghk^2)^{-1}\lambda^2]^{-1/2}$ for a wavenumber k large enough to make this real.) It seems that bottom friction does not provide a resolution.

On the other hand, we note that Gill's (1977) functional approach can be applied to (5.16) and shows that long wave solutions of (5.16) are, in fact, stationary at a control point where $\overline{u} = M_2^{-1/2}(gh)^{1/2}$. This is easily seen directly by adding a depth-averaged current perturbation $\overline{u}'$ and an associated perturbation h' to the surface height. Perturbation of the momentum and continuity equations then gives $M_2\overline{u}ik\overline{u}' + gikh' = 0$ and $h'\overline{u} + h\overline{u}' = 0$ for a stationary wave with wavenumber k. Hence $\overline{u} = M_2^{-1/2}(gh)^{1/2}$. Thus the speed of long waves with respect to the mean flow in a system governed by (5.16) is actually $M_2^{-1/2}(gh)^{1/2}$. The difference between this and the speed of inviscid waves must somehow be associated with the internal frictional term on the right hand side of (5.13).

We first note that the vertical integral of (5.13) is actually

$$M_2\overline{u}\frac{d\overline{u}}{dx} + g\frac{d}{dx}(h+H) = -\frac{\tau_b}{h} \tag{5.21}$$

where τ_b is the bottom stress. This equation replaces the first equation in (5.16) and can, of course, be obtained directly from a momentum budget. Using also $h\overline{u} = Q$, the volume flux, the problem appears very similar to that for a slab flow with bottom friction, as discussed in section 4.1.2. Control is achieved with $\overline{u} = M_2^{-1/2}(gh)^{1/2}$ and at a location where $dH/dx = -M_2^{-1}C_d$ if we express the bottom drag τ_b as $C_d\overline{u}^2$.

If we examine the difference between (5.13) (in which, as remarked earlier, the advective

terms may be written as $P^2\,\overline{u}\,d\overline{u}/dx$) and its vertical integral (5.21), we require that

$$\frac{\partial \tau}{\partial z} = \left(P^2 - M_2\right)\overline{u}\frac{d\overline{u}}{dx} - \frac{\tau_b}{h}\,. \tag{5.22}$$

Even in the absence of bottom friction, adding this to the right hand side of (5.17) will alter the long wave speed from that given by (5.19) to the value $M_2^{-1/2}(gh)^{1/2}$, as derived above. The reason for this change in long wave speed, from that for inviscid waves given by (5.19), is that the right hand side of (5.17) acquires an extra "frictional" term $(P^2 - M_2)\,\overline{u}\,d\overline{u}'/dx$ which depends on the flow derivative. It thus alternates in sign, providing no net damping for the wave but changing its propagation speed. These conclusions would need to be adjusted if τ_b depended on flow derivatives rather than just the local flow properties. In that case it, too, could be moved to the left hand side of the momentum equation, with consequent changes in the long wave speed and control condition.

We conclude that there is really no paradox. For a flow with a fixed shape of its velocity profile, the long waves for the governing equations are indeed arrested at the control, which occurs where the mean flow speed is less than the speed of waves for an inviscid flow. Moreover, as for the slab flow, bottom friction, provided it is dependent on the local flow speed and not its derivative, shifts the control section downstream of the crest of a bump.

Control conditions for an Inviscid Shear Flow

While the above discussion seems to have resolved an apparent paradox for a homogeneous shear flow with a fixed shape of the velocity profile, the question remains about conditions for control in a more general situation. One extreme is for a flow with shear but no friction. The momentum equation is then simply

$$u\frac{\partial u}{\partial x} + w\frac{\partial u}{\partial z} + g\frac{d}{dx}(h + H) = 0. \tag{5.23}$$

Combined with the continuity equation, $\partial u/\partial x + \partial w/\partial z = 0$, (5.23) may be integrated to give

$$\frac{1}{2}u^2 + gh = g[a(\psi) - H], \tag{5.24}$$

which is just Bernoulli's equation for a vortical flow, with a a function of the stream function ψ rather than constant as for the unsheared flow (e.g. Kundu, 1990, page 107).

A first remark is that, if the flow originated in a deep reservoir with a sluggish flow, then (5.24) implies equal acceleration on all streamlines, so that the velocity difference from top to bottom actually becomes smaller[2]. Another way of seeing this is that, for the assumed channel of constant width, the vorticity $\partial u/\partial z$ is conserved along streamlines, again implying a reduction in top-to-bottom velocity difference as the flow thins. Thus a purely inviscid shear flow is unlikely. One has to imagine a flow in which the shear is maintained by friction until the flow approaches a ridge crest in the vicinity of which the friction is unimportant in comparison with the inertial terms.

The problem may then be cast in terms of a functional connection between h and H by writing the continuity equation as

$$h = \int_H^{H+h} dz = \int_0^Q \frac{d\psi}{u} \tag{5.25}$$

where $u = \partial\psi/\partial z$ and Q is the volume flux. This assumes a single-valued connection between ψ and z, equivalent to assuming a unidirectional flow. Combining (5.24) and (5.25) leads to

$$\mathcal{J}(h;H) = \int_0^Q \frac{d\psi}{(2g)^{1/2}[a(\psi) - (H+h)]^{1/2}} - h = 0. \tag{5.26}$$

Note that this is of exactly the form $\mathcal{J}(h;H) =$ constant required for the applicability of Gill's (1977) arguments. (Pratt & Armi (1987) used a similar approach to derive a condition for control in a rotating flow that was unsheared in the vertical, but sheared across the channel.)

We investigate $\mathcal{J}(h;H)$ by first non-dimensionalising ψ with Q and a, H, h with $(Q^2/g)^{1/3}$ (but retain the same symbols for the non-dimensionalised variables). The functional equation (5.26) then becomes

$$\mathcal{J}(h;H) = \int_0^1 \frac{d\psi}{2^{1/2}[a(\psi) - (H+h)]^{1/2}} - h = 0. \tag{5.27}$$

For constant a (no shear) and with $b = a - H$, $\mathcal{J}(h;H) = 2^{-1/2}(b-h)^{-1/2} - h$, as shown in figure 5.2A. It has a minimum of $3/2 - b$ at $h = b - 1/2$, so solutions of (5.27) only

[2]To see this use that (5.24) is conserved on the surface and bottom streamlines. Denote with $u_{S0} > 0$ and $u_{B0} = 0$ surface and bottom velocity upstream of a sill where $H = 0$, and with u_{SC} and u_{BC} surface and bottom velocity at the crest of the sill where $H > 0$. Combining the Bernoulli equations for both streamlines gives $u_{BC}^2 = u_{SC}^2 - u_{S0}^2$, so that the velocity difference between surface and bottom at the crest $u_{SC} - u_{BC} = u_{S0}^2/(u_{SC} + u_{BC})$ is smaller than the velocity difference upstream which is just u_{S0}.

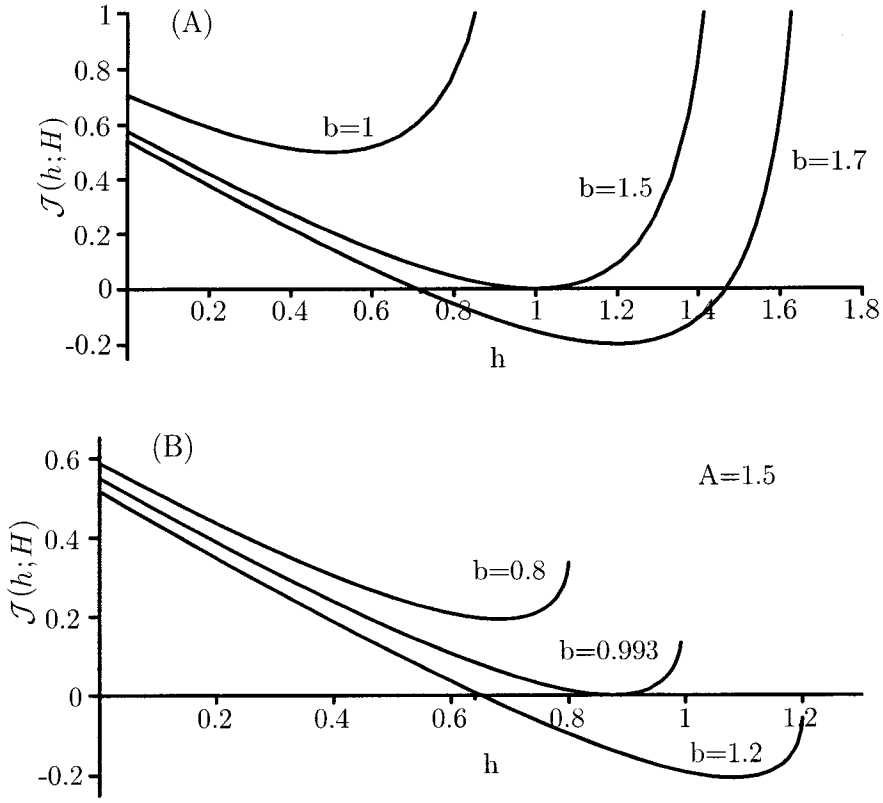

Figure 5.2.: *A) The non-dimensionalised functional of (4.5) for constant a, shown for* $b = a - H = 1, 3/2, 2$. *B) As in (A), but with* $a = a_{min} + 1.5\psi$ *and for* $b = a_{min} - H = 0.8, 0.993, 1.2$.

exist if $b \geq 3/2$. Control occurs at the ridge crest if $b = 3/2$ there. This is just a slightly different way of looking at the problem in section 5.1.

The same general shapes occur if a is allowed to vary with ψ (now with shear), in the sense that the functional starts positive at $h = 0$, then generally decreases to a minimum before increasing as h tends to the minimum value of $a(\psi) - H$, but there is no simple general solution to (5.27). Figure 5.2B shows the functional in (5.27) for various values of $b = a_{min} - H$ with the linear function $a = a_{min} + A\psi$ and $A = 1.5$. Here A is in fact the vertical shear $\partial u/\partial z$. The controlled solution for $A = 1.5$ occurs for $b = 0.993$ and $h = 0.875$; it has non-dimensional speeds of 0.49 and 1.80 at the bottom and free surface respectively. A feature worth noting in figure 5.2B for $b = 1.2$ is that there is no subcritical solution (large h). This is because, at a slow average flow, the shear would not be compatible with a positive velocity at the bottom.

As discussed earlier, the functional formalism automatically implies that long waves are arrested at the control section. It is interesting to confirm this directly. Control applies for a solution that satisfies (5.24) and also occurs at the minimum of $\mathcal{J}(h;H)$ regarded as a function of h, i.e. for $\partial\mathcal{J}/\partial h = 0$. Using (5.26) and also applying (5.24), as is appropriate for a solution, leads to the result that

$$\int_0^Q \frac{g\,d\psi}{u^3} = 1 \tag{5.28}$$

and this may be written as

$$\int_H^{H+h} \frac{g\,dz}{u^2} = 1. \tag{5.29}$$

This is identical to (5.19) with $c = 0$, implying that long waves are indeed arrested at the control section. Note that this is an independent derivation of the connection between the speed of long waves and hydraulic control which extends the previously established connection for uniform flows to sheared flows.

5.3. Discussion and Implications for Hydraulic Control at the Bosphorus

The apparent paradox concerning the hydraulic control of a frictionally influenced homogeneous fluid with a fixed velocity profile has been resolved by showing that it does actually fit in with standard approaches if one studies in detail the form of the frictional terms required to maintain the shape. The conclusion for practical purposes is that control is achieved with a depth-averaged current speed less than $(gh)^{1/2}$, and at a location downstream of the control for an inviscid flow. Pawlak & Armi (1997) present an experimental and analytical study of two-layer arrested wedge flows influenced by side-wall friction. They modify the two-layer hydraulic equations to include the effects of flow non-uniformity by means of the Coriolis coefficient α defined by

$$\alpha = \frac{\int u^3 dz}{\overline{u}^3 h}\,. \tag{5.30}$$

As mentioned earlier, this coefficient represents the correction necessary to compute the velocity head of a homogeneous fluid when velocity is not uniform; the velocity head changes from $u^2/(2g)$ to $\alpha\,\overline{u}^2/(2g)$ (Chow, 1959; Henderson, 1966). (In our notation

$\alpha = M_3 = \int_0^1 P^3 \, d\zeta$.) In essence, Pawlak & Armi (1997) use $F^2 = 1/\alpha$ as control condition instead of $F^2 = 1$. Curiously that is different than the control condition $F^2 = 1/\beta \equiv 1/M_2$ we derived in this chapter. The numerical difference between $1/\alpha$ and $1/\beta$ is, however, small for most velocity profiles so that we may defer a discussion of this issue to the end of this chapter.

Pawlak & Armi (1997) then investigate the effect of non-uniformity on the value of the non-dimensionalised barotropic component U_0 at which the two-layer exchange transitions to an arrested wedge flow and, in particular, they obtain equations for the wedge front location b_f for weak and strong barotropic flows:

$$b_f = U_0 \sqrt{\alpha} (3\alpha^{1/3} U_0^{2/3} - 2)^{-1/2} \qquad \text{for} \qquad U_0 < 1\sqrt{\alpha}\,, \tag{5.31a}$$

$$b_f = U_0 \sqrt{\alpha} \qquad \text{for} \qquad U_0 > 1\sqrt{\alpha}\,. \tag{5.31b}$$

With α between 1.25, 1.27, and 1.35 for $U_0 = 0.7$ (weak), 0.8 (medium) and 1.12 (strong), (5.31) predicts values for b_f that are 12, 13 and 24% larger than for the case $\alpha = 1$ (uniform flow). For the weak and medium barotropic flow case ($U_0 = 0.7$, $\alpha = 1.25$) the predicted value for b_f agrees well with the measured wedge front location and the use of the Coriolis coefficient is necessary to obtain this agreement. In the strongly forced case the front occurs upstream of the predicted value, i.e. α appears to be small. Pawlak & Armi (1997) argue that the discrepancy is due to boundary layer effects and cross-stream variations. In any event, this study provides experimental support for defining hydraulic control in non-uniform flows by using the 'Engineering Approach'. However, it is the only such study that I am aware of.

In the other limit, we found that an inviscid shear flow is controlled when the depth-averaged current speed equals the long wave speed, and this speed is greater than $(gh)^{1/2}$. In this situation, however, the velocity difference from bottom to top evolves with distance downstream, decreasing in an accelerating flow. It seems that a key issue is the nature of the frictional forces. If these depend only on local flow properties, then the control section will be shifted, but the speed of inviscid long waves at the control section will still be zero. If, on the other hand, the frictional forces involve along-channel derivatives of the flow variables, as for a fixed velocity profile, then the speed of long waves is changed and the control condition is no longer the same.

Many real situations might lie between these two limits, in being influenced by friction but not maintaining the shape of the velocity profile. It is not clear that there are any general results to apply in such cases, so that the governing equations would need to be examined for any assumed forms of bottom and internal friction. This is currently being investigated, but is beyond the scope of this thesis.

Only a rectangular channel of constant width was considered. Allowing for width variations would be trivial, though variations in cross-sectional shape would introduce further difficulties as in inviscid hydraulics. The effect of stratification has also not been addressed. In the inviscid case Killworth (1992) has shown that control occurs where the long wave speed vanishes. It is perhaps possible to extend the functional (5.26) to include stratification by beginning with $\frac{1}{2}\varrho u^2 + \varrho g z + p(z) = a(\psi)$ instead of (5.24) because $a(\psi)$ is then still constant on each stream surface.

In the context of this study the important question is, if and/or how the above results affect the determination of hydraulic control in the Bosphorus. Note that the control at the North Sill is not being questioned, because the lower layer velocity was approximately uniform and, more importantly, the hydraulic jump provided undisputable proof of the existence of a control. For the Contraction, South Sill and South Exit the situation is less clear, because neither are the layers uniform nor did we actually observe a hydraulic jump.

If we were to assume that the flow was inviscid then (5.20) tells us that the actual speed of the waves is larger than that obtained using layered theory, or, in other words, we would need larger average layer velocities to reach criticality. On the other hand, if we assumed that the flow maintained a similarity profile, i.e. used $F^2 = \overline{u}^2/(gh) = 1/M_2$ (or $1/\beta$ in engineering notation) as control condition, hydraulic control would be more likely because of the significant shear in the Bosphorus. Therefore, it is crucially important to utilise the correct method.

As pointed out before, the assumption of inviscid flow requires the velocity shear to decrease as the layer thins. This is clearly contrary to what we observe along the upper layer as it moves from the Contraction toward the South Exit (see figures 3.19 to 3.23). Furthermore the assumption of inviscid flow in the Bosphorus would be inconsistent with

previous findings that friction and entrainment are important. As a matter of fact, the velocity profiles between transects 7, 8 and 2 (figure 3.23) are quite similar, that is the similarity assumption seems to approximately hold. Velocity is nearly linear in the upper layer so that $M_2 \approx 4/3$. In section 3.4.4 I had calculated $F_1^2 = \overline{u}_1^2/(g'h_1) \approx 0.9$ and had concluded that the flow was between marginally subcritical and critical. But, in fact, $F_1^2 \approx 0.9 > 0.75 = 1/M_2$ which means that the flow was actually supercritical. If the flow obeyed the rules of inviscid hydraulic theory, somewhere further south a hydraulic jump should have occurred. We did not acquire observations to test this. In fact it is doubtful that a clear hydraulic jump could exist because of the shallowness of the upper layer and the influence of friction. The situation is similar to that observed at the eastern end of the Strait of Gibraltar where supercritical flow adjusts to subcritical flow through a frictional change with no obvious hydraulic jump (Farmer & Armi, 1988).

In summary, the analysis in this chapter provides support for the view that the exchange through the Bosphorus was bounded by two controls, i.e. that the exchange was maximal. The form of the frictional term (with $d\overline{u}/dx$) required for the similarity assumption is, however, unusual so that the application of the theory is somewhat preliminary. Further theoretical analysis and eventually comparison with experiments is required.

Comment on the use of $\mathbf{F^2 = 1/\alpha}$ or $\mathbf{F^2 = 1/\beta}$ as Control Condition

For a frictionally influenced homogeneous fluid with a fixed velocity profile the control conditions was shown to be $F^2 = 1/\beta$. In the engineering literature (Chow, 1959; Henderson, 1966; Pawlak & Armi, 1997), however, the commonly used control condition is $F^2 = 1/\alpha$. This discrepancy seems to arise because the Coriolis coefficient is usually introduced to adjust the velocity head term in the Bernoulli equation, that is (4.7a) is changed to

$$\alpha \frac{\overline{u}^2}{2g} + h + H = E_R \,, \tag{5.32}$$

from where the control condition $F^2 = 1/\alpha$ can be derived as usual. This approach, however, ignores that it is not possible to obtain a Bernoulli equation of the form (5.32) through integration of the momentum equation because of the presence of the frictional term on the right-hand side of (5.21).

Numerically the condition $F^2 = 1/\alpha$ is approximately the same as $F^2 = 1/\beta$ for most

near-uniform velocity distributions. However, the stronger the shear the larger will be the discrepancy. For uniform flow we obviously have $\alpha = \beta = 1$, but for linear velocity profiles, as in the southern Bosphorus, we find $1/\beta = 3/4$ to be significantly larger than $1/\alpha = 1/2$.

6. The Orkoz

The Orkoz seems to have been first described by Artüz & Uğuz (1976) who called an increase of surface salinity in the southern Bosphorus an "Orkoz". They reported daily observations of the hydrographic conditions during the period of 1967 to 1970 (reproduced by Özsoy *et al.* (1995)) and showed that surface salinity may increase to about 26 psu for a few days during winter (November to January). In later publications these events are associated with a blocking of the upper layer flow (e.g Özsoy *et al.*, 1995, 1998; Cetin, 1999) during which Black Sea water reaches only a few kilometres into the strait while the southern section fills with surface water from the Sea of Marmara. The lower layer consists, as usual, of highly saline Mediterranean water. A complete reversal of the upper layer flow has not been described in the literature although it is certainly known to occur, as we were told by Dr. Hüsne Altiok[1]. Furthermore, the commuter ferries, which we took every day to meet our survey vessel, seemed to be familiar with the reversed and very strong surface currents[2].

6.1. Observations

The Orkoz began on April 5 at 12:00 UTC. At that time the upper layer still flowed southward but had slowed down to about $-0.5\,\mathrm{m\,s^{-1}}$. Its speed was zero at 15:00 (figure 3.7, page 42). It then picked up speed in the other direction and reached a maximum of

[1] Dr. Altiok joined our survey for a few days and happened to be with us during the Orkoz event. She is with the Institute of Marine Sciences and Management, Istanbul University.

[2] At the morning of the Orkoz it appeared to me during the cross-over on the ferry that something was different. However, I did not realise at that time that the ferries were approaching the terminals from a different direction than usually. Only after we had started the ADCP on the survey vessel, did I notice that the flow was going the "wrong" way. So much for observational oceanography!

$1.35\mathrm{m\,s^{-1}}$ at 18:30. The Orkoz lasted almost exactly two days. The upper layer speed was again zero at 14:00 on April 7.

Wind Forcing

As mentioned in section 3.2.2, p. 39 the reversal of the upper layer was caused by an increase in sea-level in the Sea of Marmara above the level in the Black Sea. This was caused by a storm with strong southwesterly winds with centre somewhere over the Aegean Sea. Figure 6.1 shows wind-speeds recorded in 2000 at the Strait of Canakkale (Dardanelles), at Istanbul, and at Zonguldak in the western Black Sea (figure 2.1). Exceptionally strong southwesterly winds up to $30\mathrm{kmh^{-1}}$ occurred at Canakkale on April 5. At the same time wind speeds at Tekirdag at the southern Sea of Marmara (not shown here) and at Istanbul reached $18\mathrm{kmh^{-1}}$. One day later wind speeds were $20\mathrm{kmh^{-1}}$ at all locations, and finally on April 7 wind speed had decreased to $10\mathrm{kmh^{-1}}$ at Canakkale and Tekirdag but remained at $20\mathrm{kmh^{-1}}$ at Istanbul. Conditions were back to normal on April 8. In the western Black Sea at Zonguldak the influence of the storm was weak; southeasterly winds of $10\mathrm{kmh^{-1}}$ were noticed on April 5, but weakened to $5\mathrm{kmh^{-1}}$ westerlies the next day. At the Bosphorus the wind began to increase in the morning of April 5 and was maximal in the evening[3] (figure 3.7, page 42). It weakened overnight, increased again on April 6, decreased almost to zero in the evening, and increased again significantly on April 7. This pattern was repeated in the Golden Horn sea-level data and consequently also in the upper layer current data.

The lower layer current followed the pattern of the upper layer current with one notable exception on April 6 at 01:00 UTC. When the sea-level difference decreased briefly, the current at 49m depth decreased much more than in the upper layer.

Stratification

Figure 6.2 shows ADCP and CTD data which are complementary to the observations displayed shown in figure 3.7, p. 42. During exchange conditions we see high back-scatter

[3]During our survey the sea surface became increasingly choppy because the current and wind were opposite to each other. A few kilometres south of the contraction we had to cancel our survey because wave heights at Istanbul were said to reach 1m and a storm warning was in effect.

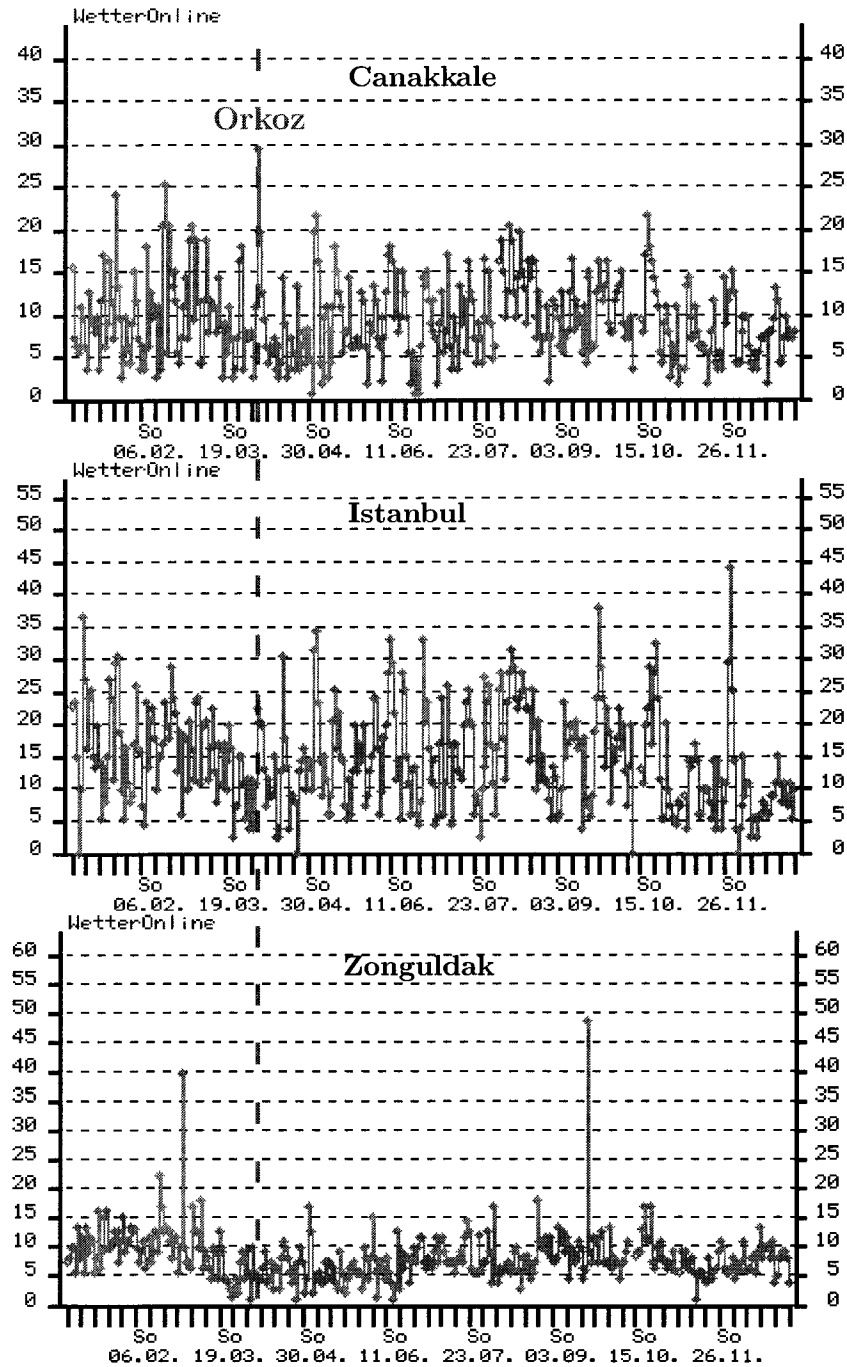

Figure 6.1.: *Wind speeds in* km/h *in year 2000 in Canakkale (upper panel), Istanbul (middle panel), and Zonguldak (lower panel). The vertical red line indicates the time of the Orkoz. The data were obtained from and are used with permission of Wetteronline Meteorologische Dienstleistungen GmbH, Bonn (www.wetteronline.de).*

intensity along the interface caused by shear induced microstructure. At the beginning of the Orkoz the shear decreases and the back-scatter intensity decreases as well. The high back-scatter intensity above the sea-floor is curious. It seems unlikely that it originated from salinity and temperature microstructure because below 50m the water was homogeneous. My guess is that it was caused by floating sediments. These might have been stirred from the sea-floor by the exceptionally strong currents.

About 4.5h after the onset of the Orkoz we observed a vertical band of slightly increased back-scatter in the upper layer. This might indicate the arrival of the Sea of Marmara water in the contraction because one would expect density microstructure at the front between Sea of Marmara and Black Sea water. The distance between the South Exit and the ADCP was 11km and assuming average layer speeds of $0.6\,\mathrm{m\,s^{-1}}$ to $0.9\,\mathrm{m\,s^{-1}}$ the travel time was between 5 and 3.5h which is consistent with the 4.5h given above. From this is also clear that the Sea of Marmara water must have reached the Black Sea after about 18h (Estimated from 30km/11km $\times$ 4.5h plus some additional time because the northern section is wider and hence the current must have been smaller than along the southern section.). In other words, Black Sea water was completely flushed out of the Bosphorus even before the end of the first Orkoz day.

Contours of temperature and density were derived from CTD casts that we carried out in proximity of the bottom-mounted ADCP. Recall that during exchange conditions fresh and cold upper layer water flows southward and salty and warm lower layer water northward. During the Orkoz the upper layer had a salinity of 22.5 psu which indicates that it originated in the Sea of Marmara. Temperature was at first 10°C uniformly throughout the layer. Later the layer was temperature stratified, presumably because southwesterly winds brought warm air (confirmed by air-temperature data that are not shown here) to the Sea of Marmara causing heat to be mixed into the upper 10 to 15m (see temperature profile in figure 6.3).

The lower layer showed increased temperature and decreased salinity/density during the Orkoz. The continuous temperature record from the bottom mounted ADCP (3m above the sea-floor) shows that temperature dropped immediately after the onset of the Orkoz. Temperature reached a minimum on April 6 at about 12:00, shortly after layer velocities had decreased sharply. It then increased again, remained at about 14°C for roughly 12h

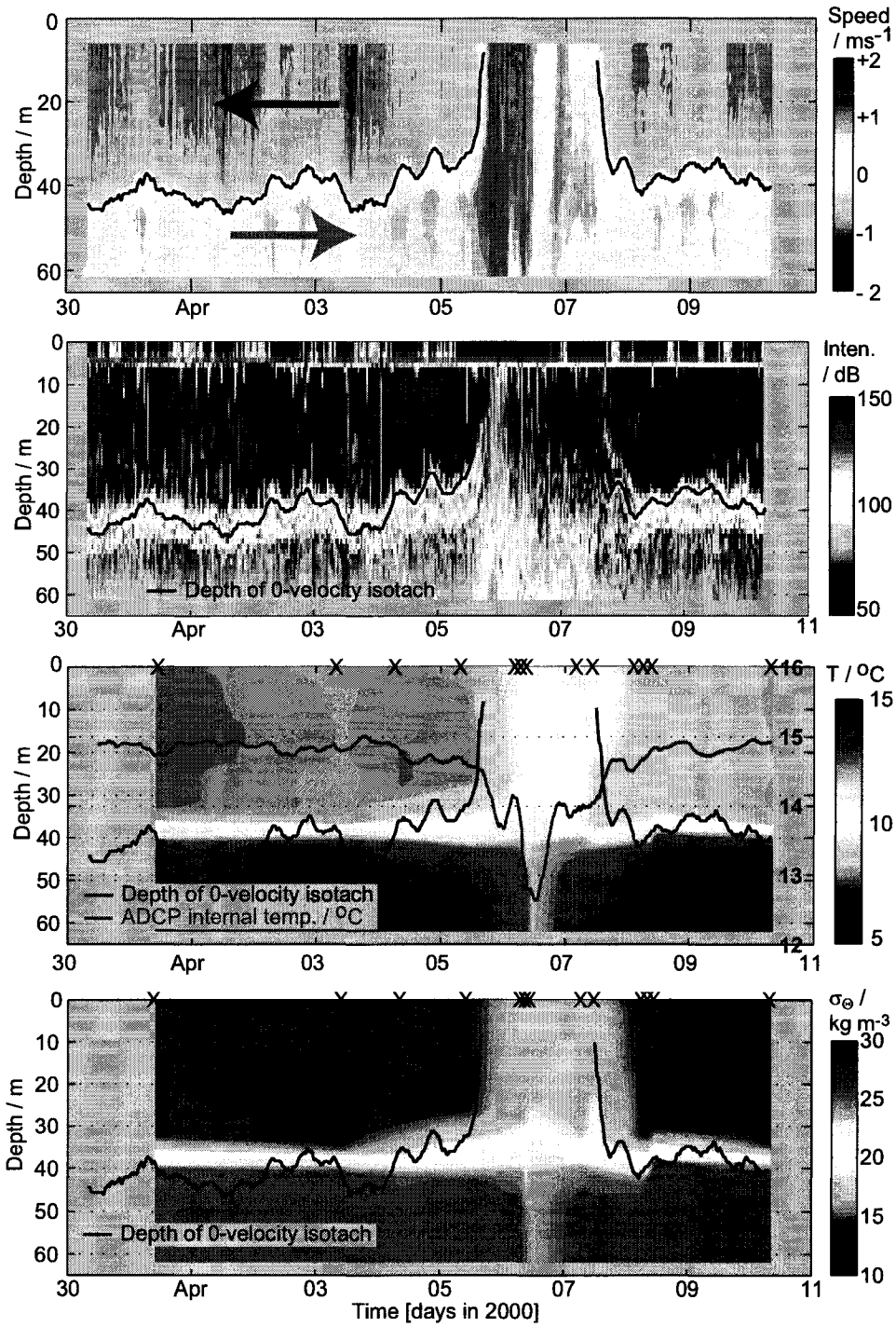

Figure 6.2.: ***1st panel:*** *Along-channel component of horizontal current from the bottom-mounted ADCP.* ***2nd panel:*** *Average (4 beam) back-scatter intensity. Intensity has been corrected for beam spreading and absorption. The black line indicates the depth of the zero-velocity iso-tach.* ***3rd panel:*** *Contour of temperature data from CTD casts carried out near the ADCP. The crosses indicate the time of the casts and the red line the temperature recorded by the internal sensor of the ADCP.* ***4th panel:*** *Density in units of σ_θ. Salinity is not shown as it is very similar to density.*

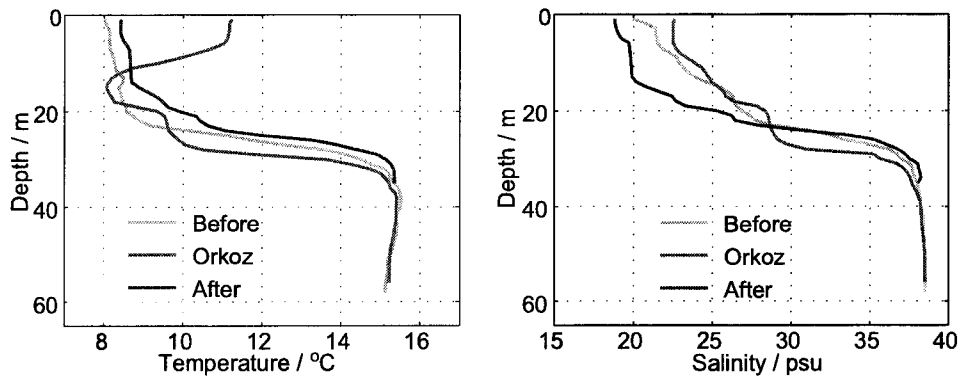

Figure 6.3.: *Comparison of temperature and salinity profiles from before, during, and after the Orkoz. Two profiles were taken at thalweg position −1km at the Sea of Marmara on March 31 (green) and April 7, 12:00 UTC (red) and the third profile was taken on April 10 (blue) at thalweg position* +1km *at Istanbul.*

on April 7, and increased back to normal at the end of the Orkoz. This pattern can be explained by entrainment of colder and fresher upper layer water into the lower layer. The other explanation would be that temperature and salinity of the lower layer in the Sea of Marmara had decreased, possibly due to increased wind mixing. Salinity and temperature profiles from the South Exit (figure 6.3) show, however, that this was not the case - at least not during the second Orkoz day (April 7). The entrainment hypothesis appears a bit inconsistent with the fact, that minimum temperatures were observed not during the period of maximum current at the beginning of the Orkoz but later, shortly after the second period of strong currents (April 6, 14:00 UTC). Perhaps wind mixing did influence the lower layer on April 6 when winds were stronger than on April 7.

Temperature, salinity, and density contours along the southern section of the Bosphorus are shown in figure 6.4. The CTD profiles were carried out on cross-channel transects that are shown in figures 6.5 and 6.6. Because of bad weather and logistical constraints[4], we were not able to do a continuous run along the channel and neither could we obtain any data from the northern part of the strait

The data from the second Orkoz day (April 7) clearly show temperature and salinity stratification within the upper layer. The temperature stratification is absent in the data

[4]On April 6 currents were so strong that the vessel had difficulties with manoeuvring. In addition storm warnings were in effect so that we were advised to stay in the sheltered central section of the Bosphorus. On April 7 we had to go to the Golden Horn to retrieve data from the sea-level recorder.

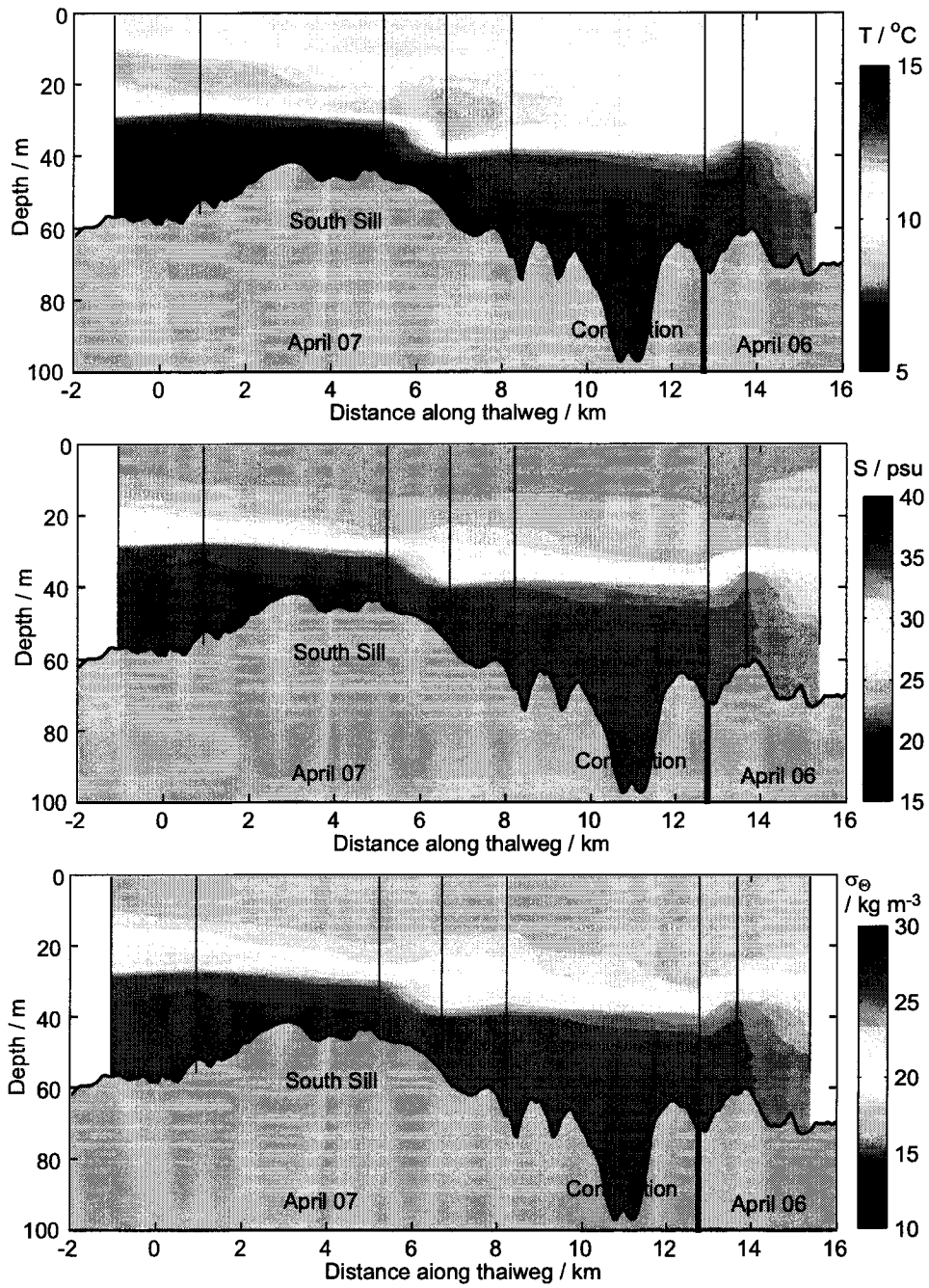

Figure 6.4.: *Composite of survey data obtained on April 6 and April 7, 2000, during the Orkoz. The data from the two days are merged at thalweg position* 12.8km, *indicated by the vertical black line. On both days a CTD cast was carried out at this position.* ***1st panel:*** *Contours of temperature. The location and depth of the CTD casts is shown by the black vertical lines.* ***2nd panel:*** *Salinity.* ***3rd panel:*** *Density in units of* σ_θ.

from April 6 because of reasons mentioned before. Stratification was most pronounced at the South Exit (figure 6.5). It was reduced somewhat by turbulence as the layer moved northward but was still noticeable at the contraction. Most of it was lost in the contraction where currents were strongest. Compare the almost homogeneous profiles from transect 1, during which the Orkoz was very strong, with the structured ones from transect 7 at the end of the Orkoz.

The lower layer was homogeneous at the South Exit and remained so up to the South Sill. It was thick enough to pass over the central ridge whereby it was strongest on the western side of the ridge. (I note in passing that this is characteristic of a strong lower layer flow, as observed by Gregg & Özsoy (2002), whereas for weaker flow the flow is concentrated on the eastern side as shown by transect T7 in figure 3.23, p. 67). During the passage over the South Sill its salinity decreased indicating that it entrained less saline upper layer water. Thereby it also became stratified, but between transect #2 and transect #1 it became again homogeneous - presumably because of turbulence.

Throughout this thesis back-scatter intensity from the ADCPs and the echo-sounder was used not only as indicator for turbulence but also an approximate tool for quantifying turbulence and/or mixing intensity. Some justification was given in section 3.4 in connection with figure 3.16. The data shown in figure 6.2 provide additional support for the assumption that the backscatter is from microstructure because as soon as interfacial shear became zero, back-scatter became zero as well. An alternative explanation is that the back-scatter was caused by zooplankton which moved away from the density interface when the shear disappeared. However, I do not know whether this would be the usual behaviour of zooplankton, so that for my purposes it seems more plausible to assume that main reason for back-scatter was microstructure.

Hydraulic Controls

In the contraction upper and lower layer currents reached speeds of $1.3\mathrm{m\,s^{-1}}$ at the beginning of the Orkoz. If we exclude the recirculation zones near the shores, that are evident in transect #1 in figure 6.5, the average layer speeds were between 1 and $1.2\mathrm{m\,s^{-1}}$. The density interface with $\sigma_\theta = 20\mathrm{kgm^{-3}}$ was at 35m and the layers were stratified 7m above and below this interface. Above 28m the upper layer had a constant density of $\sigma_\theta \approx 17\mathrm{kgm^{-3}}$

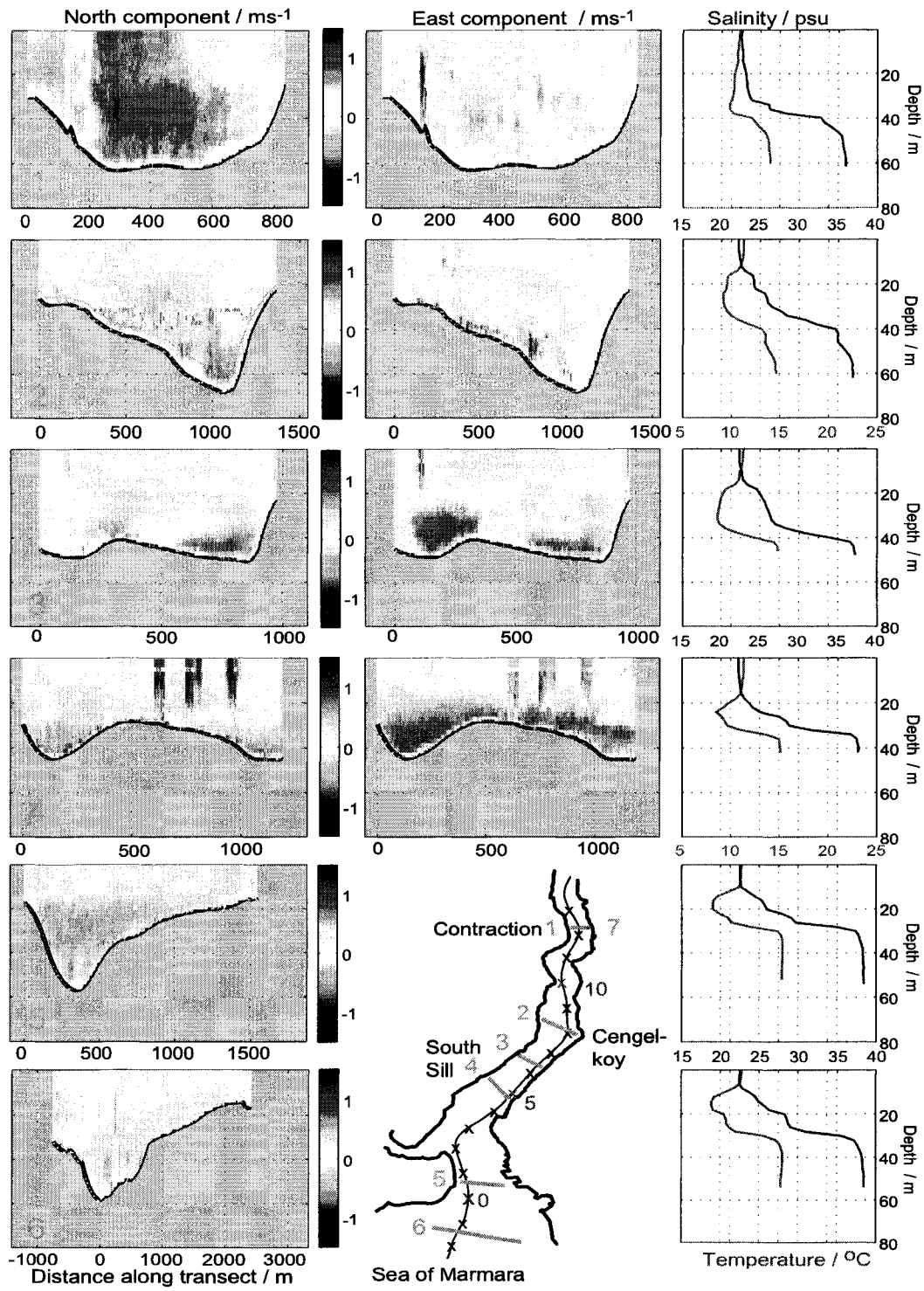

Figure 6.5.: *Velocity, temperature, and salinity data from 6 cross-channel transects from April 7, 2000, the 2nd Orkoz day. The left and middle column show the north and east component of the horizontal velocity. For transects 5 and 6 the east component (not shown) was practically zero. Note that vertical scales are identical on all plots but horizontal scales vary. The map shows the location of the transects.*

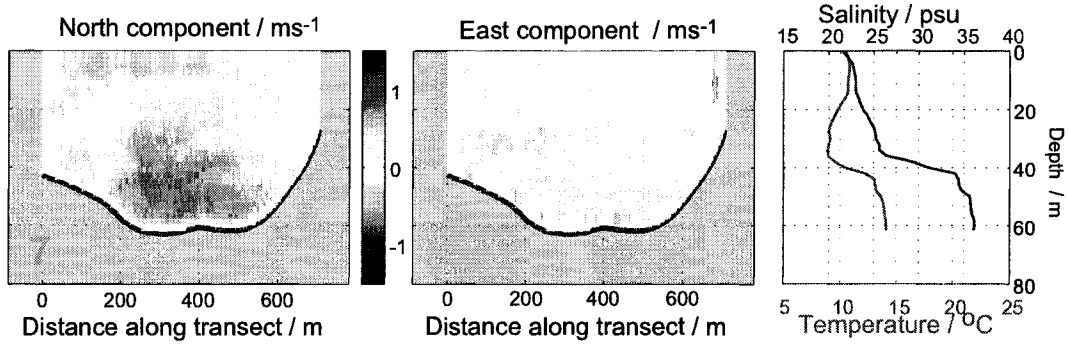

Figure 6.6.: *As in figure 6.5. Transect 7 was carried out at the same location as transect 1 but at the end of the survey day when the Orkoz was about to end.*

and below 42m the lower layer density was $\sigma_\theta \approx 26\text{kgm}^{-3}$. Hence, reduced gravity was between 0.08 and $0.09\text{m}\,\text{s}^{-2}$. With $h_1 = 35\text{m}$ and $h_2 = 30\text{m}$ the upper and lower layer Froude numbers were $F_1^2 \approx 0.3$ to 0.5 and $F_2^2 \approx 0.4$ to 0.6, so that G^2 was between 0.7 and 1.1 and the flow was between marginally subcritical to supercritical. This possible control could have lasted only until April 6, 07:00 UTC (before our survey) when the lower layer velocity dropped by about $0.5\text{m}\,\text{s}^{-1}$. Afterwards velocities were almost certainly too small for a control in the Contraction.

Along the southern and northern section of the strait the upper layer is wider than in the contraction so that velocities were certainly lower. This means that F_1^2 probably did not exceed values of 0.3 anywhere else. On the other hand, the lower layer Froude number probably reached values of 1, i.e. the flow was critical, at various other locations. For instance, recall that during exchange conditions with $Q_2 \approx 5000\text{m}^3\,\text{s}^{-1}$ (on April 5, figure 3.17) we found $F^2 \gtrsim 1$ at the North Sill and so did Gregg & Özsoy (2002) for $Q_2 \approx 10000\text{m}^3\,\text{s}^{-1}$. During the Orkoz $Q_2 \approx 10000\text{m}^3\,\text{s}^{-1}$ and $g' \lesssim 0.8$ so that very likely $F_2^2 \gtrsim 1$ and the flow was controlled at the North Sill. In conclusion, this means that the flow in the strait was almost certainly isolated from any changes in interface depth in the Black Sea - if those actually occurred.

At the South Sill the central ridge (see the bathymetry in figure 3.21) divided the lower layer into flows along the eastern and western shore. Although the western sea-floor lies higher than the eastern one, the flow was stronger west of the ridge because the deep channel, coming from the Sea of Marmara, steered the flow that way. On transect #4

across the South Sill lower layer velocities reached $1.7\mathrm{m\,s^{-1}}$ in the western channel and the average velocity was about $1.4\mathrm{m\,s^{-1}}$. With $h_2 \approx 15\mathrm{m}$ and $g' \approx 0.09$ the Froude number is $F_2^2 \approx 1$. In the eastern channel $F_2^2 \lesssim 0.7$. North of the South Sill the western channel ends so that in the bend at Cengelkoy (see figures 2.4 and 6.5) the water joined the flow in the deeper eastern channel. Consequently currents were strong at the northern end of the eastern channel and $F_2^2 \gtrsim 1.2$, that is the flow was supercritical. It responded violently to little bumps and holes along the sea-floor, as shown in figure 6.7. We sailed southward starting at Cengelkoy and passed a 10m elevation at 8.5km and a smaller one at 9.4km. The data show nicely the transition of the flow from subcritical to supercritical and back to subcritical through a hydraulic jump when the flow passed over the first bump. An internal wave with $\approx$ 15m amplitude was generated and vertical velocities reached $\pm 0.2\mathrm{m\,s^{-1}}$. The wave propagated along the pycnocline at 40m depth. In fact, it served as a useful guide for defining the interface between upper and lower layer.

6.2. Discussion

Time Dependence

In section 3.2.2 we concluded that during exchange conditions the flow could be considered quasi-steady. Not surprisingly, this approximation was not valid at the beginning and end of the Orkoz because at these times the magnitude of the time dependent term in the along channel momentum equation term was approximately 200% and 50%, respectively, of the horizontal pressure gradient terms (see appendix C). On the other hand, during the Orkoz the flow was again relatively steady for some periods of time.

Differences to Previously Reported Orkoz Events

The Orkoz that we observed had some of the characteristics that are described in the literature, but was different in other respects:

Previously an Orkoz was believed to occur only during winter months when the sea-level difference is minimal. In spring and summer, when an increased freshwater influx to the Black Sea increases the sea-level difference, one should expect a blocking of the lower layer rather than an Orkoz. As a matter of fact, the upper layer flow was very strong at the

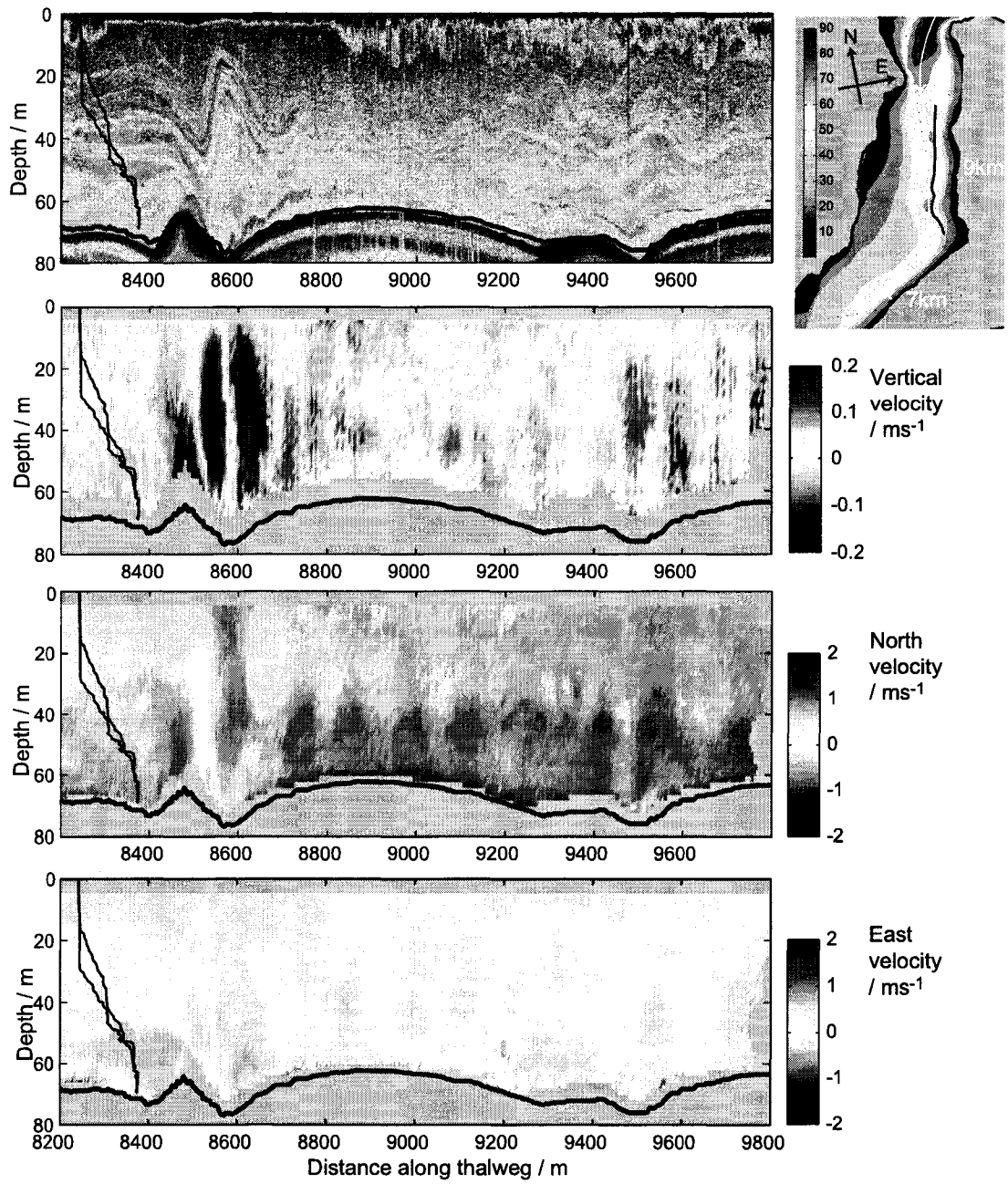

Figure 6.7.: *Echo-sounder and ADCP velocity data from a south-north run along the eastern side of the strait. The ship's track is shown as black line on the map. Density data from a CTD cast (down and up) at thalweg* 8km *are superimposed on the sounder and velocity contours. Discrepancies between the depths shown by our sounders and those in the map are most likely due to inaccuracies in the bathymetry data. The official Turkish navigational charts seem more accurate but also could not answer with certainty whether the elevations extend across the canyon or whether they are just isolated bumps.*

beginning of our experiment and on April 3 the lower layer came almost to a halt with $u_2 \approx 0.2\mathrm{m\,s^{-1}}$. Nevertheless, a sufficiently strong meteorological event as the storm over the Aegean Sea and Sea of Marmara was able to reverse the sea-level difference and hence the upper layer flow. This emphasises the rather unpredictable character of the flow in the Bosphorus.

The flow maintained a distinct two layer density character at all times. The density difference between the layers was only a little smaller than during exchange conditions because the upper layer consisted of Sea of Marmara water with a salinity of about 23 psu instead of Black Sea water with $S \approx 18$ psu. The Sea of Marmara water showed some stratification both in temperature and salinity which persisted throughout the southern strait. This is, however, different than the three layer stratification described by Özsoy *et al.* (1995) which was caused by a blocking of the upper layer rather than by a complete reversal, during which Black Sea water was completely flushed out of the Bosphorus.

Artüz & Uğuz (1976) defined the Orkoz as the occurrence of surface salinity values larger than 24 psu in the southern section of the strait. Curiously during our Orkoz surface salinity never exceeded 23 psu. A possible explanation is as follows: in the Sea of Marmara surface salinity is approximately 23 ± 2 psu and reaches its maximum during winter as a result of increased wind mixing and reduced influx of fresh water from the Black Sea (Beşiktepe *et al.*, 1994). The previously reported Orkoz events all occurred during the winter which could explain the salinities above 24 psu. On the other hand, "our" Orkoz occurred in spring when $S \approx 23$ psu.

Control of Lower Layer Flow

At the South Exit the interface, which we may define to be the surface $\sigma_\theta = 20\mathrm{kgm^{-3}}$ was at a depth of about 20m. This is approximately the same depth as observed during exchange conditions (see figures 3.10 and 3.11). The density gradient between the Sea of Marmara and the Black Sea was unchanged so that one should expect the lower layer to attain a significantly larger velocity than the upper layer during the Orkoz. Curiously this was not the case. Upper and lower layer velocities measured by the bottom-mounted ADCP were almost identical and their fluctuations showed very similar patterns, as we have seen in earlier figures and as shown in detail in figure 6.8. Although we do see some

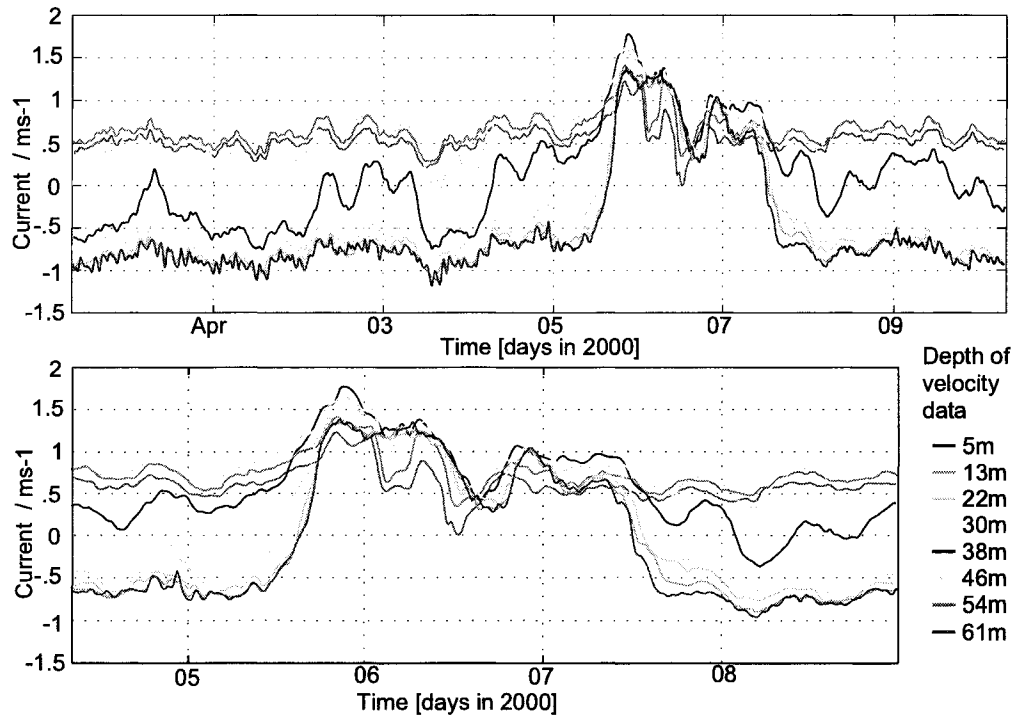

Figure 6.8.: *Along-channel component of horizontal current from different depths measured by the bottom-mounted ADCP. The upper panel shown data from the entire ADCP record, whereas the lower panel focusses on the Orkoz. The black line shows the current at* 38m *depth which is the approximate position of the zero-velocity interface. Red coloured lines present lower layer velocities and blue/green coloured lines upper layer velocities.*

small differences between the layers, which can mostly be explained by the influence of bottom friction or by the larger inertia of the upper layer compared to the lower layer, the two layers behaved as if "locked together". Finally note that even at times of large lower layer velocities (April 6, 10:00 UTC) the lower layer transport Q_2 was hardly more than $10\,000\mathrm{m}^3\,\mathrm{s}^{-1}$ which is what Gregg & Özsoy (2002) obtained for Q_2 during exchange conditions. (Total transport was approximately $25\,000\mathrm{m}^3\,\mathrm{s}^{-1}$.)

How can we explain this most striking behaviour?

The layers could have indeed been "locked together" by a sufficiently large exchange of momentum. However, interfacial friction of the form form $C_I(u_1 - u_2)|u_1 - u_2|$ could not have done this because the velocity difference between the layers was small at all times. Entrainment and/or mixing was observed and this must have exchanged some momentum. But considering that during exchange conditions downward entrainment is not sufficient

to halt the lower layer, it appears unlikely that is was sufficient to reduce the momentum of the lower layer during the Orkoz[5]. A third possibility is the momentum transfer through interfacial waves such as those in figure 6.7 which we observed on both Orkoz days. But again the question is whether this would have been sufficient. This seems unlikely since we did not observe similar waves anywhere else, consistent with the fact that elsewhere currents were probably not strong enough for reaching critical flow states. Of course, the limited data coverage does not allow us to be certain.

Let us try an alternative explanation, i.e. assume that only the lower layer flow was limited in some way. The hydraulic controls only prevented information from the Black Sea from propagating southward, but nothing prevented information from the Sea of Marmara, i.e. changes in the interface position or of the density difference between the layers, from being communicated into the strait. In other words, the hydraulic controls were not the limiting factor. Interfacial shear was ruled out above. Then it seems that only bottom/side-wall friction could have limited the lower layer flow. Let us investigate whether this is possible by considering the force-balance in the lower layer: the along channel momentum equation for the lower layer is given by (4.56b) and (4.57), p. 99 and can be approximated as

$$\underbrace{\frac{U_2}{g}\frac{\Delta U_2}{L}}_{!} = \underbrace{\frac{\varrho_1}{\varrho_2}\frac{\Delta\eta_1}{L}}_{1/200\,000} + \underbrace{\frac{\Delta\varrho}{\varrho_2}\frac{\Delta\eta_2}{\varrho_2}}_{1/90\,000} + \underbrace{\frac{H_1}{\varrho_2}\frac{\Delta\varrho_1}{L}}_{1/60\,000} + \underbrace{\frac{H_2}{2\varrho_2}\frac{\Delta\varrho_2}{L}}_{1/100\,000} - \underbrace{\gamma\frac{C_H}{g}\frac{U_2^2}{H_2}}_{!} \tag{6.1}$$

where we have used that during the Orkoz the flow was steady for limited periods of time, that is the time-dependent terms were dropped. The dimensionless terms on the right-hand side represent the surface gradient, the interface gradient, the density gradient in the upper layer, the density gradient in the lower layer and the drag due to bottom friction. The parameter γ represents the fact that the friction changes with the shape of the cross-section (e.g. Bormans & Garrett, 1989*b*). $\gamma = 1$ and $\gamma = 2$ represent rectangular and triangular cross-sections respectively. We evaluate the values between the southern and northern sea-level recorder and consider the time of maximal sea-level difference when $\Delta\eta_1 \approx 0.1\text{m}$. We use $H_2 = 30\text{m}$ and estimate the change in interface elevation to be $\Delta\eta_2 = 20\text{m}$ and the velocity difference ΔU_2 to be between $0.5\text{m}\,\text{s}^{-1}$ and $1\text{m}\,\text{s}^{-1}$. The

[5]We were not able to determine entrainment rates during the Orkoz because the interface between the layers was poorly defined due to the absence of a zero-velocity isotach.

$\Delta U_2/\mathrm{m\,s^{-1}}$	$C_H \times 1000$	γ	$U_2/\mathrm{m\,s^{-1}}$
0.5	2.3	1	2.2
1	2.3	1	2.1
0.5	3.5	1	1.8
0.5	2.3	2	1.6
0.5	3.5	2	1.3

Table 6.1.: *Solutions of equation* (6.1) *for combinations of parameters* ΔU_2, C_H *and* γ.

other variables are as specified in appendix C, page 180. Then we obtain the values set under the curly brackets in (6.1) whereby the exclamation marks indicate the terms with the unknown velocity U_2 which we need to solve for. The results are shown in table 6.1 for various values of C_H and γ.

We first note that the uncertainty in ΔU_2 has a negligible influence on the results. The main result then is that in order to obtain lower layer velocities of about $1.5\mathrm{m\,s^{-1}}$, which is a value supported by our observations, we have to take into account that the wetted perimeter of the lower layer is not rectangular and/or we have to use a friction coefficient larger than $C_H = 2.3 \times 10^{-3}$. Both are plausible assumptions. It is hence possible that it was indeed bottom friction which limited the lower layer transport during the Orkoz, and this might have been facilitated by momentum transfer between the layers due to entrainment and internal waves.

7. Summary

7.1. Summary and Conclusions

This work presents detailed observations of the exchange flow through the Bosphorus. Although there have been numerous previous surveys, almost all but the most recent (Gregg *et al.*, 1999) were limited to hydrographic measurements. Worsening environmental problems call for a better understanding of the currents and flows in the Bosphorus. Furthermore, this study improves, through simplified theoretical description, our understanding of the effects mixing and frictionally induced shear on the dynamics of exchange flows. These effects have only recently received increased attention as many previous studies were geared towards classical inviscid hydraulic theory. This works well in short, deep and narrow straits, such as Gibraltar, but is less appropriate in long, narrow and shallow straits, such as the Bosphorus.

Observations

Our observations consist of ADCP, CTD and sonar measurements from survey vessels supplemented by continuous records of sea-level and currents. Measurements are particularly challenging in the southern Bosphorus, because the surface layer becomes extremely shallow at this location and escaped previous measurements which were limited by instrument depth and other factors. We designed our measurements to minimise this problem. Detailed measurements along transects across the channel provided accurate estimates of horizontal volume and salt fluxes allowing us, for the first time, to quantify vertical mixing between the layers.

Baroclinic forcing between the Black Sea and Sea of Marmara is believed to be constant on time-scales less than a few months (e.g. Özsoy *et al.*, 1998). This assumption is consis-

tent with our observations of nearly constant density at both ends of the strait. On the other hand, sea-level and current data showed fluctuations of various origins ranging from periodic, but small tidal forcing to strong and highly irregular meteorological forcing. As if to confirm the importance of the latter, strong southwesterly winds caused for two days a highly unusual, and for the time of the year unexpected, reversal of the upper layer flow, locally called an 'Orkoz'. During the Orkoz the total northward transport reached $27\,000\mathrm{m}^3\,\mathrm{s}^{-1}$, compared to average upper and lower layer transports of $-17\,000\mathrm{m}^3\,\mathrm{s}^{-1}$ and $+4\,000\mathrm{m}\,\mathrm{s}^{-1}$, respectively, during exchange conditions. Using an analysis developed by Helfrich (1995), I find that the exchange was to a good approximation quasi-steady. On the other hand, a simple order of magnitude estimate of the terms in the equations of motion shows that the flow was unsteady at the beginning and the end of the Orkoz.

During exchange conditions we observed the well known two-layer structure with upper layer water moving from the Black Sea toward the Sea of Marmara over an undercurrent consisting of Mediterranean water moving in the opposite direction. Along the northern section, between the North Sill and the Contraction, both layers were approximately uniform in velocity and homogeneous in density, and the interface was relatively thin, not occupying more than 10% of the total water depth. It sloped throughout the strait with the average slope about twice as large along the southern section of the strait than along the northern section. At the crest of the North Sill the flow was critical, confirmed by a hydraulic jump downstream. Despite numerous bends along the northern section, mixing between the layers was small because strong stratification effectively limited the effect of shear induced turbulence at the interface. The speed of the upper layer increased substantially in the contraction reaching $-1\mathrm{m}\,\mathrm{s}^{-1}$ along the centre-line and $-2\mathrm{m}\,\mathrm{s}^{-1}$ at some lateral protuberances. Interfacial shear and turbulence created by the interaction of the flow with the topography caused lower layer water to be entrained by the upper layer. The lower layer lost about 20% of its volume to the upper layer. In contrast to previous claims based on hydrographic measurements and numerical modelling studies (Ünlüata *et al.*, 1990; Oğuz *et al.*, 1990; Yüce, 1996; Özsoy *et al.*, 1998), but in agreement with observations by Gregg *et al.* (1999), we did not observe critical flow in the Contraction. Owing to bends as well as ridges and channels along the sea-floor, the flow was complicated between the Contraction and the South Exit. During our measurements upward entrainment was

only slightly less than along the Contraction so that in total the lower layer lost about 30% of its transport to the upper layer through entrainment between the South Exit and the Contraction. These numbers are averages of a few daily values observed in August 1998 and March/April 2000 and are probably not equal to long-term averages which ought to be smaller according to long term salt balances. The upper layer was stratified and showed strong vertical shear which increased steadily between the Contraction and the South Exit. Contrary to Gregg & Özsoy (2002) our observations do not indicate that the flow was critical at the South Sill. On the other hand, we were able to observe the shallow upper layer flow toward the Sea of Marmara and found $F_1^2 = \overline{u}_1^2/(g'h_1) \approx 0.9$, i.e. the flow appeared to be marginally subcritical or critical according to classical two-layer hydraulic theory.

In two-layer numerical simulations of the exchange Oğuz *et al.* (1990) assumed a bottom friction coefficient of $C_H = 2.3 \times 10^{-3}$. Our velocity data from bottom-mounted ADCP provided a first opportunity to check the validity of this value. By identifying the logarithmic boundary layer above the seabed I was able to estimate the bottom stress. From that I determined the friction coefficient C_H which ranged from 1.9×10^{-3} to 2.5×10^{-3}. The log-layer was not the result of skin-friction but rather caused by form drag along an irregular sea-floor (Lueck & Lu, 1997; Sanford & Lien, 1999). It appears likely that the friction coefficient is larger along some isolated lateral protuberances which exert form drag on the flow. However, we are lacking the data to test this assumption.

The Orkoz was caused by a storm with strong southwesterly winds which raised the sea-level at the Sea of Marmara side of the Bosphorus above the level at the Black Sea side. Being a rare and irregularly occurring phenomenon little is known about the Orkoz in the literature. Even the information that is reported (e.g. Özsoy *et al.*, 1995, 1998) was only partly in agreement with our observations. For instance, we did not observe a three layer stratification, but the usual two layer structure whereby the only difference was that the upper layer consisted of water from the Sea of Marmara instead from the Black Sea. Furthermore, the Orkoz did not occur during the winter, when the sea-level in the Black Sea is at a minimum, but in spring when one should expect to see the opposite, i.e. a blocking of the lower layer. This confirms that the exchange was very much at the mercy of irregular meteorological forcing. Curiously upper and lower velocity were

quite similar despite the fact that baroclinic forcing was the same as during exchange conditions. The most likely explanation appeared to be that the lower layer flow was limited by bottom/side-wall friction.

Our observations provide new and detailed information on the flow in the Bosphorus. As far as the northern section of the strait is concerned, discrepancies to other studies (e.g. Möller, 1928; Tolmazin, 1985; Ünlüata *et al.*, 1990; Yüce, 1996; Özsoy *et al.*, 1998; Gregg & Özsoy, 2002) are minor. On the other hand, the complicated geometry along the southern section causes very complicated flow patterns, the exact shape of which seems to depend on the strength of the exchange. For example, during strong lower layer flow the water is directed mainly along the western side of the South Sill, whereas for weaker lower layer flow it is concentrated along the eastern side. This explains why Gregg & Özsoy (2002) believed the flow to be controlled at the South Sill whereas we did not observe a control there during exchange conditions. Although there is no doubt that geometrical features make the Bosphorus predisposed for sill, contraction and exit controls, it appears that the existence of the controls depends on the fluctuating barotropic forcing. It is therefore perhaps not surprising that a complete picture has yet to emerge. Long-term current measurements are needed to provide accurate observations of variability from hourly to annual times scale. A relatively easy, though perhaps expensive, method seems to be the use of a bottom-mounted ADCP. After calibration the current data can transformed into accurate estimates of layer transports (section 3.2.2). If two ADCPs are deployed, at the South Exit[1] and in the Contraction say, it might indeed be possible to obtain a continuous record of vertical mixing along the southern section of the strait. The benefit for determining the pathways of pollutants brought into the strait is obvious. Furthermore, if the ADCPs were connected by cable to shore-stations, the exchange could be monitored in real-time, possibly greatly reducing the risk of marine accidents.

The Effects of Mixing on the Dynamics of the Exchange

The interface along the Bosphorus is markedly sloped rising from north to south. In principle, the slope can be explained with the influence of bottom/sidewall and interfacial

[1] Here one would probably need to deploy two ADCPs in order to be able to account for the non-uniformity of the flow across the channel.

friction as shown, for instance, by Assaf & Hecht (1974) and Bormans & Garrett (1989*b*). However, both studies ignore mixing. In the Bosphorus we observed a significant amount of upward entrainment in the southern half of the strait, and clearly one must wonder about the effect of the exchange of volume, mass and momentum on the dynamics of the flow.

I have analysed this question by extending previous frictional single and two-layer models to include entrainment. A reduced gravity single-layer flow beneath a deep inactive layer was discussed first. Consideration of momentum conservation in a control volume led to relationships for the evolution of flow properties. Expressions were derived for the local change of Froude number and layer thickness as a function of the entrainment velocity. It was shown that entrainment, like friction, acts to force the flow toward criticality, although the layer thickness can increase if the Froude number is smaller than 1/2. For certain Froude numbers the effects of friction and entrainment on the layer thickness and the hydraulic state of the flow were found to be of comparable magnitude. Pratt (1986) pointed out that friction can cause purely subcritical flows to become asymmetric, i.e. to appear as an inviscid critical flow. It was shown that this can also occur as the result of entrainment.

Along the Contraction and South Sill both layers were active so that the effect of entrainment needed to be described with a two layer model. The principal conclusions were found to be the same as for the single layer model. Consideration of the special case of an exchange flow with $F_1^2 = F_2^2$ and $Q_1 + Q_2 = 0$ showed that (for a rectangular channel) interfacial and bottom friction had the same effect if $C_H = 8C_I$ emphasising the possible importance of interfacial friction. For the same case entrainment was found to have only a small effect on the layer thicknesses if $G^2 \approx 0.5$. This showed that a large entrainment need not necessarily have a large effect on the dynamics - although it will if $Q_1 + Q_2 \neq 0$ which might be true for most exchange flows.

In order to qualitatively test the theory, I compared the observed rise of the interface along the contraction with the value predicted by the theory using measured entrainment rates, friction coefficients and horizontal layer transports. After making some necessary and, in my opinion, well founded corrections, the agreement was reasonable. This indicates that the theory is qualitatively correct, and hence useful for gaining insight in the

effects of mixing/entrainment on the dynamics of reduced gravity flows and strait flows. It is also clear from the comparison that a layered one-dimensional model is not adequate to precisely reproduce the complicated flow in the Bosphorus. It seems that better descriptions will ultimately require realistic three-dimensional numerical models with proper parameterisations of mixing and precise bathymetry.

Hydraulic Control of Homogenous Shear Flows

Classical inviscid hydraulic theory assumes homogeneous and uniform layers. Then the Froude number is well defined and an internal hydraulic control is identified by $G^2 = 1$. However the assumption of uniformity does not hold along the southern section of the Bosphorus where the velocity in the upper layer was strongly sheared. The literature provides two approaches for defining hydraulic control of homogeneous shear flows. Curiously these yield contrary results.

If the shear flow of a homogeneous fluid preserves the shape of its velocity profile, a standard formula for the condition for hydraulic control suggests that this is achieved when the depth-averaged flow speed is less than $(gh)^{1/2}$. On the other hand, shallow water waves have a speed relative to the mean flow of more than $(gh)^{1/2}$, suggesting that information could propagate upstream. This apparent paradox is by showing that the internal stress required to maintain a constant velocity profile depends on flow derivatives, thus altering the wave speed without introducing damping. By contrast, an inviscid shear flow does not maintain the same profile shape, but it can be shown that longs waves are stationary at a position of hydraulic control. Many real situations will lie between these two limits, in being influenced by friction but not maintaining the shape of the velocity profile. It is not yet clear that there are any general results to apply in such cases. This problem is currently being investigated.

In the Bosphorus the upper layer becomes thinner as it progresses from the contraction to the Sea of Marmara. Simultaneously the shear increases indicating that the flow cannot be assumed to be inviscid. Furthermore, the assumption of inviscid flow would ignore earlier findings that friction and entrainment are important. On the other hand, the similarity assumption approximately holds. On the basis of this theory, the flow would have been supercritical at the exit toward the Sea of Marmara, instead of marginally

subcritical or critical as predicted by classical inviscid theory. This in turn means that the exchange was bounded by two hydraulic controls, i.e. it would have been maximal.

The analysis was carried out for a homogeneous single layer flow in a rectangular channel. Effects of stratification and non-rectangular cross-section were not taken into account but should have no effect on the main problem which is that in dispersive flows waves are dispersive as well. So, as we introduce friction, entrainment and viscosity into the problem, is it appropriate to define control by means of the speed of an inviscid long wave? This was discussed by Hogg *et al.* (2001*b*) who examined the propagation of waves through a stratified shear flow through a constricted channel. They did find an extension of the usual concept of control, in that waves, in particular so-called vortical modes, did not seem to be able to significantly affect the depth of isopycnals. In this sense they appeared to conform to the behaviour of the interfacial mode in two-layer theory, but the situation is complicated as various different waves may occur. Perhaps, one should, when considering sheared and viscous flows, return to the physically most convincing meaning for hydraulic control which comes from showing that solutions to the momentum and continuity equations no longer exist if one tries to, say, reduce the upstream reservoir level further. It is not clear to me, whether this can be done by analytical means. If not, a numerical simulation could provide answers.

7.2. Recommendations for Future Work

This thesis has revealed previously unknown details and complications of the flow in the Bosphorus. Simplified theoretical analysis has shed light on some issues but probably raised as many questions as it answered.

Two most interesting scientific issues, which await future investigation, concern the hydraulic state of the Bosphorus exchange at the exit toward the Sea of Marmara and the physical processes that cause mixing between the layers.

Exit Control at the Sea of Marmara

The exchange in the Bosphorus will be maximal if it is bounded by a sill control on the side of the basin with less dense water (the Black Sea) and by an exit control on

the side toward the denser water (the Sea of Marmara). Our observations confirmed the control at the North Sill. On the other hand, the control at the South Exit remains somewhat uncertain, because, first, the classical two-layer control conditions $G^2 = 1$ was only marginally fulfilled and, second, the effect of shear on the hydraulic control condition is not yet fully understood.

Therefore the question arises how else the existence of the exit control could be determined. A definitive indicator would be a hydraulic jump. An easily observable jump would, however, probably not occur because the shallow supercritical flow would eventually adjust to subcritical flow through a frictional change with no obvious jump.

A more compelling point might be that at times the surface flow from the Bosphorus enters the Sea of Marmara as a shallow and narrow turbulent buoyant jet. The significance of this is that the exchange is isolated from changes in the interface depth in the Sea of Marmara[2], which is the precise meaning of a control.

Our surveys did not extend into the Sea of Marmara. Therefore, we do not know if the surface flow on transect T2 (figure 3.23) continued as a jet flowing into higher density Sea of Marmara water. If it did not, then the exit region could have filled with Black Sea water, thereby lowering the interface. The control would have been lost, or "flooded" as this process is also called. There are indications in the literature that both scenarios occur.

The satellite images shown in figures 2.4 and 3.12 indicate a jet-like outflow for June 16, 2000, but without any information about the sub-surface density structure of the flow, it is difficult to draw any conclusions from those images. Beşiktepe *et al.* (1994) describe the larger scale salinity distribution in the Sea of Marmara during spring and summer (figure 7.1). The upper layer entering the Sea of Marmara had a salinity of 19 to 20 psu during both times, but whereas the jet stood clearly out from the more saline surrounding waters in May 1987, it was hardly detectable in September 1988. The authors present some current measurements from the exit region and conclude that a well defined jet is more likely to occur during strong outflow conditions, but that its existence might also depend on the variable wind-conditions and circulations patters in the Sea of Marmara.

[2]The analogy would be the water jet coming out of a garden-hose where any change of the jet would not affect the flow within the hose.

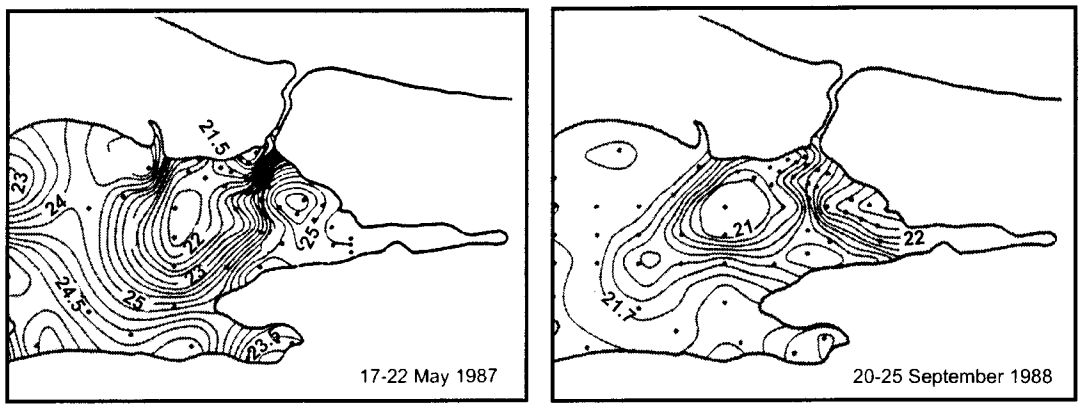

Figure 7.1.: *Distribution of surface salinity (from* 5m *depth) in the eastern Sea of Marmara for May 1987 (left) and September 1988 (right). The figure is adapted from figure 9 in (Beşiktepe* et al., *1994).*

Hence, to answer the question whether the jet indicates a hydraulic control, future observations should focus on the Bosphorus - Sea of Marmara junction region. Detailed hydrographic and current observations, preferably supplemented by continuous current and sea-level measurements within the strait, should be compared with predictions from numerical models (e.g. Wang, 1987) and laboratory experiments (e.g Whitehead & Miller, 1979). Theoretical analysis would be necessary to determine the appropriate control condition for a thin strait outflow, influenced by friction, mixing and possibly rotation.

The Physical Reasons for Entrainment and Mixing

Mixing across gravitationally stable density interfaces is an important process, both when studying geophysical phenomena, such as the development of the upper-ocean mixed layer, and in engineering applications, for example, the spreading of hot water discharges from power plants. However, as stated by Fernando (1991), despite almost a century of research we still lack universal laws quantifying this fundamental process.

Figure 7.2 depicts the situation of a two-layer flow with a sheared density interface and turbulent layers below and above. Very much simplifying the results of previous studies (e.g. Pedersen, 1980; Turner, 1986; Christodoulou, 1986; Lawrence *et al.*, 1991; Fernando, 1991; Sullivan & List, 1994; Silva *et al.*, 1996), we may distinguish three main regimes: For small values of the so-called layer bulk Richardson number Ri_b the flow is everywhere

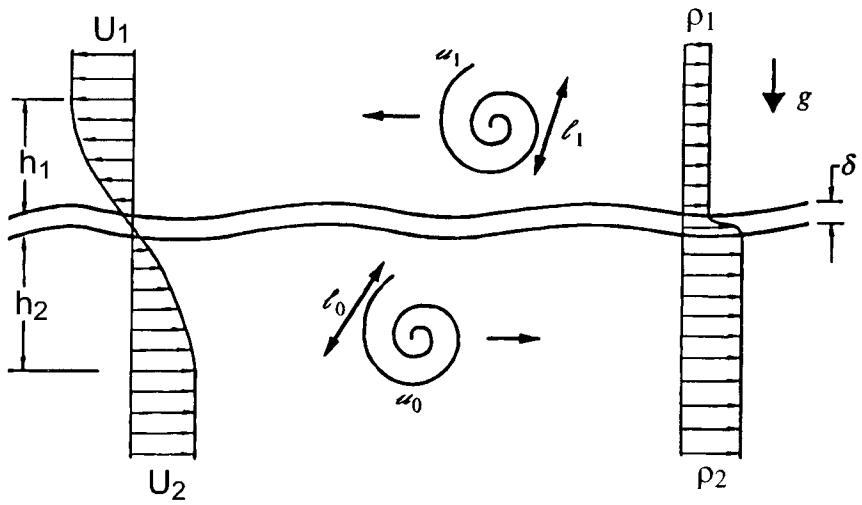

Figure 7.2.: *Idealised two-layer flow with a density interface with thickness δ embedded in a turbulent shear flow with turbulent structures of size l. Adapted from figure 11 in (Sullivan & List, 1994).*

turbulent, even in the pycnocline separating the two layers. Small-scale turbulence penetrates the density interface and lifts fluid from the interface into the turbulence layers where it is rapidly mixed. For intermediary values of Ri_b, where the density interface itself is no longer turbulent, large scale turbulent eddies in the turbulent layers scour fluid of intermediate density from the edge of the interface. The intermediate density fluid may be created by Kelvin-Helmholtz or Homboe instabilities which are formed at sheared density interfaces under certain conditions in which the destabilising effect of shear overcomes the stabilising effect of the density gradient. For even higher Ri_b-values, instabilities do not arise. Instead interfacial waves are formed, presumably generated by random pressure fluctuations induced by turbulent eddies, which may eventually break due to the destabilising effect of the main shear. However, when these waves break much less mixing appears to occur than in the case of Kelvin-Helmholtz instabilities.

The observations shown in section 3.4 suggest that in the Bosphorus mixing might operate mainly in the second regime, because we observed both interfacial instabilities and turbulence within the layer (generated by interaction of the flow with the topography).

Perhaps, finding turbulence to be stronger in the upper than in the lower layer would explain why entrainment is primarily upwards along the southern section of the Bosphorus. An alternative explanation would be a displacement between the density interface

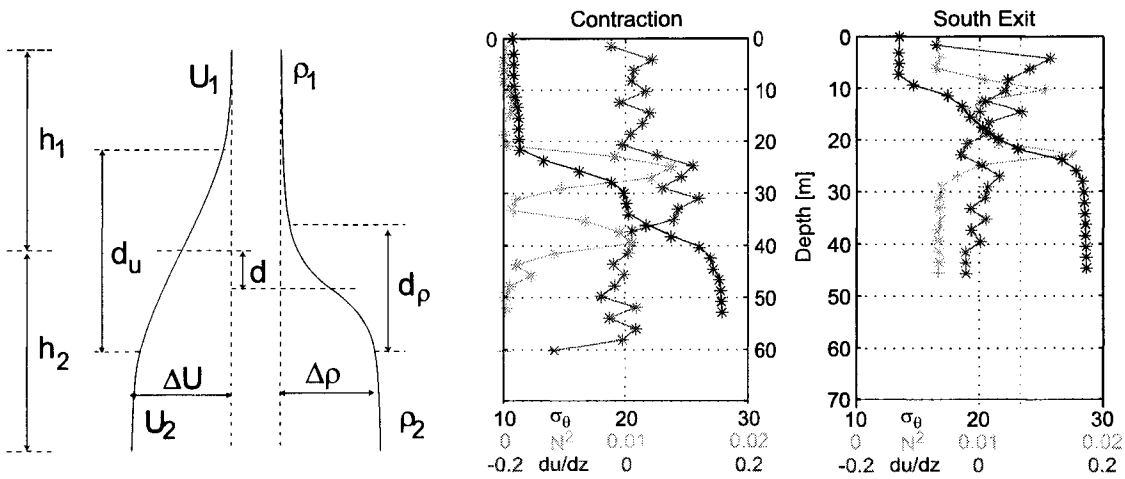

Figure 7.3.: ***Left:*** *Illustration of a stably stratified two-layer shear flow. Two-layers with densities ϱ_1 and ϱ_2 have got different velocities U_1 and U_2. The velocity jump and density jump across the shear-layer are ΔU and $\Delta\varrho$, respectively. δ_u is the thickness of the shear layer and δ_ϱ is the thickness of the density interface. d is the possible displacement between the centre of the shear layer and velocity interface. The flow is assumed to be 2-dimensional, that is homogeneous in y-direction.* ***Middle:*** *Profiles of σ_θ [kgm^{-3}] (blue), vertical velocity shear du/dz [s^{-1}] (red), and buoyancy frequency N^2 [s^{-2}] (green) from the contraction (August 24, 1998). The yellow star shows the depth of the zero-velocity iso-tach. Vertical resolution is* 2m. ***Right:*** *From the South Exit (August 20, 1998).*

and velocity interface as schematised on the left-hand side of figure 7.3. A configuration in which the velocity interface lies above the density interface (or better, where the surface of maximal shear lies above the surface of maximal density gradient) should favour instabilities to "grow" towards the upper layer (see (Lawrence *et al.*, 1991) and (Yonemitsu *et al.*, 1996) for laboratory simulations and mathematical details), thereby causing entrainment rather than symmetric mixing. The profiles of density, buoyancy frequency, and shear in figure 7.3 indicate that the vertical resolution of our data might be sufficient to attempt a stability analysis of the flow in the Bosphorus. The sounder images would have to be analysed for indications of instabilities.

If future observations to this end were to be undertaken in the Bosphorus, it would probably be better to do continuous ADCP and sonar measurements as well as CTD yo-yoing from a stationary instead a moving vessel. Obviously this would be a challenging effort under strong currents and heavy ship traffic. Considering, however, that there have

been very few studies of interfacial instability outside laboratories and theoretician's heads, it might be worth the trouble.

7.3. A Three Century Old Concluding Remark

This is the end of this thesis, and of several years of work. Let me conclude by quoting Marsigli who more than 300 years ago wrote

> "... However the observed motions make this clear and give reason for thinking of more profound investigation on the universal system of the movement of water, which needs more corresponding observations and more leisure to discuss them in depth, and I am sure that Your Majesty will already have realised from a similar attempt that my weakness is not equal to Your shrewd intelligence. You will forgive me and supply me with better reasons in which I will glory, as taught by Your Majesty, who, to the amazement of the World, knows and judges similar material so well. ... "

Bibliography

1997 *GPSPACE. GPS Positioning from ACS Clocks and Ephemerides. Version 3.2.* Geodetic Survey Division. Geomatics Canada.

AKSU, A. E., HISCOTT, R. N., MUDIE, P. J., ROCHON, A., KAMINSKI, M. A., ABRAJANO, T. & YASAR, D. 2002 Persistent holocent outflow from the Black Sea to the Eastern Mediterranean contradicts Noah's flood hypothesis. *GSA Today* **12** (5), 4–10.

AKYARLI, A. & ARISOY, Y. 1995 Evaluation of hydrodynamic characteristics of the Bosphorus regarding the performance of the marine outfall systems. *Water Science and Technology* **32** (2), 85–93.

ALPAR, B. & YÜCE, H. 1998 Sea-level variations and their interactions between the Black Sea and the Aegean Sea. *Estuarine, Coastal and Shelf Science* **46**, 609–619.

ANATI, D. A., ASSAF, G. & THOMPSON, R. O. R. Y. 1977 Laboratory models of sea-straits. *Journal of Fluid Mechanics* **81**, 341–351.

ARISOY, Y. & AKYARLI, A. 1990 Long term current and sea level measurements conducted at Bosphorus. In *The Physical Oceanography of Sea Straits* (ed. L. J. Pratt), pp. 225–236. Kluwer Academic Publishers.

ARMI, L. 1986 The hydraulics of two flowing layers with different densities. *Journal of Fluid Mechanics* **163**, 27–58.

ARMI, L. & FARMER, D. 1985 The internal hydraulics of the Strait of Gibraltar and associated sills and narrows. *Oceanologica Acta* **8** (1), 37–46.

ARMI, L. & FARMER, D. 1987 A generalization of the concept of maximal exchange in a strait. *Journal of Geophysical Research* **92** (C13), 14679–14680.

ARTÜZ & UĞUZ 1976 Daily observations on the hydrographic conditions of the Bosphorus during the period of 1967-1970. *Tech. Rep.*. Faculty of Science, University of Istanbul, (in Turkish).

ASSAF, G. & HECHT, A. 1974 Sea straits: A dynamical model. *Deep-Sea Research* **21**, 947–958.

BAINES, P. G. 1995 *Topographic Effects in Stratified Flows.* Cambridge University Press.

BARINGER, M. O. & PRICE, J. F. 1997 Momentum and energy balance of the Mediterranean outflow. *Journal of Physical Oceanography* **27**, 1678–1692.

BEŞIKTEPE, S. T., ÖZSOY, E. & LATIF, M. A. 1995 Sewage outfall plume in the two-layer channel: An example of Istanbul outfall. *Water Science and Technology* **32** (2), 69–75.

BEŞIKTEPE, S. T., SUR, H. I., ÖZSOY, E., LATIF, M. A., OĞUZ, T. & ÜNLÜATA, Ü. 1994 The circulation and hydrography of the Marmara Sea. *Progress in Oceanography* **34**, 285–334.

BENTON, G. S. 1954 The occurence of critical flow and hydraulic jumps in a multi-layered fluid system. *Journal of Meteorology* **11**, 139–150.

BORENAS, K. M. & PRATT, L. J. 1990 A review of rotating hydraulics. In *The Physical Oceanography of Sea Straits* (ed. L. Pratt). Boston: Kluwer.

BORMANS, M. 1988 A model of the exchange through the Strait of Gibraltar. PhD thesis, Dalhousie University, Halifax, Nova Scotia.

BORMANS, M. & GARRETT, C. 1989*a* The effect of rotation on the surface inflow through the Strait of Gibraltar. *Journal of Physical Oceanography* **19**, 1535–1542.

BORMANS, M. & GARRETT, C. 1989*b* The effects of nonrectangular cross section, friction, and barotropic fluctuations on the exchange through the Strait of Gibraltar. *Journal of Physical Oceanography* **19**, 1543–1557.

BRAY, N. A., OCHOA, J. & KINDER, T. H. 1995 The role of the interface layer in exchange through the Strait of Gibraltar. *Journal of Geophysical Research* **100**, 10755–10776.

BRYDEN, H. L. & KINDER, T. H. 1991*a* Recent progress in strait dynamics. *Reviews of Geophysics, Supplement* pp. 617–631.

BRYDEN, H. L. & KINDER, T. H. 1991*b* Steady two-layer exchange through the Strait of Gibraltar. *Deep-Sea Research* **38** (Suppl. 1), S445–S463.

BRYDEN, H. L. & STOMMEL, H. M. 1984 Limiting processes that determine basic features of the circulation in the Mediterranean Sea. *Oceanologica Acta* **7** (3), 289–296.

BURNS, J. C. 1953 Long waves in running water. *Proc. Camb. Phil. Soc.* **49**, 695–706.

CETIN, N. 1999 Analysis of the exchange flow through the Bosphorus Strait. Master's thesis, Graduate School of Marine Sciences, Middle East Technical University.

CHOW, V. T. 1959 *Open-Channel Hydraulics*. McGraw-Hill.

CHRISTODOULOU, G. C. 1986 Interfacial mixing in stratified flows. *Journal of Hydraulic Research* **24** (2), 77–92.

CORMACK, D. E., LEAL, L. G. & IMBERGER, J. 1974 Natural convection in a shallow cavity with differentially heated endwalls. Part 1. Asymptotic theory. *Journal of Fluid Mechanics* **65**, 209–229.

DALZIEL, S. B. 1991 Two-layer hydraulics: A functional approach. *Journal of Fluid Mechanics* **223**, 135–163.

DALZIEL, S. B. 1992 Maximal exchange in channels with nonrectangular cross sections. *Journal of Physical Oceanography* **22**, 1188–1206.

DEACON, M. B. 1971 *Scientist and the Sea. 1650-1900 a Study of Marine Science.*. Academic Press.

DEACON, M. B., ed. 1978 *Oceanography. Concepts and History, Benchmark Papers in Geology*, vol. 35. Dowden, Hutchinson & Ross, Inc.

DEACON, M. B. 1985 An early theory of ocean circulation: J.S. Von Waitz and his explanation of the currents in the Strait of Gibraltar. *Progress in Physical Oceanography* **14**, 89–101.

DEFANT, A. 1961*a* *Physical Oceanography*, , vol. 1. Pergamon.

DEFANT, A. 1961*b* *Physical Oceanography*, , vol. 2. Pergamon.

DI IORIO, D., FARMER, D., CARTIER, W. & GENG, X. 1999 Scintillation instrument for remote environmental analysis (SIREN). *Tech. Rep.* SM-354. Saclant Undersea Research Centre, La Spezia, Italy.

DI IORIO, D. & YÜCE, H. 1999 Observations of Mediterranean flow into the Black Sea. *Journal of Geophysical Research* **104** (C2), 3091–3108.

ERGIN, M., BODUR, M. N. & EDIGER, V. 1991 Distribution of surficial shelf sediments in the northeastern and southwestern parts of the Sea of Marmara: Strait and canyon regimes of the Dardanelles and Bosporus. *Marine Geology* **96**, 313–340.

FARMER, D. & ARMI, L. 1986 Maximal two-layer exchange over a sill and through a combination of a sill and contraction with barotropic flow. *Journal of Fluid Mechanics* **164**, 53–76.

FARMER, D. & ARMI, L. 1988 The flow of Mediterranean water through the Strait of Gibraltar. *Progress in Oceanography* **21** (1), 1–105.

FARMER, D. & ARMI, L. 1999 Stratified flow over topography: The role of small-scale entrainment and mixing in flow establishment. *Proceedings of the Royal Society London A* **455**, 3221–3258.

FERNANDO, H. J. S. 1991 Turbulent mixing in stratified fluids. *Annual Review of Fluid Mechanics* **23**, 455–493.

FREEMAN, N. C. & JOHNSON, R. S. 1970 Shallow water waves on shear flows. *Journal of Fluid Mechanics* **42** (part 2), 401–409.

GARRETT, C., BORMANS, M. & THOMPSON, K. 1990 Is the exchange through the Strait of Gibraltar maximal or submaximal? In *The Physical Oceanography of Sea Straits* (ed. L. J. Pratt), pp. 271–294.

GARRETT, C. & GERDES, F. 2002 Hydraulic control of homogeneous shear flows. *Journal of Fluid Mechanics* Accepted.

GERDES, F., GARRETT, C. & FARMER, D. 2002 On internal hydraulics with entrainment. *Journal of Physical Oceanography* **32** (3), 1106–1111.

GILL, A. E. 1977 The hydraulics of rotating-channel flow. *Journal of Fluid Mechanics* **80**, 641–671.

GILL, A. E. 1982 *Atmosphere-Ocean Dynamics*. Academic Press.

GÖKAŞAN, E., DEMIBAĞ, E., OKTAY, F. Y., ECEVITOĞLU, B., ŞIMŞEK, M. & YÜCE, H. 1997 On the origin of the Bosphorus. *Marine Geology* **140**, 183–199.

GÖNENÇ, I. E., MÜFTÜOGLU, O., BAYKAL, B. B., DOGAN, E., YÜCE, H. & GÜREL, M. 1995 The Black Sea factor influencing the wastewater disposal strategy for Istanbul. *Water Science and Technology* **32** (7), 63–70.

GORDON, L. 1996 *Acoustic Doppler Current Profiler - Principles of Operation: A Practical Primer*, 2nd edn.

GREGG, M. C. & ÖZSOY, E. 2002 Flow, water mass changes, and hydraulics in the Bosphorus. *Journal of Geophysical Research* **107** (C3).

GREGG, M. C., ÖZSOY, E. & LATIF, M. A. 1999 Quasi-steady exchange flow in the Bosphorus. *Geophysical Research Letters* **26** (1), 83–86.

GRUBERT, J. P. & ABBOTT, M. B. 1972 Numerical computation of stratified nearly horizontal flows. *Journal of Hydraulics Division, ASCE* **98** (HY10), 1847–1865.

HANSEN, I., VESTED, H. & LATIF, M. 1995 Environmental model studies for the Istanbul master plan. Part I: Hydrodynamical design basis and marine disposal of wastewater. *Water Science and Technology* **32** (2), 141–148.

HELFRICH, K. R. 1995 Time-dependent two-layer hydraulic exchange flow. *Journal of Physical Oceanography* **25** (3), 359–373.

HENDERSON, F. M. 1966 *Open Channel Flow*. MacMillan Publishing.

HÉROUX, P. & KOUBA, J. 1995 GPS precise point positioning with a difference. In *Geomatics 1995*. Ottawa, Ontario, Canada.

HOGG, A. M., IVEY, G. N. & WINTERS, K. B. 2001*a* Hydraulics and mixing in controlled exchange flows. *Journal of Geophysical Research* **106** (C1), 959–972.

HOGG, A. M., WINTERS, K. & IVEY, G. 2001*b* Linear internal waves and the control of stratified exchange flows. *Journal of Fluid Mechanics* **447**, 357–375.

JOHNS, B. & OĞUZ, T. 1990 The modelling of the flow of water through the Bosphorus. *Dynamics of Atmosphere and Oceans* **14**, 229–258.

KILLWORTH, P. D. 1992 On hydraulic control in a stratified fluid. *Journal of Fluid Mechanics* **237**, 605–626.

KRAUS, E. B. 1972 *Atmosphere-Ocean Interaction*. Oxford: Clarendon Books.

KUNDU, P. K. 1990 *Fluid Mechanics*. Academic Press.

LANE-SERFF, G. F., SMEED, D. A. & POSTLETHWAITE, C. R. 2000 Multi-layer hydraulic exchange flows. *Journal of Fluid Mechanics* **416**, 269–296.

LAWRENCE, G. A. 1990 On the hydraulics of Boussinesq and non-Boussinesq two-layer flows. *Journal of Fluid Mechanics* **215**, 457–480.

LAWRENCE, G. A., BROWAND, F. K. & REDEKOOP, L. G. 1991 The stability of a sheared density interface. *Physics of Fluids A* **3** (10), 2360–2370.

LISITZIN, E. 1974 *Sea-Level Changes*. Elsevier Scientific Publishing.

LONG, R. R. 1954 Some aspects of the flow of a stratified fluid. II. Experiments with a two-fluid system. *Tellus* **6** (2), 97–115.

LUECK, R. G. & LU, Y. 1997 The logarithmic layer in a tidal channel. *Continental Shelf Research* **17** (14), 1785–1801.

MACCREADY, P. & PAWLAK, G. 2001 Stratified flow along a corrugated slope: Separation drag and wave drag. *Journal of Physcial Oceanography* **31**, 2824–2839.

MÖLLER, L. 1928 *Alfred Merz' Hydrographische Untersuchungen in Bosporus und Dardanellen, Neue Folge A,*, vol. 18. University of Berlin.

OFFICER, C. B. 1976 *Physical Oceanography of Estuaries (and Associated Coastal Waters)*. John Wiley & Sons.

ORHON, D. 1995 Scientific basis for wastewater treatment and disposal in Istanbul. *Water Science and Technology* **32** (2), 199–208.

OĞUZ, T., ÖZSOY, E., LATIF, M., SUR, H. & ÜNLUATA, Ü. 1990 Modelling of hydraulically controlled exchange flow in the Bosphorus Strait. *Journal of Physical Oceanography* **20**, 945–965.

OĞUZ, T. & SUR, H. I. 1989 A two-layer model of water exchange through the Dardanelles Strait. *Oceanologica Acta* **12** (1), 23–31.

ÖZSOY, E. 1999 Sensitivity to global change in temperate Euro-Asian seas (the Mediterranean, Black Sea and Caspian Sea): A review. In *The Eastern Mediterranean as a Laboratory Basin for the Assessment of Contrasting Ecosystems* (ed. P. Malanotte-Rizzoli & V. N. Eremeev), *NATO Science Series 2, Environmental Security*, vol. 51, pp. 281–300. Kluwer Academic.

ÖZSOY, E., LATIF, M. A., SUR, H. I. & GORYACHKIN, Y. 1996 A review of the exchange flow regime and mixing in the Bosphorus Strait. In *Dynamics of Mediterranean Straits and Channels* (ed. F. Briand), *Bulletin de l'Institut Oceanographique* 17, pp. 187–203. Monaco: Musee oceanographique, CIESM Science series no. 2.

ÖZSOY, E., LATIF, M. A., ŞÜKRÜ T. BEŞIKTEPE, CETIN, N., GREGG, M. C., BELOKIPYTOV, V., GORYACHKIN, Y. & DIACONU, V. 1998 *The Bosporus Strait: exchange fluxes, currents and sea level changes. NATO TU-Black Sea Project: Ecosystem*

Modelling as a Management Tool for the Black Sea, , vol. 2, pp. 1–28. Netherlands: Kluwer Academic Publishers.

ÖZSOY, E., LATIF, M. A., TÜGRUL, S. & ÜNLÜATA, Ü. 1995 Exchanges with the Mediterranean, fluxes, and boundary mixing processes in the Black Sea. In *Lers Mers Tributaires de Mediterranee* (ed. F. Briand), *CIESM Science Series N° 1* numero special 15, pp. 1–26. Monaco: Bulletin de l'Instiut oceanographique.

ÖZSOY, E. & ÜNLÜATA, Ü. 1997 Oceanography of the Black Sea: A review of some recent results. *Earth-Science Reviews* **42** (4), 231–272.

ÖZTÜRK, B. & ÖZTÜRK, A. A. 1996 On the biology of the Turkish straits system. In *Dynamics of Mediterranean Straits and Channels* (ed. F. Briand), *Bulletin de l'Institut Oceanographique* 17, pp. 187–203. Monaco: Musee oceanographique, CIESM Science series no. 2.

PAWLAK, G. & ARMI, L. 1997 Hydraulics of two-layer arrested wedge flows. *Journal of Hydraulic Research* **35** (5), 603–618.

PAWLOWICZ, R. 2001 A tracer method for determining transport in two-layer systems, applied to the Strait of Georgia/Haro Strait/Juan de Fuca estuarine system. *Coastal and Estuarine Shelf Science* **52** (4), 491–503.

PAWLOWICZ, R., BEARDSLEY, R. B. & LENTZ, S. 2002 Classical tidal harmonic analysis including error estimates in MATLAB using T_TIDE,. *Computers and Geosciences* **28**, 929–937.

PEDERSEN, F. B. 1972 Gradually varying two-layer stratified flow. *Journal of the Hydraulic Division* **98** (HY1), 257–268.

PEDERSEN, F. B. 1980 A monograph on turbulent entrainment and friction in two-layer stratified flow. PhD thesis.

PEDERSEN, F. B. 1986 *Environmental Hydraulics: Stratified Flows*. Springer-Verlag.

PEDLOSKY, J. 1996 *Ocean Circulation Theory*. Springer.

PENEVA, E., STANEV, E., BELOKOPYTOV, V. & TRAON, P.-Y. L. 2001 Water transport in the Bosphorus Straits estimated from hydro-meteorological and altimeter data: Seasonal to decadal variability. *Journal of Marine Systems* **31**, 21–33.

PEREGRINE, D. H. 1976 Water waves in channels. In *Unsteady Flow in Open Channels* (ed. H. S. Stephens & S. K. Hemmings), pp. 1–11. BHRA Fluid Engineering.

POLAT, Ç. & TÜGRUL, S. 1996 Chemical exchange between the Mediterranean and the Black Sea via the Turkish Straits. In *Dynamics of Mediterranean Straits and Channels* (ed. F. Briand), *Bulletin de l'Institut Oceanographique* 17, pp. 187–203. Monaco: Musee oceanographique, CIESM Science series no. 2.

PRATT, L. J. 1986 Hydraulic control of sill flow with bottom friction. *Journal of Physical Oceanography* **16**, 1970–1980.

PRATT, L. J. & ARMI, L. 1987 Hydraulic control of flows with nonuniform potential vorticity. *Journal of Physical Oceanography* **17**, 2016–2029.

PRATT, L. J., DEESE, H. E., MURRAY, S. P. & JONES, W. 2000 Continuous dynamical modes in a strait having arbitrary cross section, with application to the Bab al Mandab. *Journal of Physical Oceanography* **30**, 2515–2534.

PRATT, L. J., JONES, W., MURRAY, S. P. & KATSUMATA, K. 1999 Hydraulic interpretation of direct velocity measurements in Bab al Mandab. *Journal of Physical Oceanography* **29** (11), 2769–2784.

PRATT, L. J. & LUNDBERG, P. A. 1991 Hydraulics of rotating strait and sill flow. *Annual Review of Fluid Mechanics* **23**, 81–106.

PRICE, J. F. & BARINGER, M. O. 1994 Outflows and deep water production by marginal seas. *Progress in Oceanography* **33**, 161–200.

RYAN, W. B. F., III, W. C. P., MAJOR, C. O., SHIMKUS, K., MOSKALENKO, V., JONES, G. A., DIMITROV, P., GORÜR, N., SAKINC, M. & YÜCE, H. 1997 An abrupt drowning of the Black Sea shelf. *Marine Geology* pp. 119–126.

SANFORD, T. B. & LIEN, R.-C. 1999 Turbulent properties in a homogeneous tidal bottom boundary layer. *Journal of Geophysical Research* **104** (C1), 1245–1257.

SEIM, H. E. 1999 Acoustic backscatter from salinity microstructure. *Journal of Atmospheric and oceanic technology* **16** (11), 1491–1498.

SILVA, I. D., FERNANDO, H., EATON, F. & HEBERT, D. 1996 Evolution of Kelvin-Helmholtz billows in nature and laboratory. *Earth and Planetary Science Letters* **143**, 217–231.

SIMPSON, M. R. & BLAND, R. 2000 Methods for accurate estimation of net discharge in a tidal channel. *IEEE Journal of Oceanic Engineering* **25** (4), 437–445.

SOULSBY, R. L. 1983 *The Bottom Boundary Layer of Shelf Seas, Elsevier Oceanography Series*, vol. 35, chap. 5, pp. 189–266. Elsevier.

SÖZER, A. & ÖZSOY, E. 2002 A three-dimensional model of Bosphorus Strait dynamics. In *The 2nd Meeting on the Physical Oceanography of Sea-Straits*, pp. 207–210. Villefranche.

STASHCHUK, N. & HUTTER, K. 2001 Modelling of water exchange through the Strait of the Dardanelles. *Continental Shelf Research* **21**, 1361–1382.

STOMMEL, H. & FARMER, H. G. 1952 Abrupt change in width in two-layer open channel flow. *Journal of Marine Research* **11**, 205–214.

STOMMEL, H. & FARMER, H. G. 1953 Control of salinity in an estuary by a transition. *Journal of Marine Research* **12**, 13–20.

SULLIVAN, G. D. & LIST, E. J. 1994 On mixing and transport at a sheared density interface. *Journal of Fluid Mechanics* **273**, 213–239.

TAYLOR, J. R. 1997 *An Introduction to Error Analysis*, 2nd edn. Sausalito, California: University Science Books.

TENNEKES, H. & LUMLEY, J. L. 1972 *A first course in turbulence*. The MIT Press.

THOMPSON, P. 1949 The propagation of small surface disturbances through rotational flow. *Annals of the New York Academy of Sciences* **51**, 463–474.

TOLMAZIN, D. 1984 Economic impact on the riverine-estuarine environment of the USSR: The Black Sea basin. *Environmental Management* **8** (6), 1–16.

TOLMAZIN, D. 1985 Changing coastal oceanography of the Black Sea. II: Mediterranean effluent. *Progress in Oceanography* **15** (4), 277–316.

TROWBRIDGE, J. H., CHAPMAN, D. C. & CANDELA, J. 1998 Topographic effects, straits and the bottom boundary layer. In *The Sea* (ed. K. H. Brink & A. R. Robinson), , vol. 10, pp. 63–88. John Wiley & Sons.

TURNER, J. S. 1973 *Buoyancy effects in fluids*. Cambridge University Press.

TURNER, J. S. 1986 Turbulent entrainment: The development of the entrainment assumption, and its application to geophysical flows. *Journal of Fluid Mechanics* **173**, 431–471.

ÜNLÜATA, Ü., AUBREY, D. G., BELBEROV, Z., BOLOGA, A., EREMEEV, V. & VINOGRADOV, M. 1993 International program investigates the Black Sea. *EOS* **74** (36), 401,407,412.

ÜNLÜATA, Ü., OĞUZ, T., LATIF, M. A. & ÖZSOY, E. 1990 On the physical oceanography of the Turkish Straits. In *The Physical Oceanography of Sea Straits* (ed. L. J. Pratt), pp. 25–60. Kluwer Academic.

WAJSOWICZ, R. C. 1993 Dissipative effects on inertial flows over a sill. *Dynamics of Atmospheres and Oceans* **17**, 257–301.

WANG, D. 1987 The strait surface outflow. *Journal of Geophysical Research* **92** (C10), 10807–10825.

WESSON, J. C. & GREGG, M. C. 1988 Turbulent dissipation in the Strait of Gibraltar and associated mixing. In *Small-Scale Turbulence and Mixing in the Ocean* (ed. J. C. J. Nihoul & B. M. Jamart), pp. 201–212. Amsterdam: Elsevier.

WHITEHEAD, J. & MILLER, A. 1979 Laboratory simulation of the gyre in the Alborean Sea. *Journal of Geophysical Research* **84**, 3733–3742.

WHITEHEAD, J. A. 1998 Topographic control of oceanic flows in deep passages and straits. *Reviews of Geophysics* **36** (3), 423–440.

WHITEHEAD, J. A., LEETMAN, A. & KNOX, R. A. 1974 Rotating hydraulics of strait and sill flows. *Geophysical Fluid Dynamics* **6**, 101–125.

WINTERS, K. B. & SEIM, H. E. 2000 The role of dissipation and mixing in exchange flow through a contracting channel. *Journal of Fluid Mechanics* **407**, 265:290.

YONEMITSU, N., SWATERS, G. E., RAJARATMAN, N. & LAWRENCE, G. A. 1996 Shear instabilities in arrested salt-wedge flows. *Dynamics of Atmospheres and Oceans* **24**, 173–182.

YÜCE, H. 1990 Investigation of the Mediterranean water in the Strait of Istanbul (Bosphorus) and the Black Sea. *Oceanologica Acta* **13**, 177–186.

YÜCE, H. 1996 Mediterranean Water in the Strait of Istanbul (Bosphorus) and the Black Sea Exit. *Estuarine, Coastal and Shelf Science* **43**, 597–616.

YÜCE, H. & ALPAR, B. 1997 Subtidal sea-level variations in the Sea of Marmara, their wind interactions with neighboring seas and relations to wind forcing. *Journal of Coastal Research* **13** (4), 1086–1092.

ZHU, D. Z. & LAWRENCE, G. A. 1998 Non-hydrostatic effects in layered shallow water flows. *Journal of Fluid Mechanics* **355**, 1–16.

ZHU, D. Z. & LAWRENCE, G. A. 2000 Hydraulics of exchange flows. *Journal of Hydraulic Engineering* **126** (12), 921–928.

A. Differential GPS Corrections

Differential GPS (DGPS) operations provide a method to cancel errors introduced by selective availability (SA), which was the main source of error in GPS code positioning, and atmospheric delays that originate along the signal. SA was used by the United States military as intentional degradation of the positioning precision of civilian GPS systems to about 100m (Héroux & Kouba, 1995). SA was switched off in May 2000 - two weeks after our March/April 2000 survey.

Along, for instance, the North-American coast, it is standard to eliminate the effects of SA by operating the GPS differentially with respect to known reference positions. A dense network of stations broadcast differential correction information which can be used by differential GPS receivers. Unfortunately along the Bosphorus such a permanent system does not exist. Therefore the positioning accuracy of GPS data was rather poor everywhere along the Bosphorus.

The error can be as large a 100m which is significant considering that the Bosphorus is only 700m wide at some places. Indeed, track-lines based on standard GPS data from October 1997 frequently showed the vessel steaming across the shore-line. It was clear that this would be a problem for the determination of layer transports and entrainment rates.

The problem was solved as follows: GPS data were acquired with a Motorola VP Oncore system which was able to record satellite pseudo-range (or satellite clock) data. SA dithers the satellite clocks through a random process. The dithering can be removed, in post-processing, once an accurate representation of the true GPS satellite clock is known. These accurate representations (satellite clock correction data) are computed on a daily basis by the International GPS Service for Geodynamics (IGS) from a multitude of high-quality GPS receivers stationed all over the world. This processing step is conveniently done with

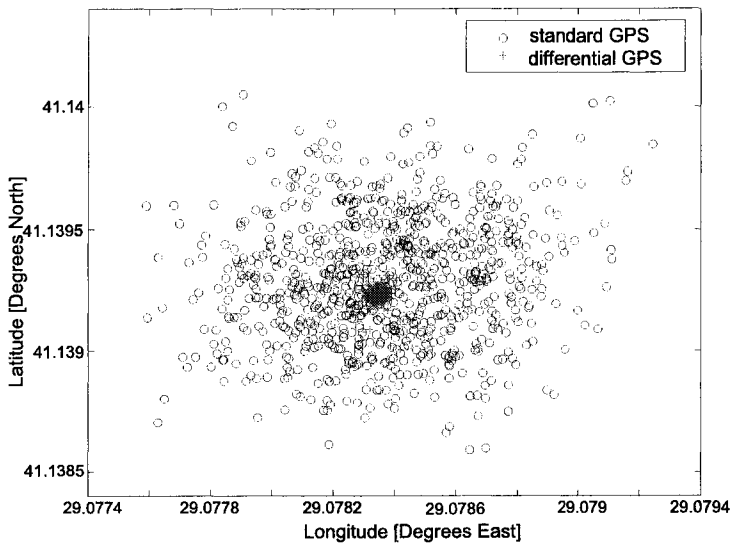

Figure A.1.: *Scatter plot of 19 hours of standard and differential GPS data. The sampling rate was* 0.5Hz*; the figure shows only every 30th sample. The data were obtained during an overnight GPS logging while the vessel did not move.*

software and clock correction files from the Geodetic Survey Division of Geomatics Canada (Héroux & Kouba, 1995; gps, 1997). The more difficult step was the logging of the satellite clock data and the conversion of these data into a format suitable for post-processing. I have documented details in a data processing report which is available on request.

Figure A.1 illustrates the improvement in positioning accuracy achieved by the post-processing. Before post-processing 68% of the estimates lie in a circle with radius 40m around the mean position, or put more negatively, 5% of the estimates deviate from the mean by 75 to 110m in any direction. After post-processing only 5% of the estimates deviate from the mean by more than 4.5m and 68% deviate by less than 3m from the mean.

For the March/April 2000 survey DNHO had installed a shore station with was able to broadcast differential corrections in real-time to be used by a Sercel DGPS receiver on the TCG Mesaha I. However, these DGPS data turned out to have a worse precision than the post-processed data from our Motorola GPS which we had brought as a backup system. Furthermore the shore station seemed to have a limited range so that its signal could not be received in the northernmost and southernmost parts of the strait. I decided to again post-process the Motorola GPS data.

Ionospheric delays of the GPS signals are another source of error, but I estimated that these cause errors not larger than about 1.5m in the horizontal. This is negligible.

B. Tidal & Spectral Analysis of Sea-level Data

To a good approximation an increase of air-pressure by 1mbar suppresses the sea-level by 1cm (Lisitzin, 1974). Low frequency air-pressure fluctuations of up to 10mbar were observed during our experiment. In order to avoid that these show up in the tidal analysis as long-period constituents, for instance as a the fortnightly MSF constituent, I added the Sariyer air-pressure to the Anadolukavagi sea-level data and the Goztepe air-pressure to the Golden Horn sea-level data. Each record was reduced by its mean value.

For the following only the sea-level data obtained between 00:00 AM, March 27 and 12:00 PM, April 5 were used, that is the time-series ends before the Orkoz begins. The tidal analysis was done in MATLAB using T_TIDE (Pawlowicz *et al.*, 2002). Nodal corrections were applied to amplitude and phase. Shallow water constituents were not taken into account because it was not clear which shallow water constituents (if any) are important at the Bosphorus. Figures B.1 and B.2 show the results of the analysis for the northern and southern sea-level data, respectively.

In the north at Anadolukavagi tidal amplitudes are at most 3cm. The tide is mixed but mainly semi-diurnal as it is in the Black Sea (see Alpar & Yüce, 1998). 25% of the variance is explained by the tidal fit. In the Golden Horn the tidal amplitude is at most 4cm. The tide is mixed but mainly diurnal. Here, 50% of the variance is explained by the tidal fit.

I repeated the analysis (not shown here) using the entire sea-level record with a length of 21 days. Then the tidal fit explains 30% of the variance at Anadolukavagi and 28% of the variance at the Golden Horn. The difference to the previous results is due to the inclusion of the Orkoz event which increases the sea-level variance in the south.

In conclusion, between 25% and 50% of the variance in sea-level is due to diurnal and semi-diurnal tides. Higher frequency tidal components are unimportant. The remaining

part of the variance is under normal circumstances due to meteorological forcing with time-scales of a few days. But short-lived meteorological events as the Orkoz may contribute to the variance as well.

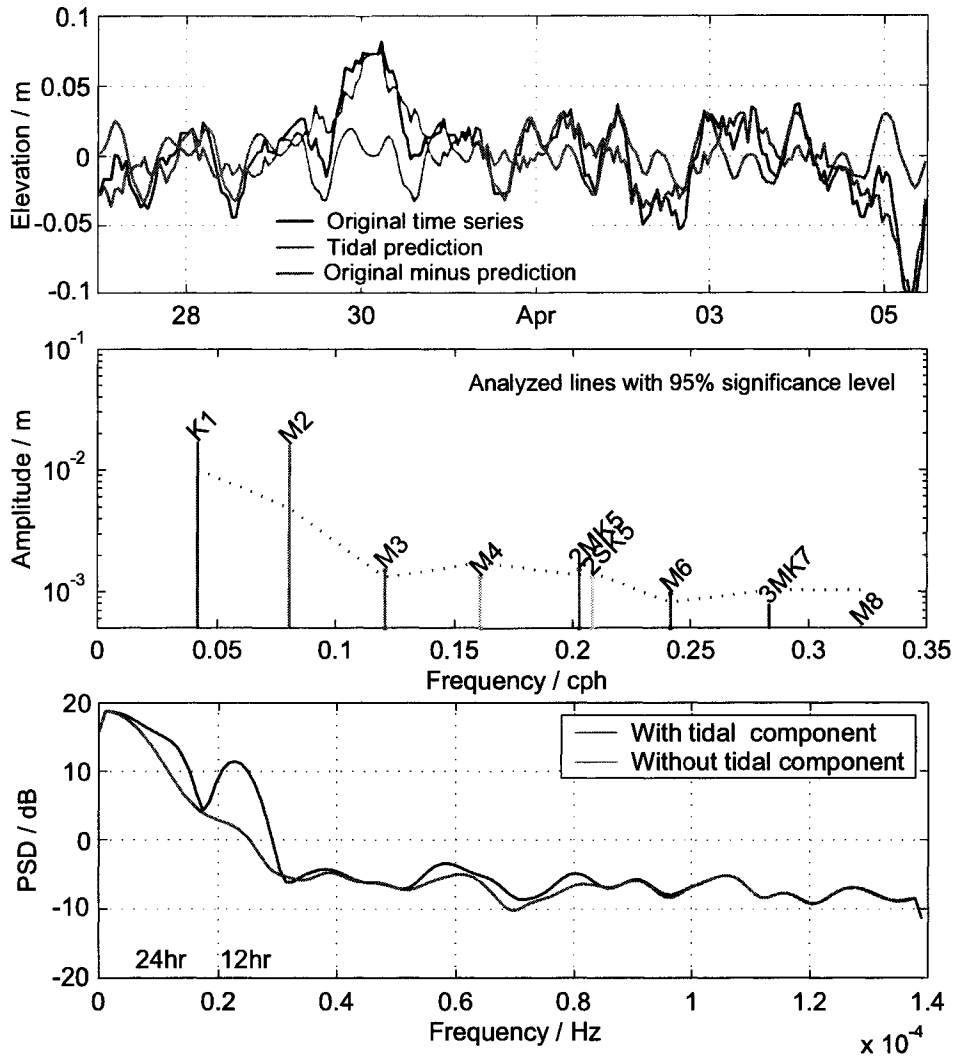

Figure B.1.: *Analysis for Anadolukavagi (northern) sea-level record. Upper: Original sea-level record, tidal prediction, and original sea-level minus tidal prediction. Middle: Analysed tidal constituents. Lower: Power spectrum of original sea-level and original sea-level minus tidal prediction. T_TIDE output: nobs = 228, ngood = 227, record length (days) = 9.50, start time: 27-Mar-2000 00:30:00, rayleigh criterion = 1.0, Greenwich phase computed with nodal corrections applied to amplitude and phase relative to center time, x0= 0.00012, x trend= 0, var(x)= 0.0010632, var(xp)= 0.00026269, var(xres)= 0.00080031, percent var predicted/var original= 24.7, tidal amplitude and phase with 95% CI estimates.*

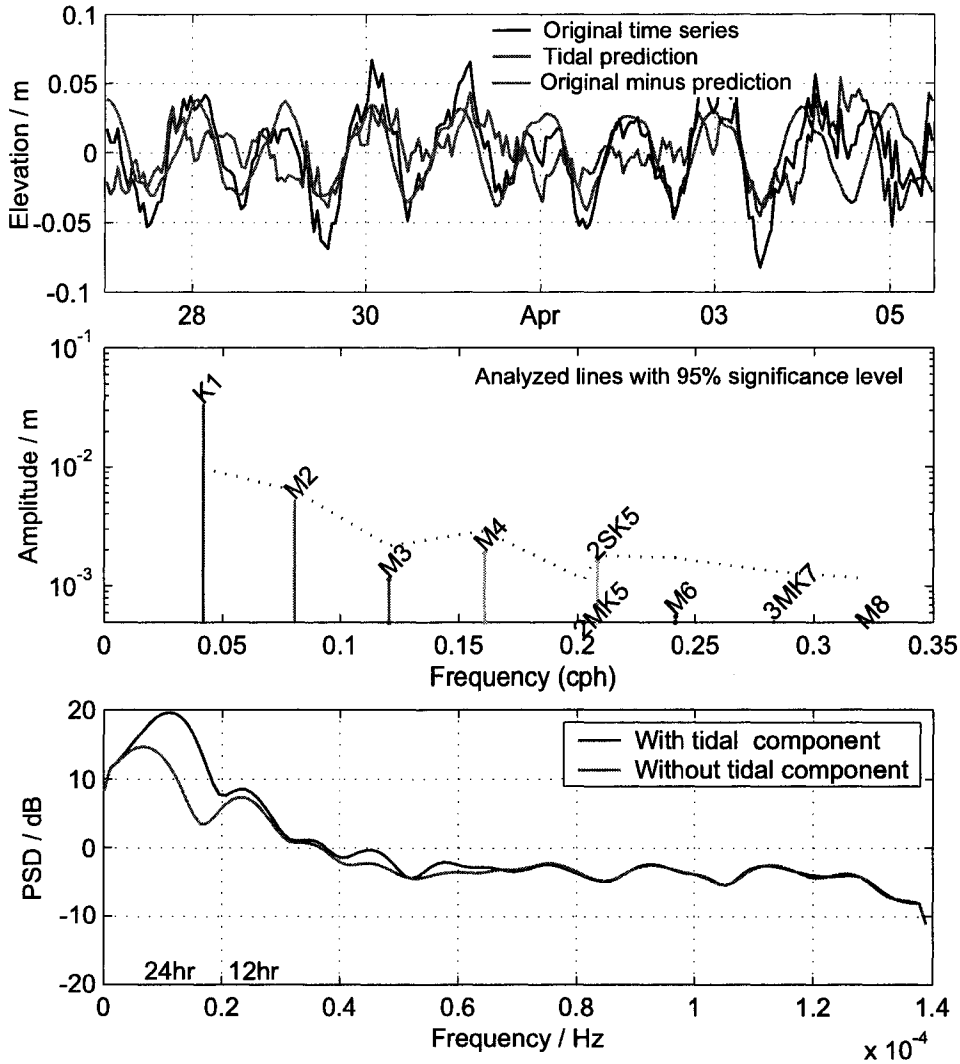

Figure B.2.: *Analysis for Golden Horn (southern) sea-level record. Upper: Original sea-level record, tidal prediction, and original sea-level minus tidal prediction. Middle: Analysed tidal constituents. Lower: Power spectrum of original sea-level and original sea-level minus tidal prediction. T_TIDE output: nobs = 228, ngood = 227, record length (days) = 9.50, start time: 27-Mar-2000 00:30:00, rayleigh criterion = 1.0, Greenwich phase computed with nodal corrections applied to amplitude and phase relative to center time, x0= -0.000454, x trend= 0, var(x)= 0.00094073, var(xp)= 0.00050888, var(xres)= 0.00043247, percent var predicted/var original= 54.1*

C. Determination of Offset of Sea-level Data

DNHO provided sea-level data from two stations, the northern one at Anadolukavagi and the southern one at the Taskizak Navy ship-yard in the Golden Horn (figure 2.4). We expected the two sea-level recorders to be geodetically levelled but apparently they were not. Data from the Anadolukavagi station have been used in several studies (e.g Di Iorio & Yüce, 1999: Gregg *et al.*, 1999; Cetin, 1999) in which they are compared to data from Fenerbahce which is in the Sea of Marmara, about 10km east of the South Exit. Presumably these two stations are geodetically levelled which suggests that the problem is with the Taskizak station.

I communicated the problem to Lt.JG Ahmet Unlu from DNHO. For a different period of time he compared the Taskizak data with those from another station and concluded that the Taskizak data might be too large by 22cm. He also said that another error of some sort might have been made so that I should add another 6cm. In total I should subtract 28cm from the southern sea-level data. However, he emphasised strongly that these numbers were not based on actual measurements but more on his guesswork. Hence they are uncertain.

I independently tried to establish the offset in two different ways:

Method A: Table C.1 summarises information from the literature on the relation between layer currents or transports and sea-level difference. Most useful for my purpose are the current data from Cetin (1999) and Gregg *et al.* (1999) (identical data-sets) because they are from current meters which were deployed at almost the same location as our bottom-mounted ADCP. The readings are from single depths and, hence, might be different from average values. During exchange flow conditions our upper layer currents varied between $-0.9\mathrm{m\,s^{-1}}$ and $0.5\mathrm{m\,s^{-1}}$ (see figure 3.8). According to table C.1 the corresponding sea-

	Date or Season	SL stations	SL diff.	Curr. or Transp.
Alpar & Yuce (1998)	Spring '85	Ana.Kav. - Ortakoy	26 ± 7cm	not available
	Spring '86	Ana.Kav. - Ortakoy	34 ± 7cm	not available
DiIorio & Yuce (1999)	Nov/Dec '95	Ana.Kav - Fenerb.	≈ 20cm	$Q_2 \approx 10000\text{m}^3\,\text{s}^{-1}$
	Nov/Dec '95	Ana.Kav - Fenerb.	≈ 30cm	$Q_2 \approx 5000\text{m}^3\,\text{s}^{-1}$
Cetin (1999)	Sept 8, '94	Ana.Kav - Fenerb.	40cm	$u_1 = -0.8\text{m}\,\text{s}^{-1}$, $u_2 = 0.65\text{m}\,\text{s}^{-1}$
equal to	Sept 10-12, '94	Ana.Kav - Fenerb.	25cm	$u_1 = -0.4\text{m}\,\text{s}^{-1}$, $u_2 = 0.75\text{m}\,\text{s}^{-1}$
Gregg et. al (1999)	Sept 13, 94	Ana.Kav - Fenerb.	37cm	$u_1 = -0.65\text{m}\,\text{s}^{-1}$, $u_2 = 0.75\text{m}\,\text{s}^{-1}$

Table C.1.: *Sea-level difference and current/transport data pairs from the literature. Ortakoy is located at thalweg* 7km. *Di Iorio & Yüce (1999) estimated the lower layer transport at the North Sill. Cetin (1999) and Gregg* et al. *(1999) measured the currents with current metres, the location of which was close to that of our bottom-mounted ADCP. Their measurements are from a single depth.*

level differences between Anadolukavagi (figure 2.4) and Fenerbahce (about 10km east of South Exit) in Sea of Marmara) lie between 30cm and 40cm. Assuming that sea-levels at Fenerbahce and at the South Exit are identical, this means that the sea-level change is about 35cm over a distance of 25km (from Anadolukavagi to the South Exit) which gives an average slope of 1.4cm/km. According to Alpar & Yüce (1998) the surface slope is about twice as large in the south as in the north. Hence, I will assume that the surface slope in the south was 2cm/km. The distance between the mouth of the Golden Horn and the South Exit is 4km so that we would expect the sea-level in the Golden Horn to be about 8cm less than at the South Exit. Therefore this analysis suggests that our observed sea-level differences (during exchange) should have been between 20cm and 30cm. However, these values must be too large, because with them the sea-level difference would be 0cm when the upper layer current reached maximum northward velocities of $1.2\text{m}\,\text{s}^{-1}$ at the peak of the Orkoz.

Method B: Because of the Orkoz, the upper layer current was zero at two times (see figure 3.8). Friction along the side-walls was zero. Interfacial friction was even smaller than during exchange conditions because of the reduced velocity difference between upper and lower layer. Hence, the upper layer momentum equation reads (derived from (2.1))

$$\frac{\partial u_1}{\partial t} + g\frac{\partial h_1}{\partial x} + g\frac{h_1}{2\varrho_1}\frac{\partial \varrho_1}{\partial x} = 0\,. \tag{C.1}$$

which can be approximated as

$$\underbrace{\frac{1}{g}\frac{\Delta U_1}{\Delta T}}_{1/140{,}000(begin),-1/360{,}000(end),1/500{,}000(average)} + \underbrace{\frac{\Delta H_1}{L}}_{?} + \underbrace{\frac{H_1}{2\varrho_0}\frac{\Delta \varrho_1}{L}}_{\approx -1/265{,}000} = 0 \quad \text{(C.2)}$$

where $H_1 \approx 40$ is the upper layer thickness, ΔH_1 the unknown sea-level difference, $L \approx$ 21km the distance between Anadolukavagi and the mouth of the Golden Horn, $\varrho_0 \approx$ 1015kgm^{-3}, $\Delta\varrho_1 \approx 4$kgm^{-3} the density difference between the Black Sea and Sea of Marmara, and ΔU_1 the change of upper layer velocity over the time interval ΔT.

Although time-dependence can normally be neglected in the Bosphorus, it is significant during the Orkoz because the upper layer changed direction in a relatively short period of time. On April 5, 12:00, when it began to reverse, it moved southward with $-0.5\,\mathrm{m\,s^{-1}}$. 6.5h later it reached a maximum speed of $1.3\,\mathrm{m\,s^{-1}}$. With these values the du/dt term is almost twice as large as the density gradient term. The opposite process at the end of the Orkoz was slower; the upper layer velocity decreased from $+0.6\,\mathrm{m\,s^{-1}}$ to $-0.5\,\mathrm{m\,s^{-1}}$ in 11h.

The magnitude of the three different terms is indicated below each in (C.2). The du/dt term shows three values which represent the beginning and end of the Orkoz, and the average of the two. The corresponding solutions for ΔH_1 are then -0.07m, $+0.13$m and 0.03m. The last solution makes the reasonable assumption that the density gradient between the basins remained constant.

Conclusion: I have used the result from method B to establish the correct sea-level difference, that is I subtracted 28cm from the southern sea-level record. This happens to be the value suggested by Lt.JG Ahmet Unlu, but it is about 15cm less than asked for by the result of method A. Considering the approximations made the discrepancy with method A is not surprising: a) according to Lt.JG Ahmet Unlu geodetic levelling at the Bosphorus has an uncertainty of $\pm$5cm and my method A calculations could easily be wrong by the same amount, b) there could be a sea-level difference between Fenerbahce and the South Exit and/or the sea-level slope is larger than assumed, and c) the upper layer currents reported by Cetin (1999); Gregg *et al.* (1999) might be smaller than the average layer speeds if the current meter was close to the interface which might be the case because the current meter must have been set sufficiently deep to avoid big ships.

D. Determination of Entrainment Rates

In his 1966 nobel lecture Richard Philips Feynman (1918 - 1988) said *'We have a habit in writing articles published in scientific journals to make the work as finished as possible, to cover up all the tracks, to not worry about the blind alleys or describe how you had the wrong idea first, and so on. So there isn't any place to publish, in a dignified manner, what you actually did in order to get to do the work.'* If I took this criticism to heart this appendix would turn into a saga which would not be in anybody's interest. As a compromise I will try to describe in detail the steps toward the determination of the entrainment rates and their uncertainty.

D.1. Basic Equations

Due to the two-layer structure of the flow in the Bosphorus, it is possible to find the entrainment fluxes Q_{12} and Q_{21} by making use of the steady state salt and volume conservation equations (figure D.1). The layer volume fluxes Q_1 and Q_2 are obtained by integrating the velocity over the cross-section

$$Q_1 = \int dy \int_{\eta_2}^{\eta_1} dz\, u_1(y,z) \qquad \text{and} \qquad Q_2 = \int dy \int_{H}^{\eta_2} dz\, u_2(y,z)\,, \tag{D.1}$$

and the layer salt fluxes are given by

$$\begin{aligned} SF_1 &= \int dy \int_{\eta_2}^{\eta_1} dz\, u_1(y,z) S_1(y,z) \varrho_1(y,z)\,, \\ SF_2 &= \int dy \int_{H}^{\eta_2} dz\, u_2(y,z) S_2(y,z) \varrho_2(y,z)\,. \end{aligned} \tag{D.2}$$

Here, H, η_2 and η_1 are the position of the bottom, interface, and surface, respectively. The interface is defined by the depth of the zero isotach (where $u = 0$). The subscripts 1 and 2 are for upper and lower layer, and the subscripts M and B indicate the cross-section

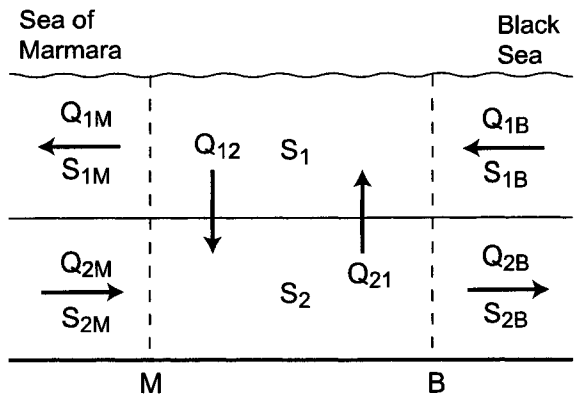

Figure D.1.: *Compartment flows in the Bosphorus two-layer system. The subscript M and B indicate the flows through the boundaries toward the Sea of Marmara and Black Sea, respectively. All quantities are positive.*

closest to the Sea of Marmara and the Black Sea, respectively. In general, the variables will vary over the cross-section.

Conservation of volume is described by

$$Q_{1M} + Q_{12} = Q_{1B} + Q_{21} \qquad \text{and} \qquad Q_{2M} + Q_{12} = Q_{2B} + Q_{21}\,, \tag{D.3}$$

and conservation of salt by

$$SF_{1M} + \int dy \int dx\, u_{12}(x,y) S_1(x,y) \varrho_1(x,y) = SF_{1B} + \int dy \int dx\, u_{21}(x,y) S_2(x,y) \varrho_2(x,y)\,, \tag{D.4a}$$

$$SF_{2M} + \int dy \int dx\, u_{12}(x,y) S_1(x,y) \varrho_1(x,y) = SF_{2B} + \int dy \int dx\, u_{21}(x,y) S_2(x,y) \varrho_2(x,y)\,, \tag{D.4b}$$

where $S_{1,2}$ and $\varrho_{1,2}$ are the salinities and densities of the waters entrained with velocities u_{12} and u_{21}. The quantities may vary with x and y.

To a good approximation we have $\varrho_{(1,2)M}(y,z) = \varrho_{(1,2)B}(y,z) = \varrho_{1,2}(x,y)$ so that density can be eliminated from (D.4). The maximum error, based on minimum and maximum densities observed at the Black Sea and Sea of Marmara exits, respectively, is $(1028 - 1011)/1028 \approx 1.6\%$. For my calculations the density differences are smaller so that the error is about 1%. Because we do not know how the entrainment velocities vary between the cross-sections M and B, we might as well assume that they are constant[1]. Then we

[1] Qualitatively one may be able to infer variations from the echo-sounder images but for the sake of simplicity I will ignore that possibility for now.

may also assume the salinities of the entrained water to be constant so that (D.4) simplifies to

$$SF_{1M} + Q_{12}S_1 = SF_{1B} + Q_{21}S_2 \qquad \text{and} \qquad SF_{2M} + Q_{12}S_1 = SF_{2B} + Q_{21}S_2\,, \tag{D.5}$$

where the salt fluxes SF are defined as in (D.2) but without density variables in the integrand, and where

$$S_1 = \frac{1}{2}(S_{1M} + S_{1B}) \qquad \text{and} \qquad S_2 = \frac{1}{2}(S_{2M} + S_{2B})\,. \tag{D.6}$$

The set of equations (D.3) and (D.5) can be solved for the entrainment fluxes Q_{12} and Q_{21}:

$$Q_{12}^{up} = \frac{1}{S_2 - S_1}(SF_{1M} - SF_{1B} - S_2(Q_{1M} - Q_{1B})\,, \tag{D.7a}$$

$$Q_{12}^{low} = \frac{1}{S_2 - S_1}(SF_{2M} - SF_{2B} - S_2(Q_{2M} - Q_{2B})\,, \tag{D.7b}$$

$$Q_{21}^{up} = \frac{1}{S_2 - S_1}(SF_{1M} - SF_{1B} - S_1(Q_{1M} - Q_{1B})\,, \tag{D.7c}$$

$$Q_{21}^{low} = \frac{1}{S_2 - S_1}(SF_{2M} - SF_{2B} - S_1(Q_{2M} - Q_{2B})\,. \tag{D.7d}$$

We see that, if S_1 and S_2 are given by (D.6), we need to know all four salinity variables (for upper and lower layer and at both cross-sections), but only two volume flux variables (either the upper or lower layer fluxes). If salinity is constant over the layer cross-section then we may use $SF = Q \cdot S$, and if velocity is constant but not salinity then we may use $SF = Q \cdot S$ where $S = \frac{1}{A}\int dy \int dz S(y,z)$ is salinity averaged over the cross-section. With this approximation (D.7) becomes

$$Q_{12}^{up} = \frac{1}{S_2 - S_1}(Q_{1M}S_{1M} - Q_{1B}S_{1B} - S_2(Q_{1M} - Q_{1B})\,, \tag{D.8a}$$

$$Q_{12}^{low} = \frac{1}{S_2 - S_1}(Q_{2M}S_{2M} - Q_{2B}S_{2B} - S_2(Q_{2M} - Q_{2B})\,, \tag{D.8b}$$

$$Q_{21}^{up} = \frac{1}{S_2 - S_1}(Q_{1M}S_{1M} - Q_{1B}S_{1B} - S_1(Q_{1M} - Q_{1B})\,, \tag{D.8c}$$

$$Q_{21}^{low} = \frac{1}{S_2 - S_1}(Q_{2M}S_{2M} - Q_{2B}S_{2B} - S_1(Q_{2M} - Q_{2B})\,. \tag{D.8d}$$

It might seem odd that I have presented two expressions for Q_{12} and Q_{21} although it is clear that $Q_{12}^{up} = Q_{12}^{low}$ and $Q_{21}^{up} = Q_{21}^{low}$ must be valid. This is true in theory but the measurement reality is that some quantities might have been measured with better

accuracy than others (or some have not been measured at all) so that we might prefer one equation over the other in order to reduce the uncertainty of the estimate for the entrainment fluxes. I will discuss this in detail in the following section.

D.2. Uncertainty of Entrainment Estimates

Whereas the determination of the entrainment rates is a simple matter in theory and also when the variables are obtained from numerical simulations (e.g. Stashchuk & Hutter, 2001), it turned out to be a rather cumbersome process for our observations from the Bosphorus. The main reason was that many sources of error needed to be considered and their impact on the entrainment estimates evaluated. In what follows I explain how this was done.

D.2.1. General Expression for Uncertainty of Entrainment Estimates

The uncertainty in a function q of several variables $x_1 \ldots x_N$ measured with uncertainties $\delta x_1 \ldots \delta x_N$ is given by (e.g. Taylor, 1997)

$$\delta q = \left(\left(\frac{\partial q}{\partial x_1} \, \delta x_1 \right)^2 + \ldots + \left(\frac{\partial q}{\partial x_N} \, \delta x_N \right)^2 \right)^{1/2} \tag{D.9}$$

provided the uncertainties in $\delta x_1 \ldots \delta x_N$ are independent and random. In any case, the uncertainty is never larger than

$$\delta q \leq \left| \frac{\partial q}{\partial x_1} \right| \delta x_1 + \ldots + \left| \frac{\partial q}{\partial x_N} \right| \delta x_N \, . \tag{D.10}$$

The uncertainty of Q_{12} and Q_{21} can be evaluated by applying (D.9) and (D.10) to expressions (D.7) and (D.8) as soon as the uncertainties of the layer transports and layer salinities (or of the salt fluxes) have been determined. The resulting expressions, which I do not show here because of their length, are derived and evaluated easily with the aid of a computer algebra system. I have used Maple from Waterloo Maple Inc..

D.2.2. Sources of Error

I distinguish between four kinds of errors. The first two are the systematic and the random errors. These can be well estimated. The third kind are, what I call, 'errors

due to incomplete measurement' which occur because a part of the total volume and salt flux has to be estimated rather than measured. And the fourth kind is due to the time-dependence of the flow.

Systematic Errors

Systematic errors in the salinity measurements are of no concern because the entrainment estimates do not change if an arbitrary constant is added to all salinity values or if all values are multiplied by the same factor (e.g. Pawlowicz, 2001).

On the other hand, systematic errors in the ADCP discharge measurement will have an effect on the entrainment estimates, but it can be estimated easily. For example, if all discharge estimates are too large (small) by 1% (5%,10%) then the entrainment estimates will be too large (small) by the same percentages. There are many sources of ADCP systematic errors (see, for instance, (Simpson & Bland, 2000)), but the most important one in the Bosphorus seems to be errors in the speed of sound c which is used by the ADCP to calculate current velocity and the channel depth. The ADCP uses either a fixed value for c or calculates its using the temperature measured at the transducer face and a fixed salinity value. Because the calculated sound speed deviated slightly from the one based on the CTD measurements, I applied a simple correction (e.g. Gordon, 1996), after which the ADCP's bottom-track velocity agreed with the GPS derived velocity to $\pm 1 \mathrm{cms}^{-1}$. Stratification causes the sound speed to vary with depth. This does not affect the horizontal velocities, however the depth measurement is biased. I corrected this using the measured sound-speed profile (Gordon, 1996). The correction assumed zero horizontal sound-speed gradient which was in general a good approximation save on a few transects. I estimate that after all corrections the bias in the **measured** part of the layer transports to be about 2% and for a few bad cases to be about 5%.

Random errors

Discharge Measurement The effect of random errors on discharge determined from broad-band ADCP measurements is discussed by Simpson & Bland (2000). The equa-

tion for estimating the random error in a discharge measurement is given by

$$\sigma_Q = \left[\frac{1}{0.75 N_b N_s N_{wp}} \left(100 \frac{\sigma_w}{V_m} \right)^2 + \frac{1}{N_s N_{bp}} \left(100 \frac{\sigma_b}{V_m} \right)^2 + \frac{\sigma_p^2}{N_b N_s} + \frac{\sigma_{bt}}{N_s} \right]^{1/2} , \qquad \text{(D.11)}$$

where σ_Q is the standard error of a typical measurement of full-channel discharge in percent, σ_w is the single-ping, single-bin water velocity uncertainty in cms^{-1}, V_m is the mean stream speed in cm, σ_b is the single-ping bottom track velocity uncertainty in cms^{-1}, σ_p is the standard deviation of single-bin velocity measurements due to natural stream pulsations, in percent of mean speed, σ_{bt} is the standard error of measured depth, in percent of mean speed, N_b is the average number of depth bins, N_s is the total number of subsection measurements, N_{wp} is the number of water pings per subsection measurement, N_{bp} is the number of bottom pings per subsection measurement, and the constant 0.75 takes into the account the ADCP bin-to-bin correlations (roughly 15%). The four error terms are assumed to be statistically independent, and the stream pulsations are assumed to be uncorrelated from bin to bin.

For a cross-channel transect between Rumelihisari and Anadoluhisari (Transect T310300_1a on March 31, 2002 at 09:50 UTC) the values of the error parameters and typical values of the other variables are as follows: $\sigma_w \approx 10\text{cms}^{-1}$; $\sigma_b \approx 1\text{cms}^{-1}$; $V_m \approx 100\text{cms}^{-1}$; $\sigma_p = 12\%$ (Simpson & Bland, 2000); $\sigma_{bt} \approx 2\%$ (RD Instruments Inc. estimate for a four-beam ADCP (Simpson & Bland, 2000)); $N_b \approx 20$ for one layer; $N_{wp} = 2$; and $N_{bp} = 1$. These values lead to a value of

$$\sigma_Q = 0.3\% . \qquad \text{(D.12)}$$

If the assumption of uncorrelated random errors is not true σ_Q might be larger. In particular, the channel pulsations are likely to be correlated vertically between bins and horizontally between adjacent ensembles. For their example Simpson & Bland (2000) estimate that this might increase σ_Q by a factor of 4. For my purposes I will assume that the random error in the **measured** part of the layer transports is not larger than 1.5%.

Salinity and Salt Flux Measurement Salinity was measured with a Seabird 19 CTD profiler. The manufacturer gives an initial accuracy for salinity of about $\delta S = 0.005\,\text{psu}$. The uncertainty of the layer averaged salinity will be of the order of $\delta S / N^{1/2}$ where N is

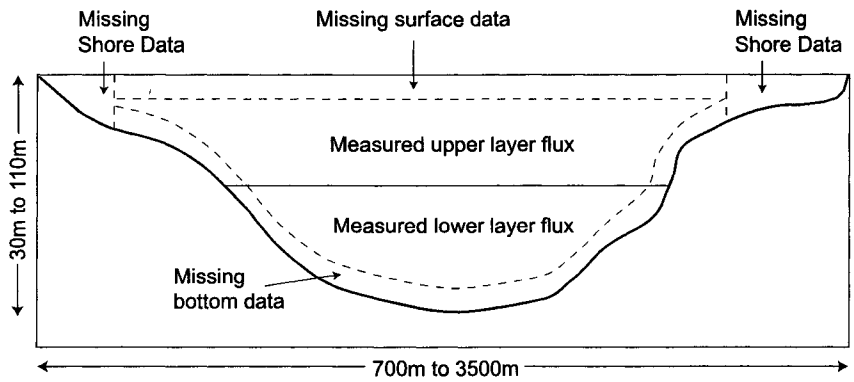

Figure D.2.: *Sketch of cross-section of the Bosphorus with measured and unmeasured parts of the total layer transports.*

the number of samples. Clearly this is negligible. Hence, the random error of the salt flux estimates approximately equals that of the discharge estimates.

Errors due to incomplete measurements

Layer Volume Fluxes Our measurements of the layer volume transports were always incomplete because of three reasons: a) there was an unmeasured distance of 3.2m near the surface due transducer mounting depth as well as transducer and electronics settling time (Gordon, 1996), b) signal-loss due to side-lobe interference occurred in the deepest 6% of the measured depth (Gordon, 1996), and c) we could not measure the flow near the shores of the strait because of limitations by the vessel hull depth, propeller draft, and maneuverability (Figure D.2).

The transport Q_{top} in the missing about 3m thick surface layer was estimated by using either a constant extrapolation from the average of the last two measured velocity bins or by a linear extrapolation from the last 3 to 4 measured velocity bins. For uniform flow both methods give the same result, whereas for sheared flow the constant extrapolation underestimates the flux. I generally used the linear extrapolation method to estimate the transport and used the difference of the results obtained with the two methods as rough indicator of the accuracy. The contribution of Q_{top} to the total upper layer flux $Q_{1,\text{total}}$ was as small as 7% in the north were the upper layer is thick, and as large as 30% in the south when the upper layer was only 15m thick.

The transport Q_{bot} in the missing bottom layer was estimated similarly whereby the

linear extrapolation assumed zero velocity at the bottom. The constant and linear extrapolation method always overestimate and underestimate the true flux, respectively. For a few test cases I compared these two estimates with estimates obtained using a logarithmic velocity profile (which should be the true profile) or a one-sixth power velocity profile (Simpson & Bland, 2000) and found the average of the 'constant' and 'linear' estimate to be a good approximation. Over flat bottom the thickness of the bottom layer was about 6% of the total depth (as predicted for a 20° beam angle ADCP (Gordon, 1996)), but about 8% on slopes. The contribution of Q_{bot} to the total lower layer flux $Q_{2,\text{total}}$ was generally between 10 and 15% and up to 30% for transects with a shallow lower layer.

Finally, the unmeasured transports $Q_{1,\text{east}}$ and $Q_{1,\text{west}}$ of the upper layer close to the eastern and western shore, respectively, had to be estimated. Whenever possible we extended the end-points of our transects into areas where the currents were nearly zero so that the transports would be negligibly small. This was impossible to achieve a) in large bays which were too shallow to sail into, and b) around the contraction were the currents were large even very close to the steep sides. I then estimated $Q_{1,\text{east}}$, $Q_{1,\text{west}}$ and their uncertainties by use of some assumed bottom profiles and horizontal and vertical velocity profiles. For instance, I assumed the bottom to be constant or linearly increasing to the surface, and the current to remain constant or to decrease linearly to zero along the side-walls. The distance between the transects end-points and the shore was calculated using our differential GPS data and coastline data from a database which was derived from Turkish navigational charts. The accuracy of the distance estimates is about ±20m. (Whereas I know the accuracy of our GPS data (see appendix A), I had to estimate the accuracy of the coastline data. We sometimes sailed very close to shore and never did the corrected GPS data indicate that we crossed the shoreline. Furthermore, we frequently docked at terminals at Anadoluhisari and at the Turkish Hydrographic Office, the charted position of which agreed well with the GPS derived position.) Nevertheless the uncertainty of $Q_{1,\text{east}}$ and $Q_{1,\text{west}}$ is probably as large as 50% to 100%. This does not constitute a big problem as for most transects the contribution of $Q_{1,\text{east}}$ and $Q_{1,\text{west}}$ to the total upper layer flux was only 0% to 2%. However, on some transects it contributed about 5%.

Layer Salinities and Salt Fluxes Along the northern part of the Bosphorus the layers were generally found to have an almost constant salinity in the horizontal and also in the vertical save close to the interface. It was therefore sufficient to derive the layer salinities from a single CTD profile.

On the other hand, south of the contraction, and in particular over the South Sill we did observe some variation of salinity across the channel. Because of heavy ship traffic and time constraints we were often limited to only one CTD cast per transect. I estimated the resulting uncertainty in the layer salinities (or layer salt fluxes) using the horizontal variation in salinity that we did measure along some transects and which was then based on 2 to 3 CTD casts. I also I checked that my error estimates are consistent with more detailed observations of density across the South Sill by Gregg & Özsoy (2002).

Generally I tried to estimate the layer salinities consistently from transects to transects, because, as pointed out earlier, salinity biases of equal sign and magnitude have no effect on the entrainment rates.

Time-dependence Errors

Equations (D.3) and (D.4) assume a steady state. From the discussion in section 3.2.2 it is clear that this is only approximately true because the layer transports can change significantly over a few hours in a highly irregular manner. This was frequently evidenced by discrepancies in total volume fluxes obtained at different cross-sections.

In August 1998 we had no knowledge about the magnitude and direction of these fluctuations which rendered the determination of the entrainment rates almost impossible. On the other hand, in April/March 2000 the bottom-mounted ADCP provided continuous current measurements from which I derived the continuous record of layer transports as shown in figure 3.9 in section 3.2.2. I will briefly explain how the layer transports were obtained:

I calculated the layer transports from 12 cross-channel transects in the vicinity of the bottom-mounted ADCP between Rumelihisari and Anadoluhisari, whereby I applied all the corrections explained in the previous section. (We did a total of 16 cross-channel transects at that location but 4 were done during the Orkoz. For the latter the interface was poorly defined.) From the data of the bottom mounted ADCP I derived layer thicknesses

and vertically averaged velocities. I then compared the layer transports with the vertically averaged velocities and with the product of the vertically averaged velocities and the layer thicknesses as shown in figure D.3. The second comparison shows a very good linear relation. Naturally, it is better than the first, because it takes into account the variation of the interface depth. Using the obtained regression coefficients the ADCP velocity samples were transformed into layer transports. Theoretically, an even better regression can be done if it is taken into account that the strait has a non-rectangular cross-section, that is that the layer areas do not change linearly with the layer thickness. However, this requires a very good knowledge of the cross-sectional shape which our data could not provide (for instance, because the transects were not all done at exactly the same locations). Furthermore, at the level of the interface the channel sides are relatively steep and, because of friction, the currents are small.

Having derived the continuous record of layer transports it was possible to decide whether they had changed significantly between two transects. I also took into account the corresponding change in sea-level. If the changes were large it was difficult to use the layer transports to calculate the entrainment rates. For instance, it was generally impossible to compare transects from the northern end of the strait with those from the southern end because the time difference was a couple of hours during which the flow changed significantly. On the other hand, if the change was small I applied a small correction to the layer transports from one of the cross-sections so that they would represent the transports at the time of the other cross-section. One flaw of this method is that, strictly speaking, I should also have adjusted the layer salinities, because entrainment depends on the layer velocities. Unfortunately the data base was somewhat too slim for a systematic investigation of this problem.

Expressing the time-dependence error in numbers was difficult. It was also not always clear whether this would constitute a random or a systematic error. The most consistent method was the comparison of the net transports from two cross-channel transects.

Summary

In summary, the time dependence errors often turned out to be as large or larger than the sum of all the other errors, that is it accounts for about 50% of the uncertainty in

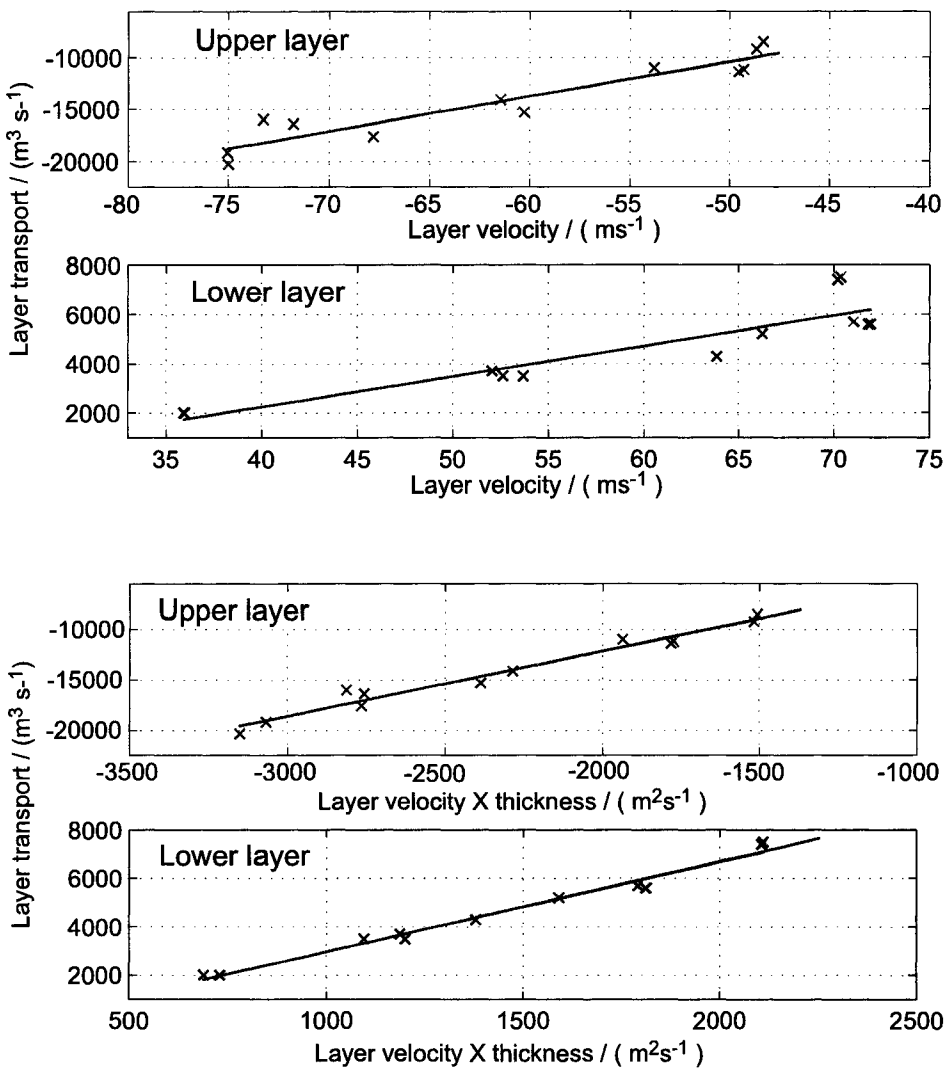

Figure D.3.: *Upper two panels: Comparison between layer transports and average layer velocities measured by the bottom-mounted ADCP. Lower two panels: Similar, but the average layer velocities were multiplied with the layer thicknesses. The layer transports were derived from cross-channel transects between Rumelihisari and Anadoluhisari, that is in the vicinity of the bottom-mounted ADCP.*

the entrainment estimates which varied between 100 and 300$m^3 s^{-1}$. Clearly the time-dependence error could have been reduced to zero if cross-channel transects had been done simultaneously from two vessels.

E. Detrainment From an Active Into a Passive Layer

We ignore friction and topographic effects and use $w_{21} = 0$. Then (4.61) becomes

$$\frac{\partial h_2}{\partial x} = \frac{1}{1 - F_1^2 - F_2^2} \times \left\{ w_{21} \frac{2F_1^2}{u_1} \left(1 - \frac{1}{2}\frac{u_2}{u_1} + \frac{1}{2}\frac{u_1}{u_2}\frac{F_2^2}{F_1^2} - \frac{1}{4}F_1^{-2} \right) \right\} . \tag{E.1}$$

We modify this expression in order to be able to approximate it appropriately if $F_1^2 \ll 1$. Using $\frac{u_i}{u_j} = \frac{F_i}{F_j}\sqrt{\frac{h_i}{h_j}}$ we obtain

$$\frac{\partial h_2}{\partial x} = \frac{F_2^2}{1 - F_1^2 - F_2^2} \times \left\{ 2\frac{w_{21}}{u_1} F_2^{-2} \left(F_1^2 + \frac{1}{2}F_1 F_2 \frac{h_1 - h_2}{\sqrt{h_1 h_2}} - \frac{1}{4} \right) \right\} . \tag{E.2}$$

Certainly when $F_1^2 \ll 1$ we obtain

$$\frac{\partial h_2}{\partial x} = \frac{F_2^2}{1 - F_2^2} \times \left\{ 2\frac{w_{21}}{u_1} F_2^{-2} \left(\frac{1}{2}F_1 F_2 \frac{h_1 - h_2}{\sqrt{h_1 h_2}} - \frac{1}{4} \right) \right\} . \tag{E.3}$$

The first term in the innermost pair of parenthesis can be rewritten as

$$\frac{1}{2}F_1 F_2 \frac{h_1 - h_2}{\sqrt{h_1 h_2}} = \frac{1}{2}\frac{u_1 u_2}{g'} \left(\frac{1}{h_2} - \frac{1}{h_1} \right) . \tag{E.4}$$

In addition to $F_1^2 \ll 1$ we now also assume that the upper layer is thicker than the lower layer ($h_1 > h_2$). Then our final expression for $\frac{\partial h_2}{\partial x}$ becomes

$$\frac{\partial h_2}{\partial x} = \frac{F_2^2}{1 - F_2^2} \times \left\{ 2\frac{w_{21}}{u_1} F_2^{-2} \left(\frac{1}{2}\frac{u_1}{u_2} F_2^2 - \frac{1}{4} \right) \right\} . \tag{E.5}$$

The last approximation might not always be justified. If $h_1 \gtrapprox h_2$ the first term in the innermost pair of parenthesis in (E.3) becomes very small compared to 1/4 and may be ignored completely so that we obtain

$$\frac{\partial h_2}{\partial x} = \frac{F_2^2}{1 - F_2^2} \times \left\{ -\frac{1}{2}\frac{w_{21}}{u_1} F_2^{-2} \right\} . \tag{E.6}$$

To derive the expression for $\frac{\partial F_2^2}{\partial x}$ we insert (E.3) into

$$\frac{\partial F_2^2}{\partial x} = F_2^2 \left(\frac{2}{Q_2} \frac{\partial Q_2}{\partial x} - \frac{1}{g'} \frac{\partial g'}{\partial x} - \frac{3}{h_2} \frac{\partial h_2}{\partial x} \right) \tag{E.7}$$

and use

$$\frac{\partial Q_2}{\partial x} = -w_{21} \qquad \text{and} \qquad \frac{1}{g} \frac{\partial g'}{\partial x} = -\frac{w_{21}}{Q_1} \,. \tag{E.8}$$

The result is the following rather complicated expression

$$\begin{aligned} \frac{\partial F_2^2}{\partial x} =& \frac{-F_2^2}{1 - F_2^2} \frac{w_{21}}{Q_2} \\ & \left\{ 2 + F_2^2 - \frac{u_2}{u_1} \left[\frac{3}{2} + \frac{h_2}{h_1} \left(1 - F_2^2 \left(1 + 3 \frac{u_1}{u_2} \right) \right) \right] \right\} \,. \end{aligned} \tag{E.9}$$

The term $(2 + F_2^2)$ is due to the loss of fluid. This causes the flow to become less critical. The unpleasantly complicated remainder is due to the density gradient in the upper layer. If $u_1 < u_2$ and $h_1 > h_2$ it can be approximated by $-(3u_2)/(2u_1)$. In an exchange flow this term causes the flow to become less critical, too.